Adsorption of Heavy Metal Ion Species from Aqueous Solution on Activated Carbon

Yongfeng Jia

A Thesis Submitted for the Degree of Doctor of Philosophy

University of Newcastle-upon-Tyne

2000

Acknowledgement

I would like to thank my supervisor Professor K. Mark Thomas for offering me the opportunity of doing a PhD at Northern Carbon Research Laboratories and his invaluable supervision throughout my research, especially at some crucial points of the project.

I also wish to thank Dr Carl J. Steele for his help and advise at the beginning of my research in this lab.

Many thanks go to Dr Ian A. S. Edwards for all his help and assistance throughout my study at NCRL. I would like to thank Dr. Paul A. Christensen for allocating me some valuable *in-situ* FTIR time in his lab. I also thank Dr Brian Eastwood for his assistance on the FTIR.

I would like to thank Dr Mike May at ICI for measuring the pore size distribution of some active carbons in a friendly way. Many thanks go to Dr Ian P. Hayward at the University of Leeds for allowing me to use the Raman spectroscopy and Dr Ian Kirkman at Daresbury Laboratory for his assistance on the beam line.

I would also like to thank the technicians in the Department of Chemistry, Steve, Dave, John the glassblower, George, Martin, Bruce, Gary, Eddie. I also thank Grant at the Materials Analytical Service for the EDA analysis.

I thank Dr Qian Zhu and my other colleagues at NCRL for the friendliness and help.

I will cherish the days with my friend at Newcastle over the last few years, whose encouragement and love help me complete this course.

Finally, I would like to thank every member of my family for their understanding, patience and loving support during my study here.

ABSTRACT

Activated carbons are used widely for the adsorption of environmentally unfriendly species from both liquid and gas phases, the separation of gases and adsorption of species from aqueous solution. Examples of the processes are the adsorption of $Au(CN)_2^-$ and $Ag(CN)_2^-$ from aqueous solution for the recovery of precious metals, the treatment of waste water containing organic chemicals and toxic metal species and the preparation of metal catalysts supported on carbon. This investigation has involved the study of the influence of porous structure and surface functional groups on the adsorption of both anionic and cationic metal species in order to understand the mechanism of adsorption of these species on active carbon from aqueous solution.

Various types of oxygen functional groups were introduced onto the surface of coconut shell derived activated carbon through oxidation using nitric acid. Fourier transform infrared spectroscopy (FTIR), temperature programmed desorption (TPD) and selective neutralisation were used to characterise the surface oxygen functional groups. The oxidised carbons were also heat treated to provide a suite of carbons where the oxygen functional groups of various thermal stability were varied progressively. It was found that acidic oxygen functional groups mainly as carboxylic acid groups were incorporated into activated carbon by HNO_3 oxidation. The phenol and quinone groups were also introduced by the oxidation process while the lactone groups were formed during heat treatment. The oxygen functional groups had a range of thermal stabilities with carboxylic acid groups being the least stable.

A coconut shell derived active carbon was treated with ammonia and nitric acid followed by ammonia to incorporate nitrogen functional groups into the carbon. Active carbon with high nitrogen content was also prepared from nitrogen-rich precursor polyacrylonitrile (PAN). X-ray absorption near edge structure spectroscopy (XANES) and FTIR were used to investigate the structures of the nitrogen functional groups in carbons. The possible nitrogen functional groups present on carbon surface were pyridinic, pyrrolic (or indolic), pyridonic and aromatic amine-like structures.

The adsorption characteristics of gold and silver cyanide anionic species on a suite of active carbons derived from coconut shell, polyacrylonitrile and chemical modification of the coconut shell carbon were investigated. The gold and silver cyanide adsorption capacities for coconut shell derived carbons correlate with total pore volume. Nitric acid oxidation treatment of the carbon was detrimental to gold adsorption in spite of the incorporation of oxygen content of carbon. The influence of nitrogen functional groups in the carbon structure on gold and silver adsorption was investigated using carbons derived from polyacrylonitrile. The addition of ethanol and butanol to the solution had an adverse effect on gold adsorption. Adsorption of silver cyanide ionic species on the active carbon was suppressed in the presence of excess free cyanide ions in solution whereas gold cyanide adsorption was not greatly affected at room temperature. The adsorption of gold cyanide was suppressed by the excess free cyanide and sodium sulphide at 70 °C.

The adsorption of cadmium ions was enhanced dramatically by oxidation of the carbon. The ratio of released proton to adsorbed cadmium on oxidised carbon was approximately 2 indicating cation exchange was involved in the adsorption process. Na^+ exchange studies with the oxidised carbon gave a similar ratio. After heat treatment of the oxidised carbons to remove oxygen functional groups, the ratio of

H^+/Cd^{2+} decreased significantly as well as the adsorption capacity. Both reversible and irreversible adsorption were involved in the process of cadmium adsorption with reversible adsorption having higher enthalpy. The irreversible adsorption resulted from cation exchange with carboxylic acid groups whereas the reversible adsorption probably involved physisorption of the partially hydrated cadmium ion.

The nitrogen functional groups may act as ligands which can coordinate with transition metal cations. The adsorption of transition metal cations such as Cd^{2+}, Ni^{2+} and Cu^{2+} on active carbon was appreciably increased by the nitrogen functional groups present on carbon surface whereas ammonia treatment of the carbon showed little effect on the adsorption of alkali earth metal cation Ca^{2+}. There is little difference in the adsorption capacities of cadmium ions on coconut shell derived carbon at pH 4.1 and pH 7 whereas the adsorption of cadmium ions was significantly enhanced with increasing pH for the carbons with high nitrogen content. The nitrogen rich carbons show selectivity towards various transition metal cations reflected by adsorbing more Cu^{2+} than Cd^{2+}. This is consistent with the fact that the coordination compound of Cu^{2+} with pyridine has higher stability constant than that of cadmium.

Content

Chapter 1

STRUCTURES IN CARBON

1.1 Introduction

This chapter gives a overview of the basic structural features of carbon materials, the carbon forms and various principle approaches and techniques used to investigate the structure of solid carbon materials.

The formation of σ and π bonds between carbon atoms and with other atoms provides extensive and complex structures which constitute a whole branch of chemistry, organic chemistry. However the carbon science, strictly speaking, deals only with the materials comprised of carbon atoms bonding with themselves via sp^3 or sp^2 hybrid orbitals to give diamond-like, graphite-like and fullerene structures and various derivatives from them.

Element carbon exists in several crystallographic forms, namely diamond with its tetragonal bonding imparting the hardness to the crystal, and graphite which has a lamellar structure in which each lamella is composed of carbon atoms arranged in six-membered ring. The recently discovered fullerenes possess spherical or cylindrical structure based on the structure of graphite lattice. Perfect graphite is a rare form of carbon, the majority of carbon is found as less ordered structures which are chemically heterogeneous and composed of mainly graphitic subunits such as coals, cokes, chars, carbon blacks, carbon fibres and active carbons. The variety of carbons and their structure is mainly dominated by the origins and the processing conditions.

1.2 Allotropes of Carbon

1.2.1 The Element Carbon

The element carbon has an atomic weight of 12.011 and atomic number of 6. It is the first element in group IV of the periodic table. Eight isotopes so far are known to exist, ^{9}C, ^{10}C, ^{11}C, ^{12}C, ^{13}C, ^{14}C, ^{15}C and ^{16}C. The stable isotopes have natural abundance of approximately 98.90 % for ^{12}C and 1.10 % for ^{13}C. ^{14}C is a radioactive isotope of element carbon with a half life of 5730 years, which makes it useful as a tracer in organic reaction as well as for dating archaeological artefacts. Although the abundance of isotopes varies accordingly from one carbon to another, the $^{12}C/^{13}C$ ratios remain relatively stable in carbons derived from different precursors.

Carbon has the electronic configuration of $1s^2 2s^2 2p^2$ in ground state and the valences of either 2, 3 or 4. Carbon can bond to itself by σ bonds via sp^3 hybrid to give diamond-like materials, and *sp* hybrids as in ecetylene π bonds via sp^2 hybrid to give graphite-like materials. At least four different crystalline forms of element carbon are known to exist: diamond, graphite, carbyne and fullerene.

1.2.2 Diamond

Diamond is made up of a regular three dimensional network of σ bonds via four sp^3 hybrid orbitals, providing a very rigid and stable structure. This makes it one of the hardest materials known to exist. The density of diamond is 3.51 g cm^{-3} which is much higher than 2.25 g cm^{-3} of graphite. Diamond is thermodynamically less stable than graphite at ambient temperature and pressure. However the situation is in opposite way at pressure > 60 GPa at room temperature principally due to its higher density. The electrical conductivity is very low due to lacking of delocalised electrons

since in diamond lattice all four valence electrons of carbon atom are engaged in tetrahedral bonds (via sp^3 hybrid) forming σ bonds between carbon atoms. The structure of diamond is shown in **Figure 1.1**.

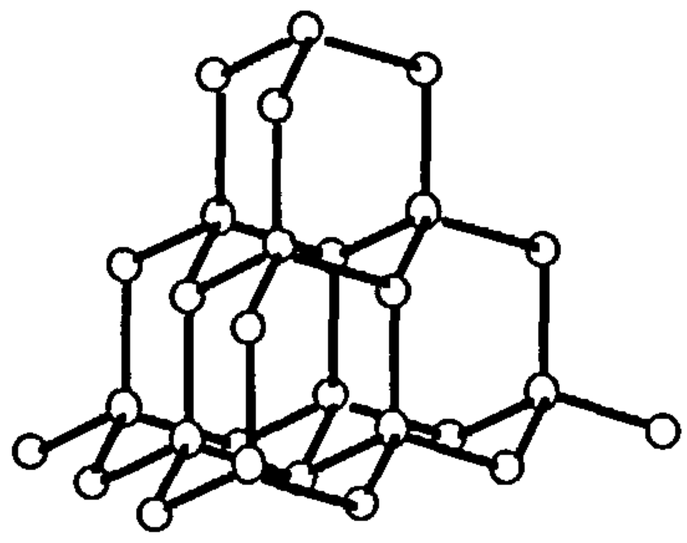

Figure 1.1 Structure of diamond

1.2.3 Graphite

The structure of the graphite crystal was first established as a result of X-ray studies by Bernal in 1924 [*1*]. The graphite crystal consists of layers of carbon atoms in the form of fused benzene rings. In the plane each carbon atom symmetrically bonds to three nearest neighbours through both σ and π bonds which forms the hexagonal two-dimensional networks. The planar structure is stabilised by the resonance and mobility of the delocalised π electrons in the plane while these layers are held together loosely by van der Waals forces. These structural features make graphite a good electrical conductor and a solid lubricant. The bond length of the adjacent carbon-carbon atoms within the rings is 1.42 Å while the separation of the planes (the *d*-spacing) is 3.354 Å. The alternate planes are normally arranged with ABAB stacking sequence so that the structure is hexagonal. Due to the weak Van der Waals attractive force between lamellae the stacking defects can occur. The

rhombohedral form is slightly less stable in which the stacking sequence of the planes is ABCABC rather than ABAB. The rhombohedral form can irreversibly convert to the hexagonal lattice upon heat treatment at 2400 K whereas grinding can increase the proportion of the rhombohedral form in the graphite.

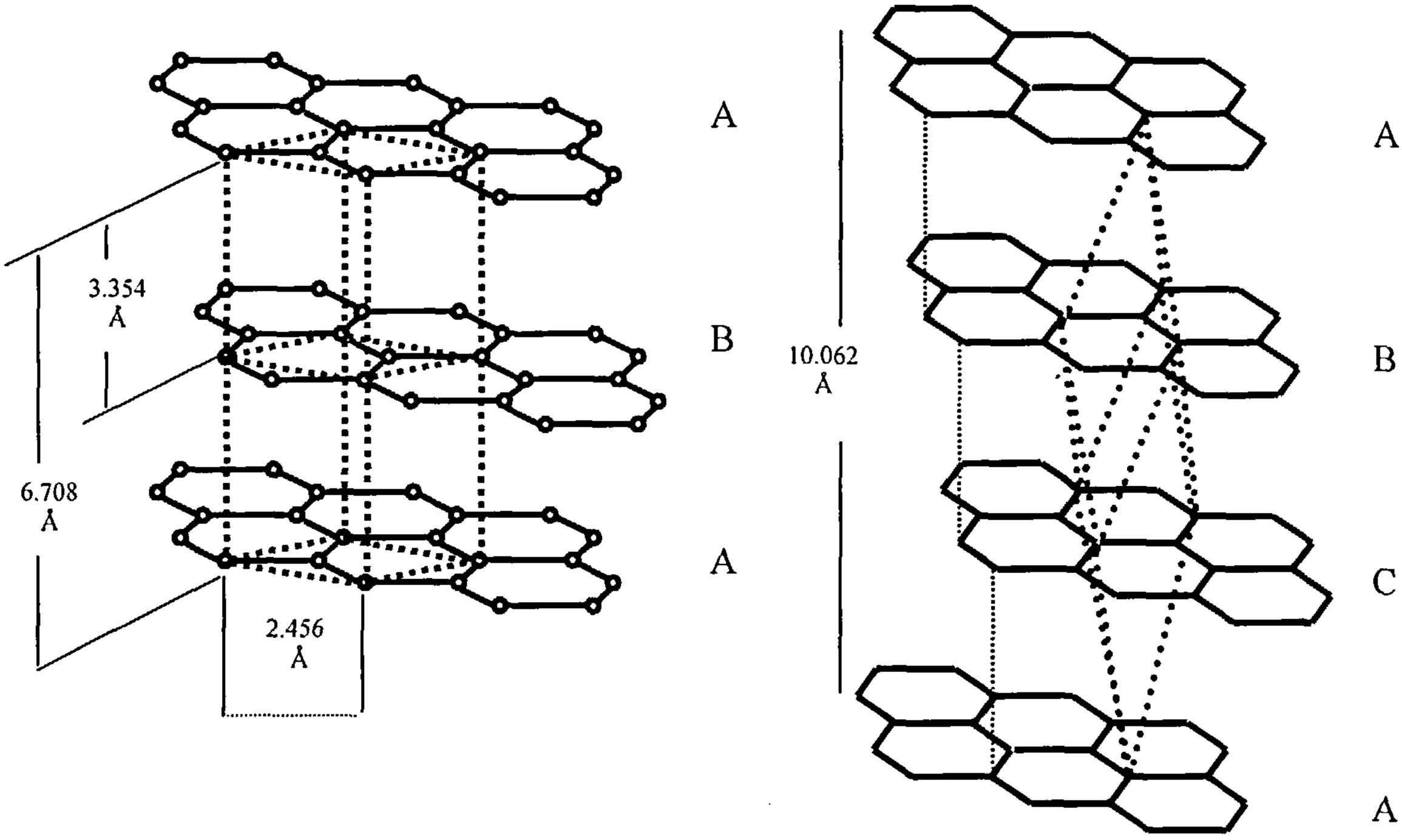

Hexagonal Unit Cell **Rhombohedral stacking**

Figure 1.2 Graphite structure

Graphite possesses conjugated π bonding within the planes which provides a means of conducting electricity owing to the delocalised π electrons throughout the planar structure. However there is little electron movement between layers therefore the electrical conduction across the layer is low. This gives a an excellent example of the anisotropy exhibited by graphite. The graphite structure is illustrated in **figure 1.2**.

1.2.4 Carbyne

Carbyne as an allotrope of carbon was reported to be synthesised by Kasatochkin et al [*2*]. It has an amorphous and crystalline structure which retains the chain structure of carbon macromolecules of polyyne or cumulene, as shown in **Figure 1.3**.

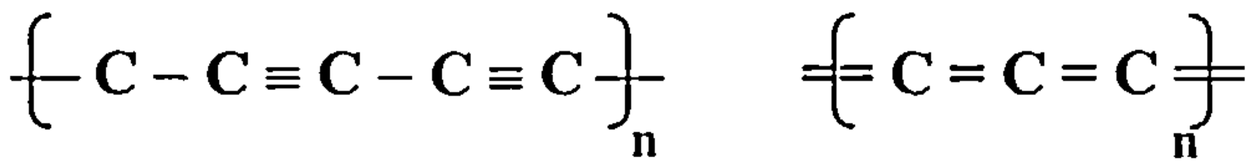

Polyyne **Cumulene**

Figure 1.3 Structure of carbyne

Two polymorphous modifications, α and β of carbyne monocrystals are known to exist which possess a hexagonal crystal structure in which the carbon chains are aligned parallel to the crystallographic c-axis. The β carbyne with higher density due to its higher intermolecular order is more stable than α carbyne.

1.2.5 Fullerenes

It was not until recently when the existence of fullerenes as a family of carbon allotropes which constitute one form of pure carbon has been established by Kroto and Smalley and co-workers [*3*]. It is the fourth allotropic and first molecular form of carbon, named after Buckminster Fuller, an architect renowned for his geodesic dome structure. The main species observed are C_{60} and C_{70} (C_{60}/ C_{70} ratio typically 5:1) but there are many possible cage isomers of the fullerenes. The most geodesically stable

cages for the C_{60} and C_{70} molecules have I_n and D_{6h} symmetry. The high stability of C_{60} is attributed to the closed cage structure consisting of 12 pentagons and 20 hexagons (See **Figure 1.4**).

In C_{60} all carbon atoms are connected via sp^2 bonds with remaining 60 delocalised π electrons distributed in the structure.

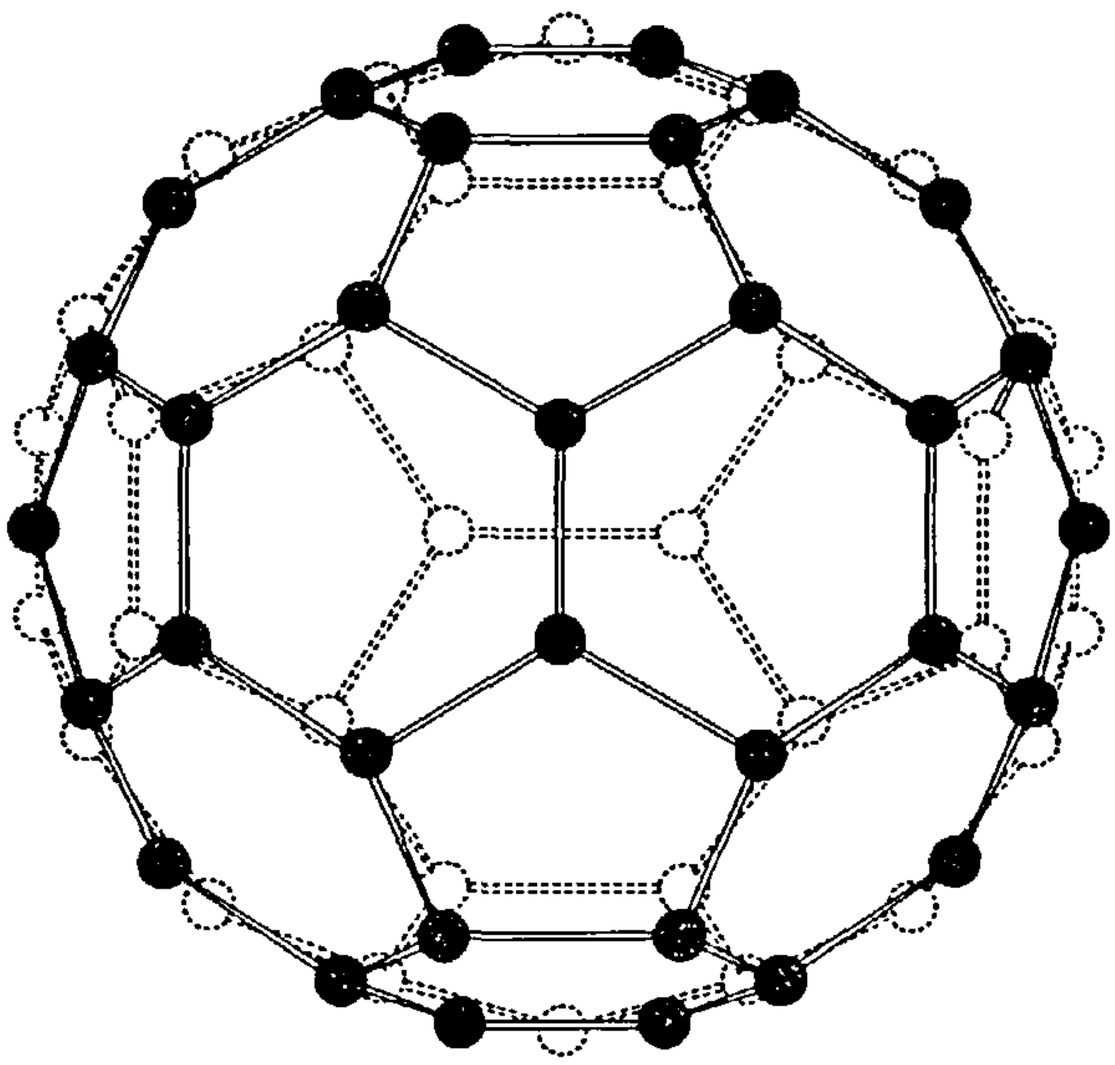

Figure 1.4 The model of C_{60} molecule

In 1990, Krätschmer, Huffman *et al* [*4*] reported the preparation of macroscopic quantities of C_{60} by resistive heating of graphite under an inert atmosphere. The truncated icosahedral structure of C_{60} resembling a soccer ball, has been firmly established [*5-8*]. Specifically, it was proposed that these molecules with the composition C_{20+2m} can take the stable form of hollow closed nets composed of 12 pentagons (five-membered ring) and m hexagons (six-membered ring). The higher fullerenes such as C_{76}, C_{78} and C_{84} were also isolated and identified [*9*]. Cylindrical fullerene-type structure also exist and are termed as carbon nanotube.

1.3 Carbon Forms and Origin

Until comparatively recently the natural and artificial forms of carbons were regarded as either crystalline (graphite or diamond) or amorphous. However the application of X-ray diffraction methods to the amorphous carbons led to the view that the latter were also graphitic with their apparently amorphous character arising from the very minute size of the crystallites. Solid carbons are derived from organic precursors. The various types of carbons are divided into two categories: graphitic and non-graphitic depending upon the degree of crystallographic ordering and represent an intermediate between the organic precursor and single crystal graphite. Non-graphitic carbons are further divided into two categories: graphitisable and non-graphitisable carbons. The definition and nomenclature for classification of carbons are available in the literature [*10-13*] and can be summarised in **Figure 1.5**.

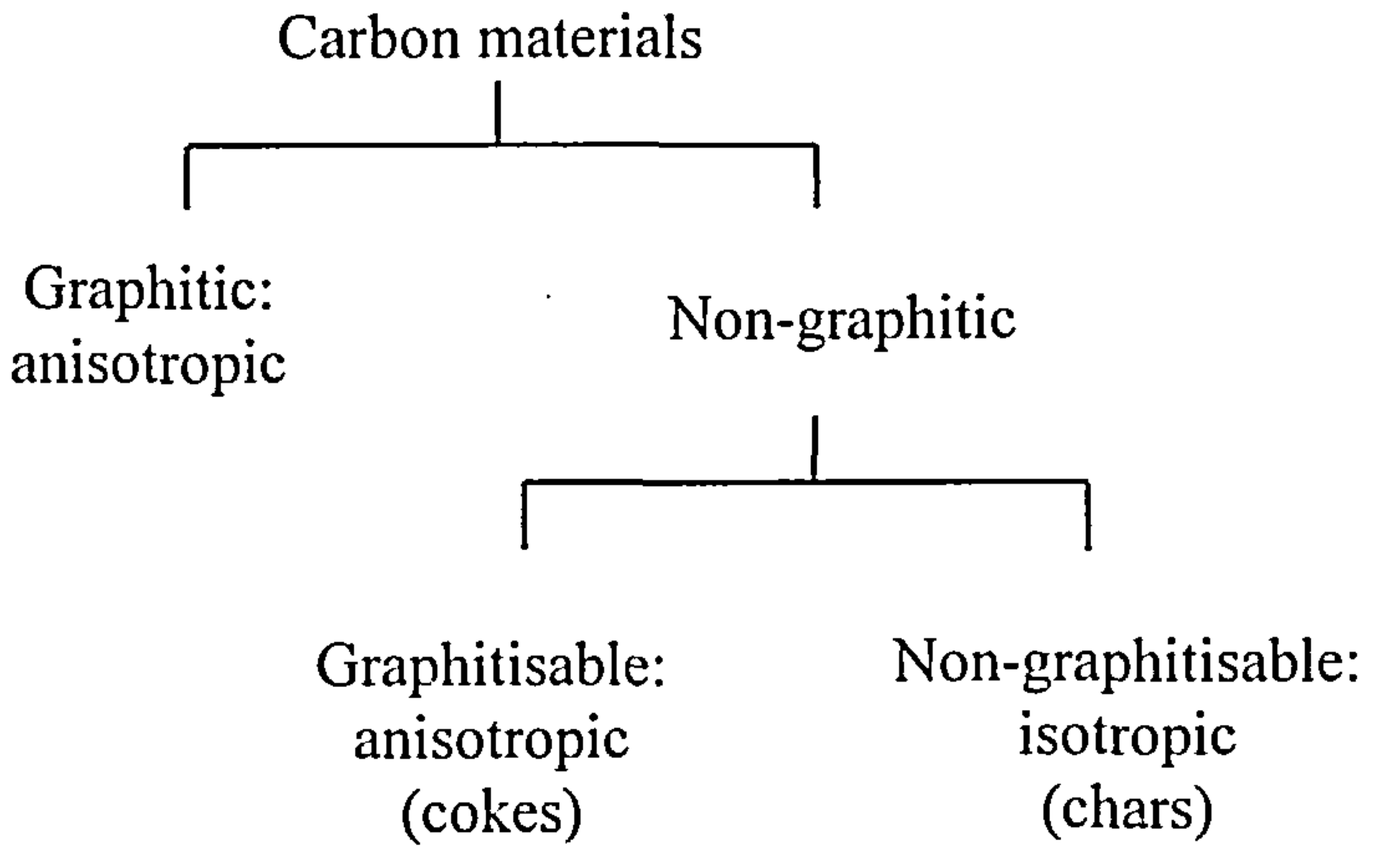

Figure 1.5 Diagram illustrating the classification of carbon materials

1.3.1 Graphitic and Non-graphitic Carbons

Graphitic carbons possess three-dimensional symmetry and non-graphitic do not. Graphitic carbons are all varieties of substances consisting of the element carbon in the allotropic form of graphite irrespective of the presence of structural defects, including natural and synthetic graphites. Non-graphitic carbons are all varieties of substances consisting mainly of the element carbon with two-dimensional long range order of the carbon atoms in planar hexagonal networks, but without any significant crystallographic order in the third direction (c-direction) apart from more or less parallel stacking. Graphitisable carbons can be converted into graphitic carbons by heat treatment to above 2500 K. Such conversion is called graphitisation.

1.3.2 Graphitisable and Non-Graphitisable Carbons

Graphitisable carbons are non-graphitic carbons which can be converted into graphitic carbons by heat treatment [*14*]. The degree of graphitisation depends on the heat treatment temperature (HTT) and the time allowed at temperature to anneal the structure. Non-graphitisable carbons are non-graphitic carbons which cannot be transformed into graphitic carbons solely by heat treatment (under inert conditions) up to temperature of 3500 K under atmospheric or lower pressure. The graphitisable carbons, called *cokes*, are formed commercially by the pyrolysis of aromatic petroleum and coal-tar pitches and some coals. In addition, model polyaromatic compounds and polyvinyl chloride ($C_2H_2Cl_2$) also carbonise to graphitisable, anisotropic cokes. The crystallinity of coke is established via the association, or layering together, of large lamellar polyaromatic hydrocarbon-type molecules (~1000

amu) formed during the carbonisation process. This association of molecules is a new phase termed aromatic, nematic, discotic liquid crystals (or mesophase) formed from within the fluid phase of carbonisation systems.

The liquid crystals of pitch and coal carbonisation are generated in the pyrolysis process. Initially the average molecular weight of pitch at 200 °C is about 200 amu and the liquid is Newtonian and isotropic. Pitch pyrolysis chemistry is dominantly dehydrogenative polymerisation. At temperature >400 °C, molecular weights reach 600-900 amu and the molecules remain attached to each other following a collision because cohesive energy exceeds translational energy. They collect further mesogen molecules of similar size and shape until the clusters can be observed by optical microscopy as anisotropic reflecting spheres of >1 μm diameter. During the initial growth stages of mesophase, the discotic mesogen molecules are stacked parallel and vertical to each other. However, due to the dictates of minimum surface energy, the growing mesophase adopts a spherical shape. However, in some systems such as coal and very reactive pitches, the growth units may never be of sufficiently low viscosity to assume a spherical shape but remain irregular. Structure within the growth sphere is described in **Figure 1.6**. The constituent lamellar molecule of the sphere are parallel to an equatorial plane. Optical microscopy indicates that the layers become orientated towards the poles of the spheres and that they approach the surface of the sphere at right angle. An alternative structure, the onion shaped structure also exists when a sphere of mesophase is trapped within the porosity of a coke or in a second immiscible fluid.

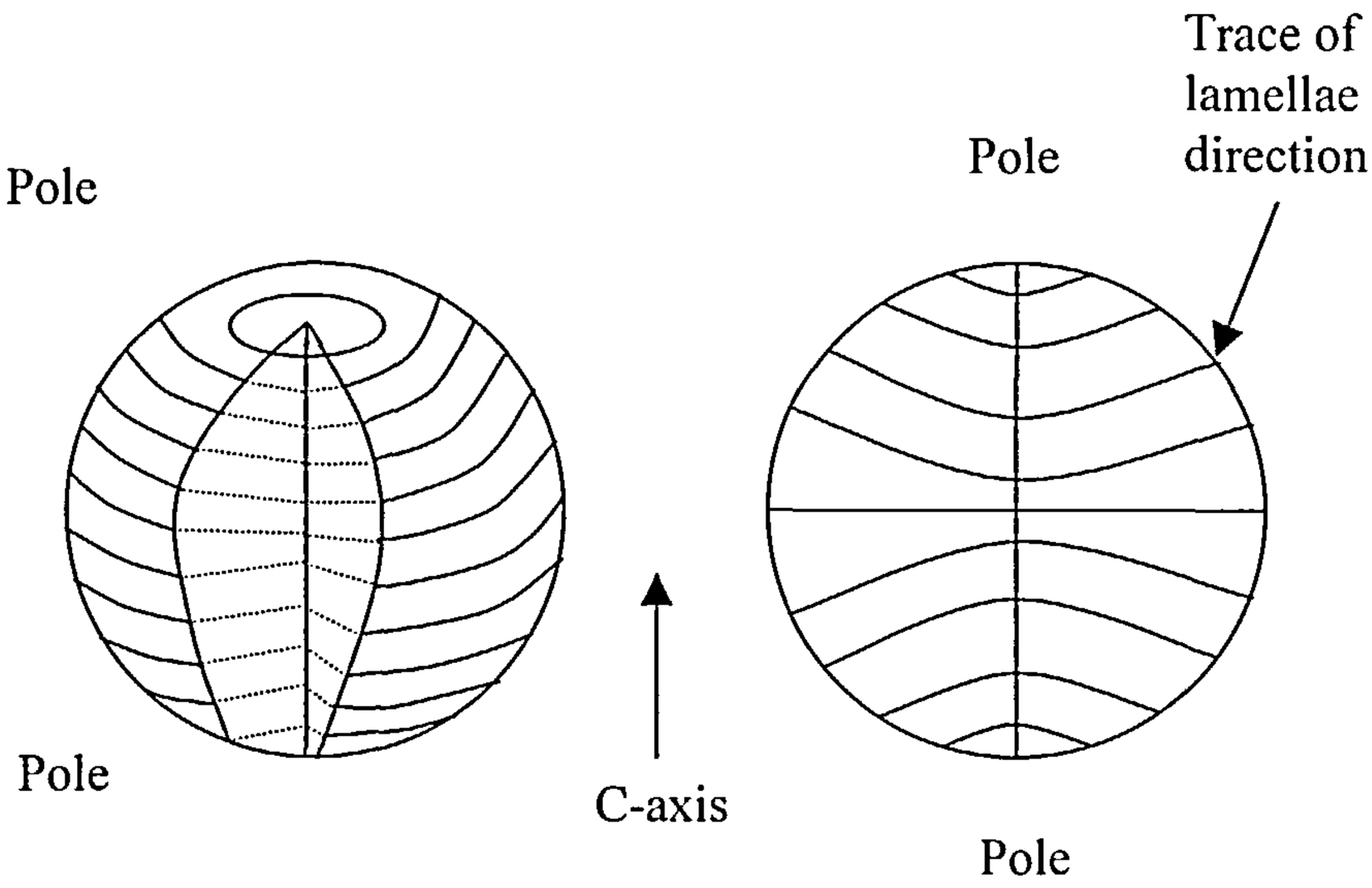

Figure 1.6 Structure of anisotropic nematic liquid crystals as sphere of mesophase within pyrolysing isotropic pitch

The non-graphitisable carbons, called *chars*, or isotropic carbons originate from materials which are already macro molecular in nature, *e.g.* the cellulose or lignin compounds of woods and nutshells, or the specific cross-linked structures (C-O-C bondings) of low rank coals such as peats, lignites, brown coals and non-caking bituminous coals. Synthetic resins of the chemical industry such as phenolic resin, polyfurfuryl alcohol and polyvinylidene chloride are of similar nature. The cross-linkage natures of the isotropic carbons either inherit from the heavily cross-linked precursors or are developed in the early stage of carbonisation. Such parent materials do not pass through a fluid phase during pyrolysis and carbonisation. Chars have a short range structural order, < 10 nm, roughly layered and are isotropic in all properties.

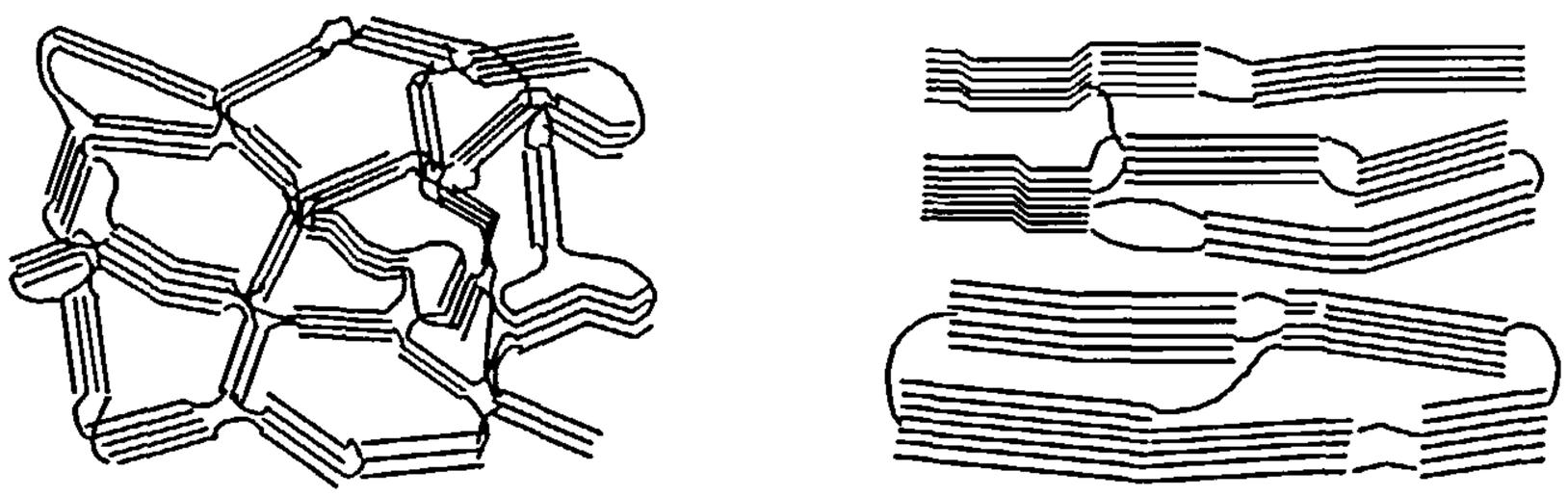

Isotropic **Anisotropic**

Figure 1.7 Two-dimensional orientation of carbon lamellae of isotropic and anisotropic carbons

The graphitisable, anisotropic carbons have essentially approximately parallel arrangements of lamellae which assume increased order on heat treatment to give graphitic carbons. The non-graphitisable, isotropic carbons are comprised of small structural units of graphene lamellae with bent, twisted and defect structures. Both the graphitisable, anisotropic and non-graphitisable, isotropic carbon structures are shown in **Figure 1.7**.

1.3.3 The Building of Graphitic Structures

The schematic building of graphitic structures with heat treatment temperature (HTT) is show in **Figure 1.8** [*15*]. The carbon materials and coals can still be considered as molecular solid at below 1000 – 1100 °C, with a large proportion of heteroatoms and non-aromatic C-C bonds. Their structure is characterised by "structure units" (S.U), which are molecules constituted of less than 10-12 condensed aromatic rings, their size is in the order of 8-10 Angström units and they are stacked

by two or three these molecules (**Figure 1.8 A**). There is no general organisation of these units except a possible preferred orientation, usually local but sometimes extending more or less through the whole solid. The effect of increasing HTT is mainly a progressive purification due to the removal of heteroatoms.

When the HTT increased to 1000-1600 °C there are few heteroatoms left and most of them are probably bound laterally to the aromatic molecules. The S.U. will orient themselves parallel to one another and to build columnar structures like stacks of plates. However these stacks are bent and very irregular. The number of aromatic layers associated in such parallel stacking increases with HTT, as shown in **Figure 1.8 B**.

Graphitisation occurs between 1600 and 3000 °C in two steps: a two dimensional growth from 1600 °C to 2000-2100 °C, and a three dimensional organisation from 2100 °C upwards. Hard carbons usually deviate from the graphitising behaviour at this stage. They do not acquire the complete three dimensional ordered lattice of graphite even at the highest treatment temperatures.

The two dimensional growth of the aromatic systems results from the gradual removal of the various defects (heteroatoms, sp_3 bonds, twists and dislocations) located at the periphery of the structural units. This allows the coalescence of the columnar associations which then constitute very large "wrinkled" parallel sheets of aromatic carbons (**Figure 1.8 C**). The continuing elimination of defects progressively rubs out the S.U. boundaries, and very extended rigid two dimensional parallel graphitic layers are obtained at 2000-2100 °C (**Figure 1.8 D**).

These two dimensional structures are named "graphenes" which are different from the true three dimensional graphite structures. Graphenes have no three

dimensional organisation and are usually called "turbostratic". In the final step the "turbostratic" stacking is ordered into regular ABABAB... sequence of hexagonal graphite.

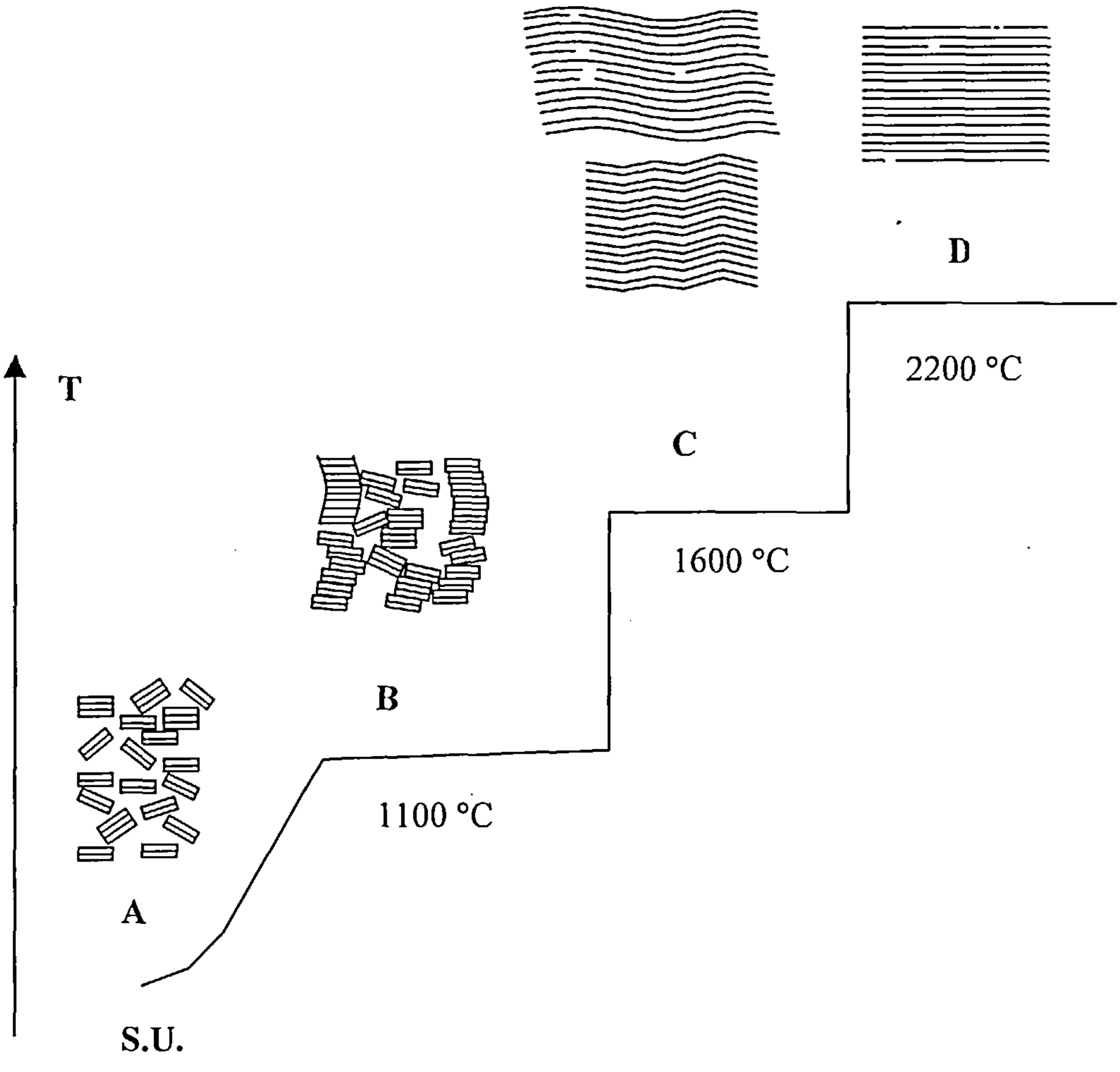

Figure 1.7 A Schematic building of graphitic structure

1.4 Porosity in Carbon

1.4.1 Origin of Porosity

The porosity in carbon is formed by the spaces or voids between the lamellae due to irregular stacking arrangement in carbons. It results either from the manufacturing process or from inheritance in the microstructure of the raw materials. The voids in carbon may be developed or created as a result of mechanical, chemical or heat treatment or exposure to nuclear radiation. There are both open pores and closed pores in carbon, the former referring to the pores connected to the external surface and the latter referring to the voids which are not so connected. The various pore types are schematically shown in **Figure 1.9** [*16*].

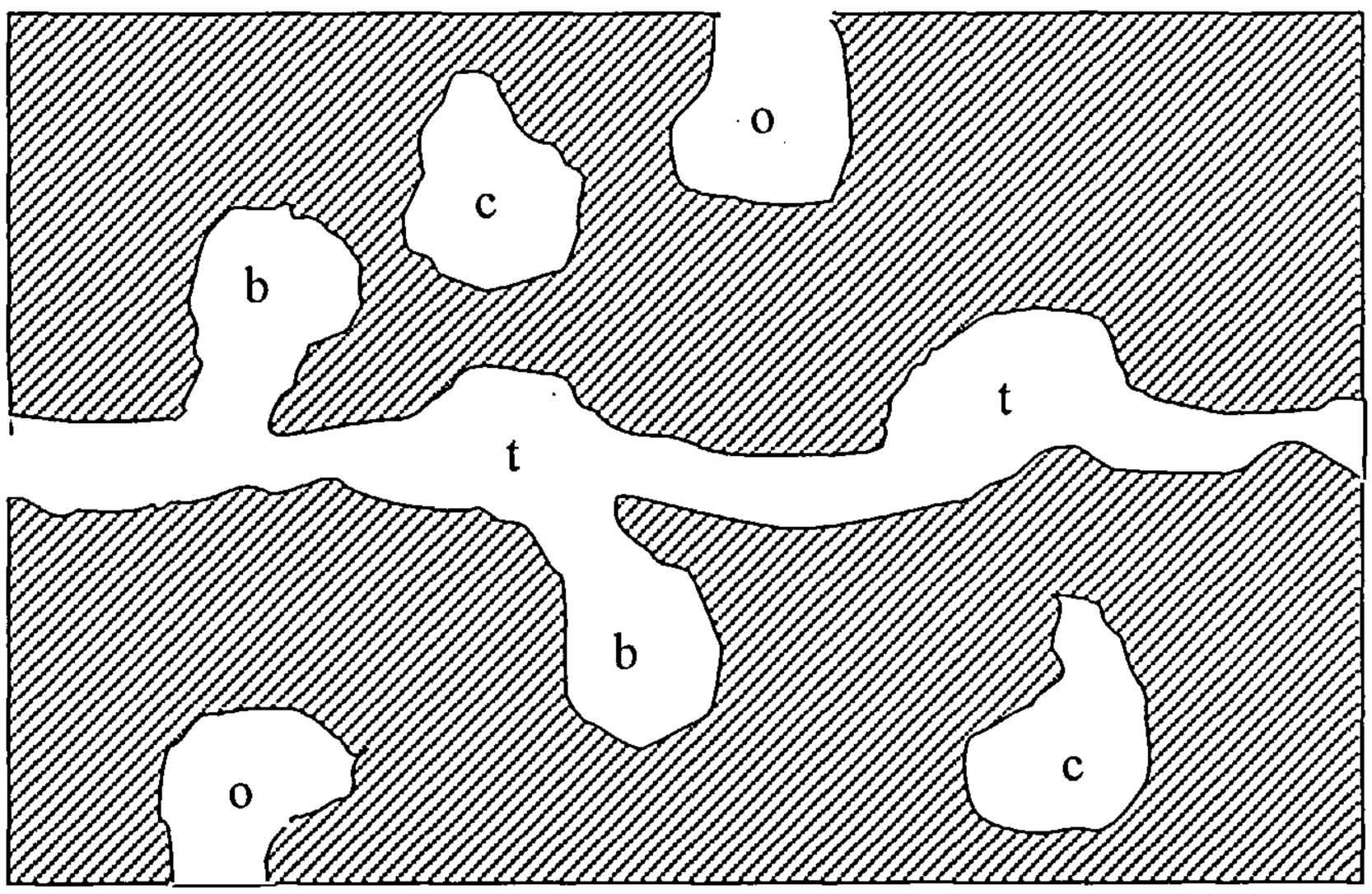

Figure 1.9 Different types of porosity in a porous solid. o – open pores: c – closed pores; t – transport pores; b – blind pores.

1.4.2 Classification of Pores

In addition to the classification of pores by their types, pores in carbons and graphite may also be classified by their size and shape. An arbitrary but widely adopted classification based on pore size was based on the adsorption characterisation of porous solids. It was proposed by International Union of Pure and Applied Chemistry (IUPAC) [*17*] as follows:

Micropores: width less than 2 nm;

Mesopores: width between 2 and 50 nm;

Macropores: width greater than 50 nm.

It has also been useful to classify micropores further into:

Ultra-microporosity: < 0.5 nm;

Super-microporosity: 1.0-2.0 nm

Micropores are considered to be about the size of adsorbate molecules in their cross section and accommodate one, two or perhaps three molecules. Mesopores are wider and are characterised by hysteresis loops during adsorption and desorption at high relative pressures of adsorption.

1.5 Adsorption of Gas on Carbon

1.5.1 Classification of Adsorption

Adsorption occurs when a solid is exposed to a gas or vapour. The concentration of gas/vapour at the surface of solid (*i.e.* within a distance of a molecule or atom) is greater than that in the gas/vapour phase. There are two types of adsorption:

physisorption and ***chemisorption***, according to the nature of the interaction between adsorbate and adsorbent. The physisorption process is very general and is comparable to condensation or liquification with adsorbate molecule attached to the surface by weak forces without being chemically changed (van der Waals, dispersion forces or London forces). Physisorption occurs more or less for all gases/vapours with all solid surfaces, increasing with increasing pressure and decreasing temperature. On the other hand, chemisorption involves the formation of chemical bonds with the adsorbate being chemically changed.

1.5.2 Classification of Adsorption Isotherms

In order to quantify the adsorption process, the extents of adsorption are related to the equilibrium partial pressure at constant temperature to derive the isotherms. The following information can be obtained by studying the adsorption isotherms:

- Estimates of surface area/ pore volumes;
- Estimates of pore size distribution;
- Assessment of the surface chemistry of the adsorbents;
- The fundamentals of adsorption process, *i.e.* the nature of the adsorbed phase;
- Assessment of the efficiency of industrial carbons employed in separation / purification techniques.

There are many adsorption isotherms in the literature of the subject, measured for wide range of adsorptives and on a variety of solids. Nevertheless, the majority of these isotherms which resulted from physical adsorption may conveniently be grouped into five classes: the five types I to V of the classification originally proposed by Brunauer, Deming, Deming and Teller (BDDT) [*18*]. This is sometimes referred to as

the Brunauer, Emmett and Teller (BET) [*19*], or simply the Brunauer [*20*] classification. The essential features of these types of isotherms obtained from adsorption experiments are shown in **Figure 2.0**.

Type IV and V isotherms possess a hysteresis loop, the lower branch of which represents measurements obtained by progressive addition of gas to the system, and the upper branch by progressive desorption. Hysteresis effects are liable to appear in isotherms of the other types as well. The stepped isotherm of Type VI, though rare, is of particular theoretical interest. In addition to the six classical types, there are borderline cases which are difficult to be assigned to one group rather than another. There are indeed a considerable number of isotherms which are difficult to fit into the classical classification.

Type I Isotherm

Type I isotherms are characterised by a plateau which may cut the $p/p^0 = 1$ axis sharply or show a tail as saturation pressure is approached. The incidence of hysteresis varies: many Type I isotherms usually have no hysteresis loops at all, while others display a definite loop. In the simplest case, adsorption in a microporous solid leads to Type I isotherms, where micropore filling occurs significantly at relatively low partial pressure < 0.1 p/p^0 with the adsorption process being essentially complete at ~0.5 p/p^0. The micropores in the solid are no more than a few molecular diameters in width. Therefore, the potential fields from neighbouring walls will overlap and the interaction energy of the solid with the gas molecule will be correspondingly enhanced resulting in increased adsorption. There is considerable evidence that the interaction may be strong enough to bring about complete filling of the pores at a quite low

relative pressure. Examples include the adsorption of nitrogen on microporous carbon at 77 K and adsorption of ammonia on charcoal at 273 K.

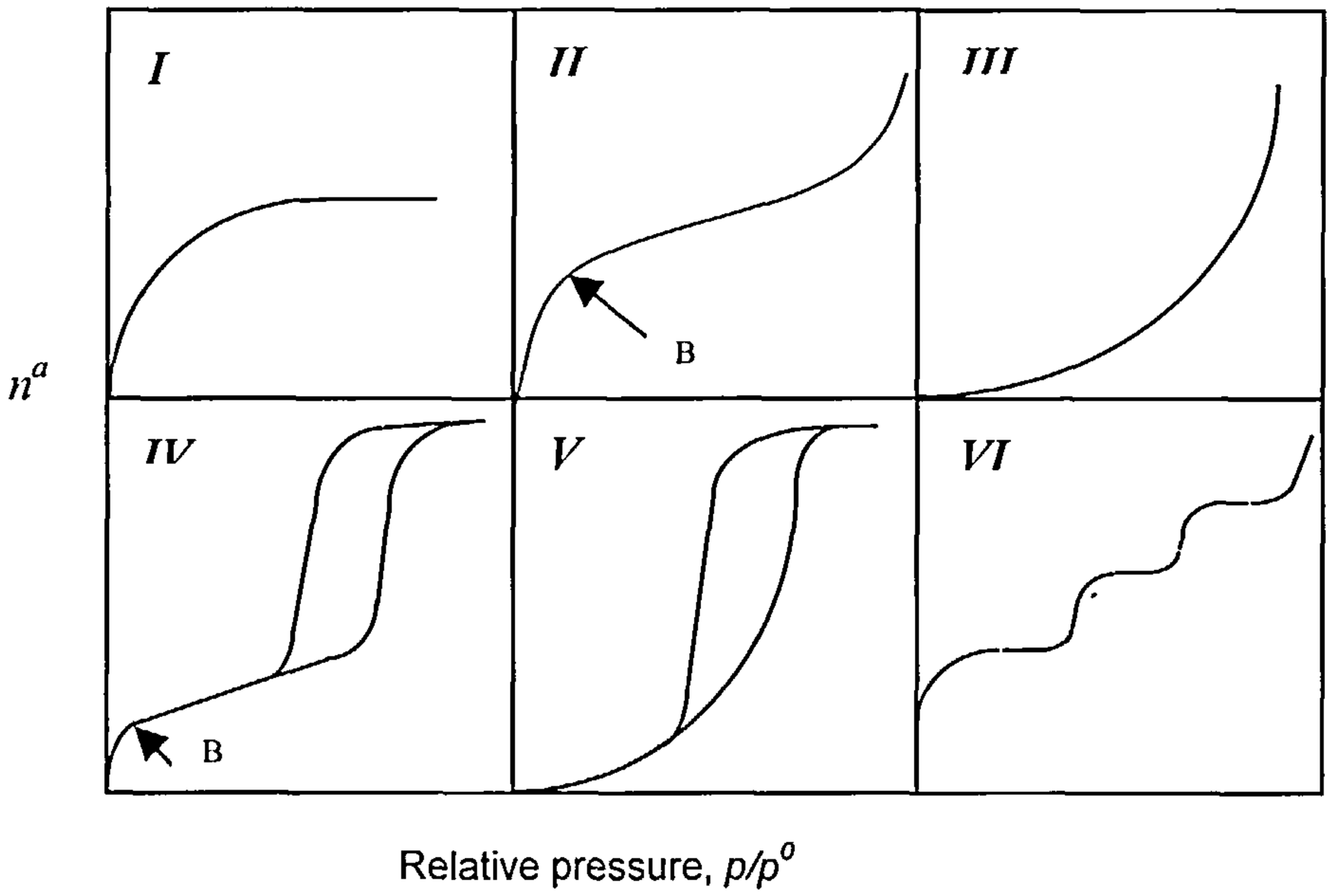

Figure 2.0 The five types of adsorption isotherms in the classification of BDDT [*17*], together with Type VI, the stepped isotherm [*21*].

Type II Isotherm

Type II adsorption isotherms describe unrestricted monolayer/multilayer adsorption on a solid material which is either non-porous or macroporous. The isotherm rises as monolayer coverage is established and continues to rise as multilayers are formed at higher p/p^0. Point 'B' represents the monolayer coverage. Type II isotherms can also be obtained from carbons with mixed micro- and mesoporosity.

Type III and Type V Isotherm

Both Type III and Type V isotherms are characterised by convex curvature towards the relative pressure axis. In Type III isotherms the convex persists throughout the isotherm, whereas in Type V isotherms there is a point of inflection at fairly high relative pressure (often ~0.5 or even higher) so that the isotherm reaches a plateau at high relative pressure. These two types of isotherm are characteristic of weak gas-solid interaction [*22*]. The Type III isotherms usually describe the adsorption of adsorptives on non-porous or macroporous solids whereas Type V isotherms describe the adsorption on mesoporous or microporous solids. The weak adsorbent-adsorbate forces will cause the uptake at low relative pressure to be small. Once the molecules are adsorbed, the adsorbate-adsorbate force will promote further adsorption. Thus the isotherms will become convex to the pressure axis. Type III and Type V isotherms may originate through the adsorption of either polar or non-polar molecules.

Type IV Isotherm

A characteristic feature of Type IV isotherms is that they possess a hysteresis loop which is associated with capillary condensation taking place in the mesopores and limiting uptake at high relative pressure. The amount adsorbed is always greater at any given relative pressure along the "desorption" branch than along the "adsorption branch on the hysteresis loop. Type IV isotherms are very common isotherms which have played an essential role in the development of adsorption theory and practice. Adsorption of N_2 at 77 K on mesoporous carbon usually gives Type IV isotherms and in this case BET model is applicable.

1.5.3 Mathematical Models

A number of mathematical models have been developed based on the interpretation of adsorption isotherms to describe the adsorption process. The first successful model describing adsorption process is Langmuir model, on which the Brunauer-Emmett-Teller (BET) model is based and the Dubinin-Radushkevich (D-R) model was developed for microporous materials.

Langmuir Model

Langmuir model [*23*] was derived based on the following three simplified assumptions:

1. The solid surface is composed of a two-dimensional array of energetically homogeneous sites.
2. Only a monolayer can occur and only one molecule can adsorb on a site.
3. The adsorption is localised and there are no adsorbate-adsorbate interaction.

Based on these assumptions Langmuir used a direct kinetic derivation to describe the adsorption in terms of an equation:

$$\frac{P}{V} = \frac{1}{V_m b} + \frac{P}{V_m} \qquad (1.1)$$

where P = pressure of gas;

V = equilibrium amount of gas adsorbed per unit mass of adsorbent at relative pressure p/p^0, ($mmolg^{-1}$);

V_m = amount of gas required for monolayer coverage of adsorbent ($mmolg^{-1}$);

b = adsorption coefficient, dependent on temperature but independent of surface coverage and describing in some way the energetics of the surface;

The plot of $\frac{P}{V}$ against P will yield a straight line with a slope of $\frac{1}{V_m}$. The specific surface area S can be calculated using the following equation:

$$S = V_m A_m L \qquad (1.2)$$

where S = specific surface area;

A_m = the average area occupied by a adsorbate molecule at monolayer coverage;

L = Avogadro's constant.

Langmuir model is useful to describe Type I adsorption isotherms. This model has limitations based on the original assumptions. It is certain that these assumptions are invalid for any carbon. However the equation is applicable to many isotherms and provide useful approximation values for adsorption parameters and the determination of surface area for Type I adsorption isotherms.

Brunauer Emmett Teller (BET) Theory

The Brunauer Emmett Teller (BET) equation [*24*] was devised to improve the Langmuir model to account for the multilayer adsorption of gases on a wide range of porous and non-porous solids. Type II adsorption isotherms describe unrestricted multilayer formation whereas Type IV adsorption isotherms describe restricted multilayer formation. In addition to the assumptions proposed by Langmuir, it also

assume that the energy of adsorption of the second and subsequent layers of molecules is equal to that of liquification and the total amount adsorbed is the amount on all layers. The BET equation is usually expressed in the linear form to describe unrestricted multilayer adsorption:

$$\frac{p}{n(p^0 - p)} = \frac{1}{n_m c} + \frac{(c-1)}{n_m c} \bullet \frac{p}{p^0} \qquad (1.3)$$

where p^0 = saturation vapour pressure;

n = the molar amount adsorbed at pressure p;

n_m = the molar amount of adsorbate required for complete monolayer coverage;

c = dimensionless constant which relates to adsorption energy and is expressed as:

$$c = e^{(q_1 - q_L)/RT} \qquad (1.4)$$

where q_1 = the heat of adsorption in the first layer;

q_L = the heat of adsorption in the second and subsequent layers (*i.e.* the heat of condensation);

$q_1 - q_L$ = net heat of adsorption.

The plot of $\frac{p}{n(p^0 - p)}$ against $\frac{p}{p^0}$ will yield a straight line with a slope of $\frac{c-1}{n_m c}$ and an intercept of $\frac{1}{n_m c}$. The values of c and n_m can be obtained thereafter.

The BET equation is probably the most widely used model for the interpretation of isotherms obtained from the adsorption of N_2 at 77 K and for the determination of surface area. The model has been subjected to a number of criticisms:

- Unsuitable for highly microporous carbons [*20*, *25*];
- Energetically homogeneous surface never exist [*26*];
- Adsorbate-adsorbate interactions are not taken into consideration[*27*,*28*];
- The enthalpy and entropy terms predicted by the model do not agree with those obtained experimentally [*16*,*27*,*29-31*], *i.e.* the value of c only provides a rough guide to the size of the heat of adsorption;
- Purely localised adsorption is unlikely to occur above 77 K [*28*,*32-35*].

Dubinin-Radushkevich (D-R) Model

Pierce *et al* [*36*] in 1949 and independently, Dubinin [*37*] postulated that in very fine pores the mechanism of adsorption is pore filling rather than surface coverage. Thus the plateau on Type I isotherm represents the filling up of the pores with adsorbate by a process similar to but not identical with capillary condensation, rather than a layer by layer building up of a film on the pore walls. Dubinin, in collaboration with Radushkevich [*38*] put forward an equation for the estimation of the micropore volume from low and medium pressure parts of the adsorption isotherm. Their treatment represented an adaptation of the earlier Polanyi theory of adsorption [*39*], an essential parameter of which is the quantity A defined by the expression:

$$A = RT\ln(\frac{p^{o}}{p}) \qquad (1.5)$$

Where A was originally termed by Polanyi the adsorption potential, but Dubinin preferred the designation differential molar work of adsorption. According to Dubinin' s idea, the process involved is volume filling of the micropores rather than layer-by-layer adsorption on the pore walls. Therefore the degree of filling of the micropores is defined by:

$$\theta = \frac{W}{W_0} \tag{1.6}$$

where W_0 is the total volume of the micropore system and W is the volume that has been filled at relative pressure $\frac{p}{p^0}$. On the assumption that the pore size distribution is Gaussian, Dubinin and Radushkevich arrived at the expression:

$$\theta = \exp\left[-k\left(\frac{A}{\beta}\right)^2\right] \tag{1.7}$$

where k is characteristic parameter related to pore size distribution. β is adsorbate affinity coefficient. By combining equations (1.5), (1.6) and (1.7), an expression can be obtained:

$$W = W_0 \exp\left[-k\left(\frac{RT}{\beta}\right)^2 \ln\left(\frac{p^0}{p}\right)^2\right] \tag{1.8}$$

or

$$\frac{W}{W^0} = \exp\left[-B\left(\frac{T}{\beta}\right)^2 \log^2\left(\frac{p^0}{p}\right)\right] \tag{1.9}$$

where $B = (2.303R)^2 k$ (2.0)

For plotting, equation (1.9) can be transformed into:

$$\log W = \log W^0 - D\log^2\left(\frac{p^0}{p}\right) \quad (2.1)$$

where $D = B\left(\frac{T}{\beta}\right)^2$ (2.2)

W is simply the amount adsorbed expressed as a liquid volume and is given by $W = \frac{n}{\rho^*}$, where ρ^* is the density of the adsorbate in micropores. At a temperature well below the critical point ρ^* may be taken as equal to the ordinary density ρ_L of the bulk liquid adsorbate.

According to equation (2.1), the D-R plot of *log W* against $\log^2\left(\frac{p^0}{p}\right)$ should be a straight line having an intercept equal to the total micropore volume W_0. For a substantial number of systems the D-R plot is indeed a good straight line. However, the D-R graph deviates from linearity in a number of ways. Sometimes the plot is convex to the $\log^2\left(\frac{p^0}{p}\right)$ axis and sometimes concave. In these cases, it is questionable to extrapolate from the low pressure, reasonably linear part of the isotherm.

Figure 2.1 shows the relationship between deviation from linearity in the shape D-R graph and the associated pore size distribution [*39-41*].

- Isotherm A indicates that the adsorption is a pore filling progresses from the smallest to largest micropores until all porosity is filled at $\log(p^0/p) = 0$, *i.e.* $p^0/p = 1$.

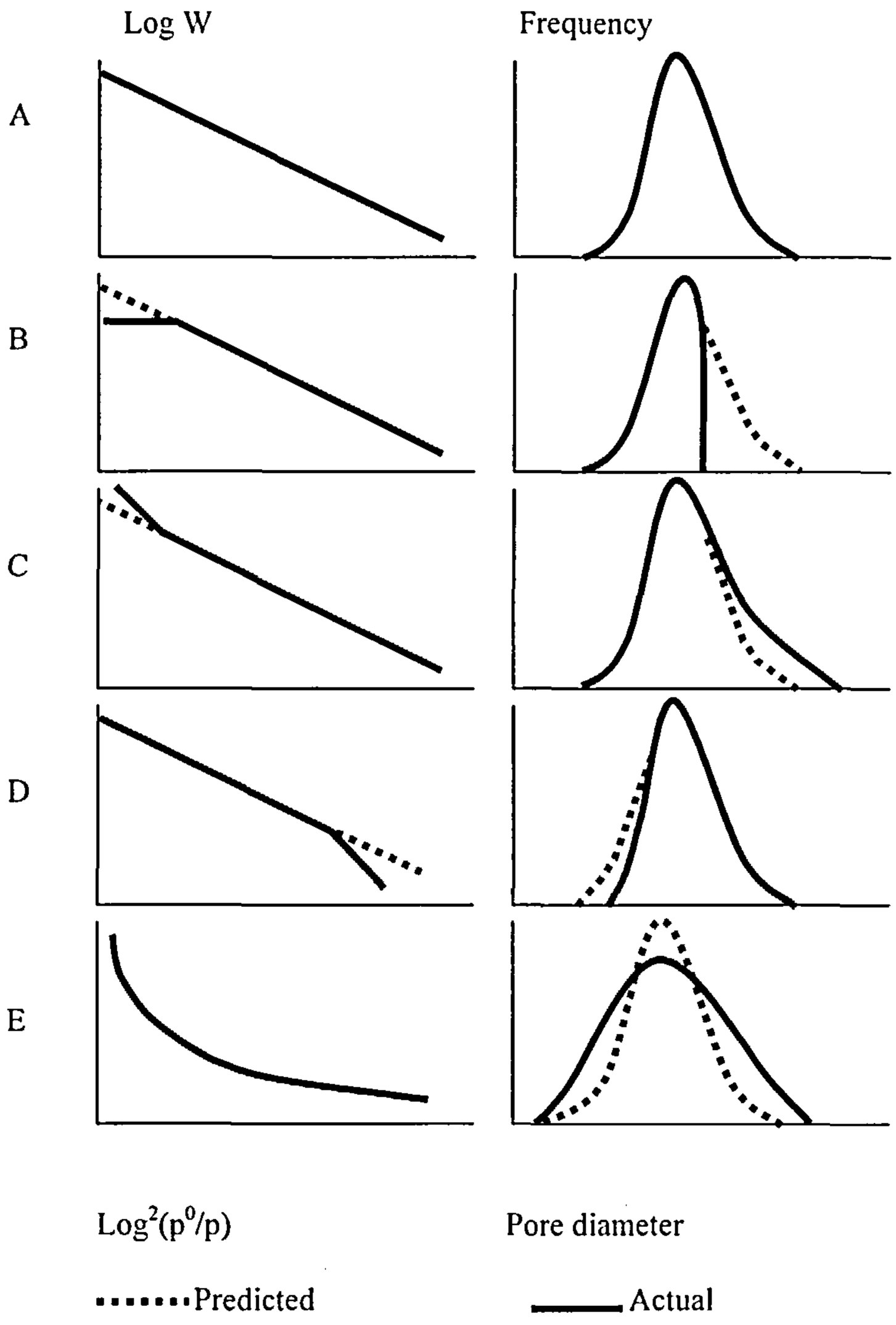

Figure 2.1 Schematic diagram of the deviation in D-R plots explained in terms of distributions of site energy (after Marsh [*40*])

- Isotherm B occurs with microporous carbons and indicates either that the larger size of porosity is absent or the entire distribution of microporosity is filled at a relative pressure of less than unity. The position of the cut-off on the x-axis indicates the width of the pore size distribution. The lower the relative pressure of the cut-off position, the narrower and smaller the pore size distribution.

- Isotherm C shows an upward deviation at high values of relative pressure, *i.e.* more uptake than predicted. This excess adsorption may be due to the filling of supermicropores or mesopores, or multilayer adsorption on non-porous surfaces. Extrapolation of the D-R line gives the micropore volume in this case.
- Isotherm D, which shows a negative deviation at low relative pressure, may be due to a activated diffusion and/or molecular sieve effects.
- Isotherm E may result from the carbon in which microporosity is either just developing or closing [*40*]. Here the micropore size is very narrow and the measured isotherm is not an equilibrium isotherm and therefore cannot legitimately be processed by D-R equation.

Freeman *et al* [*42*] discussed criticisms of the D-R equation and suggested that the D-R equation is correct if the distribution of adsorption energies within the micropores could be expressed mathematically, *i.e.* a Gaussian type distribution. Overall the surface area obtained on some adsorbents may vary accordingly depending on the adsorbate selected. Therefore it is not valid to quote absolute value of surface areas and micropore volumes, but rather to make comparison of the surface areas and micropore volumes for the same adsorbate used. Langmuir and BET methods are applied to the relative pressure in the range of 0.05-0.4 from the adsorption isotherm. D-R equation is applied to a much lower relative pressure region of < 0.03.

1.5.4 Determination of Surface Area from Gas Adsorption

Gas adsorption has been extensively employed for the investigation of the porous structures of carbon, including the determination of specific surface area and pore volume from the adsorption isotherms. The specific surface area of carbon is

most usually determined from gas adsorption by standard gravimetric or volumetric techniques using Brunauer-Emmett-Teller (BET) theory. Nitrogen at its boiling point (77 K) is the recommended adsorptive, although argon at 77 K is also used. For carbons and graphites with low surface area (less than 5 m^2g^{-1}), krypton at 77 K may be preferred as the adsorptive due to its low saturation vapour pressure and higher molecular weight.

It is unlikely that calculation of a true value of the true surface area can be obtained using the BET equation if the isotherm is of either Type I or Type III. BET method is suitable for both Type II and Type IV isotherm, provided that the value c is not too high and that the BET plot is linear for the region of the isotherm containing point B. If the value of c is found to be higher than normal for particular gas-solid system, it is possible that the adsorbent contains microporosity even if the isotherm is of Type II or Type IV. The BET surface area should be then checked by the α_s-method in order to ascertain how closely the shape of the isotherm conforms to that of the standard isotherm in monolayer range.

For Type I isotherm, if there is a nearly constant adsorption at high relative pressure, the micropore volume is given by the amount adsorbed in the plateau region (converted to liquid volume). If the Type I isotherm has a finite slope at high relative pressure, both the external area and the micropore volume can be evaluated by the α_s-method provided that a standard isotherm on a suitable non-porous solid is available.

For both the micropore volume and apparent surface area obtained on the carbons, there are different behaviour:

- $N_2 < CO_2$: carbonised materials, molecular sieve carbons and activated carbons with very low burn-off (<10 %). N_2 surface area is low due to activated diffusion effects.

- N_2 ~ CO_2 : activated carbon with low to medium burn-off and some molecular sieve carbons. The microporosity is relatively narrow and rather homogeneous;
- N_2 > CO_2: activated carbon with medium to high burn-off. The microporosity is wider and very heterogeneous. The difference between the two adsorbates increases with increasing burn-off. In this case the N_2 surface area may have contributions from pore filling.

References

1. Bernal, J.D. *Proc. R. Soc.* **A106**, 749 (1924)
2. Kasatochkin, V.I.; Sladkov, A.M.; Kudryavtsev, Yu.P.; Popov, N.M.; Korshak, V.V. *Dokl. Chem.* **177**, 1031 (1967)
3. Kroto, H.W.; Heath, J.R.; O'Brien, S.C.; Curl, R.F.; smalley, R.E. *Nature*, **318**, 162 (1985)
4. Krätschmer, W.; Lamb, L.D.; Fostiropoulos, K.; Huffman, D.R. *Nature*, **347**, 354 (1990)
5. Diederich, F.; Whetten, R.L. *Angew. Chem.* **103**, 695 (1991)
6. Diederich, F.; Whetten, R.L. *Angew. Chem. Int. Ed. Engl.* **30**, 678 (1991)
7. Curl, R.F.; Smalley, R.E. *Sci. Am.* **54**, (1991)
8. Kroto, H.W.; Allaf, A.W.; Balm, S.P. *Chem. Rev.* **91**, 1213 (1991)
9. Diederich, F.; Whetten, R.L. *Acc. Chem. Res.* **25**, 119 (1992)
10. Kochling, K.H.; McEnaney, B.; Rozploch, F.; Fitzer, E. *Carbon*, **20**, 445 (1982)
11. Kochling, K.H.; McEnaney, B.; Neumann, S.; Fitzer, E. *Carbon*, **21**, 517 (1983)
12. Kochling, K.H.; McEnaney, B.; Muller, S.; Fitzer, E. *Carbon*, **23**, 601 (1985)
13. Franklin, R.E. in *Proceedings of the Royal Society London, Ser.* **A209**, p196 (1951)
14. Marsh, H. *Carbon*, **29**, 703 (1991)
15. Marchand, A. In *Carbon and Coal Gasification*, Edited by Figueiredo, J.L. and Moulijin, A. Martinus Nijhoff Publisher, 1986, p93.
16. McEnaney, B and Mays, T. J. In *Introduction to Carbon Science*, edited by Marsh, H., Butterworths, p153 (1989).
17. Sing, K.S.W.; Everett, D.H.; Haul, R.A.W.; Moscou, L.; Pierotti, R.A.; Rouquerol, J. and Siemieniewska, T. *Pure Appl. Chem.* **57**, 603 (1985).
18. Brunauer, S.; Deming, L.S.; Deming, W.S. and Teller, E. *J. Amer. Chem. Soc.* **62**, 1723 (1940).
19. Brunauer, S.; Emmett, P.H and Teller, E. *J. Amer. Chem. Soc.* **60**, 309 (1938).
20. Brunauer, S. *The Adsorption of Gases and Vapours*, Oxford University Press (1945).

21. Gregg, S.J. and Sing, K.S.W. *Adsorption, Surface Area and Porosity*, Academic Press, London (1982).
22. Kiselev, A.V. *J. Colloid Interface Sci.* **28**, 430 (1968).
23. Langmuir, I. *J. Am. Chem. Soc.* **38**, 2221 (1916).
24. Brunauer, S.; Emmett, P.H. and Teller, E. *J. Am. Chem. Soc.* **60**, 309 (1938).
25. Dubinin, M.M. In *Progress in Surface and Membrane Science*, edited by Cadenhead, D.A. Danielle, J.F. and Rosenburg, M.D. Vol.9, pp1-70, Academic Press (1975).
26. Dubinin, M.M. In *Chemistry and Physics of Carbon*, edited by Walker (Jr), P.L. Vol. 2, pp.51-120 (1996).
27. Gregg, S.J. *Colloids and Surfaces*, **21**, 109 (1986).
28. McClellan, A.J. and Harnsberger, H.F. *J. Colloid Interface Sci.*, **23**, 577 (1967).
29. Davis, R.T. and Dewitt, T.W. *J. Am. Chem. Soc.* **70**, 1135 (1948).
30. Kingston, G.L.; Beebe, R.A; Polley, M.H. and Smith, W.R. *J. Am. Chem. Soc.* **72**, 1775 (1950).
31. Kingston, G.L. and Aston, J.G. *J. Am. Chem. Soc.* **73**, 1929 (1951).
32. Hill, T.L. *J. Chem. Phys.* **14**, 263 (1946).
33. Pierce, C. and Ewing, B. *J. Phys. Chem.* **68**, 2562 (1964).
34. Zettlemoyer, A.C. *J. Colloid Interface Sci.* **28**, 343 (1968).
35. Carruthers, J.D.; Payne, D.A.; Sing, K.S.W. and Stryker, K.J. *Colloid Interface Sci.* **36**, 205 (1971).
36. Pierce, C.; Wiley, J.W. and Smith, R.N. *J. Phys. Chem.* **53**, 669 (1949).
37. Dubinin, M.M. and Zaverina, E.D. *Zhur. Fiz. Khim.* **23**, 1129 (1949).
38. Dubinin, M.M. and Radushkevich, L.V. *Proc. Acad. Sci. USSR.* **55**, 331 (1947).
39. Marsh, H. and Byme, J.F. *Porosity in carbons: Characterisational Applications,* Edited by Patrick, J.W., Edward Arnold, London, pp1-48 (1995).
40. Marsh, H. *Carbon*, **25**, 49 (1987).
41. Marsh, H. and Rand, B. *J. Colloid Interface Sci.* **33**, 101 (1970).
42. Freeman, E.M.; Siemieniewska, T.; Marsh, H. and Rand, B. *Carbon*, **8**, 7 (1970).

Chapter 2

ACTIVATED CARBON

2.1 Introduction

Activated carbon is a processed carbon material with a highly developed porous structure and a large internal specific surface area. It consists principally of carbon (generally 87 - 97 %) but also contains such elements as hydrogen, oxygen, sulphur and nitrogen, as well as various inorganic compounds either originating from raw materials used in its production or generated during its manufacture. The compounds mainly originate from mineral substances in coal or bio-inorganic compounds in biomass materials. These substances may be removed by acid washing.

Activated carbon has the ability to adsorb various substances both from gas and liquid phases. Their application in water purification can be dated back to 2000 BC when the ancient Egyptians used charcoal to purify water for medical purposes [*1*]. However, the rational use of activated carbon for industrial purposes was started at the end of 18^{th} century. The Swedish chemist Karl Wilhelm Scheele was the first to discover (1773) the phenomenon of adsorption of gases on charcoal. A dozen years later (1785) the Russian academician Lovits found that charcoal, when immersed in tartaric acid solution, decolourised it by adsorbing the organic contaminants present. This discovery led to the first industrial application of charcoal in the sugar industry in England in 1794, where it was used as a decolourising agent for sugar syrup. This event initiated research on adsorption from the liquid phase. The major development of activated carbon began during the First World War, when hard granular activated

carbon (GAC) was manufactured for use in gas masks. In the last 50 years, the technology involved in active carbon manufacture has advanced. Powdered active carbon (PAC) is extensively used in water purification processes together with granular activated carbon. PAC is associated with larger pore diameter than GAC. Activated carbon are used for gas and liquid phase adsorption processes. Approximately 80 % of about 300,000tons per year is used for liquid phase applications whereas 60,000 tons per year for gas phase application [*2*]. Granulated active carbons are mainly employed for gas adsorption and separation.

2.2 Manufacture of Activated Carbons

The manufacture of activated carbons involves two main steps: the carbonisation of carbonaceous raw materials at temperatures below 800 °C in the absence of oxygen which is followed by the activation of the carbonised products. Thus carbonaceous materials can be converted into activated carbon, although the properties of the final products will be different, depending on the nature of the starting materials used, the nature of the activating agent and the conditions of the activation process. The large internal surface areas of the activated carbons results from the porous structure developed in the carbonisation process and the activation process. The activation methods used to increase porosity generally are chemical and physical activation. Chemical activation involves the addition of chemical agents such as $ZnCl_2$ and H_3PO_4 to the parent feedstock prior to carbonisation. Due to the environmental concern, chemical activation process is not now favoured by industry. Physical activation refers to the char gasification process using gas mixtures such as carbon

dioxide and steam at 700-1000 °C, which are commonly used in the production of activated carbon.

2.2.1 Raw Materials

Activated carbons can be manufactured from a wide variety of materials. Cheap materials with a high carbon content and low inorganic content are normally used as raw materials for the production of activated carbon. Those most frequently used on a commercial scale are peat, coal, lignite, wood and coconut shell [*2*]. The principal properties of manufactured activated carbons especially the structure of pores and pore size distribution depend mainly on the type and properties of the raw materials used and the activation procedure. Active carbons produced from coconut shell usually exhibit high adsorption capacity and a large volume of micropores. However, one of the problems of using agricultural by-products to produce active carbon is the variability in feed stock resulting in limited control over extent and size distribution of resultant porosity. Therefore, in addition to the raw materials from natural products, other precursors are required from which to produce carbons with reproducible pore size distribution to meet specifications. Such precursors are the synthetic resins and other polymeric materials such as polyvinylidene chloride.

The basic requirements of a raw material are:

1. High carbon and low inorganic contents.
2. High density and low volatile content.
3. Ability to develop a porous structure.
4. Ability to be regenerated and a long storage life.
5. Low cost and volume

Low inorganic substance content are essential in order to keep the ash content low in the final product because the ash does not contribute greatly to the adsorption capacity. Due to catalytic gasification effects, mineral matter is responsible for preferential gasification during the activation process resulting in meso- and macropore channelling and pitting, and not the preferred microporosity. High density contributes to enhanced bulk strength and resistance to abrasion thereby reducing losses during use and increase the life span of the activated carbons.

Practically five different types of carbonaceous materials are being used for industrial scale production of activated carbon. These raw materials in the order of their importance and in terms of activated carbon production capacity are the following [*2*]:

Raw material	Capacity (tons / year)
Wood	130,000
Coal	100,000
Lignite	50,000
Peat	35,000
Coconut shell	35,000
Others	10,000

The porous structure and chemical properties and the applications of the activated carbons are predominantly determined by the raw materials. The properties of some of the raw materials and the most general uses of the activated carbons obtained from them are show in **Table 2.1** [*2*]

Table 2.1 Properties of some raw materials used in the manufacture of activated carbon

Raw materials	Carbon (wt% a.r.)	Volatile (wt% a.r)	Density (kg dm^{-1})	Ash (wt% a.r.)	Texture of Activated carbon	Application of Activated carbon
Soft wood	40 - 45	55 - 60	0.4 - 0.5	0.3 - 1.1	Soft, large pore volume	Aqueous phase adsorption
Hard wood	40 - 42	55 - 60	0.55 - 0.80	0.3 - 1.1	Soft, large pore volume	Aqueous phase adsorption
Lignin	35 - 40	58 - 60	0.3 - 0.4	-	Soft, large pore volume	Aqueous phase adsorption
Nutshells	40 - 45	55 - 60	1.4	0.5 - 0.6	Hard, large micropore volume	Vapour phase adsorption
Lignite	55 - 70	25 - 40	1.0 - 1.35	5 - 6	Hard, small pore volume	Wastewater treatment
Soft coal	65 - 80	20 - 30	1.25 - 1.50	2 - 12	Medium hard, medium micropore volume	Liquid and vapour phase adsorption
Petroleum coke	70 - 85	15 - 20	1.35	0.5 - 0.7	Medium hard, medium pore volume	Wastewater treatment
Semihard coal	70 - 75	10 - 15	1.45	5 - 15	Hard, large pore volume	Gas vapour adsorption
Hard coal	85 - 95	5 - 10	1.5 - 1.8	2 - 15	Hard, large pore volume	Gas vapour adsorption

2.2.2 Carbonisation

Carbonisation is the first step of manufacturing activated carbons, which involves thermal decomposition of carbonaceous materials, eliminating heteroatomic species and producing a carbon mass with a rudimentary pore structure. This process is generally conducted in a rotary kiln or multiple hearth furnace at a temperature below 800 °C with the protection of flowing inert gas. The heating rate, maximum

temperature and the soaking time at the final temperature are the most important factors in controlling the quality and the yield of char. Pyrolysis with lower heating rate results in lower volatilisation and higher char yield [*4*]. These factors also have a marked influence on activation and the quality of the final product [*5*].

2.2.3 Activation

The char obtained after removal of the volatile compounds of a carbonaceous precursor by heat treatment in an inert atmosphere and without addition of chemical agents is only slightly porous. A suitable activation process has to be applied to the char to produce active carbon due to its low adsorption capacity. The objective of the activation process is to develop porosity in the carbon including enhancement of the volume of the pores created during pyrolysis, creation of new porosity and the opening of closed porosity. However, the porous structure and pore size distribution are largely predetermined by the nature of the raw materials and the carbonisation process. Some activated carbons are manufactured by chemical activation which involves the carbonisation of process of a mixture of raw materials with a activating agent such as phosphoric acid, zinc chloride or potassium hydroxide. However, most commercial activated carbons are produced by a process termed "physical activation", in which the char obtained from carbonisation is activated by partial gasification using gaseous activating agents such as carbon dioxide, air, steam or a combination of these agents.

Chemical Activation

Chemical activation is carried out at temperature lower than that in physical activation process, usually between 400 and 800 °C. In this process, the starting

material is impregnated with concentrated solution of the activating agent usually by mixing and kneading. The mixture is extruded and carbonised in a rotary kiln to give a product which is then washed to remove the activating agent which is recycled. During the carbonisation, the activating agent dehydrates the starting material to result in charring and aromatisation of the carbon skeleton and the creation of the porous structure. Although a number of activating agents were suggested [*6*] for chemical activation such as alkali metal carbonates, potassium thiocyanate, potassium hydroxides, potassium sulphide and calcium, magnesium and iron chlorides, only phosphoric acid, zinc chloride and sulphuric acid are widely and frequently used in industries. The common feature of these chemicals is their ability to act as a dehydrating agent which influences the pyrolytic decomposition and inhibits the formation of tar. They also lower the formation of acetic acid, methanol and other by-products in order to enhance the yield of carbon.

Chemical activation is usually carried out when the starting materials are of wood origin. For example, sawdust is usually activated using phosphoric acid at 350 - 500 °C. The characteristics of the product are mainly determined by the following factors:

1. Degree of impregnation, *i.e.* the ratio of P_2O_5 to wood.
2. Heating rate.
3. Maximum temperature at which the wood-acid mixture is kept in oven.
4. Composition of the combustion gas used for heating.

The pore size distribution of the activated carbon is largely determined by the degree of impregnation with the larger degree of impregnation producing larger pore diameter in the carbon. The shapes of the pores in activated carbon are different for chemical activation compared with the physical activation process. When the carbon

is produced by chemical activation, the pores are usually bottle shaped whereas cone shaped in physical activation [*7*].

Although chemical activation is usually limited to wood precursors in industry, there were some reports on the production of chemical activated carbons from other types of raw materials. Wennerberg *et al* [*8*] prepared active carbons of high surface area from coal, coke, petroleum coke and their mixtures by chemical activation using hydrated potassium hydroxide. The carbons obtained by this method were highly microporous and had cagelike with bottle shaped pores structures. Microporous carbons were also prepared by Donnet *et al* [*9*] who carried out the pyrolysis of coals in the presence of potassium hydroxide and sodium hydroxide. Kwok *et al* [*10*] suggested a method for preparing chemically activated carbon from petroleum coke by treating it with polyphosphoric acid of > 74 % wt P_2O_5, which was followed by a steam activation process at 700 - 900 °C.

Physical Activation

Physical activation is the process to develop the porosity in carbonised product by gasification with an oxidising gas at a temperature of 800 - 1100 °C. The oxidising gases commonly used in physical activation are steam, carbon dioxide, air or any mixture of these gases. Several types of oven can be used in the manufacture of activated carbons, *i.e.* rotary kilns, multiple hearth furnaces and fluidised beds. The properties of activated carbon produced are partially determined by the type of oven used. A decreasing mesoporosity is obtained in the following order: fluidised bed > multiple hearth furnace > rotary kiln [*11*]. The heat for the activation process is provided by the combustion of coke oven gas or natural gas economically. Both the

required heat and the activating agent are supplied simultaneously. Extra steam is usually added in directly fired activators to moderate the temperature.

The activation with steam involves a complex set of chemical reactions, but it is generally assumed that during the activation process the most important gasification reactions of the carbon are as following reactions:

$$C + H_2O \rightleftharpoons CO + H_2 \qquad \Delta H = +1185 \text{ kJ mol}^{-1} \qquad (2.1)$$

$$CO + H_2O \rightleftharpoons CO_2 + H_2 \qquad \Delta H = -42.3 \text{ kJ mol}^{-1} \qquad (2.2)$$

$$C + CO_2 \rightleftharpoons 2CO \qquad \Delta H = +159 \text{ kJ mol}^{-1} \qquad (2.3)$$

The chemical reaction rate (r) of the reaction can be expressed by a Langmuir-Hinshelwood type rate expression [*12*]

$$r = \frac{kP_{H_2O}}{1 + K_1 P_{H_2O} + K_2 P_2} \qquad (2.4)$$

Where P_{H_2O} and P_{H_2} are the partial pressures of H_2O and H_2 respectively, k is a rate constant, K_1 and K_2 are adsorption constants.

Steam is the preferred activating gas because the water molecule has smaller dimensions than the carbon dioxide molecule. The use of steam in an activation process has the following positive effects:

1. faster diffusion into the porous network;
2. easier access into the micropores; and
3. a faster reaction rate (about three times faster than carbon dioxide).

However, the steam reaction is product-inhibited due to the strong adsorption of hydrogen on the active centre of the carbon surface which reduces the reaction rate.

Gasification of the carbonised materials with carbon dioxide occurs by the following endothermic reaction:

$$C + CO_2 \rightleftharpoons 2\,CO \qquad \Delta H = +159\ kJ\ mol^{-1} \qquad (2.3)$$

For the reaction of carbon with carbon dioxide, the rate expression is:

$$r = \frac{KP_{CO_2}}{1 + K_1 P_{CO} + K_2 P_{CO_2}} \qquad (2.5)$$

where P_{CO} and P_{CO_2} are the partial pressures of CO and CO_2 respectively.

Activation with carbon dioxide is inhibited by carbon monoxide with the back reaction. The addition of carbon monoxide to the reacting gas resulted in the development of a better microporous structure in addition to decreasing the rate of gasification [*13*].

Gasification of the carbonised carbon with air or oxygen is based on the following reactions:

$$C + O_2 \rightleftharpoons CO_2 \qquad \Delta H = -406.0\ kJ\ mol^{-1} \qquad (2.6)$$

$$C + O_2 \rightleftharpoons 2CO \qquad \Delta H = -123.0\ kJ\ mol^{-1} \qquad (2.7)$$

The above equations are simplified expression of the reaction of carbon with oxygen. The mechanism is not yet fully understood, although it is assumed that both CO and CO_2 are primary products [*12*].

When gasifying conditions are optimised in terms of oxidising gas, temperature, flow rate and pressure, an acceptable compromise exists between selective burn-off of

carbon atoms and external burn-off which is simply removal of carbon atoms without development of porosity. This generally happens with fast burn-offs, *e.g.* as with oxygen. Therefore the extent of development of porosity and the characteristics of the porosity are determined by:

- the structure of char
- the inorganic impurities in the char
- the oxidising gas
- temperature of gasification
- pressure of gas
- duration of gasification
- particle size of carbon

The slower gasification rate usually generates extensive development of porosity within the carbon particle. The use of different activating gases generally produces a different distribution of porosity. During the study of the activation of the two brown coals carbonised at 900 °C with steam, carbon dioxide, Tourkow *et al* [*14*] observed that steam resulted in the development of mesoporosity to a large extent than carbon dioxide. The difference in porosity created by different activating gases is significant at higher burn-offs. Activation with steam resulted in a progressive development and widening of all sized pores. The activated carbon obtained at burn-off of 70 % contained a well developed porous system with a wide pore size distribution. The activation between 50 - 70 % burn-off appreciably increased total pore volume but slightly affected surface area.

Activation with carbon dioxide developed mainly microporosity over the entire range of burn-offs. About 73 % total adsorption pore volume and 90 % of total surface

area are contributed by micropores for carbon dioxide activation, whereas only 33 % and 63 % of the total pore volume and total surface area respectively for steam activated carbons.

Activation with oxygen showed different effects on porosity compared with steam and carbon dioxide. Microporosity was produced at very low burn-off, which changed very little with further burn-off. The micropore volume increase from 0.002 cm^3 g^{-1} for the non-activated carbon to 0.2 cm^3 g^{-1} for the carbon with burn-off of 1 %. However the micropore volume increased very slightly to 0.23 and 0.27 cm^3 g^{-1} for the burn-offs of 8 and 25 % respectively. Higher burn-off caused decrease of micropore volume.

2.2.4 Classification of Activated Carbons

Activated carbons are classified on the basis of particle size and particle shape into powdered, granulated, spherical or pelleted activated carbons.

Powdered Activated Carbons

Powdered activated carbons are generally produced from sawdust by chemical activation. They have a fine granulometry less than 0.1 mm with average diameter between 0.015 and 0.025 mm. Therefore they have a large external surface and a small diffusion distance. The adsorption rate is very high and the problems related to mass transfer are negligible. The powdered activated carbons are preferably used for the adsorption from solution due to low diffusion rate in the liquid phase. The application of powdered activated carbon includes decolourisation and medicinal carbons.

Granulated Activated Carbons

Granulated activated carbons can be prepared by physical activation from various raw materials such as bituminous, sub-bituminous and lignite coals, petroleum or tar residues, synthetic and natural rubbers. Granulated activated carbons have a relatively larger size of carbon particles compared with powdered activated carbons. Therefore diffusion of the adsorbate in carbons is an important factor. They are usually used for the adsorption of gases and vapours. The granule size is an important factor because the gases or vapours pass through a bed of activated carbon. The small particle size causes a large pressure drop along the bed whereas greater size of a granular carbon bed lowers the rate of adsorption. Granulated activated carbons are also used for the adsorption from solution, *e.g.* for decolourisation and recovery of precious metals.

Spherical Activated Carbons

Spherical activated carbons were prepared from pitch [*15*] with the addition of naphthalene or tetralin by ammonia treatment and physical activation using steam or carbon dioxide. The activated carbon spheres obtained have a high mechanical strength and excellent SO_2 and NO_2 adsorption capacity. Spherical activated carbon in the form of bellow spheres [*16*] and in the form of granulated spherical pellets [*17*] have also been obtained.

2.3 Structure of Activated Carbon

Both the porous structure and the chemical nature of the surface of activated carbon are significantly related to its crystalline constitution. The graphite-like micro-

crystalline structure is the basic structural unit of activated carbon. The formation of the crystalline structure of activated carbon begins early in the carbonisation process. Thus sets of condensed aromatic rings of various numbers which are the nascent centres of graphite-like microcrystallites, are formed. Although their structure resembles that of a crystal of graphite, there exist deviations from that structure. It is composed of stacks of graphene layers cross-linked in a random manner. Most of the sheets are wrinkled which helps to create porosity. The wrinkles are possibly due to the presence of five and seven membered rings. The deviations from the ordering characteristics of graphite which can be described by the term 'turbostratic structure' [*18*]. The disordering of the crystal lattice may be caused by its defects (*e.g.* vacant lattice sites) and the presence of built-in heteroatoms. This results from the nature of the starting material and the method and conditions used to produce the activated carbon. In addition to disordering within the internal structure of the crystallites, the second significant difference between the structure of graphite and that of active carbon lies in the quantity of and mutual orientation of the crystallites. The range of order of the crystal structure which is very high in the case of graphite, is very limited for active carbons. Carbons featuring a chaotic mutual arrangement of micro crystallites with strong cross-linking between them are characterised by a well developed porous structure, considerable hardness and a small degree of graphitisation.

The pore size distribution of an activated carbon depends upon the nature of the precursors as well as the carbonisation and activation processes. For instance, the intrinsic pore structure of coal based and coconut shell based materials (both are used as raw materials in industrial production of activated carbon) are inherently different

in pore shape and pore size distributions with coconut shell derived carbon having higher micropore volume.

2.4 Chemical Nature of the Surface of Activated Carbon

The chemical nature of the surface of activated carbon significantly influences its adsorption, electrochemical, catalytic, acid-base, redox, hydrophilic-hydrophobic and other properties. In graphite, which has a highly ordered crystalline structure, the adsorption capacity is determined mainly by the dispersion component due to London forces. The random ordering of the aromatic sheets in active carbons causes a variation in the arrangement of electron clouds in the carbon skeleton and results in the creation of unpaired electrons and incompletely saturated valences, which would undoubtedly influence the adsorption behaviour. In addition, activated carbons are also invariably associated with appreciable amounts of heteroatoms such as oxygen, hydrogen, nitrogen, chlorine and sulphur. These heteroatoms are inherited from the starting materials and become a part of the carbon as a result of carbonisation. They are also incorporated into carbon during activation or during subsequent treatments. The heteroatoms are usually bonded at the edges of the aromatic sheets and form surface compounds, *i.e.* surface complexes and surface groups. They can also be incorporated within the carbon layers forming heterocyclic ring systems.

All carbons can chemisorb oxygen on exposure to air or oxygen, which can only be desorbed as an oxide of carbon on high temperature evacuations. It is also well known that all active carbons contain chemically bonded hydrogen which can not be eliminated completely even on outgassing at 1000 °C. Activated carbons can also possess nitrogen functionality on treatment with ammonia or using nitrogen rich

organic compounds or polymers as precursors. Sulphur can be incorporated into activated carbon by the treatment with hydrogen sulphide, carbon disulphide or sulphur while halogens are introduced by treatment with halogen in gaseous or liquid phase.

2.4.1 Oxygen Functional Groups on Carbon Surface

A. Acidic and Basic Carbons

Surface oxygen functional groups in activated influence the surface characteristics and surface behaviour of carbons. The carbon surface is very complex and difficult to reproduce. Therefore, the surface oxygen functional groups can never be simply treated as ordinary organic compounds. The surface functional groups interact differently in different environments. They behave as combined structures presenting numerous mesomeric forms depending on their location on the same polyaromatic frame. Activated carbons usually have acid-base character. Thus active carbon can be classified into acidic carbon and basic carbon. ***Acidic carbons*** are defined as those carbons that show acidic behaviour and react with appreciable amounts of bases but very little acids. The acidic carbons are generally obtained when carbons outgassed at high temperatures under vacuum or inert gases are exposed to oxygen between 200 - 700 °C. They can also be prepared by oxidising carbons with oxidants in gaseous or liquid phase. The optimum temperature for the development of acidic functional groups with maximum capacity to adsorb bases by air oxidation is around 400 °C. The ***basic carbons*** are those which show basic characters and adsorb acids and little alkali. The basic carbons are prepared by outgassing carbons in the

absence of oxidising agents or treating carbons with hydrogen. Several theories were proposed to explain the basic properties of carbons. Such as the electrochemical theory by Burstein and Frumkin [*19*, *20*], the oxide theory by Shilov *et al* [*21*, *22*], the chromene theory by Garten and Weiss [*23*] and the pyrone theory by Boehm and Voll [*24*].

Steenberg [*25*] used the uptake of inorganic acid and base as a method of characterising the carbons activated and oxidised at different temperatures: classifying those low-temperature oxidised carbons which adsorb primarily hydroxide as ***L carbons***. Those which were activated at high temperatures and thus adsorb acids were classified as ***H carbons***.

B. Types of Oxygen Functional Groups on Carbon Surface

Oxygen surface compounds are usually divided into two main types: functional groups of acidic nature (undergoing neutralisation by bases) and basic groups which may be neutralised by acids.

Nearly every type of oxygen functional groups known in organic chemistry has been suggested as being present on the surface of activated carbon [*26-38*]. The most often suggested acidic groups are illustrated in **Figure 2.1**, *i.e.* (1) carboxyl groups (2) phenolic hydroxyl groups (3) quinone-type carbonyl groups (4) ether, peroxide and ester groups in the forms of lactone and (5) fluorescein-like lactones (cyclic esters) (6)carboxylic acid anhydrides (7) cyclic peroxide.

Basic groups are much less well-characterised compared with acidic oxygen functional groups because of the experimental difficulties. The structures corresponding to chromene [*23*, *38*] or pyrone-like [*39*, *40*] structures were usually

suggested to attribute to them. However, it should be noted that the basic properties of particular sites on the active carbon surface are not necessarily associated with the presence of oxygen. It is proposed that basal planes show basic properties [*41*] as well as some nitrogen functional groups on carbon surface.

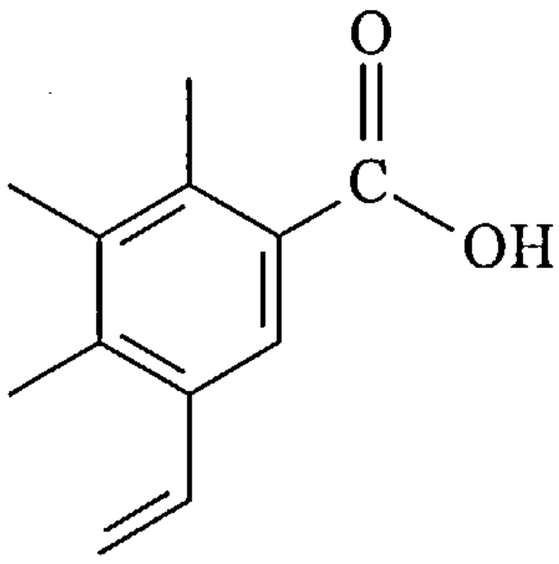

(1)

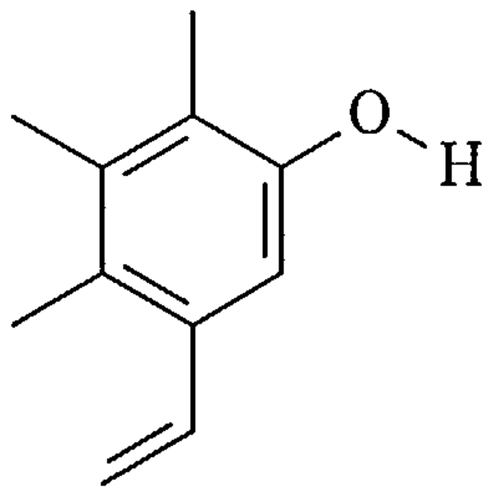

(2)

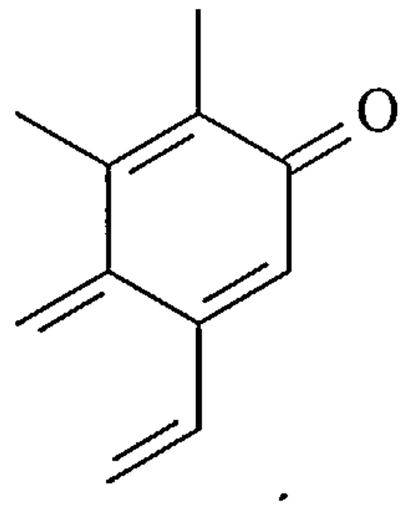

(3)

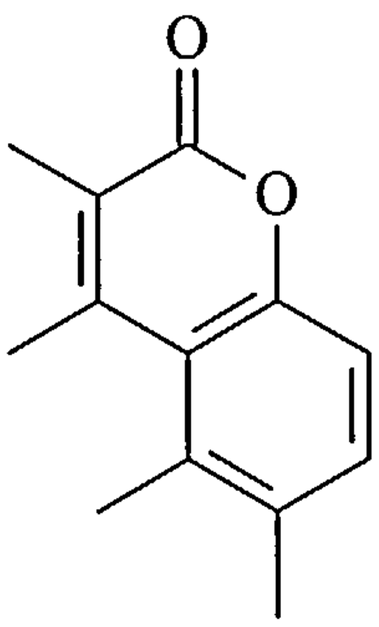

(4)

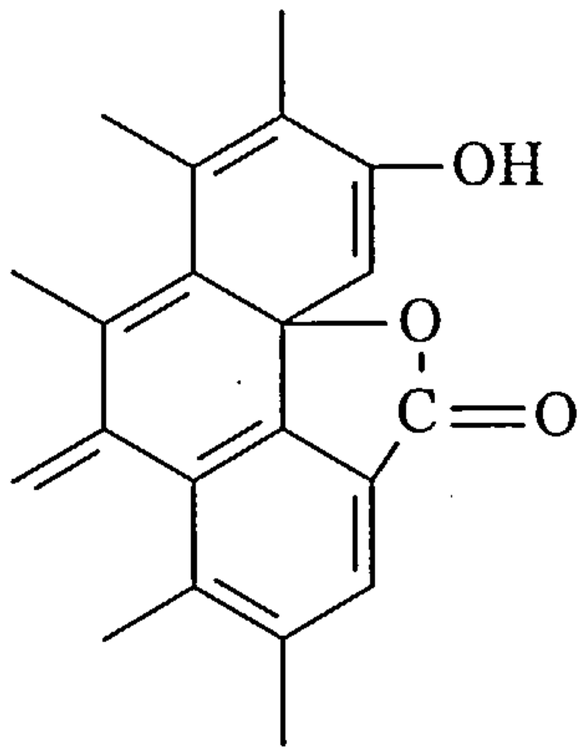

(5)

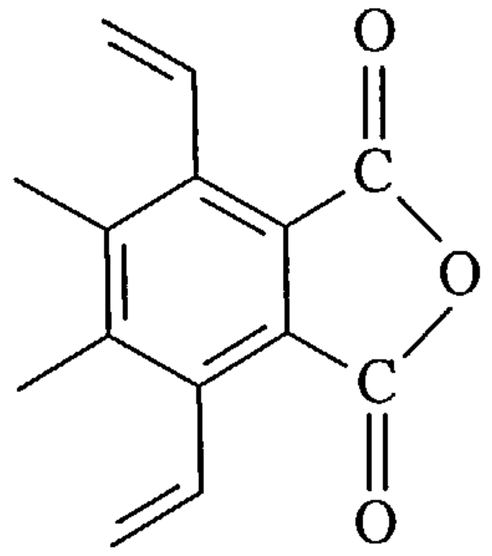

(6)

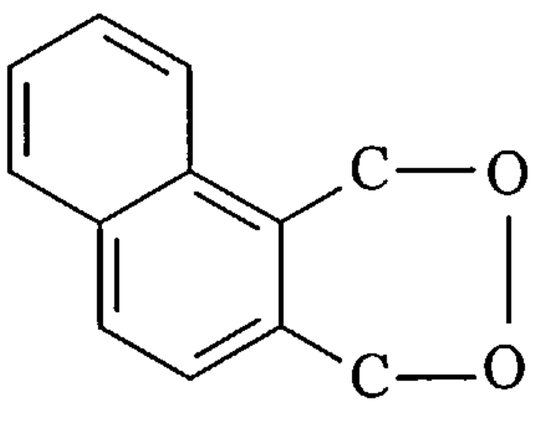

(7)

Figure 2.1 The most often suggested acidic oxygen functional groups on carbon surface

A model of a fragment of oxidised active carbon surface was proposed by Tarkovaskya *at al* [*42*] to illustrate the general chemical character of the active carbon surface, which is shown in **Figure 2.2**.

The oxygen containing functional groups, even of given type, can display different reactivity owing to direct interaction with adjacent groups of the same or other type and to electronic interactions with more distant groups via surface carbon crystallites. The amounts of oxygen functional groups on carbon surface are increased by oxidation, and decreased as a result of outgassing at high temperature exceeding 1000 °C in inert atmosphere or under vacuum. The oxygen functional groups on carbon surface thermally decompose to produce CO_2, CO, H_2O and H_2 when the carbon undergo outgassing heat treatment in an inert atmosphere.

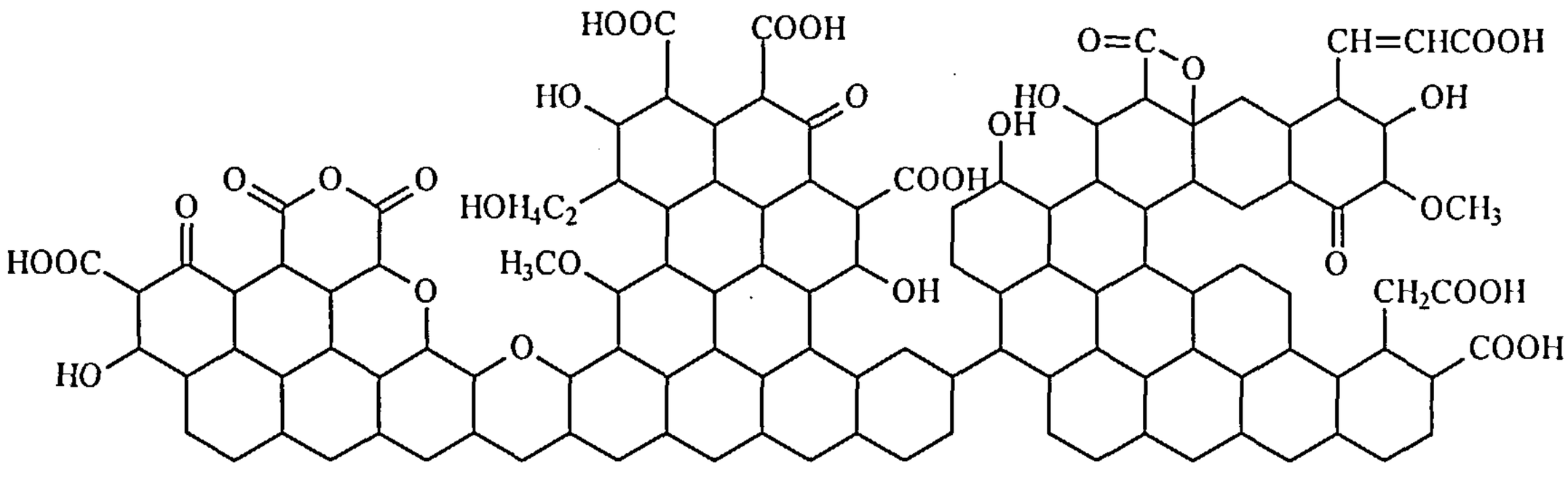

Figure 2.2 Model of a fragment of an oxidised active carbon surface

C. Characterisation of Surface Functional Groups

Attempts have been made to identify the surface oxygen functional groups using physical, chemical and physicochemical methods which include selective neutralisation, temperature programmed desorption (TPD), Fourier transform infrared spectroscopy (FTIR), specific chemical reaction, potentiometric, polarography and X-ray photoelectron spectroscopy and XANES. The functional groups proposed as a result of these investigation are carboxyls, lactones, phenols, anhydrides, ketones, quinones, hydroquinones, aldehydes and ethereal structures.

Neutralisation of Bases

Titration with alkalis can be employed to determine the nature and amounts of the acidic surface groups on carbon and graphite. The alkali solution used should be sufficiently strong (0.1-0.2 N) and the contact time should be long enough (24-72 hr) to obtain reproducible neutralisation results. Boehm [*26*] proposed a method to differentiate the acidic groups present on oxidised charcoals and carbon blacks by selective neutralisation techniques using bases of different strengths. This method was based on the assumption that the following groups become neutralised as follows. The strongly acidic functional groups neutralised by $NaHCO_3$ were postulated as COOH groups, where those neutralised by $NaCO_3$ but not by $NaHCO_3$ were believed to be lactone groups. The weakly acidic groups neutralised by NaOH but not by $NaCO_3$ were postulated as phenolic groups. The reaction with C_2H_5ONa was not considered as true neutralisation reaction since it did not involve exchange of H^+ by Na^+ ions. The groups reacting with C_2H_5ONa but not with NaOH were suggested to be carbonyls which were created by the oxidation of disorganised aliphatic carbon. Boehm [*26*] observed that the neutralisation capacity of the four bases for most of the carbons was

in the simple ratio 1:2:3:4, which according to Boehm, is not by chance but implies that four different groups occurred side by side on the carbon surface in equivalent amounts. This stoichiometry ratio was observed only when the carbons were completely oxidised.

This approach is to some extent simplified since it does not take into account long-range interaction between functional groups through conjugated π system which can influence acidity. Puri [*43*] questioned the reliability of the selective neutralisation technique for the determination of acidic groups of varying strengths. In his opinion the same acidic groups would neutralise different amounts of alkalis of varying strengths.

Potentiometric alkalimetric titration, using one strong base, *e.g.* sodium hydroxide, can also be applied to determine surface acidity in carbon [*34,44,45*]. The contribution of functional groups of various acidity can be determined by the analysis of the shape of the titration curves.

Thermal Desorption

The method based on the quite significant differences in the thermal stability of particular kinds of functional groups was also applied to characterise the surface functional groups in activated carbons. These differences in thermal stability are due to the varying energies necessary to decompose particular chemical bonds. Therefore during the heat treatment at a carbon under vacuum or in a inert atmosphere, particular surface compounds decompose at different characteristic temperatures [*33*, *46-48*] yielding such products as following:

CO_2: from decomposition of carboxylic acid and lactone groups, in the range of 200 - 800 °C.

CO: from decomposition of quinone, phenol and ether groups, in the range of 500 - 1000 °C.

H_2O: from decomposition of phenolic groups, in the range of 200 - 500 °C.

H_2: from recombination of hydrogen atoms liberated as a result of splitting of C–H bonds, in the range of > 500 - 700 °C.

Puri *et al* [***49-51***] studied a number of sugar and coconut charcoals before and after outgassing treatment and extensive oxidation in oxygen [***31***] as well as in oxidising solutions such as potassium persulphate, nitrate, and iodate [***52***], aqueous chlorine [***53***] and hydrogen peroxide [***54***]. The base neutralisation capacity of the charcoal was correlated with the oxygen functional groups evolved as CO_2 on evacuation at 1200 °C. The amount of alkali neutralised by the carbon was close to the amount of CO_2 evolved which was termed as CO_2 complex. As the amount of the CO_2 complex decreased on outgassing and increased on oxidation, the amount of neutralised base by the carbon decreased or increased correspondingly. When the entire amount of CO_2 complex was eliminated after outgassing at around 750 °C, the carbon could react with little alkali even though it still contained appreciable amounts of combined oxygen.

Oxidation with nitric acid also resulted in the fixation of considerable amounts of oxygen, most of which was desorbed as CO_2 during heat treatment. The base neutralisation capacity of the oxidised sample increased in proportion to the amount of CO_2 complex formed. The decomposition of CO_2 complex during outgassing caused a corresponding decrease in the base adsorption capacity.

Fourier Transform Infrared Spectroscopy

Infrared spectroscopy has been widely used for the characterisation of chemical structures of coals. carbon blacks, chars and activated carbons. Direct information on the structure of bulk of carbon materials and the various surface functional groups may be obtained from IR studies. The most common IR bands of carbon materials are 3400 -3500 cm^{-1}, 1760 -1880 cm^{-1}, 1700 - 1720 cm^{-1}, 1550 -1675 cm^{-1}, 1100 - 1200 cm^{-1} bands. Zhuang *et al* [*55*] investigated the surface oxygen complexes formed during carbon gasification using DRIFT. They observed two clear bands at 1770 and 1610 cm^{-1} and a broad band at 1250 cm^{-1}. The 1770 cm^{-1} band was assigned as C=O stretching in lactone and/or acid anhydride. The peak at 1610 cm^{-1} band was assigned as carboxyl groups which are highly conjugated with the polyaromatic matrix, *i.e.* quinone groups. The broad peak at 1250 cm^{-1} was attributed to the C-O stretching band either from ether type complexes or from lactone/anhydride. Bautista-Toledo *et al* [*56*] studied the HNO_3 oxidised carbon and attributed the 3500 cm^{-1} band to carboxylic acid groups (ν OH) and 1717 cm^{-1} band to carbonyl groups of carboxylic acid. Ishizaki *et al* [*57*] assigned the 1760 - 1710 cm^{-1} band to carboxylic groups and 1600 cm^{-1} band to carboxylate groups after neutralisation by alkali. The 1000 - 1180 cm^{-1} overlapping band was assigned to phenolic C-O stretching vibrations. Starsinic *et al* [*58*] applied FTIR to a study of oxidised Saran char and observed a few bands common to other carbon materials. They attributed the 1720 cm^{-1} band to carbonyl groups of carboxylic acid and 1250 cm^{-1} band to C-O stretching and OH bending modes of carboxylic acid groups. The 3400 cm^{-1} band was possibly due to water adsorbed in carbon or in KBr during grinding. After the char was treated with NaOH solution, the 1720 cm^{-1} band completely disappeared, leaving a weak peak at 1690 cm^{-}

[1] while a band at 1570 cm^{-1} was superimposed on the 1585 cm^{-1} vibration. Based on this evidence, the authors concluded that the 1720 cm^{-1} was due to COOH groups and that there was no evidence for the formation of lactones which absorb in the region of 1750 -1790 cm^{-1}. The 1585 cm^{-1} band of the oxidised char was assigned as carboxylate COO^- formed during KBr disc preparation and aromatic ring stretching vibrations.

Zawadzki [*59*] studied the oxidised carbon film prepared from polyfurfuryl alcohol and observed an intensity increase of the bands 1700, 1600, 820 cm^{-1}. The author proposed that these carbon oxygen surface complexes were probably ionoradical structures C⁼⁼O absorbing at 1600 cm^{-1} range and C=O groups absorbing at 1700 cm^{-1}. The carbonaceous aromatic structures reacting with HNO_3 form nitro groups absorbing at 1530 cm^{-1} (ν_{as} NO_2) and 1330 cm^{-1} (ν_s NO_2). The experiment was also carried out for the oxidised carbon film derived from cellulose by HNO_3 treatment at 80 °C, and a similar spectrum was recorded. The formation of band at 1665 cm^{-1} was ascribed to the surface quinone groups which were probably formed as result of an intramolecular rearrangement of ionoradical forms of chemisorbed oxygen. An absorption increase at 1720 cm^{-1} together with the parallel intensity increase of OH stretching vibrations band at 3500 cm^{-1} was caused by the formation of carboxyl structures. The density of these structures on the surface was found to rise rapidly after oxidation of the same sample at 100 °C.

X-ray Absorption Near Edge Structure Spectroscopy (X ANES)

Oxygen K-edge XANES is a powerful technique for the identification of oxygen functional groups in carbonaceous materials. It can readily distinguish between

anhydrides and lactones [*60,61*]. The oxygen XANES results [*60,61*] show that carbonyl-type complexes predominate in the partially combusted char samples. The author suggested that the oxygen functional groups evolved at ~1000 K during TPD were acids/anhydrides and carbonyls for the partially combusted chars.

2.4.2 Nitrogen Functional Groups on Carbon Surface

Nitrogen functional groups on activated carbon surface have not been studied extensively compared with the numerous studies on surface oxygen functionality. Stöhr *et al* [*62*] investigated the reaction of activated carbon with ammonia using XPS and assigned the peak at 398 – 399 eV to pyridine and/or nitrile groups and the peak at 400 – 401 eV to amino groups (NH_2-). The reaction of ammonia with activated carbon proposed by the authors is shown in **Figure 2.3**. The catalytic activity of activated carbon in oxidation reactions of SO_2 with O_2 was enhanced after treatment with NH_3.

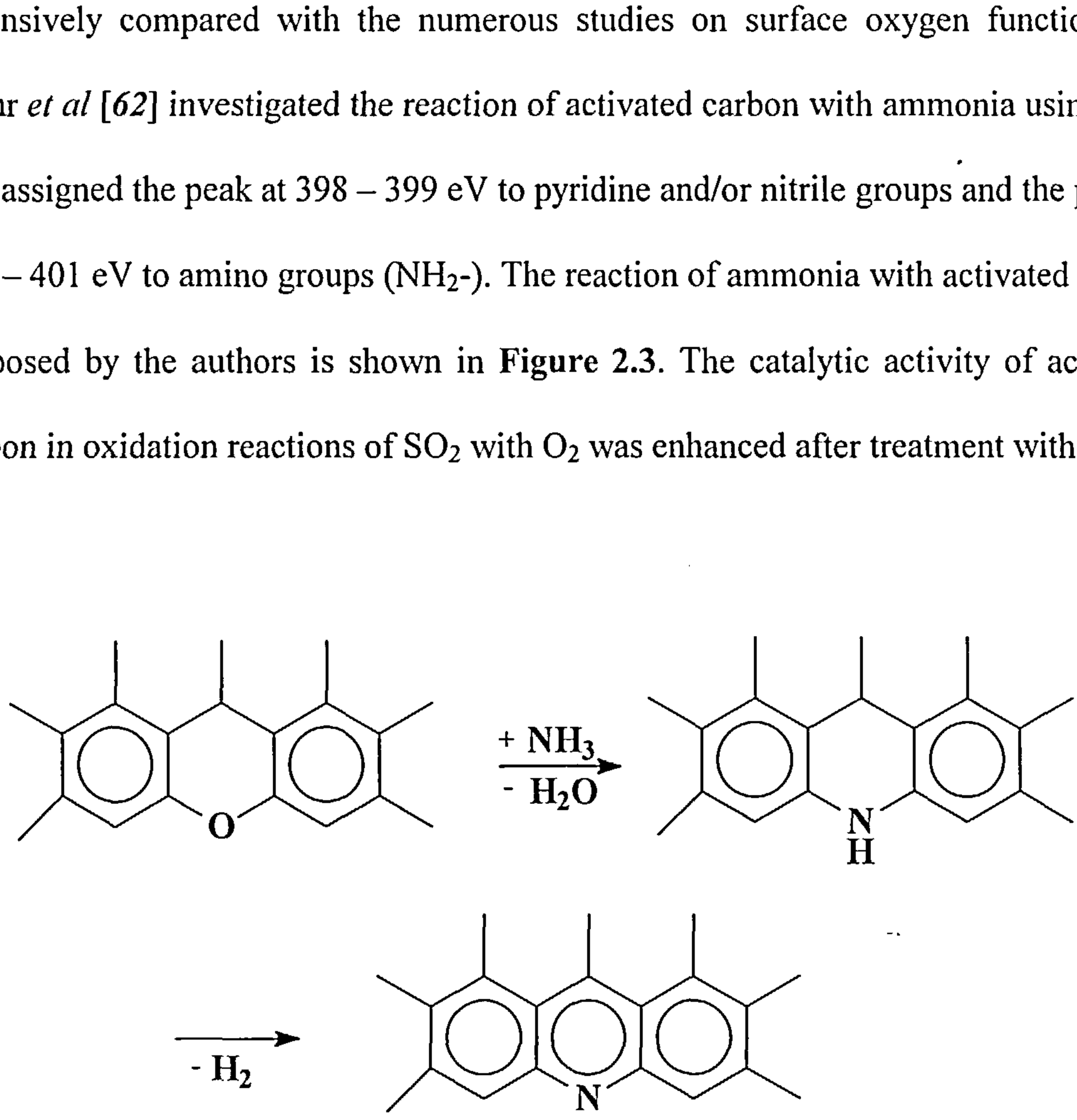

Figure 2.3 Reaction scheme for conversion of chemisorbed oxygen (ether-like) into imine and pyridine groups in the reaction with ammonia

Jansen *et al* [***63***] found that the nitrogen functional groups are mainly amides in the carbon treated with a mixture of ammonia and air (ratio 1:5) at 420 °C. The aminated carbon which was prepared by HNO_3 oxidation followed by ammonia treatment at 230 °C had mainly lactam and imide functional groups. Lactam and imide groups were the principle nitrogen functionality after the aminated carbon was heat treated below 400 °C. With increasing heat treatment temperature, the nitrogen functionality were mainly pyridine and pyrrolic groups, however lactam and imide groups were still present after treatment at 800 °C. The possible nitrogen functional groups and reactions is shown in **Figure 2.4** [***64***].

Pels *et al* [***65***] used XPS to investigate the fate of nitrogen functionality present in lignite and its chars and chars derived from the model compounds acridine, carbazole and polyacrylonitrile (PAN). The distribution of the nitrogen functional forms changes with pyrolysis conditions. Under mild pyrolysis conditions, firstly unstable functionalities like pyridones, protonated pyridinic nitrogen and N-oxide of pyridinic nitrogen are converted to pyridinic nitrogen. Secondly pyrrolic nitrogen is converted to pyridinic nitrogen during condensation of carbon matrix. During the condensation process, nitrogen atoms are incorporated into the graphene layers replacing carbon atoms. After severe pyrolysis all nitrogen is eventually present in 6-memebered rings located at the edges of the graphene layers as pyridinic nitrogen or in the interior as quaternary nitrogen. Upon exposure to air, N-oxides of pyridinic nitrogen can be formed.

Stanczyk *et al* [***66***] studied the transformation of nitrogen structures during carbonisation process of model compounds using XPS. Nitrogen containing chars were prepared by low temperature carbonisation (460 °C) of compounds containing

pyrrolic, pyridinic, amino and cyano groups. At low temperature carbonisation, pyrrolic, pyridinic and quaternary nitrogen were observed. The pyrrolic and pyridinic nitrogen structures decrease with increasing temperature, whereas the amount of quaternary nitrogen increases.

Zhu *et al* [*67*] investigated the nitrogen functional groups in ammonia treated PVDC carbon and PAN derived carbon using X-ray absorption near edge structure (XANES) spectroscopy. It was found that ammonia treatment of PVDC carbon incorporated pyridinic, pyridone or CN and pyrrolic nitrogen functional groups into the carbon. PAN carbon had mainly pyridinic and pyrrolic functionality and some quaternary nitrogen as well. **Figure 2.5** shows the possible nitrogen forms proposed by the authors. Partial gasification studies revealed that pyridone functional groups were formed by combustion in air at 600 °C (char).

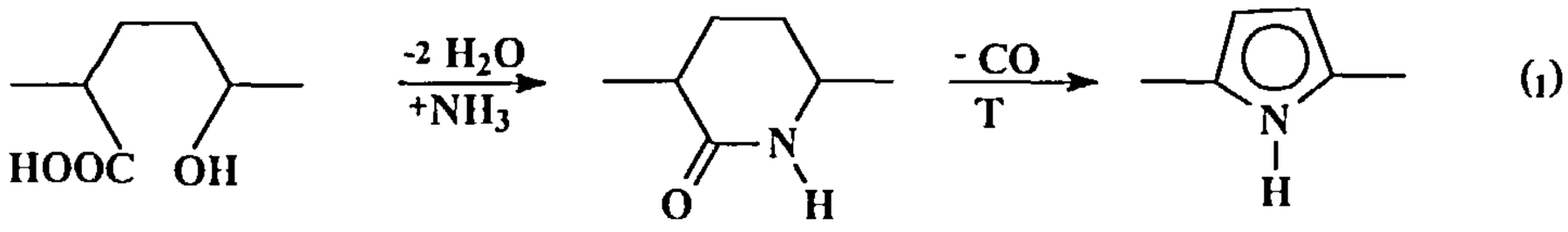

Figure 2.4 The reaction path of five types of carboxylic groups, first step: reaction with ammonia gas resulting in *amide* (2,4), *imide* (3,5) and *lactam* (1) groups. Second step: heat treatment resulting in *pyrroles* (1,4) and *pyridines* (2,3,5)

a) Nitrogen forms in carbons

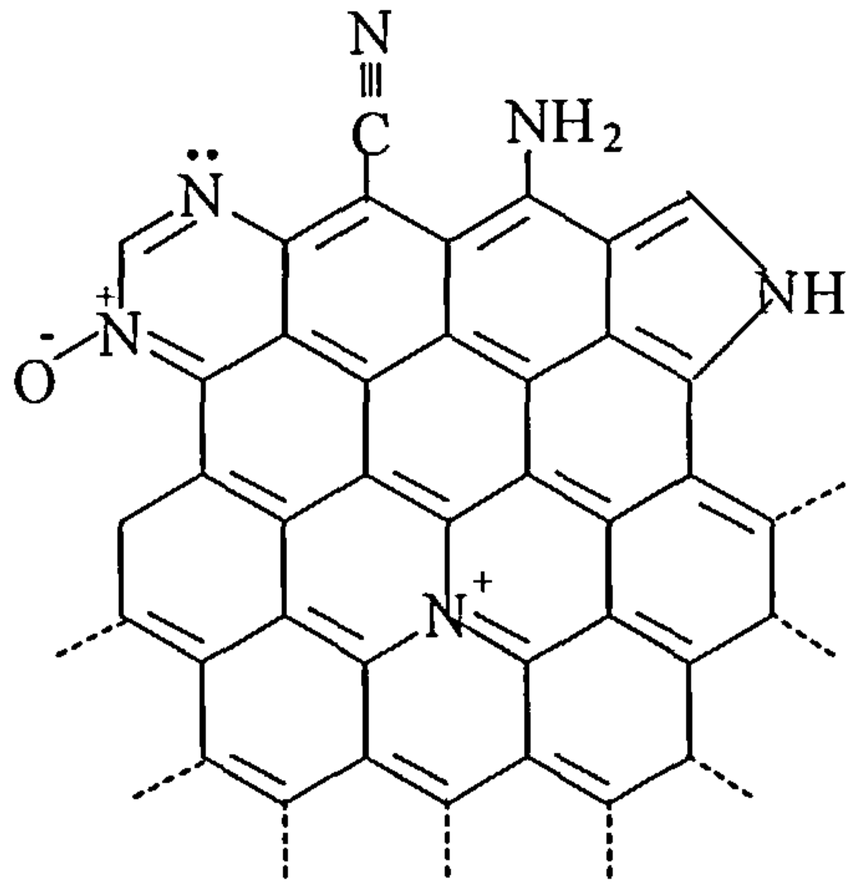

b) Nitrogen forms in partially gasified carbons

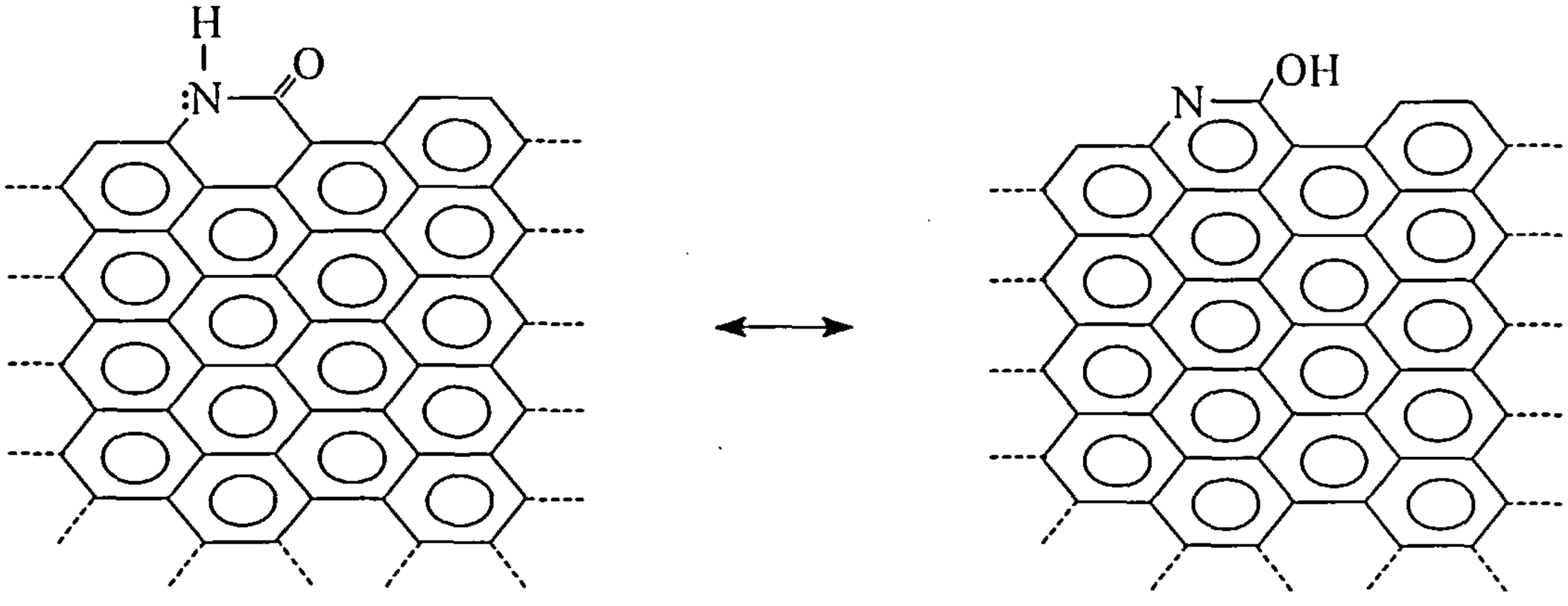

Figure 2.5 Nitrogen forms in carbons and partially gasified carbons [*67*]

References

1. Faust, S. D. and Aly, O. M. 1983, *Chemistry of Water Treatment*, London, Butterworth.
2. Bansal, R. C., Donnet, J. B. and Stoeckli, H. F. *Active Carbon*, New York, Marcel Dekker, 1988.
3. Mattson, J. S. and Mark, H. B. (Jr.) *Activated Carbon, Surface Chemistry and Adsorption from Solution*, New York, Marcel Dekker, 1971.
4. Mackay, D. M. and Roberts, P. V. *Carbon*, 1982, **20**, 95.
5. Mackay, D. M. and Roberts, P. V. *Carbon*, 1982, **20**, 105.
6. Smisek, M. and Cerny, S. *Active Carbon*, Elservier, Amsterdam, 1970.
7. Kadlec, O., Varhanikova, A. and Zukal, A. *Carbon*, 1970, **8**, 321.
8. Wennerberg, A. N. and O' Grady, T. M. *U. S. Patent*, 4,082,694, Apr. 4, 1978.
9. Kraehenbuehl, F., Stoeckli, H. F., Ehrburger, P., Addour, A. and Donnet, J. B. *Carbon*, 1986.
10. Kwok, J. and Miller, A. *U. S. Patent*, 3,767,592, Oct. 23, 1973.
11. Wigmans, T. *Carbon*, 1989, **27**, 13.
12. Walker, P. L. (Jr.), Rusinko, F. and Austin, L. G. *Adv. Catal.* 1959, **11**, 133.
13. Rand, B. and Marsh, H. *Carbon*, 1971, **9**, 79.
14. Tourkow, K., Siemieniewska, T, Czeckowski, F. and Gankowska, A. *Fuel*, 1977, **56**, 121.
15. Katori, K., Nagai, H. and Shüki, Z. *U. S. Patent*, 4,045,368, Aug. 30, 1977.
16. Kobayashi, K., Watari, S., Kato, T., Shiraishi, M. and Kawana, Y. *U. S. Patent*, 3,891,574. Jun. 24, 1975.
17. Voet, A. and Lamond, T. G. *U. S. Patent*, 3,533,961, Oct. 31, 1970.
18. Biscoe, J. and Warren, B. E. *J. Appl. Phys.* 1942, **13**, 364.
19. Burstein, R. and Frumkin, A. *Z. Phys. Chem.* 1929, **A141**, 219.
20. Frumkin, A. *Kolloid Z.* 1930, **51**, 123.
21. Shilov, N. *Kolloid Z.* 1930, **52**, 107.
22. Shilov, N., Shatunovsha, H. and Larowskaja, D. *Z. Phys. Chem.* 1930, **A150**, 421.
23. Garten, V. A. and Weiss, D. E. *Aust. J. Chem.* 1957, **10**, 309.
24. Voll, M. and Boehm, H. P. *carbon*, 1971, **9**, 481.

25. Steenberg, B. *Adsorption and Exchange of Ions On Activated Charcoal*, Almquist & Wiksells, Uppsala, Sweden, 1944.

26. Boehm, H. P. *Advan. Catal.* 1964, **16**, 179.

27. Boehm, H. P., Diehl, E., Heck, W. and Sappok, R. *Angew. Chem. Int. Ed.* 1964, **3**, 669.

28. Coughlin, R. W. and Ezra, F. S. *Environ. Sci. Technol.* 1968, **2**, 291.

29. Puri, B. R. In *the Proceedings of the 5th Conference on Carbon*, Vol. I, Pergamon Press, New York, 1962, p.165.

30. Puri, B. R., Singh, D. D. and Sharma, L. R. *J. Phys. Chem.* 1958, **62**, 756.

31. Puri, B. R., Singh, D. D., Nath, J. and Sharma, L. R. *Ind. Eng. Chem.* 1958, **50**, 1071.

32. Puri, B. R., Murari, K. and Singh, D. D. *J. Phys. Chem.* 1961, **65**, 37.

33. Puri, B. R. and Bansal, R. C. *Carbon*, 1964, **1**, 451.

34. Puri, B. R. and Bansal, R. C. *Carbon*, 1964, **1**, 457.

35. Puri, B. R. *Carbon*, 1966, **4**, 391.

36. Zarif'yanz, Y. A., Kiselev, V. F., Lezhnev, N. N. and Nikitina, D. V. *Carbon*, 1967, **5**, 127.

37. Garten, V. A., Weiss, D. E. and Willis, J. B. *Aust. J. Chem.* 1957, **10**, 295.

38. Garten, V. A., Weiss, D. E. *Rev. Pure Appl. Chem.* 1957, **7**, 69.

39. Boehm, H. P. and Voll, M. *Carbon*, 1970, **8**, 227.

40. Voll, M. and Boehm, H. P. *ibid*, 1971, **9**, 481.

41. Leon y Leon, C. A., Solar, J. M., Calemma, V. and Radovic, L. R. *Carbon*, 1992, **30**, 797.

42. Tarkovskaya, I.A., Strazhesko, D.N. and Goba, W.E., *Adsorbtsiya i Adsorbenty*, 1977, **5**, 3.

43. Puri, B. R. In *Chemistry and Physics of Carbon*, Walker (Jr.), P. L., Marcel Dekker, New York, 1970, vol. 6, p191.

44. Puri, B. R., Singh, G. and Sharma, L. R. *J. Indian Chem. Soc.* 1957, **34**, 357.

45. Matsumura, Y. *J. Appl. Chem. Biotechnol.* 1975, **25**, 39.

46. Cotharp, M. T. and Hackerman, N. *J. Phys. Chem.* 1968, **72**, 1171.

47. Barton, S. S., Gillespie, D. and Harrison, B. H. *Carbon*, 1973, **11**, 649.

48. Voll, M. and Boehm, H. P. *Carbon*, 1970, **8**, 741.

49. Puri, B. R., Meyer, Y. P. and Sharma, L. R. *J. Indian Chem. Soc.* 1956, **33**, 781.

50. Puri, B. R., Meyer, Y. P. and Sharma, L. R. *Chem. Ind.* London, B. I. F. Rev. R. 1956, 30.

51. Puri, B. R., Meyer, Y. P. and Sharma, L. R. *Res. Bull. Panjals University Chandigarh*, 1956, **88**, 53.

52. Puri, B. R., Mahajan, O. P. and Singh, D. D. *J. Indian Chem. Soc.* 1961, **38**, 135.

53. Morterra, C., Low, M. J. D. and Severdia, A. G. *Carbon*, 1984, **22**, 5.

54. Puri, B. R., Sharma, L. R. and Singh, D. D. *J. Indian Chem. Soc.* 1958, **35**, 457.

55. Zhuang, Q.L., Kyotani, T. and Tomita, A. *Energy and Fuel*, 1994, **8**, 714.

56. Bantista-Toledo, I., Rivera-Utrilla, J., Ferro_garcia, M.A. and Moreno-Castilla, C. *Carbon*, 1994, **32**, 93.

57. Ishizaki, C. and Marti, I. *Carbon*, 1981, **19**, 409.

58. Starsinic, M., Taylor, R.L., Walker (Jr), P.L. and Painter, P.C. *Carbon*, 1983, **21**, 69.

59. Zawadzki, J. In *Chemistry and Physics of Carbon*, Edited by Thrower, P.A. 1989, vol.21, p147.

60. Turner, J.A., Thomas, K.M. and Russell, A.E. *Carbon*, 1997, **35**, 983.

61. Turner, J.A. and Thomas, K. M. *Langmuir*, 1999, **15**, 6416.

62. Stöhr, B., Boehm, H.P. and Schlögl, R., *Carbon*, 1991, **29**, 707.

63. Jansen, R.J.J and van Bekkum, H., *Carbon*, 1995, **33**, 1021.

64. Jansen, R.J.J and van Bekkum, H., *Carbon*, 1994, **32**, 1507.

65. Pels, J.R., Kapteijn, F., Moulijn, J.A., Zhu, Q. and Thomas, K.M., *Carbon*, 1995, **33**, 1641.

66. Stanczyk, K., Dziembaj, R., Piwowarska, Z. and Witkowski, S. *Carbon*, 1995, **33**, 1383.

67. Zhu, Q., Money, S.L., Russell, A.E. and Thomas, K.M., *Langmuir*, 1997, **13**, 2149.

Chapter 3

ADSORPTION OF METAL ION SPECIES ON ACTIVATED CARBON

3.1 Adsorption of Gold on Activated Carbon

3.1.1 Introduction

Activated carbon was first reported to have the property of adsorbing precious metals from solutions by Lazowski [*1*] in 1848. Triggered by this discovery, Davis [*2*] patented a process for the recovery of gold from chlorination leach liquors using wood charcoal. Soon after MacArthur and the Forrest brothers [*3*] discovered that gold could be dissolved by cyanide solutions, Johnson [*4*] patented the use of wood charcoal for the extraction of gold from cyanide solutions in 1894. However, the first practical application of activated carbon to the recovery of gold in a large scale, known as carbon-in-pulp (CIP) was not established until 1973 [*5*]. Before that, the hydrometallurgical process for the treatment of gold and silver ores remained unchanged for the first 70 years of this century. The process consisted essentially of leaching in cyanide solution followed by solid-liquid separation, with the solid residues being washed as efficiently as possible. The leach liquor was treated by zinc cementation to recover the precious metals.

Cyanidation of Ores

The first step in cyanidation process is to crush and mill the gold-bearing ores to a size in order to liberate the gold particles from the host rock. The milling is performed using a wet slurry of the ore with a low solid density. The milled product is thickened to 30 ~ 50 % solids contents and admitted to cyanide-leaching plant.

The slurry is blown from the bottom of the tank using compressed air which provides oxygen to oxidise gold from Au (0) to Au (I), which also keeps the slurry fully in suspension as well. Cyanide is usually introduced to the system after the slurry is thoroughly preaerated and the leach solution saturated with oxygen prior to contact with cyanide. The gold bearing leach solution is then separated from the gold-depleted ore. This process is costly and inefficient therefore providing stimulus for the development of carbon-in-pulp and carbon-in-leach process.

The chemistry of the dissolution of gold and silver in alkaline cyanide solutions was proposed by Kudryk and Kellogg [*6*] as an electrochemical process with following overall stoichiometry:

$$4\ Au + 8\ CN^- + O_2 + 2\ H_2O = 4\ Au(CN)_2^- + 4\ OH^- \qquad (3.1)$$

This reaction consists of cathodic and anodic half-reactions. The anodic reaction involves the oxidation of Au (0) to Au (I):

$$4\ Au + 8\ CN^- = 4\ Au(CN)_2^- + 4\ e \qquad (3.2)$$

This is accompanied by the cathodic reaction of oxygen at the surface of the gold particle:

$$O_2 + 2\ H_2O + 4\ e = 4\ OH^- \qquad (3.3)$$

In contrast to cyanide, all the alternative leaching agents proposed (halides, thiourea, thiosulphate, thiocyanate) yield gold complexes that are considerably less stable than aurocyanide [7]. The one drawback of the cyanide / oxygen leaching chemistry for the dissolution of gold is the low solubility of oxygen in water. Under most conditions, the rate of gold leaching is controlled by diffusion of oxygen to the metal surface [7].

Cementation of Gold

The zinc cementation process for the recovery of gold and silver was introduced in 1890 at the same time as the cyanide leaching process. The major reactions are the cathodic deposition of gold and anodic corrosion of zinc, which occur on the surface of zinc particles:

$$Au(CN)_2^- + e = Au + 2\ CN^- \qquad (3.4)$$

$$Zn + 4\ CN^- = Zn(CN)_4^{2-} + 2\ e \qquad (3.5)$$

There are side reactions present in the process which affect the cost of the cementation process. The side reactions involve the simultaneous and wasteful consumption of zinc, by oxidation to Zn^{2+} and formation of zinc tetracyanide, *i.e.* if there is oxygen present in the solution, the following reaction occurs:

$$2\ Zn + 8\ CN^- + O_2 + 2\ H_2O = 2\ Zn(CN)_4^{2-} + 4\ OH^- \qquad (3.6)$$

This reaction can be minimised by deaeration of the pregnant solution in a Crowe vacuum tower.

3.1.2 Carbon-In-Pulp (CIP) Process

Much of the technology on which the CIP is based was developed by Zadra *et al* [8,9] in the laboratories of the United States Bureau of Mines. This technology paved the way for setting up the first large-scale CIP plant in 1973 at the Homestake Mining Company in the USA [*4*]. A simplified schematic diagram of the CIP process is shown in **Figure 3.1**. The CIP process is generally used to treat low grade gold ores feed though concentrated feed can also be used. The ore is ground in a ball mill with a sizing device cyclone. The ground ore overflows the cyclone at the desired particle size to a thickener to increase the slurry density to 45 ~ 50 % solids. Prior to passing through several stages of leaching, the pulp is conditioned with air and lime for a few hours to make it more amenable to leaching. In each leach tank, lime slurry, sodium cyanide and plant air are introduced and mixed into the pulp. The pulp flows from leach circuit into next stage, the CIP circuit, which consists of more than 3 tanks. As in leaching circuit. Lime slurry, plant air and sodium cyanide are added. The activated carbon, generally 6 ~ 16 mesh, is added to the last CIP tank and advanced to the first CIP tank via air lifts, whereas the pulp flows counter current to the carbon from first to last CIP tank. Between CIP tanks, the vibrating 24 mesh screens are used to separate the coarse carbon from finer pulp. The pulp is advanced to the next tank while most of the carbon retained on the screen drops back to the same tank and a determined amount is advanced to next tank counter current to the pulp flow. The barren pulp with less than 0.001 ounce of gold per ton of solution is disposed as

tailings. As the carbon is advanced from tank to tank, the gold loading on the carbon increases. The carbon normally is held in No.1 tank until the load on the carbon reaches 300 ~ 400 ounces of gold per ton. It is moved from the first tank by jet eductor to the desorption circuit to be stripped of the gold and silver. In stripping vessels the carbon is first washed with water to remove the fine slime particles. A hot solution of NaCN-NaOH is used to elute the precious metals from activated carbon. The pregnant solution is then pumped to electrowinning cells, where gold and silver are deposited on cylindrical steel wool cathodes. After sufficient loading of the wool, the cathode is removed for smelting. The metal is then remelted in a bullion furnace, where suitable fluxes are introduced to remove most of the base metal impurities. The metal from the bullion furnace is then cast into bullion and sent to refinery.

The stripped carbon is moved to a regeneration kiln for reactivation treatment. A safety screen of 20 mesh is used as a precautionary measure to remove the minus 20 mesh carbon. This can reduce losses of 24 mesh carbon in the adsorption circuit.

The CIP process has several important advantages over the conventional zinc cementation route, the counter current decantation process (CCD, as shown in **Figure 3.2**). First, due to direct application of carbon to the pulp, the costly filtration and clarification stages are obviated. Furthermore, the recovery of gold and silver is less affected in CIP process by copper and nickel *et al*. Finally, greater efficiency can be achieved for recovering gold from very dilute solution with CIP.

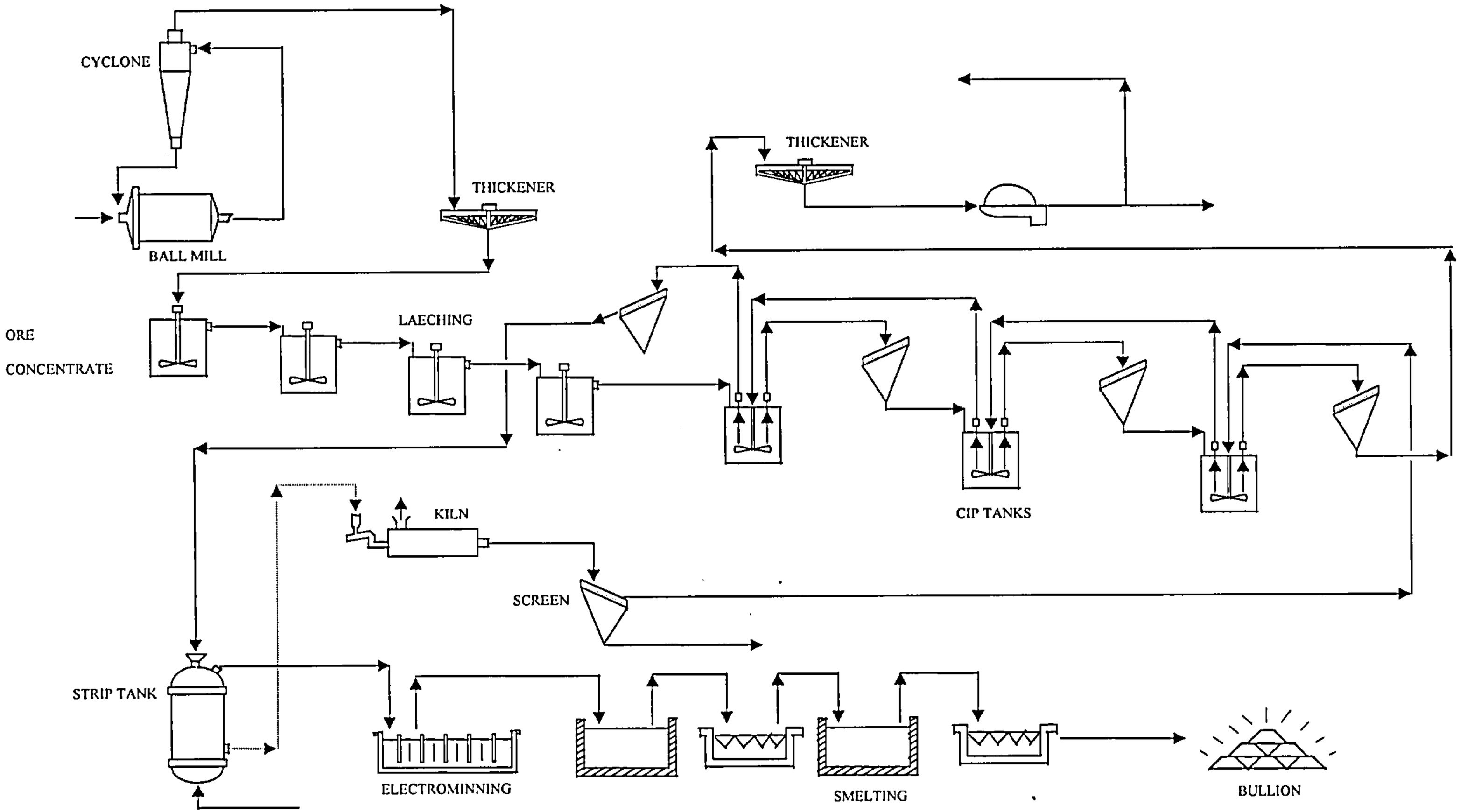

Figure 3.1 Carbon-in-pulp process schematic flowsheet

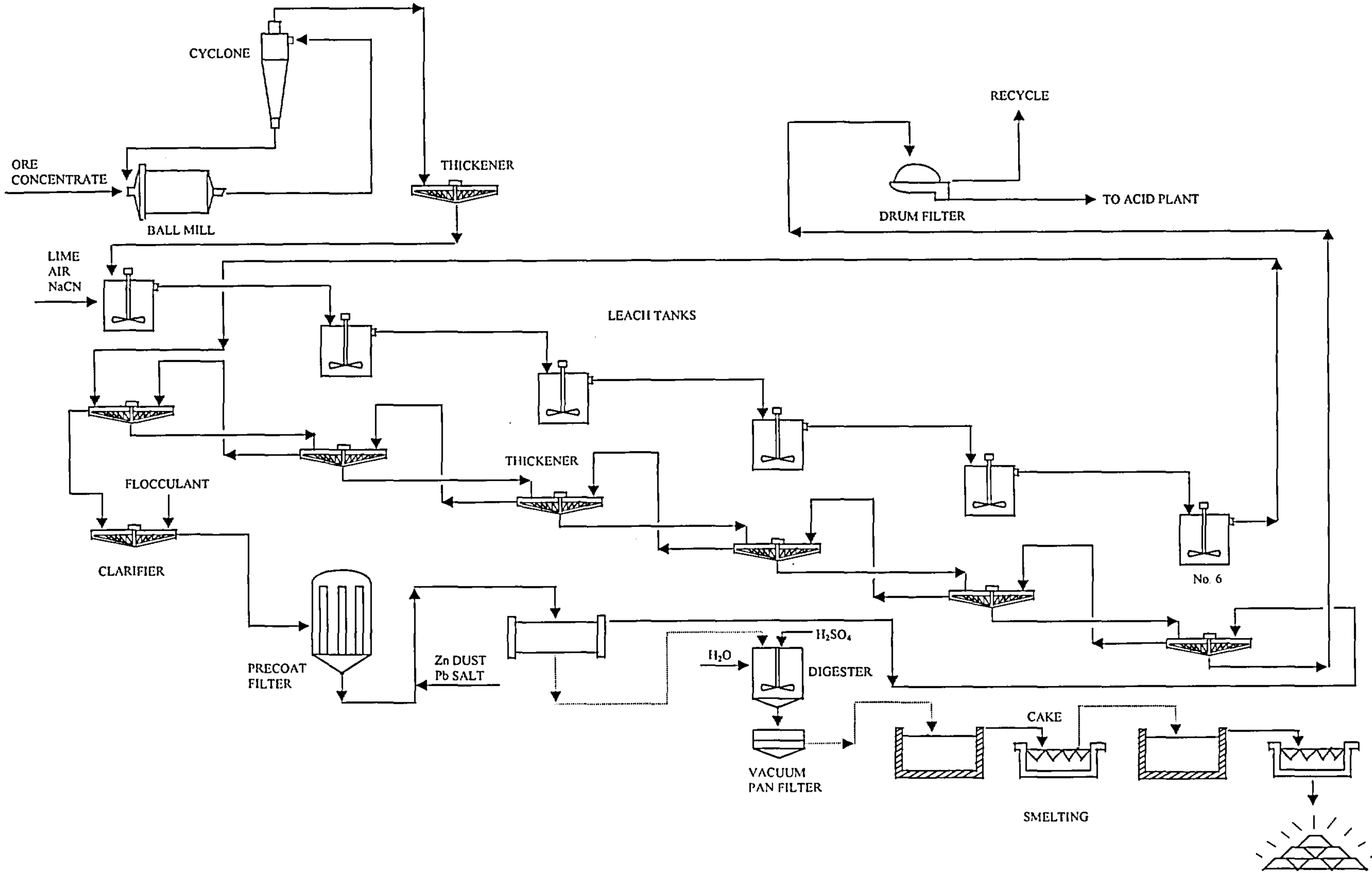

Figure 3.2 Counter current decantation process (CCD) schematic flowsheet

3.1.3 Adsorption Sites and Nature of Gold Cyanide Species on Carbon Surface

A. Early Studies

Early theories on the adsorption of gold cyanide species on activated carbon fell into two major types, namely those that proposed the adsorption of $Au(CN)_2^-$ anions without change and those that proposed the adsorption of gold through the reduction of gold cyanide to metallic gold or to some intermediate state or by precipitation as the insoluble complex AuCN on carbon surface.

In 1913, after the studies of adsorption of gold cyanide onto finely crushed wood charcoal, Green [*10*] reported that the wood charcoal turned into yellow after contact with gold cyanide solution. Therefore he proposed a adsorption mechanism involving the complete reduction of gold cyanide complex to metallic gold. However, soon after Green' s works, Feldtmaan [*11*] found that although metallic gold precipitated rapidly from chloride medium onto 10 mesh wood charcoal, the gold in an aurocyanide solution was loaded onto carbon comparatively slowly. The form of gold adsorbed in this way was neither visible metallic nor to any significant extent soluble in cyanide solutions, thereby concluding that the mechanism of the adsorption of gold cyanide on charcoal was different from that of gold chloride. Feldtmaan postulated that gold cyanide was adsorbed on charcoal by a chemical precipitation process which involved a combination of AuCN, CO and $(CN)_2$, termed as 'carbonyl aurocyanide' precipitate with the formula $AuCN{\bullet}CO(CN)_2$. Edmands [*12*] suggested that carbon monoxide occluded in the charcoal was involved in the adsorption of gold cyanide by the formation of $KAu(CN)_2CO$, or $HAu(CN)_2CO$ from acidic solution. He also investigated the effects of additional compounds and found that gold adsorption

capacity was greatly enhanced in acidic solution and suppressed by soluble sulphides. Thiocyanate and thiosulphate were not found to have measurable effects. Contrary to previous assumptions, Allen [*13*] suggested that gold cyanide was physically adsorbed as $NaAu(CN)_2$ on charcoal without undergoing chemical change. He also found that the adsorption of gold cyanide on charcoal could be accurately described by the empirical Freundlich equation:

$$x/m = k\, C^{1/n} \qquad (3.7)$$

where x is the mass of the adsorbate

m is the mass of the adsorbent

c is the equilibrium concentration

k and n are constants

However, Allen' s proposal was questioned by Williams [*14*] who showed that the sodium in the ash of the loaded, burned charcoal was far from being sufficient to account for the simple adsorption of $NaAu(CN)_2$. He assumed that it was more likely to be the anion $Au(CN)_2^-$ that was adsorbed.

In the late 1920' s, after the systematic and detailed investigation of the factors that influence the adsorption of $Au(CN)_2^-$ onto activated carbon, Gross and Scott [*15*] proposed that the $Au(CN)_2^-$ anions were adsorbed without undergoing a chemical change and retained on the carbon surface as a neutral complex, namely $M^{n+}[Au(CN)_2^-]_n$, where the cation M^{n+} were either from solution or from the ash of the carbon. The enhanced gold loading in acidic solutions was attributed to the formation of insoluble AuCN:

$$Au(CN)_2^- + H^+ \rightleftarrows AuCN + HCN \qquad (3.8)$$

The mechanisms advanced by Allen, Williams and Gross and Scott were in agreement regarding the adsorption of $Au(CN)_2^-$ anions on carbon without chemical changes but differed only with respect to the source of the cation required to maintain the electroneutrality.

B. Advances in the Theories of Adsorption

Modern theories of the gold adsorption on activated carbon can be summarised as following categories:

1. The adsorption of $M^{n+}[Au(CN)_2^-]_n$ ion pairs [*16 - 19*].
2. The electrical double layer adsorption of $Au(CN)_2^-$ anions and cations on a charged surface [*20 - 23*].
3. The ion exchange extraction of $Au(CN)_2^-$ anions by positively charged sites present on the surface of the carbon [*24 - 26*].
4. Adsorption of ion pairs $M^{n+}[Au(CN)_2^-]_n$ followed by partial reduction of the $Au(CN)_2^-$ complex to a cluster-type species [*27*].
5. Adsorption of $Au(CN)_2^-$ by ion exchange followed by degradation to AuCN [*28-30*].
6. Adsorption of $Au(CN)_2^-$ on the graphitic structures [*31 - 37*].

In 1957, Garten and Weiss [*24*] suggested an anion-exchange mechanism for $Au(CN)_2^-$ adsorption involving simple electrostatic interaction between positive and negative charges. The positive sites on the carbon surface were assumed to be carbonium ion sites which were formed by the oxidation of chromene groups to chromenol groups by the oxygen adsorbed on the carbon surface:

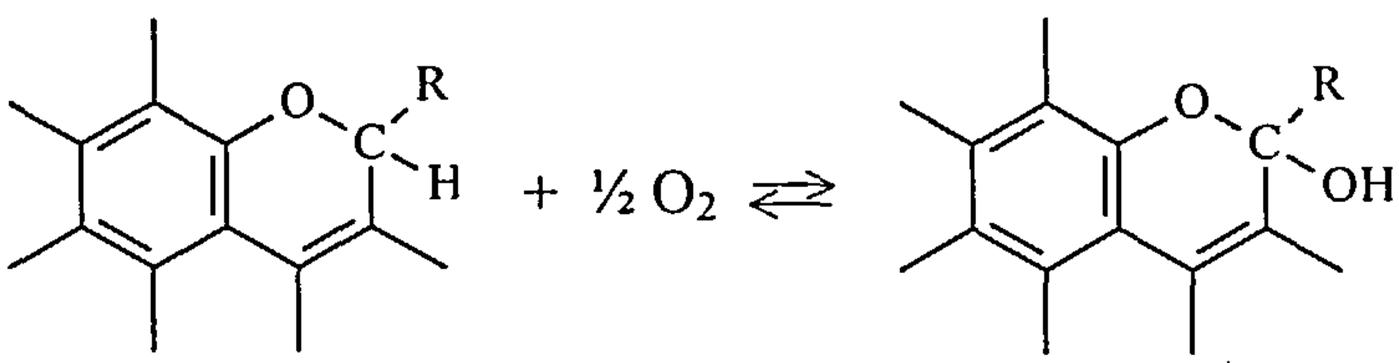

(3.9)

Therefore, $Au(CN)_2^-$ or CN^- could be adsorbed through ion exchange with OH^- anions:

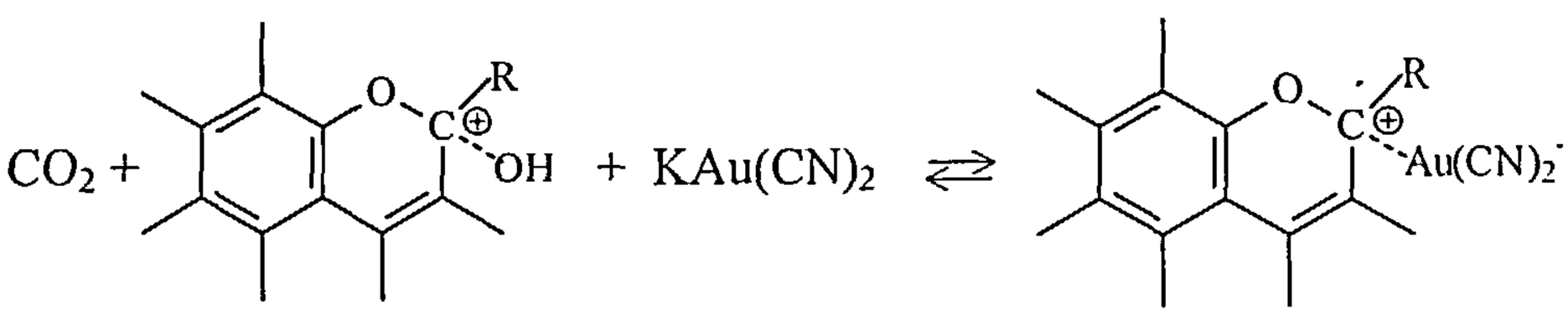

$$+ KHCO_3 \qquad (3.10)$$

The adsorption mechanism advanced by Dixon *et al* [*26*] involved an electrostatic interaction between $Au(CN)_2^-$ anions and positively charged sites on carbon surface, as preciously suggested by Plaksin [*25*] and Garten and Weiss [*24*]. They suggested that the positive sites attracting $Au(CN)_2^-$ anions were due to the Frumkin' s electrochemical mode [*38 - 40*]

$$C + O_2 + 2\,H_2O \rightleftarrows C^{2+} + 2\,OH^- + H_2O_2 \qquad (3.11)$$

The reaction would shift towards the right at low pH thereby producing more positively charged sites. Therefore the loading of $Au(CN)_2^-$ would be enhanced from acidified cyanide solutions.

However, Kuzminykh and Tjurin [*41*] questioned the electrostatic interaction mechanism since the simple anions such as Cl^- and I^- had no effect on the capacity of gold adsorption on birch or aspen derived carbons. Neutral organic compounds such as octyl alcohol and kerosene present in solution depressed the adsorption of gold on activated carbon, and this led to the proposal that gold was adsorbed as a neutral molecule. Under acidic conditions the neutral molecules $HAu(CN)_2$ was adsorbed whereas under neutral or alkaline conditions, a salt such $NaAu(CN)_2$ was adsorbed by van der Waals type interactions.

Davidson [*16*] advanced the ion pairs mechanism based on previous works by Kuzminykh and Tjurin [*41*]. He investigated the factors influencing the adsorption of $Au(CN)_2^-$ on coconut shell based activated carbon and found that the 'spectator cations' such as Ca^{2+} and Na^+ enhanced the gold adsorption capacity on carbon. The mechanism advanced by him involved the adsorption of the metal dicyanoaurate complex ion pairs $M^{n+}[Au(CN)_2^-]_n$ from solution. It was noted that the ability of M^{n+} to inhibit gold adsorption followed the sequence:

$$Ca^{2+} > Mg^{2+} > H^+ > Li^+ > Na^+ > K^+$$

This led to the conclusion that when M^{n+} was an alkaline earth metal ion (Ca^{2+} or Mg^{2+}), the ion pair was bound to the carbon more firmly. The ion pair mechanism was favoured by many researchers and was supported by the works of Adams and co-workers [*17 -29*]. They examined the effects of alkali and alkaline earth metal cations on the extraction of aurocyanide by Norit R2020 activated carbon and polymeric adsorbents and observed the enhancement of gold loading by the metal cation in the same order as in previous work by Davidson [*16*]. They ascribed the increased

adsorption to the decreased aqueous solubilities of aurocyanide salts with larger cations which were less well hydrated resulting in an enhanced extractability into the hydrophobic carbon phase. The aurocyanide would be almost entirely in the form of associated $HAu(CN)_2$ in the aqueous phase at pH 1, which would account for the enhanced adsorption under acidic conditions. The ion pair mechanism of gold adsorption was further clarified by E.S.R spectroscopy by the authors, which indicated that a specific interaction between the adsorbed ion pair and the condensed aromatic structure was also probably occurring. After a careful balance calculation of the anions and cations both in solution and on the carbon surface, Adams *et al* [*42*] also suggested that under the alkaline conditions typically encountered in a CIP plant, gold is extracted as an ion pair of the type $M^{n+}[Au(CN)_2^-]_n$ (where $M^{n+} = Ca^{2+}$, Na^+, *etc.*). At low pH (<3), gold was loaded onto activated carbon predominantly as the aurocyanide acid $HAu(CN)_2$, while at intermediate pH, the ion pair and the acid were loaded simultaneously.

Cho *et al* [*20 - 23*] applied the ionic solvation energy theory [*43*] to the study of gold and silver adsorption on carbon and proposed the electrical double layer adsorption mechanism. The specific adsorption was principally determined by the degree and type of ionic hydration. Therefore, they predicted that a large weakly hydrated anion such as $Au(CN)_2^-$ or $Ag(CN)_2^-$ would be specifically adsorbed on the carbon surface, whereas small anions with a large number of strong bound water molecules in their primary-hydration shells, for example CN^-, would not be specifically adsorbed and would therefore remain in the outer part of the electrical double layer. The observation that the adsorption capacity of $Ag(CN)_2^-$ was considerably higher than that of CN^- supported this proposal. Cho *et al* [*23*] confirmed the results that an increase in the concentration of K^+, Na^+ and Ca^{2+} cations in solution

enhanced the adsorption of silver cyanide on carbon. To explain the observation, they proposed that the silver cyanide complex was specifically adsorbed on the carbon surface and the cations were non-specifically adsorbed in the electrical double layer and these cations provided additional sites for the adsorption of anions such $Au(CN)_2^-$ and CN^-.

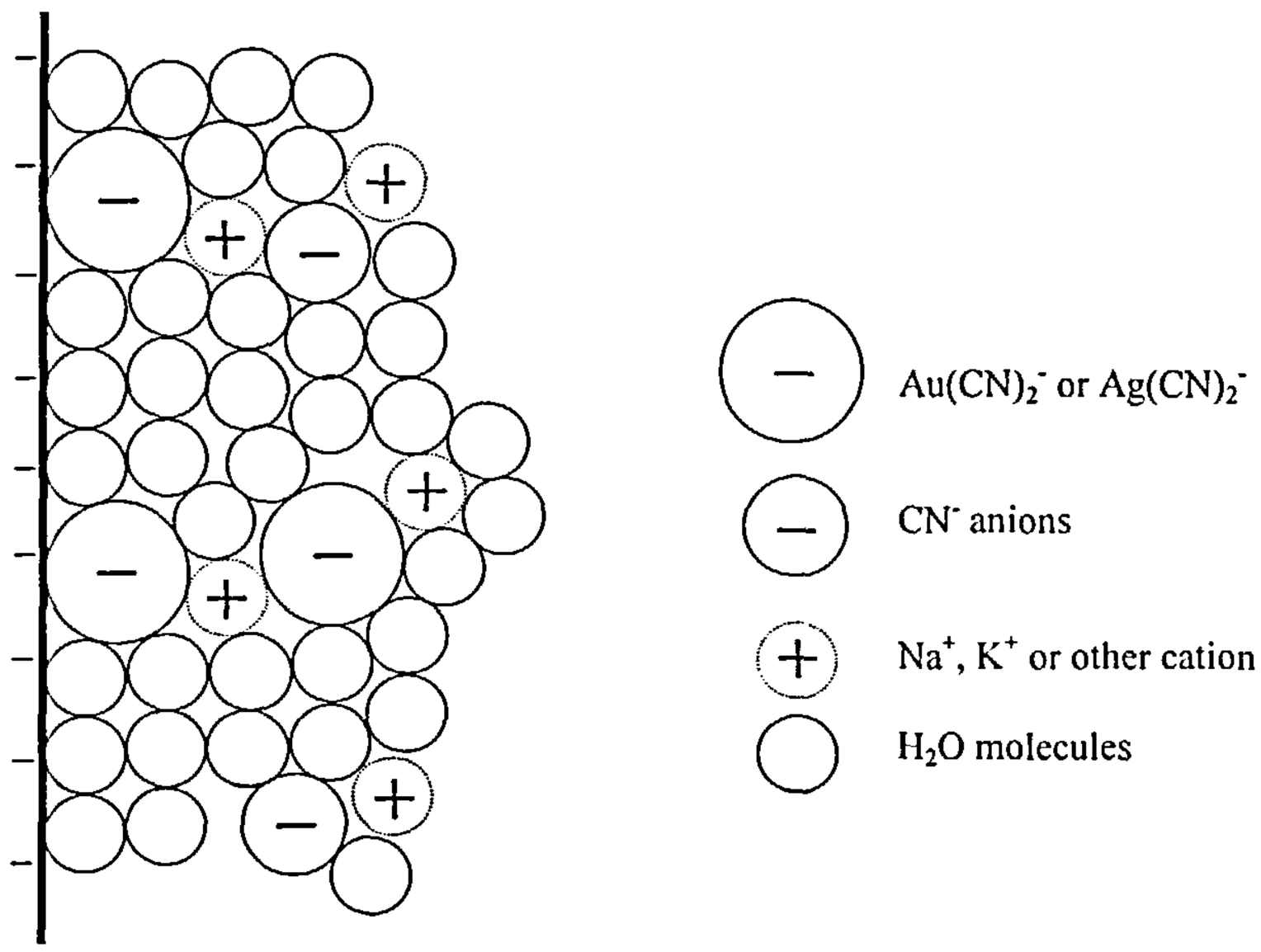

Figure 3.3 Schematic representation of the model proposed by Cho *et al* [*23*] for the adsorption of $Au(CN)_2^-$ or $Ag(CN)_2^-$ anions on coconut shell derived carbon

Figure 3.3 shows the adsorption mechanism involving the formation of multilayer ions proposed by the authors. Cho *et al* also observed that the adsorption capacity of carbon for gold was about three times higher than for silver and they attributed this to the larger ionic radius of gold (137 pm) compared with that of silver (126 pm), which was consistent with solvation energy theory. McDougall *et al* [*27*, *44*] reported the following sequence for the adsorption capacity of carbon for metal cyanide complexes in the absence of additional electrolytes:

$$Hg(CN)_2 > [Au(CN)_2]^- > [Ag(CN)_2]^- > [Ni(CN)_4]^{2-} > [Co(CN)_6]^{3-}$$

They attributed these results to the fact that the capacity was greater for ions with lower charge and larger size. Thus, the neutral molecule $Hg(CN)_2$ was adsorbed to a greater extent and could displace $Au(CN)_2^-$ on carbon surface.

McDougall *et al* [*27*] also confirmed the enhancing effect of the addition salts, even KCN, and acids on the gold capacity of coconut shell derived activated carbon. However it was found that ClO_4^- did not depress the gold adsorption capacity on carbon. Therefore, they suggested that the driving force for the adsorption of gold cyanide on coconut shell carbon was not simply electrostatic interactions in the electrical double layer or between $Au(CN)_2^-$ and positively charged sites on carbon surface. Gold adsorption capacity was dependent on temperature, which was contrary to normal anion-exchange behaviour.

McDougall *et al* [*27*] used XPS to investigate the nature of gold on adsorbed carbon surface and found that the gold atoms present on carbon surface had an oxidation number of 0.3. They also determined the nitrogen content of gold loaded carbon using elemental micro-analysis. The results showed that the amount of nitrogen was less than that required for the adsorption of gold as $Au(CN)_2^-$ anions and the ratio of gold to nitrogen was about 1 at high loading from either alkaline or acidic solutions. The authors suggested that the adsorption of aurocyanide on carbon from acidic or alkaline solutions, either in the presence or absence of electrolytes, might proceed by a reduction mechanism. They proposed a mechanism in which the gold cyanide was adsorbed as ion pair $M^{n+}[Au(CN)_2^-]_n$ (where M^{n+} is Na^+, K^+ and Ca^{2+} *et al*) in the initial adsorption stage followed by a reduction step in which either a sub-

stoichiometric $(AuCN)_x$ surface species or a cluster-type compounds of gold was formed.

Comparative studies [***30***] of the adsorption of $Au(CN)_2^-$, $Ag(CN)_2^-$ and $Hg(CN)_2$ onto activated carbon suggested that oxygen surface functional groups played an important role in the adsorption of $Au(CN)_2^-$ and $Ag(CN)_2^-$ but not in the adsorption of $Hg(CN)_2$. After the carbon was outgassed at 950 °C under vacuum the adsorption capacity for $Au(CN)_2^-$ and $Ag(CN)_2^-$ decreased by 50 % compared with untreated carbon. However in the presence of oxygen in solution, the outgassed carbon showed the same adsorption capacity as the untreated carbon. A dual mechanism for adsorption of $Au(CN)_2^-$ was proposed by Tsuchida *et al* [***30***]: cyanide complexes adsorbs on carbon surface by anion exchange with OH^- followed by the partial oxidation of $Au(CN)_2^-$ or $Ag(CN)_2^-$ to insoluble AuCN or AgCN by chemisorbed oxygen. The AuCN does not take part in the equilibrium between $Au(CN)_2^-$ in solution and on the carbon surface, thus allowing higher gold loading than on the deoxygenated carbon.

Cook *et al* [***45***] investigated the adsorption of $KAu(CN)_2$ on activated carbon and carbon black using microanalysis and X-ray photoelectron spectroscopy. They concluded that gold was adsorbed as Au(I) under all conditions used. They also confirmed that both $Au(CN)_2^-$ and AuCN would be present on the carbon. It was proposed that the adsorbed AuCN was generated through CN^- oxidation on carbon surface.

However other workers [***32***, ***42***, ***46***] confirmed the absence of any irreversible adsorbed species like AuCN or Au on their carbon by eluting all of the adsorbed gold with hot sodium hydroxide solutions. This could be achieved from carbons loaded from both alkaline and acidic solutions at room temperature [***42***]. Their results led

them to reject a mechanism in which the AuCN was assumed to be formed during adsorption.

Papirer *et al* [*47*] observed that the gold uptake was related to the content of basic groups in the non-modified carbons. Chemical modification to incorporate basic surface groups increased gold adsorption capacity noticeably. However the remaining question was whether these groups, probably of the pyrone type, intervene directly in the mechanism of $Au(CN)_2^-$ fixation, acting as a source of π electrons as suggested by electron spectroscopy [*33*], or if the same groups influence the distribution of π electrons in the graphene layers. Such repartition would facilitate the donation of electrons to the gold atoms suggested by Klauber [*31*].

The influence of oxygen on the adsorption of gold cyanide on activated carbon were also reported by other researchers [*48-51*]. Dixon *et al* [*48*] observed that less gold was adsorbed in the presence of nitrogen instead of air. They concluded that the exclusion of oxygen reduced the number of available adsorption sites on the carbon. From the changes in redox potential observed for charcoal in different solutions, Hughes *et al* [*49*] proposed an oxidation reduction mechanism for the loading of various anions. They suggested that the adsorption of complexes, such as $Au(CN)_2^-$, was controlled by the supply of an oxidant such as oxygen or quinone groups. van der Merwe *et al* [*50*] showed that considerable quantities of oxygen were consumed during the adsorption of anionic metal cyanides and that the lowering of the oxygen level in solution below the atmospheric equilibrium value of 8.2 mg/L, lowered the gold and silver adsorption capacity. They found that increasing the oxygen concentration beyond the atmospheric level increased the uptake of gold and silver only for some carbons. The authors suggested that the gold or silver cyanide was adsorbed in two ways: 1) where oxygen is required for the oxidation of carbon surface

functional groups used for adsorption, and 2) where the adsorption takes place without the use of oxygen. Peterson *et al* [***51***] showed that the oxygen played a role in the adsorption process only when oxygen-poor carbon used as an adsorbent.

The most recently developed mechanism which is widely accepted indicates the adsorption of gold cyanide in the graphitic structure. Jones *et al* [***32,33***] proposed that the $Au(CN)_2^-$ anion is adsorbed without change or chemical reaction in its normal linear form N≡C–Au–C≡N in a symmetrical environment parallel to the graphitic planes of the carbon. At pH 10 in the absence of free cyanide, the equilibrium adsorption and desorption isotherms for gold on Calgon GRC22 were identical. An Au:N molar ratio of 2 was determined on the loaded carbon using x-ray photoelectron spectroscopy (XPS). They suggested that $Au(CN)_2^-$ adsorbs reversibly via a weak carbon to gold π-donor complex. Cations have no direct role in this interaction except for H^+, where the adsorbed species is $Au_4(CN)_5^-$ and thus increases the adsorption capacity of the carbon. Cations M^{n+} (K^+, Na^+, Ca^{2+} *etc*) coadsorb at the carbon-solution interface but do not form identifiable ion pairs $M^{n+}[Au(CN)_2^-]_n$ on the carbon surface. There was no direct involvement of C-O groups in the adsorption of $Au(CN)_2^-$. The model for the adsorption on basal plane by the authors is shown in **Figure 3.4**.

Ibrado *et al* [***34***] studied the adsorption of gold cyanide on a series of carbonaceous adsorbents, including lignite, coals, anthracite, carbon black, graphite and activated carbon which covered wide variation of composition, surface acid groups content and degree of graphitisation. They found that the adsorption of gold cyanide was not related to the amounts of oxygen groups on the surface and total oxygen content of the materials. The amounts of adsorbed gold cyanide showed very strong correlation with the degree of graphitisation of the adsorbents, indicating that

the graphene layers play the most important role. They suggested that the adsorption of gold cyanide occurs on the graphene layers of the activated carbon.

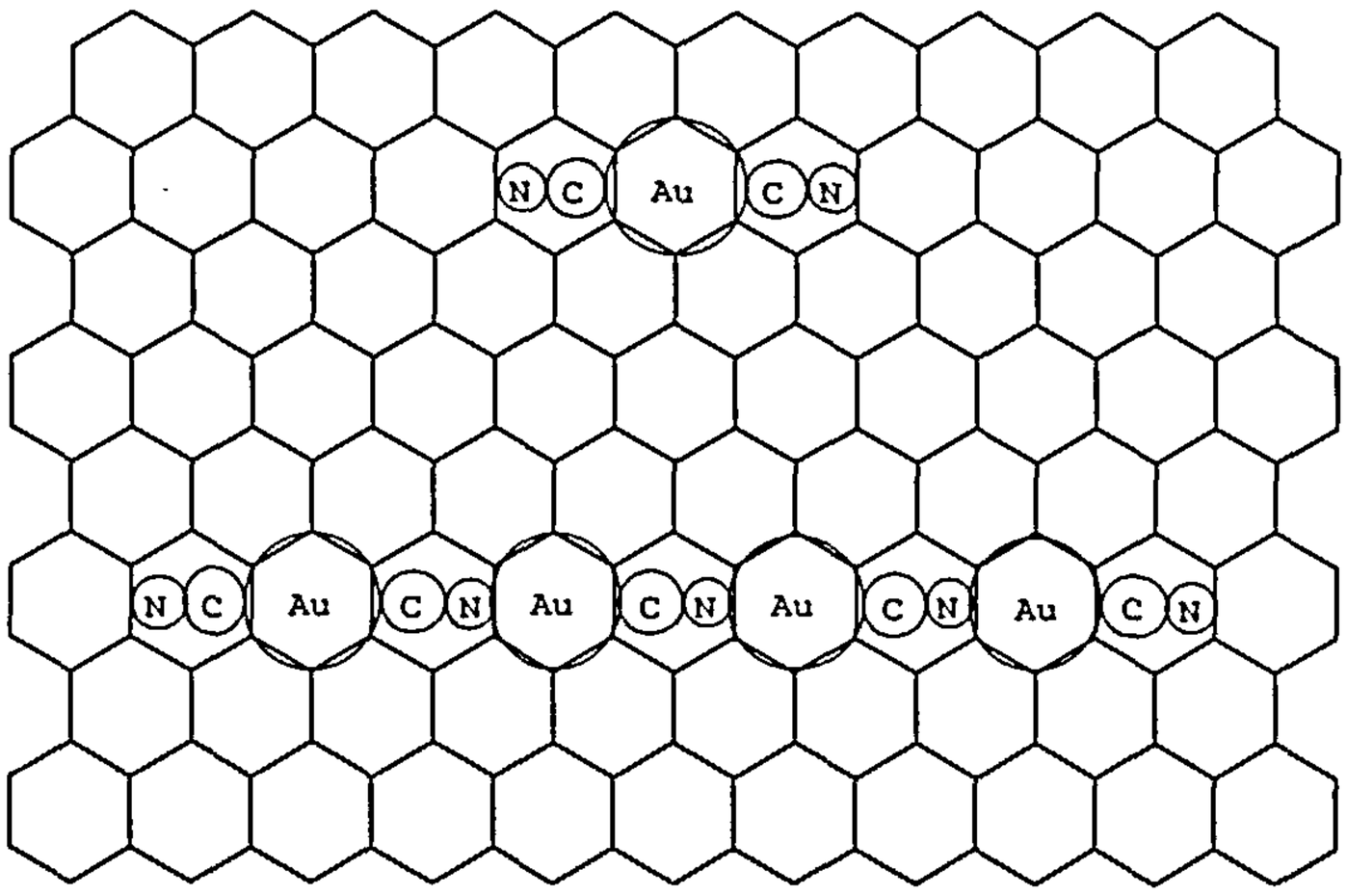

Carbon-$Au(CN)_2^-$

Au-C 2.12 Å
C-N 1.17 Å

Carbon-$Au_4(CN)_5^-$

Au-Au 5.09 Å
Au-N 1.97 Å
Au-C 1.97 Å
C-N_b 1.15 Å
C-N_t 1.17 Å

Figure 3.4 A model of aurocyanide species $Au(CN)_2^-$ and $Au_4(CN)_5^-$ adsorbed on the basal plane [*32,33*].

Klauber [*31, 35*] investigated the adsorption of $Au(CN)_2^-$ on activated carbon using XPS and found that $Au(CN)_2^-$ was adsorbed on the carbon surface without chemical change. Both of the nitrogen atoms were shown to exist in identical chemical environments which precluded any preferential interaction with the substrate by one of the terminal N atom. He suggested that $Au(CN)_2^-$ was adsorbed via π electron donation from the basal planes of the activated carbon to the central gold atom. The net charge transfer was estimated to be 0.3 - 0.5 of an electronic charge. Additional charge was also transferred to the terminal nitrogen atoms on the cyanide units, however, the nitrogen atoms did not appear to be directly involved in the adsorption. Although cations were assumed to coadsorb with $Au(CN)_2^-$, the formation

of an intimate ion pair $M^{n+}[Au(CN)_2^-]_n$ need not occur due to the nature of the highly conductive graphitic substrate. The tetramer $Au_4(CN)_5^-$ was formed by acid induced oligomerisation of $Au(CN)_2^-$ after loaded carbon was treated with hydrochloric acid. This complex bound to the basal planes by four π donor bonds to the four gold centres.

Kongolo *et al* [*52*} using Mössbauer showed that the state of the adsorbate largely depended on whether and how the samples were dried after the adsorption. They found that gold was adsorbed as $Au(CN)_2^-$ at pH 1 ~ 10. The results were explained by the π donation from carbon to gold atom. AuCN species were not found to be present on the wet carbon for the adsorption from the solution with pH 1 ~ 4. AuCN formed only on removal of virtually all of the water from the pores of the carbon by drying either in vacuum or at elevated temperatures. The coadsorbed polyvalent cations (Ca^{2+}, Gd^{3+}) were found to have no influence on Mössbauer parameters of the adsorbed gold complex. However, the absence of such an influence, according to the authors, did not rule out $M^{n+}[Au(CN)_2^-]_n$ adsorption. The effect of the cation on the electronic state of the gold may be too small to be detected.

Groszek *et al* [*36*] investigated the heats of adsorption of gold complex on carbons using flow microcalorimetry (FMC) and found that the heats of adsorption of $NaAu(CN)_2$ per unit area of graphitised carbon black were close to those of the coconut shell active carbon. They suggested that the driving force for the preferential adsorption of $Au(CN)_2^-$ was its affinity for the graphitic basal planes. As the graphitised carbon possesses only a very small amount of polar surface sites, the adsorption of $Au(CN)_2^-$ was ascribed to the formation of a surface complex of gold compounds with the basal plane surface of the graphite. It was further suggested that

the formation of these complexes was responsible for the strong adsorption of gold compounds on the surface of active carbon, a high proportion of which is constituted by basal plane sites.

The XPS and IR results by Ibrado *et al* [*37*] were consistent with the adsorption of gold cyanide by a weak donation of π electrons from activated carbon to gold. No evidence was found to support the ion-pair adsorption model so the authors suggested that the adsorbed species was most likely the unpaired dicyano complex.

3.1.4 Factors Influencing the Adsorption Capacity and Rate

A. Effect of pH

The pH of the gold solution is one of the most important factors influencing gold adsorption. Davidson [30] found that the adsorption capacity and rate decreased as the pH of solution increased. Fleming *et al* [*53*] showed that the pH value of solution had a marked effect on equilibrium loading, especially at pH < 7, which was in agreement with the observations of McDougall *et al* [*27*]. The rate of adsorption also increased slightly in acid solution. Other researchers [*19,23,30*] also observed that the adsorption of gold and silver was enhanced by the acidity of solution.

B. Effect of Ions

The cations present in solution were found to be able to increase the adsorption capacity of gold cyanide complex on activated carbon [16-19]. The strength of the adsorption of ion pair $M^{n+}[Au(CN)_2^-]_n$ follows the order:

$$Ca^{2+} > Mg^{2+} > H^{+} > Li^{+} > Na^{+} > K^{+}$$

Adams *et al* [*19*] and Fleming *et al* [*53*] found that the loading rate and adsorption capacity increased with increasing cation concentration. However, the effect on the adsorption capacity is much greater than that on the rate of adsorption.

The reports on the effects of anions were controversial. McDougall *et al* [*27*] found that ClO_4^- present in the solution even in large concentration, did not depress the gold adsorption capacity on the carbon. However the same authors [*17-19*] later reported that an excess of ClO_4^- resulted in a depression of aurocyanide loading.

Cho *et al* [*23*] reported that free cyanide caused a decrease in the adsorption of silver cyanide on charcoal. They ascribed it to the competitive adsorption between the cyanide ion and the silver cyanide ion for the active adsorption sites. Fleming *et al* [*53*] observed the an increase in the concentration of free cyanide depressed the rate of adsorption and adsorption capacity of gold on activated carbon.

C. Effect of Temperature

Dixon *et al* [*48*] and McDougall *et al* [*19,27*] found that the adsorption of gold cyanide was exothermic. Therefore the adsorption capacity decreased with increasing temperature. Fleming *et al* [*53*] reported that the increase in the adsorption rate with temperature was fairly small, in common with most diffusion-controlled processes.

3.1.5 Elution of Gold from Carbon

The adsorbed gold on carbon can be eluted using chemical reagents such as sodium sulphide/sodium sulphite/sodium hydroxide [*8*], boiling sodium

cyanide/sodium hydroxide [*9*] and pressure leaching at 150 °C with sodium cyanide/sodium hydroxide [*54*].

Two main techniques of elution are used in industry:

(1) Zadra process [*8*,*9*], in which warm cyanide solution is circulated through an elution column and electrowinning cell.

(2) The Anglo-American Research Laboratory (AARL) method, consisting of a pre-treatment step with hot caustic cyanide solution, followed by elution with hot deionised water. An Australian invention [*55*,*56*] which involved the use of organic solvents is also applied in industry.

Davidson *et al* [*57*,*58*] studied the elution of gold from activated carbon using water as the eluant and found that the temperature was the most critical parameter. The pre-treatment of gold loaded activated carbon with a relatively strong sodium cyanide solution prior to elution with deionised water at 90 ~ 125 °C had a beneficial effect on the elution of gold. It was demonstrated that the use of 0.5 bed volume of a pre-treatment agent comprising 10 % of NaCN and 1 % NaOH resulted in a virtually 100 % recovery of gold, silver and base metals on subsequent elution with demonised water. The elution process took a relatively short time about 14 hours at 90 °C or 3 hours for pressure elution at 125 °C. If the loaded carbon contains high levels of calcium carbonate, treatment with acid is to remove calcium carbonate which was known to foul the carbon in the adsorption circuit and to have a deleterious effect on the efficiency of elution. This procedure is currently in use on most CIP plants. McDougall [*59*] patented a process in which carbon was periodically removed from the adsorption circuit and treated with hot acid and then returned to the adsorption circuit.

McDougall *et al* [*27*] reported that the adsorbed gold can be effectively eluted only if an anion which could form strong complexes with gold (*e.g.* CN^-, SCN^-) was present in the eluent, or if the carbon was pre-treated with CN^- prior to its elution with hot water. Adams *et al* [*42*] found that gold could be eluted almost completely from carbon with a sodium hydroxide solution in absence of cyanide. Moreover, this could be achieved with carbons loaded with gold from both acidic and alkaline conditions and with carbons loaded to a very high gold concentrations. It was proposed that aurocyanide adsorbed on activated carbon was converted to AuCN by boiling the carbon in acid. When the carbon was subsequently treated with hot sodium hydroxide, the AuCN decomposed according to the reaction:

$$2\ AuCN + e \rightarrow Au^0 + Au(CN)_2^-\ \ (E^0 = 0.252\ V) \qquad (3.12)$$

This reaction only occurs in alkaline solution and not after treatment with boiling acid, possibly because of the formation of a more mobile intermediate species, such as $AuCNOH^-$ ion. In contrast, when the carbon was boiled in water instead of in hydroxide after the treatment with hot acid, no X-ray diffraction peaks for metallic gold were observed. The authors attributed the elution effects of sodium hydroxide to the formation of a hydrophilic, negatively charged surface which shows lower affinity for neutral species as well as anions, according to the following reaction:

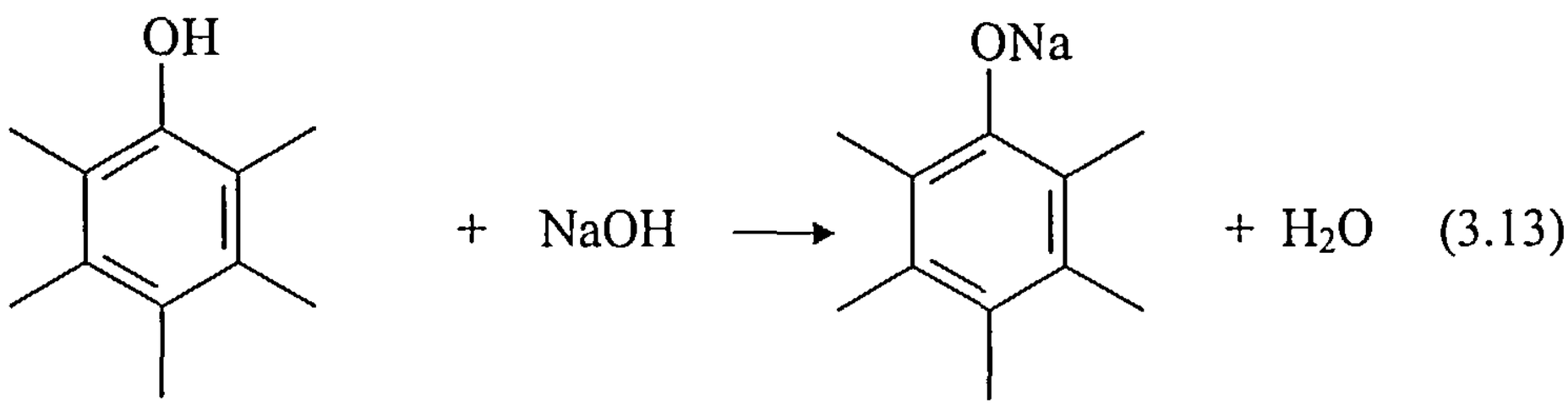

(3.13)

This was supported by the results of zeta-potential studies [***23,28,60***] which showed that the negative potentials of activated carbons increased with increasing pH possibly due to the specific adsorption of OH^- ions onto the carbon surface with Na^+ ions located in the outer Helmholtz layer.

Cyanides are usually used for the elution of gold from activated carbon. Tsuchida *et al* [***23,29,30***] suggested that there was a competitive ion exchange of CN^- for $Au(CN)_2^-$. They attributed the enhancement of elution in the presence of polar organic solvents to the increase in the activity of the CN^- ion in polar organic solvents relative to water. However, Adams *et al* [***42***] believed that the ion exchange mechanism was relatively unimportant and suggested that cyanide was involved in the specific chemical reactions on the carbon surface:

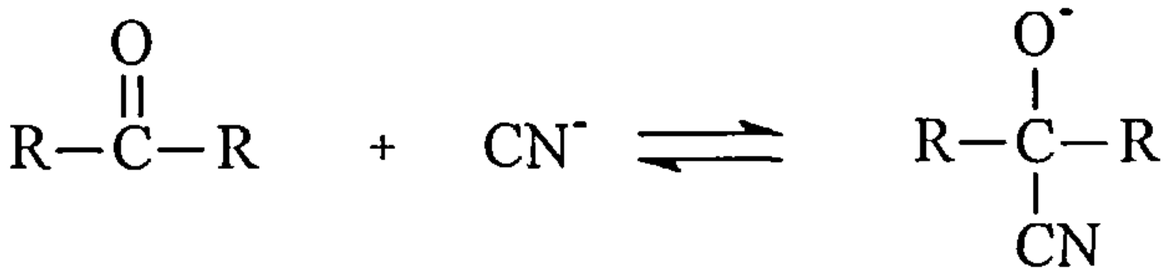

(3.14)

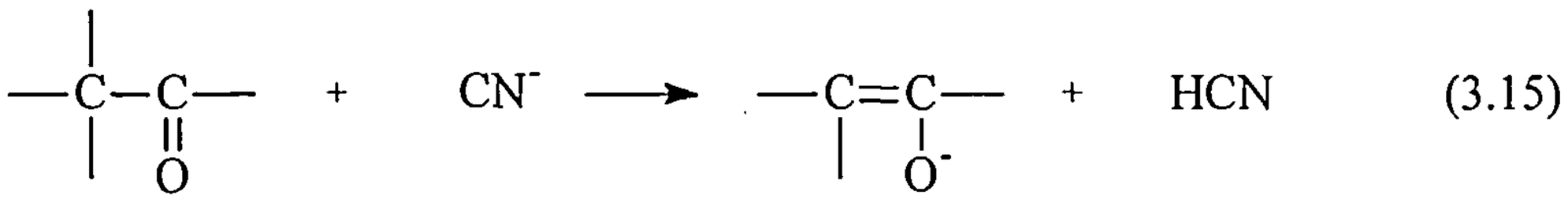

(3.15)

They proposed that these reactions could take place with carbonyl groups on the carbon surface under elution conditions, thereby increasing the negative charge density on the surface and resulting in faster elution kinetics for cyanide than hydroxide. van Deventer *et al* [***61***] also ascribed the elution of gold using CN^- to the above reactions.

3.1.6 Current Situation

Extensive research on the mechanism of adsorption of gold cyanide species on activated carbon during the past decades has not reached a consensus view of the mechanism. The main problems remaining requiring clarification are 1) the mechanism of the adsorption of gold cyanide species on the active carbon, where and how the gold cyanide species are adsorbed on the surface of activated carbon and what form of gold cyanide species are adsorbed; 2) how does the adsorption capacity relate to the porous structures and surface chemical structures of the activated carbon. Most researchers recently tend to believe that the gold cyanide species are adsorbed on graphene layers in the form of ion pairs however no direct evidence has been provided to prove the theory. Most of the studies using ex-situ spectroscopy methods such as FTIR are meaningless since one cannot tell whether the spectra were recorded from the adsorbed species or from the precipitated $KAu(CN)_2$ after drying of activated carbon with residual solution trapped in the pores. It is also hard to differentiate adsorbed $Au(CN)_2^-$ from solution species in in-situ FTIR because the shift of wave number is lower than the spectral resolution. In a recent study using FMC [*62*] it was found that the adsorption of gold cyanide species comprises of two parts: reversible adsorption and irreversible adsorption with the extent of irreversibility varying depending on carbon types. The irreversible adsorption occurs as an unpaired anion $Au(CN)_2^-$ through electrostatic interactions on the active surface functional groups sites which have polar character. The graphene layer sites are occupied by the ion-paired neutral molecule species $KAu(CN)_2$ through the action of van der Waals forces and account for the reversible adsorption.

If the graphene layers are the main sites for the adsorption of gold cyanide species, a relationship between the pore volume or surface area and the adsorption capacity could be established since the surface of unmodified activated carbon is predominantly hydrophobic graphene layers. There should also be a relationship between the adsorption capacity and pore size distribution. However no such relationship has been established yet.

3.2 Adsorption of Heavy Metal Ion Pollutants from Water

3.2.1 Introduction

The presence of most heavy metals in surface water and wastewater is generally associated with industrial discharges. The tremendous increase in the use of heavy metals over the past few decades has inevitably resulted in an increased flux of metallic pollutants in aquatic environment. The trace heavy metals in water are a significant environmental problem because they are non-degradable and therefore persistent. The removal of heavy metal pollutants at high concentration from water can be readily accomplished by chemical precipitation or electrochemical method. At low concentration, the removal of these pollutants is more effective by ion-exchange or adsorption on solid adsorbents such as activated carbon. Activated carbon is widely used for the adsorption of environmentally unfriendly species. It is a good adsorbent for the removal of organic pollutants from water and wastewater while the information available on the adsorption of inorganic species by activated carbon, specifically metallic ions, is markedly limited. The adsorption of organic species from either gas phase or liquid phase is predominantly determined by the porous structures.

In contrast, the adsorption of inorganic or ionic species from solution is usually dominated by the surface functional groups [*63*].

3.2.2 Adsorption of Cationic Heavy Metal Species on Activated Carbon

Cadmium (II), lead (II), copper (II), nickel (II), zinc (II), cobalt (II) are the most common heavy metal cations present in water and wastewater. The systematic study on the adsorption of cadmium on activated carbon was first reported by Huang *et al* [*64*] using several different activated carbons. They investigated the influence of various factors such as pH, nature of carbon surface, carbon dose and additional chelating agents, on the adsorption of cadmium (II). The amount of Cd (II) adsorbed was found to increase with increasing pH of the solution. At pH < 3 little Cd (II) was adsorbed but the adsorption increased appreciably at higher pH and became more or less constant at pH > 8. They also observed that the efficiency of adsorption of cadmium on carbon increased appreciably in the presence of chelating agents such as nitrilotriacetate (NTA) and ethylene diamine tetraacetate (EDTA). With the additional of 1 % of chelating agent on the weight of cadmium in solution, the efficiency of the carbon to remove Cd (II) increased from 20 to 40 % at pH 7. This increased adsorption was attributed to the formation of univalent cadmium complex anions which were adsorbed on the carbon positive sites.

Netzer *et al* [*65*] studied the adsorption of Cu^{2+}, Pb^{2+} and Co^{2+} on activated carbons and found that the solution pH was the most important parameter affecting the adsorption. At pH 2 the adsorption was insignificant for all the three metals while there was a slight improvement in metal adsorption at pH 3. The adsorption increased

dramatically at pH 4. The onset of adsorption for the three metals occurred before the beginning of hydrolysis (at concentration of 10^{-5} N, pH 6 for Pb^{2+} and Cu^{2+}, pH 8 for Co^{2+}). There was a competitive adsorption when two or three metals were present in the solution, indicating these metal cations were adsorbed on the same surface site. The adsorption capacity of Pb^{2+} was twice as much that of Cu^{2+} and approximately 10 times as much that of Co^{2+}.

Corapcioglu *et al* [*66*] investigated the adsorption of Cu^{2+}, Pb^{2+}, Ni^{2+} and Zn^{2+} on hydrous activated carbon. They found that the amounts of Cu^{2+} removed increased appreciably as the temperature increased from 25 to 100 °C, for example, at pH 3 the percentage of Cu^{2+} removal increased from 15 to 60 %. Since the adsorption is an exothermic reaction, the observation apparently is not in agreement with thermodynamic principle. One possible explanation suggested by the authors was that at elevated temperature, the H-carbon became oxidised and progressively converted to a L-carbon thereby increasing the Cu^{2+} removal capacity. The free metal cations M^{2+} and their hydroxo species, $M(OH)_y^{2-y}$ were suggested to be involved in the adsorption reaction by a surface complex formation model. For L-type carbon, its surface mainly displays $\underline{C}OH$ and $\underline{C}O^-$ hydroxo groups and the surface complex formation could be described by the following general equations [*66*]:

$$2(\underline{C}OH) + M^{2+} \rightleftharpoons (\underline{C}O^-)_2M^{2+} + 2H^+ \quad (3.16)$$

$$2(\underline{C}O^-) + M^{2+} \rightleftharpoons (\underline{C}O^-)_2M^{2+} \quad (3.17)$$

$$2(\underline{C}OH) + MOH^+ \rightleftharpoons (\underline{C}O^-)_2MOH^+ + 2H^+ \quad (3.18)$$

$$2(\underline{C}O^-) + MOH^+ \rightleftharpoons (\underline{C}O^-)_2MOH^+ \quad (3.19)$$

They proposed that the hydrogen bonding interaction between surface oxygen atom and the hydrogen atom of the hydrated metal ions was the more probable bonding mechanism.

Ferro-Garcia *et al* [*63*] investigated the adsorption of Zn^{2+}, Cd^{2+} and Cu^{2+} on H-type activated carbons prepared from agricultural by-products almond shells, olive stones and peach stones. It was found that at low pH the adsorption was negligible while at pH 3-5 the adsorption increased sharply, reaching a plateau at higher pH. They explained the results on the basis of the changes of the carbon surface charge at different pH. At low pH, electrostatic repulsion between cations and the positively charged surface of the carbon would take place. As the pH increased, metal cations would replace hydrogen ions from the carbon surface and therefore the adsorption was increased. The effects of temperature on the adsorption was also investigated. It was observed that the adsorption capacities of Zn^{2+} and Cd^{2+} on all three carbons were higher at 293 K than that at 313 K and this was attributed to the exothermic adsorption process. The adsorption capacities of Cu^{2+} on almond shell carbon and peach stone carbon at 293 K were lower than that at 313 K while for olive stone carbon the isotherms at two temperatures showed a crossing point. This was ascribed to that the process was endothermic. The amounts of metals adsorbed on the carbons were in following order: $Cd^{2+} < Zn^{2+} < Cu^{2+}$, which was explained on the basis of their ionic radii. The radii of the hydrated cations are: Cu^{2+} = 0.419 nm, Zn^{2+} = 0.430 nm, Cd^{2+} = 0.426 nm. Therefore the Cu^{2+} ion has a greater accessibility to the surface of certain pores than the other two cations, which led to the higher adsorption capacity. The lower adsorption capacity of Cd^{2+} compared with Zn^{2+} was ascribed to its smaller polarising power, according to the authors. The same researchers [*63*] also found that the presence of Cl^-, CN^- or SCN^- in solution increased the adsorption capacity while

EDTA present in metal ion solutions decreased the adsorption. This is due to the formation of complex anions which would be preferentially adsorbed by the H-type carbon with positive charge potential.

The adsorption of heavy metal cationic species from aqueous solution is influenced by various factors such as pH of solution, surface functionality and chemical modification procedures. Extensive work has been carried out on general studies of adsorption of heavy metal species on carbons from various precursors and the effect of concentration, pH, carbon dosage on the adsorption capacity and breakthrough point for the dynamic adsorption through carbon bed. The mechanism of the adsorption of heavy metal species was not fully understood especially the adsorption sites on the carbon surface and the effect of oxygen and nitrogen functionality incorporated by chemical modification. The mechanism of interaction between the heavy metal cation species with functional groups remains unclear. Thus further investigation into the adsorption mechanism is necessary to make the involvement of functionality well understood.

References

1. Lazowski, M. *Chem. Gas.*, **1848**, *6*, 43.
2. Davis, W. N. *U.S. Patent*, **1880**, 227,963.
3. Adamson, R. J. *Gold Metallurgy in South Africa*, Chamber of Mines of South Africa, Johannesburg, **1972**, p88.
4. Johnson, W. D. *U.S. Patent*, **1894**, 522,260.
5. Hall, K. B. *World Min.* **1974**, *27*(12), 44.
6. Kudryk, V. and Kellogg, H. H. *J. Metals* **1954**, *6*(5), 541.
7. Nicol, M. J.; Fleming, C. A. and Paul, R. L. In *The Extractive Metallurgy of Gold in South Africa*, Edited by Stanley, G. G., **1987**, *M7*, 831.
8. Zadra, J. B. *A Process for the Recovery of Gold from Activated Carbon by Leaching and Electrolysis*, U.S. Bureau of Mines, Washington, D. C., R. I. No. 4672, **1950**.
9. Zadra, J. B.; Engel, A. K. and Heinen, H. J. *A Process for Recovering Gold and Silver from Activated Carbon by Leaching and Electrolysis*, U.S. Bureau of Mines, Washington, D. C., R. I. No. 4843, **1952**.
10. Green, M. *Trans. Inst. Min. Metall.*, **1913-1914**, *23*, 65.
11. Feldtmann, W. R. *Inst. Min. Metall.*, **1914-1915**, *24*, 329.
12. Edmands, H. R. *Inst. Min. Metall.*, **1917-1918**, *27*, 277.
13. Allen, A. W. *Metall. Chem. Eng.*, **1918**, *18*(12), 642.
14. Williams, L. B. *Min. Mag.*, London, **1923**, *23*, 139.
15. Gross, J and Scott, J. W. U.S. Bureau of Mines, Washington, D. C., Technical Paper No. 378, **1927**.
16. Davidson, R. J. *J. S. Afr. Inst. Min. Metall.*, **1974**, *75*(4), 67.
17. McDougall, G.J.; Adams, M.D. and Hancock, R.D., *Hydrometallurgy*, **1987**, *18*, 125.
18. Adams, M.D.; McDougall, G.J. and Hancock, R.D., *Hydrometallurgy*, **1987**, *18*, 139.
19. Adams, M.D.; McDougall, G.J. and Hancock, R.D., *Hydrometallurgy*, **1987**, *19*, 95.
20. Cho, E.H.; Dixon, S.N. and Pitt, C.H., *Metall., Trans.*, **1979**, *10B*, 185.

21. Cho, E.H. and Pitt, C.H., *Metall., Trans.*, **1979**, *10B*, 165.
22. Cho, E.H. *Adsorption of Silver Cyanide on Activated Carbon*, PhD Thesis, University of Utah, **1978**.
23. Cho, E.H. and Pitt, C.H., *Metall., Trans.*, **1979**, *10B*, 159.
24. Garten, V. A. and Weiss, D. E. *Rev. Pure Appl. Chem.*, **1957**, *7*(June), 69.
25. Plaksin, I. N. *Metallurgy of Noble Metals*, Metallurgizolat, **1958**.
26. Dixon, S.; Cho, E. J. and Pitt, C. H. *The Interaction Between Gold Cyanide and High Surface Area Charcoal*, AIChE Meeting, Chicaco, IL, **1976**.
27. McDougall, G.J.; Hancock, R.D.; Nicol, M.J.; Wellington, O.L. and Copperthwaite, R.G., *J. S. Afr. Inst. Min. Metall.*, **1980**, *80*, 344.
28. Tsuchida, N.; Ruane, M. and Muir, D. M. *MINTEK 50, Proc. of the Int. Conf. on Mineral Science and Technology*, Edited by Haughton, L. F., Council for Mineral Technology, Randburg, South Africa, **1984**, *2*, 647.
29. Tsuchida, N. and Muir, D.M., *Metall. Trans.*, **1986**, *17B*, 523.
30. Tsuchida, N. and Muir, D.M., *Metall. Trans.*, **1986**, *17B*, 529.
31. Klauber, C., *Surface Science*, **1988**, *203*, 118.
32. Jones, W.G.; Klauber, C. and Linge, H.G. In *Randol Conference on Gold and Silver,* Perth, Australia, Randol International, Golden Co, **1988**, p. 243.
33. Jones, W.G.; Klauber, C. and Linge, H.G. In *Proceedings of 19th Biennial Carbon Conference*, American Carbon Society, Pennsylvania State University, **1989**, p.38.
34. Ibrado, A.S. and Fuerstenau, D.W., *Hydrometallurgy*, **1992**, *30*, 243.
35. Klauber, C., *Langmuir*, **1991**, *7*, 2153.
36. Groszek, A.J. and Partyka, S., Cot, D., *Carbon*, **1991**, *29*, 821.
37. Ibrado, A.S. and Fuerstenau, D.W., *Minerals Engineering,* **1995**, *8*(4/5), 441.
38. Frumkin, A. *Kolloid Z.*, **1930**, *51*, 123.
39. Frumkin, A.; Burshtein, B. and Lewin, P. *Z. Phys. Chem.*, **1931**, *157A*, 422.
40. Burshtein, B. and Frumkin, A. *Z. Phys. Chem.*, **1929**, *141A*, 219.
41. Kuzminykh, V. M. and Tjurin, N. G. *Izv. Vyssh. Ucheb. Zaved., Tsvet. Metall.*, **1968**, *11*(4), 65.
42. Adams, M.D. and Fleming, C.A., *Metall Trans.*, **1989**, *20B*, 315.
43. Anderson, T. N. and Bockris, J. O'M. *Electrochim. Acta*, **1964**, *9*(4), 347.

44. McDougall, G.J.and Hancock, R.D. *Gold Bull.*, **1981**, *14*, 138.
45. Cook, R.; Crathorne, E.A.; Monhemius, A.J. and Perry, D.L., *Hydrometallurgy*, **1989**, *22*, 171.
46. Cashion, J.D.; McGrath, A.C.; Volz, P. and Hall, J.S., *Trans. Inst. Min. Metall.*, **1988**, *97*, 129.
47. Papirer, E.; Polania-Leon, A.; Donnet, J.B. and Montagnon, P., *Carbon*, **1995**, *33*, 1131.
48. Dixon, S.; Cho, E.H. and Pitt, C. H., *A. I. Ch. E. Symposium Series*, **1978**, *74*(173), 75.
49. Hughes, H. C.; Muir, D. M.; Tsuchida, N. and Dalton, R., *Regional Conference on Gold-Mining, Metallurgy and Geology*, Aus. I,M.M., Perth, **1984**, 151.
50. van der Merve, P. F. and van Deventer, J. S. J., *Chem. Eng. Comm.*, **1988**, *65*, 121.
51. Petersen, F. W. and van Deventer, J. S. J., *Chem. Eng. Sci.*, **1991**, *46*, 3053.
52. Kongolo, K.; Bahr, A.; Friedl, J. and Wagner, F. E., *Metallurgical Transaction B*, **1990**, *21B*, 239.
53. Fleming, C. A. and Nicol, M. J., *J. S. Afr. Inst. Min. Metall.*, **1984**, *84*, 85.
54. Ross, J. R.; Salisbury, H. B. and Potter, G. M., *AIME Annual Meeting,* Chicago, Feb-Mar, **1973**.
55. Muir, D. M.; Hinchliffe, W. D.; Tsuchida, N. and Ruane, M., *Hydrometallurgy*, **1985**, *14*, 47-65.
56. Muir, D. M.; Hinchliffe, W. D. and Griffin, A., *Hydrometallurgy*, **1985**, *14*, 151-169.
57. Davidson, R. J. and Duncanson, D., *J. S. Afr. Inst. Min. Metall.*, **1977**, *77*, 254-261.
58. Davidson, R. J. and Veronese, V., *J. S. Afr. Inst. Min. Metall.*, **1979**, *79*, 437-445.
59. McDougall, G J., *S. A. Patent*, No. 4-528-166, July, **1985**.
60. Gupta, A.; Ofori-Ansah, K., *Proc. Australas. Inst. Min. Metall.*, **1984**, No. 289, 239-245.
61. van Deventer, J. S. J. and van der Merwe, *Metallurgical and Materials Transaction B*, **1994**, *25B*, 829-838.

62. Lagerge, S., Zajac, J, Partyka, S and Groszek, A.J., *Langmuir*, **1999**, *15*, 4803-4811.

63. Ferro-Garcia, M.A.; Rivera-Utrilla, J.; Rodriguez, J. and Bautista-Toledo, I., *Carbon* **1988**, *26*, 363.

64. Huang, C. P. and Ostovic, F., *J. Environ. Engg. Div. Am. Soc. Civ. Engrs.*, **1978**, *104*, 863.

65. Netzer, A. and Hughes, D. E., *Water Res.* **1984**, *18*, 927.

66.Corapcioglu, M.O. and Huang, C.P. *Water Research* **1987**, *21*, 1031.

Chapter 4

OBJECTIVES

4.1 Overall Objectives

The overall objectives of this study were 1) to investigate the mechanism of adsorption of gold and silver cyanide anionic species and heavy metal cationic species from aqueous solution on activated carbon, 2) to establish the relationship between the adsorption of these anionic and cationic metal species and the porous structure and surface functionality of the activated carbon, 3) to understand the adsorption mechanism of cationic and anionic metal species on active carbon.

4.2 Specific Objectives

4.2.1 Preparation of Activated Carbon With Various Functionality

PAN Carbon

To produce activated carbon with high nitrogen contents and with well developed porosity from polyacrylonitrile (PAN).

Nitric Acid Oxidation Treatment

To incorporate various oxygen functional groups into the coconut shell derived activated carbon by oxidation treatment using aqueous nitric acid.

Heat Treatment of Oxidised Carbon

To prepare a suite of activated carbons with various oxygen functionality by heat treatment of the oxidised carbon in helium at elevated temperature to progressively eliminate the oxygen functional groups of various thermal stability.

Ammonia Treatment

To incorporate nitrogen functional groups into the structure of the activated carbon by treating the carbon in ammonia at elevated temperature.

4.2.2 Characterisation of the Carbons

1. To characterise the porosity structures of the carbons using gas adsorption techniques;
   a) Determination of surface area and micropore volume using carbon dioxide adsorption at 273 K;
   b) Determination of total pore volumes using nitrogen adsorption at 77 K;
2. a) Determination of the C, H, O, N content;
   b) To identify the chemical structures of the oxygen and nitrogen functional groups incorporated by chemical modification, activation process or inherited from precursors;
   c) Characterisation of the surface oxygen functionality of carbons by using FTIR, TPD and titration;
   d) Characterisation of the surface nitrogen functionality of carbons by XANES, FTIR and TPD.

4.2.3 Adsorption on the Activated Carbons

1. To study the adsorption isotherms of gold and silver cyanide anionic species on a suite of active carbons with varying extents of activation;
2. To investigate the effects of oxygen and nitrogen functional groups in active carbon on the adsorption of gold and silver cyanide anionic species;
3. To study the adsorption isotherms of heavy metal cationic species on active carbons;
4. To investigate the role of functional groups on the adsorption of metal cationic species by the incorporation of surface functional groups in active carbons by chemical treatment procedures;
5. To study the ion exchange properties of the functionalised active carbons and changes of pH during the adsorption process;
6. To study the adsorption/desorption reversibility and enthalpies of the adsorption/desorption of cadmium ions on various carbons using flow microcalorimetry (FMC).

Chapter 5

EXPERIMENTAL

5.1 Materials Used

5.1.1 Reagents and Gases

Reagents

Materials	*Supplier*	*Purity*
Buta-1-nol	Aldrich, UK	99.8 % HPLC grade
$Ca(NO_3)_2 \cdot 4H_2O$	Aldrich, UK	99 %
$Cd(NO_3)_2 \cdot 4H_2O$	Aldrich, UK	98 %
$Cu(NO_3)_2 \cdot 2.5H_2O$	Aldrich, UK	98 %
Ethanol	Aldrich, UK	HPLC grade
H_3BO_3	Aldrich, UK	99.5 %
HCl	Fisons Ltd., UK	35.5-37.5 % wt
HNO_3	Aldrich, UK	70 %
KCl	Fisons Ltd., UK	99.5 %
KCN	BDH, Merck Ltd., UK	96 %
$KAg(CN)_2$	BDH, Merck Ltd., UK	99 %
$KAu(CN)_2$	Aldrich, UK	98 %
NaCl	Aldrich, UK	99 %

NaOH	Aldrich, UK	97 %
$Ni(NO_3)_2 \cdot 6H_2O$	BDH, Merck Ltd., UK	98 %
PAN	Aldrich, UK	
Pyridine	Aldrich, UK	99.8 %

Gases

Gases	***Supplier***	***Grade***	***Purity***
Air	BOC, UK	Compressed air	-
Ammonia	BOC, UK	N 3.8	99.9 %
Argon	BOC, UK	N 4.9	99.0 %
Carbon dioxide	BOC, UK	N 3.5	99.9 %
Helium	BOC, UK		
Nitrogen	BOC, UK	N 4.8	99.9 %
Oxygen	BOC, UK	N 2.6 (zero)	99.6 %

5.1.2 Commercial Activated Carbons

Four commercially available activated carbons were used in the experiments. C1, C2 and C3 were coconut shell derived active carbons whereas P1 was a peat based carbon. All these activated carbons were previously activated in a rotary kiln furnace using steam between 1173 - 1223 K to increasing extents of activation. All the commercial activated carbon were ground to give a size fraction of 0.212 - 0.600 mm and Soxhlet extracted with water to remove water soluble substance prior to use.

5.1.3 Polyacrylonitrile (PAN) Derived Carbons

Polyacrylonitrile (PAN) was pretreated under air at 250 °C for 1 hr. The pretreated PAN was heated at a rate of 30 °C min^{-1} to 900 °C under argon in a vertical furnace. The argon flow was then changed to carbon dioxide and the carbon gasified for about 4 hours at 900 °C. This gave a carbon burn-off ~60 %. PAN1 and PAN2 correspond to carbon with 63 and 60 wt% burn-offs, respectively.

5.1.4 Nitric Acid Oxidised Carbon and Heat Treatment Derivatives

Carbon C1 was chemically modified by oxidation using nitric acid in order to introduce various oxygen functional groups on the carbon surface. The procedure was as follows: carbon C was refluxed in 7.5 M HNO_3 solution (C:HNO_3 ratio = 1:5) for 4 hours and 48 hours respectively. The oxidised carbons were Soxhlet extracted with water to remove residual HNO_3 and other soluble materials and vacuum dried at 75 °C. The resultant carbons for oxidation for 4 and 48 hours were designated sample code CN1 and CN2 respectively.

Heat treatments of CN1 and CN2 were conducted at 10 °C min^{-1} under flowing helium to the desired temperature and held for 1 hour at the maximum temperature. The resultant carbons were designated as the code of original carbon followed by a number to indicate the heat treatment temperature in °C, e.g. CN1-300 represents CN1 heat treated to 300 °C and held at the heat treatment temperature (HTT) for 1 hour. Neutralisation treatment of CN2 with NaOH was carried out by mixing CN2 with 0.2 N of NaOH solution and refluxing for 8 hours. The carbon was then Soxhlet extracted with water and vacuum dried at 75 °C.

5.1.5 Ammonia Treatment of the Carbons

Carbon C1 and CN2 were treated with ammonia using the following procedure: carbon C1 and CN2 were heated to 800 °C at a rate of 3 °C min^{-1} in the flowing ammonia and held at maximum temperature for 3 hours. The treated carbon was cooled in flowing ammonia to room temperature and Soxhlet extracted with water. The sample was vacuum dried at 75 °C and designated sample code CA and CNA respectively.

5.2 Characterisation of Carbon

5.2.1 Pore Volume and Surface Area Measurements

The surface areas and pore volumes of the carbon samples were determined from the isotherms of the adsorption of nitrogen at 77 K and carbon dioxide at 273 K. A classic gravimetric McBain spring balance apparatus was used to obtain the adsorption isotherm of N_2 and CO_2. The system consists of four main components namely, a) Vacuum system which was made up of a rotary pump (Edwards model E04K) and an oil vapour diffusion pump (Edwards model E2M2), b) The gas inlet system consisting a needle valve and adsorbate cylinders, c) The sample tubes into which the aluminium foil buckets containing the samples are each suspended by a Pyrex hook from a pre-calibrated silica spring with a sensitivity of 250 mm g^{-1}, d) A mercury manometer.

Approximately 200 mg of each sample was placed in the aluminium foil bucket suspending from a silica spring. The system was evacuated to a pressure of 1.3 Pa (10

$^{-2}$ Torr) and the samples were outgassed for several hours. The samples were heated to 378 K using isomantles surrounding each tube and outgassed overnight. The samples were allowed to cool to room temperature and the isomantles were replaced by Dewars filled with an appropriate coolant (*i.e.* ice/water at 273 K for CO_2 adsorption or liquid nitrogen at 77 K for N_2 adsorption). The adsorbate was introduced into the system at various pressures up to approximately 0.1 MPa (1 atm) and the readings were taken by measuring the extension of the pre-calibrated silica spring using a cathetometer After each admission of the adsorbate, the system was left for at least one hour to reach the equilibrium with longer intervals for the first several points. Ten points were taken for each isotherm measurement.

The amounts of adsorbate adsorbed on the adsorbents can be calculated from the spring extension, based on the equation below:

$$n = (a \times 1000)/(b \times RMM) \qquad mmol\ g^{-1}$$

where:

a = Spring extension due to the adsorbate uptake (cm)

b = Spring extension due to sample

RMM = Relative molecular mass of adsorbate molecule (g mol^{-1})

The D-R equation was used in the following form to calculate CO_2 surface area:

$$Log_{10} N = log_{10} N_0 - D \times log_{10}^2 (p/p_0)$$

where N is the amount (mmol) of the adsorbate at a relative pressure of p/p_0, N_0 is the amount of adsorbate which fills the micropores and D is variable, dependent on temperature, pore size distribution and adsorbate affinity.

A plot of $log_{10}\ N$ versus $log_{10}^2(p/p_0)$ should be linear with a gradient of $-D$. Extrapolation of the graph to $log_{10}^2(p/p_0) = 0$, where $log_{10}\ N = log_{10}\ N_0$, and this represents the maximum effective micropore volume (for CO_2 adsorption) or total pore volume (for nitrogen adsorption).

The CO_2 surface areas were calculated from the maximum uptake estimated from the isotherms and referred to as minimum surface areas. Higher values of the surface areas were obtained from extrapolating the D-R plots and were referred to as maximum surface areas. Generally the minimum surface areas of the carbon were used in the interpretation of the results since the extrapolation of D-R plot gives micropore volume therefore resulting in a unrealistically higher value of surface area.

The surface area was determined by the following equation:

$$S_a = N_m \times a_m \times L$$

where:

S_a = Surface area ($m^2\ g^{-1}$)

N_m = Monolayer capacity (mmol g^{-1})

a_m = Cross section area of 1 adsorbate molecule

i.e. 1.92×10^{-19} m^2 for CO_2, 1.6×10^{-19} m^2 for N_2

L = Avogadro number (6.023×10^{23} molecules per mole)

P_0 = Saturated vapour pressure of the adsorbate

i.e. 760 Torr (0.1 MPa) for N_2 at 77 K, 26144 Torr (3.49 MPa) for CO_2 at 273 K.

The pore volume was determined by the following equation:

$$V = (N_0 \times RMM)/\sigma$$

where:

N_0 = amount of adsorbate obtained from the extrapolation of D-R plot (mol);

RMM = relative molecular mass of adsorbate molecule (g mol^{-1}), 28 for CO_2 and 44 for N_2;

σ = density of the adsorbate at the adsorption temperature (g cm^{-3}), 1.2506 for N_2 and 0.9179 for CO_2.

5.2.2 Elemental Analysis

The analytical method is based on the complete and instantaneous oxidation of the sample by 'flash combustion' which converts both inorganic and organic substances into combustion products. The resulting combustion gases were brought through a reduction furnace and are swept into the chromatographic column by carrier gas helium, where they are separated and detected by a thermal conductivity detector which give an output signal proportional to the concentration of the individual component of the mixture.

Determination of C, H, N

A Carlo Erba 1106 elemental analyser was used to determine the C, H, N contents of the carbon samples. The technique used for the measurement of C, H, N is based on the quantitative 'dynamic flash combustion' method. Approximately 1 mg of each sample was weighed into a tin container which was placed inside the autosampler drum where it was purged with a continuous flow of helium and then dropped at preset intervals into a vertical quartz tube maintained at 1293 K (combustion reactor). When the sample was dropped inside the furnace, the helium stream was temporarily enriched with pure oxygen. The sample container melt and the tin promoted a violent reaction, i.e flash combustion, in a temporarily enriched atmosphere of oxygen. Quantitative combustion was then achieved by passing the mixture of gases over a catalyst. The mixture of combustion products was then passed over copper to remove the excessive oxygen and to reduce the nitrogen oxides to element nitrogen. The resulting mixture was passed over a chromatographic column (Porapak 'S') where the individual components were separated and eluted as N_2, CO_2 and H_2O with a species detection using a thermal conductivity detector. The electrical signal detected was recorded using an integrator. The concentration of each component was determined from the integral of the signals in comparison with that of the corresponding organic chemical standard.

5.2.3 Proximate Analysis

The proximate analysis was conducted on a Stanton Redcroft STA 780 thermobalance which consists of an electronic microbalance with a hangdown

suspended from it down the centre of a water cooled furnace. A ceramic sample bucket was placed at the bottom of the hangdown. The gas flows upwards from the bottom of the furnace at a flow rate of 50 cm^3 min^{-1}.

Approximately 50 mg of carbon sample was placed in the sample bucket and the exact weight was noted. The sample was then heated in a constant flow of nitrogen to 383 K at a heating rate of 99 K min^{-1}. The sample was held at this temperature until a constant weight was achieved and the weight was recorded. Therefore the moisture contents of the carbon samples can be calculated based on the difference in weight. Then the sample was heated from 383 K to 1173 K and held at maximum temperature for 3 minutes. The weight loss between 383 K and 1173 K represents the volatile matter content.

The furnace was cooled to 1073 K and maintained at this temperature. The gas flow was changed to air at the same flow rate of 50 cm^3 min^{-1}. The char was gasified and burnt out at this temperature until the weight of the sample was constant, The remaining weight represents the ash content of the sample. The moisture, volatile, ash contents and fixed carbon were calculated as follows:

$$M\,\% = 100 \times (W_0 - W_{f1})/W_0$$

$$V\,\% = 100 \times (W_{f2} - W_{f1})/W_0$$

$$A\,\% = 100 \times (W_{f3}/W_0)$$

$$F\,\% = 100 - M\,\% - V\,\% - A\,\%$$

here M = moisture content of the sample

V = volatile content of the sample

A = ash content of the sample

F = fixed carbon of the sample

W_0 = initial weight of the sample

W_{f1} = final weight at 383 K

W_{f2} = final weight at 1173 K

W_{f3} = final weight after combustion

5.2.4 Determination of Surface Functionality in Activated Carbons

Determination of Surface Oxygen Functional Groups in Activated Carbons

Temperature Programmed Desorption (TPD)

Temperature programmed desorption (TPD) studies were carried out using a Thermal Science STA 1500 thermogravimetric analyser (TGA) connected to a VG Quadruple 300 amu mass spectrometer by a heated stainless steel capillary lined with deactivated fused silica. Approximately 7 mg of sample was placed in a sample bucket and was heated from ambient temperature to 1200 °C at a heating rate of 15 °C min^{-1} under flowing argon (50 cm^3 min^{-1}). The evolved gas was sampled and analysed by the mass spectrometer throughout the course of desorption. The mass/charge (m/z) values of 28, 30 and 44 were monitored.

Fourier Transform Infrared Spectroscopy (FTIR)

Infrared spectra were recorded on a Nicolet 20-PCIR Fourier Transform Infrared Spectrometer with a CsI optics DTGS detector. The resolution was 4 cm^{-1}. The KBr discs were prepared by mixing 0.5 % of finely ground carbon sample in KBr.

Titration Studies (Boehm' s method)

The selective neutralisation method used to evaluate the carbon surface acidity was the scheme suggested by Boehm [*1*]. The amounts of various acidic functional groups can be measured by selective neutralisation using $NaHCO_3$, Na_2CO_3 and NaOH solutions respectively. About 0.2 g of carbon was placed in 25 cm^3 of each 0.1 N of solution and the mixtures were allowed to stand for 72 hours at room temperature. The mixtures were separated by filtering. The amount of each base neutralised by the carbon was determined by back titration using 0.1 N HCl solution.

Determination of Nitrogen Functional Groups in Activated Carbon

X-ray absorption near edge structure (XANES) spectroscopy was used to identify the nature of nitrogen functional groups present on the surface of activated carbon. Nitrogen XANES spectra were obtained on beamline 1.1 of the Synchrotron Radiation Source (SRS) at Daresbury Laboratory. The SRS storage ring was operated at an energy of 2 GeV with ring current in the range of 100 - 200 mA. The monochromator was a high energy spherical grating monochromator with a Au grating and a slit width of 0.1 mm. An electron detector was used to acquire the total electron yield. All the measurements were carried out at room temperature under vacuum, i.e. 10^{-6} - 10^{-8} bar, in order to minimise the interference of atmospheric nitrogen. The vacuum of the beamline which was < 10^{-8} bar, was separated from that of the sample compartment by an aluminium window with a thickness of 150 μm.

Standard compounds were chosen from a suite of organic compounds containing well defined nitrogen functionality for identifying nitrogen functional groups in the

carbons. The suite of standards consisted of acridine, carbazole, 2-hydroxypyridine, pyridine-N-oxide, PAN, 2- aminoanthracene, 9-cyanoanthracene and 1,3,5-tribenzylhexahydro-1,3,5-triazine. The samples were ground finely and dispersed in carbon tetrachloride. A few drops of each slurry were applied to a high purity aluminium plate and the solvent was allowed to evaporate. Then the sample plates were mounted on a vertical sample holder which was fixed in the sample compartment. After outgassing to a pressure lower than 10^{-6} bar, the aluminium window was lifted and the beam was allowed into the sample compartment. The samples were scanned in the energy range of 380 - 430 eV with the resolution of 0.1 eV. A blank aluminium plate was scanned as the background in every fourth run. The standard acridine was scanned regularly as a calibration of energy drift during each circle of run. The baseline of the spectra of the carbon samples were corrected by dividing the data of sample by that of the blank plate.

5.2.5 Energy Dispersive X-ray Analysis (EDA)

The surface of carbon loaded with metal was subjected to energy dispersive X-ray analysis (EDA). EDA studies were carried out on a JEOL JSM 35 Scanning Electronic Microscope (SEM) with a LINK Q×2000 EDA analyser.

5.3 Characterisation of Solutions

5.3.1 Raman Spectroscopy

Raman spectra were obtained using a Renishaw Raman spectrometer. The spectrometer consisted of a 25 mW air cooled helium neon laser, with a wavelength of

632 nm. The laser was focused on the solution using a microscope with a x50 n.a objective. The spectra were recorded with a resolution of 1 cm^{-1} using a couple charged device (CCD) detector.

5.3.2 Inductively Coupled Plasma (ICP) Atomic Emission Spectroscopy (AES)

The concentrations of metal ions in the solution were determined using a Unicam model 701 Inductively Coupled Plasma Atomic Emission Spectrometer. The spectrometer was calibrated using a suite of standard solutions of known concentration. A linear response was found over the range of concentrations used.

The solution samples were admitted through a nebulizer and were injected as an aerosol into the flame, using argon as a carrier gas. The emitted light which was observed in the higher regions of the flame passed through a polychromator and was enhanced by photomultiplier tubes. The signals were converted from analogue to digital and recorded on a computer display.

5.4 Adsorption Experiments

5.4.1 Gold and Silver Adsorption Studies

a) Capacity Measurements

The method used was a modified version of that described previously [*2*] for the determination of gold and silver capacities on activated carbons. The carbon was ground and sieved to give a size fraction of 212–600 μm. The gold standard solution

was prepared by adding 146.3 mg of $KAu(CN)_2$ (or 100 mg of $KAg(CN)_2$ for silver adsorption studies) and 200 mg of NaCN (140 mg of KCN for silver adsorption studies) into a 1 dm^3 of volumetric flask. The pH of the solution was adjusted to 10 using borate buffer solution. The buffer solution was prepared from an aqueous solution of 3.092 g of boric acid and 3.728 g of potassium chloride in 1 dm^3 volumetric flask by adjusting the pH to 10 by addition of 1 M NaOH solution. An isotherm was obtained by adding various amounts of carbons (0.1–0.55 g with an interval of 0.05 g) to 100 cm^3 of gold or silver solution. The mixtures were allowed to stand for 72 hours in a water bath of 25 °C. The amounts of gold or silver adsorbed on the carbons were determined by measuring residual concentrations of gold or silver using Unicam 701 Inductively Coupled Plasma (ICP) atomic emission spectrometer.

b) ***Adsorption Studies in the Presence of Alcohols***

In order to investigate the effects of alcohols on the adsorption of gold cyanide species on active carbons, ethanol (7 v/v %) and butan-1-ol (6.1 v/v %) were added to the standard gold solution. In all other aspects the measurements of gold cyanide adsorption capacities were carried out by the methods described above.

c) ***The Adsorption Studies in the Presence of Excess Cyanide Ions***

The effects of excess free cyanide ions on the adsorption were examined by adjusting the ratio of CN^- to $Ag(CN)_2^-$ (or $Au(CN)_2^-$) in the absence of borate buffer solution. The experiment procedures were identical in all other details to that described above.

5.4.2 Adsorption Studies of Other Metals

The nitrate salts of cadmium, nickel, copper and calcium were used for the studies of adsorption of cationic metal species on activated carbons. The mixtures of carbon and metal salts aqueous solution were allowed to stand for 48 hours in a water bath of 25 °C. The amounts of metal adsorbed were determined by measuring solution concentration using Unicam 701 Inductively Coupled Plasma (ICP) atomic emission spectrometer. The loaded carbons were separated by filtering and rinsed with water (0 °C) to remove residual solution trapped among carbon particles. Desorption studies were carried out using Soxhlet extraction for 24 hours.

5.4.3 Flow Microcalorimetry Studies

A Microscal Model 3 Vi immersion flow microcalorimeter was used to measure the heat change of a solid/liquid interaction. Approximately 80 mg of carbon (particle size of 0.212 - 0.425 mm) was used with a flow rate of 3.3 cm^3 h^{-1}. The heat of adsorption were measured by the following procedure. 1) The carbon was equilibrated by passing water until a steady baseline was achieved. 2) Cadmium nitrate solution was passed over the sample and the heat of adsorption was measured by calibration of the thermal profile against a known current/voltage/time calibration peak. After the adsorption and calibration were finished, the water was passed over the sample to obtain the heat of desorption. 3) When a steady baseline was achieved after desorption 1, the cadmium nitrate was passed over the sample bed again to obtain the heat of adsorption for the second adsorption. 4) Finally, the heat of desorption for the second cycle was obtained by passing water over the sample.

References

1. Boehm, H.P. *Advan. Catal.* **1966**, *16*, 179.

2. Grigorova, B., *Standard Analytical Procedures for Evaluation of Activated Carbon*, AARL Reference CA 68, Johannesburg, 1987.

Chapter 6

RESULTS

6.1 Characterisation of the Activated Carbons Used

6.1.1 Proximate and Ultimate Analysis

The proximate analysis and ultimate analysis results of the carbons used in this study are show in **Table 6.1** and **Table 6.2**. It is apparent that the commercially available activated carbons C1, C2, C3 and P1 have similar chemical composition although they are from different precursors. Small amounts of nitrogen and oxygen were present in the carbons.

The chemical modification of the active carbon by HNO_3 oxidation altered both the ultimate analysis and proximate analysis results. The proximate analysis shows that the amounts of volatile species increased while ash content decreased as a result of HNO_3 treatment. The volatiles are an indication of the functional groups which are introduced by the oxidation process and decomposed during heat treatment. Treatment with HNO_3 results in increases in oxygen, nitrogen and hydrogen contents and decrease of carbon content. It is apparent that large amounts of oxygen were introduced into the carbon after nitric acid oxidation with higher oxidation time introducing more oxygen functional groups. Small amounts of nitrogen are also incorporated into the carbon by oxidation. Heat treatment decreases the oxygen and hydrogen contents gradually whereas the nitrogen content remained relatively

constant, which indicates that nitrogen was incorporated into the carbon structure as relatively stable functional groups. Heat treatment to 300 °C reduced the oxygen contents in oxidised carbons slightly with release of carbon dioxide. The chemical composition and structure of the oxidised carbons heat treated at 800 °C were similar to the original sample.

Table 6.1 Proximate analysis of activated carbons used (wt %, ar)

Sample code	Moisture	Volatile	Ash	Fixed carbon
C1	3.1	3.3	3.0	90.7
C2	2.4	3.3	1.7	92.6
C3	2.0	3.1	3.2	91.8
P1	2.6	8.9	5.5	83.1
CA	3.1	2.5	2.4	91.9
CNA	1.1	6.9	2.9	89.1
CN1	2.5	23.9	1.8	71.8
CN1-300	1.2	20.5	0.8	77.5
CN1-400	1.3	17.7	1.3	79.7
CN1-500	1.2	14.5	1.4	82.9
CN1-600	1.1	11.5	1.7	85.7
CN1-800	1.0	4.6	1.4	93.0
CN2	2.9	29.1	1.7	66.3
CN2-300	2.3	27.1	1.1	69.5
CN2-400	1.7	24.2	0.7	74.3
CN2-500	1.5	19.2	1.6	77.7
CN2-600	1.3	14.4	0.7	83.6
CN2-800	1.1	3.9	1.8	93.2

Table 6.2 Ultimate analysis of activated carbons used (wt %, daf)

Sample code	Carbon	Hydrogen	Nitrogen	Oxygen
C1	96.1	0.4	0.3	3.2
C2	96.7	0.3	0.0	2.1
C3	97.8	0.2	0.0	1.9
P1	97.0	0.2	0.3	2.5
PAN1	85.1	0.5	9.4	5.0
PAN2	84.1	0.5	8.5	5.9
CA	95.5	0.1	2.3	2.0
CNA	90.0	0.5	5.3	3.9
CN1	82.8	1.1	0.8	15.3
CN1-300	84.1	1.0	0.9	14.1
CN1-400	86.3	0.7	0.8	12.2
CN1-500	88.4	0.7	0.9	10.0
CN1-600	91.0	0.6	0.9	7.5
CN1-800	95.9	0.5	1.0	2.6
CN2	75.6	1.5	1.0	21.9
CN2-300	77.1	0.9	1.0	21.0
CN2-400	82.1	0.9	1.1	15.9
CN2-500	84.3	1.0	1.1	13.6
CN2-600	86.9	0.8	1.2	11.1
CN2-800	94.3	0.5	1.4	3.8

Table 6.3 The porous structure characterisation data of the carbons used

Sample code	Pore volume ($cm^3\ g^{-1}$)		D-R surface	V_{CO_2}/V_{N_2}
	Micropore	Total pore	area ($m^2\ g^{-1}$)	
	(CO_2, 273 K)	(N_2, 77 K)	(CO_2, 273 K)	
C1	0.32	0.32	683	0.99
C2	0.31	0.33	605	0.96
C3	0.30	0.43	647	0.71
P1	0.24	0.25	485	0.95
PAN1	0.26	0.30	545	0.87
PAN2	0.24	0.24	455	0.98
CA	0.26	0.30	546	0.85
CNA	0.20	0.30	493	0.67
CN1	0.26	0.27	455	0.96
CN1-300	0.25	0.29	537	0.87
CN1-400	0.26	0.28	557	0.93
CN1-500	0.25	0.28	538	0.90
CN1-600	0.27	0.3	574	0.91
CN1-800	0.29	0.33	619	0.90
CN2	0.14	0.21	295	0.67
CN2-300	0.16	0.21	347	0.78
CN2-400	0.19	0.24	401	0.80
CN2-500	0.22	0.24	473	0.94
CN2-600	0.21	0.27	453	0.79
CN2-800	0.26	0.27	553	0.97

The incorporation of nitrogen into the activated carbon structures were realised by treating the commercial activated carbon with ammonia and using nitrogen rich polymer as precursor. It is evident that treatment with ammonia at 800°C introduced an appreciable amount of nitrogen into the coconut shell derived carbon C1. The nitrogen content of the carbon increased from 0.3 % to 2.3 % after ammonia treatment. More nitrogen was incorporated into the carbon when the carbon C1 was oxidised using nitric acid prior to ammonia treatment. The nitrogen content of CNA is twice as that of CA. The activated carbon with even higher nitrogen content was prepared from polyacrylonitrile. It is apparent that the PAN derived carbon (PAN1) inherited very high nitrogen content (~9 %) from the nitrogen-rich polymer precursor. The high amounts of nitrogen in the carbons allowed the assessment of the role of nitrogen functional groups on the adsorption of metal cations.

6.1.2 Porous Structure Characteristics of the Carbons Used

The commercially available coconut shell based carbons C1, C2 and C3 were activated in steam at 900 °C and have a range of burn-offs. The extent of activation was in the following order C3 > C2 > C1. Both the carbon dioxide (273 K) and nitrogen (77 K) adsorption isotherms were Type I for all the coconut shell carbons. The variation of total pore volume obtained from nitrogen adsorption at 77 K and micropore volume obtained from extrapolation of the Dubinin-Radushkevich equation for the carbon dioxide adsorption at 273 K, with the extent of activation for these carbons are shown in **Table 6.3**.

The porous structure of coconut carbon C1 was modified after oxidation with HNO_3 in addition to the modification to the surface chemical structures. Nitric acid

treatment decreased both the CO_2 micropore volume and N_2 total pore volume with higher oxidation times resulting in greater reduction of pore volumes. This is possibly due to the blockage of pores by structural changes involving the incorporation of functional groups. Heat treatment increased the surface areas and pore volumes gradually. Both approaches of ammonia treatment did not greatly modify the porous structure of the activated carbon with the surface area being slightly decreased by ammonia treatment.

6.1.3 Chemical Properties of the Carbon Surface

Titration Studies

The acidic oxygen surface functional groups in carbon include 1), carboxylic acid groups 2), derivatives of carboxylic acid groups such as carboxylic anhydride, lactone and lactol groups 3), phenolic groups. These groups are weakly acidic and the acidity constants differ by several orders of magnitude [*1*]. According to Boehm [*2,3*] only the strongly acidic carboxylic groups are neutralised by $NaHCO_3$, whereas those neutralised by Na_2CO_3 are thought to be lactone, lactol and carboxyl groups. The weakly acidic phenolic groups only react with strong alkali NaOH. Therefore, by selective neutralisation using bases of different strength, the surface acidic functional groups in carbons can be characterised quantitatively and qualitatively. It is assumed that neutralisation with HCl characterises the amounts of surface basic groups. The basic properties are ascribed to surface basic groups and the π electron system of carbon basal planes.

The titration results for the original activated carbon C1, the oxidised carbons CN1, CN2 and their heat treated derivatives and the nitrogen-rich carbons (CA,CNA,

PAN1) are shown in **Tables 6.4** and **6.5**. The results indicate that carbon C1 is a basic H-type carbon since it does not react with sodium carbonate and sodium bicarbonate and therefore does not contain significant quantities of carboxylic acid groups or its derivatives such as anhydride, lactone and lactol groups. However the carbon contains a small amount of acidic groups which react with NaOH, but the dissociation is small since the carbon shows only basic properties in aqueous solution. The oxidation by HNO_3 produced considerable amounts of acidic groups in the carbon. Approximately half of the total acidity in oxidised carbons was due to carboxylic groups. Comparison of titration data for CN1 and CN2 shows that increase in oxidation time leads to the incorporation of greater amounts of oxygen functional groups into the carbon.

The trends for acidic groups of various strength after heat treatment at elevated temperatures to eliminate progressively the surface oxygen complexes in oxidised carbons CN1 and CN2 are shown in **Tables 6.4** and **6.5** and **Figures 6.1** and **6.2**. It is evident that heat treatment led to progressive loss of acidic surface groups. In contrast the amounts of HCl required to neutralise basic groups in carbons increased slightly with increasing heat treatment temperature (HTT) with the basicity being similar to starting carbon C after heat treatment to 800 °C.

Figures 6.1 and **6.2** show that the carboxylic acid groups are most sensitive to heat treatment. Approximately half of the carboxylic acid groups in the oxidised carbons CN1 and CN2 were removed by heat treatment at 300 °C for an hour, whereas the amounts of lactone and phenolic groups remained relatively unchanged at this temperature indicating that they are more stable towards heat treatment. The amounts of lactone and lactol groups decreased for heat treatment temperatures > 300 °C while the amounts of phenolic groups decreased for heat treatment > 400 °C. Small amounts

of acidity remained in the carbons after heat treatment at 800 °C and this is ascribed tentatively to phenolic groups.

The selective neutralisation studies of the nitrogen-rich carbons show that the PAN carbons and ammonia treated carbons contain neither carboxylic nor lactone groups. This is important because these acidic oxygen functional groups may be involved in strong interaction with metal cations thereby significantly increasing the adsorption of metal cations. These effects can be ruled out due to the absence of stronger acidic oxygen functional groups. Therefore the influence of nitrogen functional groups on the adsorption of metal cations can be assessed without the interposition of acidic oxygen functional groups. All the activated carbons showed similar weak acidity which may result from the presence of phenolic groups. The nitrogen-rich carbon CA, CNA and PAN1 have higher basicity than untreated carbon C1. The basic properties are probably due to the basic oxides, π electron system of carbon basal planes and the nitrogen functional groups.

Table 6.4 Selective neutralisation results of the carbons used

Sample code	HCl (meq g^{-1})	$NaHCO_3$ (meq g^{-1})	Na_2CO_3 (meq g^{-1})	NaOH (meq g^{-1})
C1	0.40	0.00	0.00	0.50
CN1	0.08	1.80	2.31	3.69
CN1-300	0.05	1.00	1.55	2.90
CN1-400	0.14	0.87	1.11	2.39
CN1-500	0.11	0.47	0.67	1.69
CN1-600	0.26	0.40	0.56	1.31
CN1-800	0.35	0.00	0.00	0.62
CN2	0.00	2.52	3.25	4.89
CN2-300	0.00	1.40	2.06	3.70
CN2-400	0.00	0.95	1.32	2.96
CN2-500	0.06	0.63	0.78	2.02
CN2-600	0.06	0.24	0.53	1.30
CN2-800	0.50	0.00	0.00	0.41
CA	0.70	0.00	0.00	0.80
CNA	0.78	0.00	0.00	0.65
PAN1	0.71	0.00	0.00	0.50

Table 6.5 Percentage of various acidic oxygen functional groups on the surface of the carbons used

Sample code	Total basicity (meq g^{-1})	Total acidity (meq g^{-1})	Carboxylic (%)	Lactone (%)	Phenolic (%)
C1	0.40	0.50	0.00	0.00	100
CN1	0.08	3.69	48.8	13.8	37.4
CN1-300	0.05	2.90	37.5	20.6	41.9
CN1-400	0.14	2.39	36.4	10.0	53.6
CN1-500	0.11	1.69	24.2	23.2	52.6
CN1-600	0.26	1.31	23.0	9.2	67.8
CN1-800	0.35	0.62	0.00	0.00	100
CN2	0.00	4.89	51.5	14.9	33.5
CN2-300	0.00	3.70	37.8	17.8	44.3
CN2-400	0.00	2.96	31.9	12.7	55.4
CN2-500	0.06	2.02	23.4	16.3	61.2
CN2-600	0.06	1.30	18.5	22.3	59.2
CN2-800	0.50	0.41	0.00	0.00	100
CA	0.70	0.80	0.00	0.00	100
CNA	0.78	0.65	0.00	0.00	100
PAN1	0.71	0.50	0.00	0.00	100

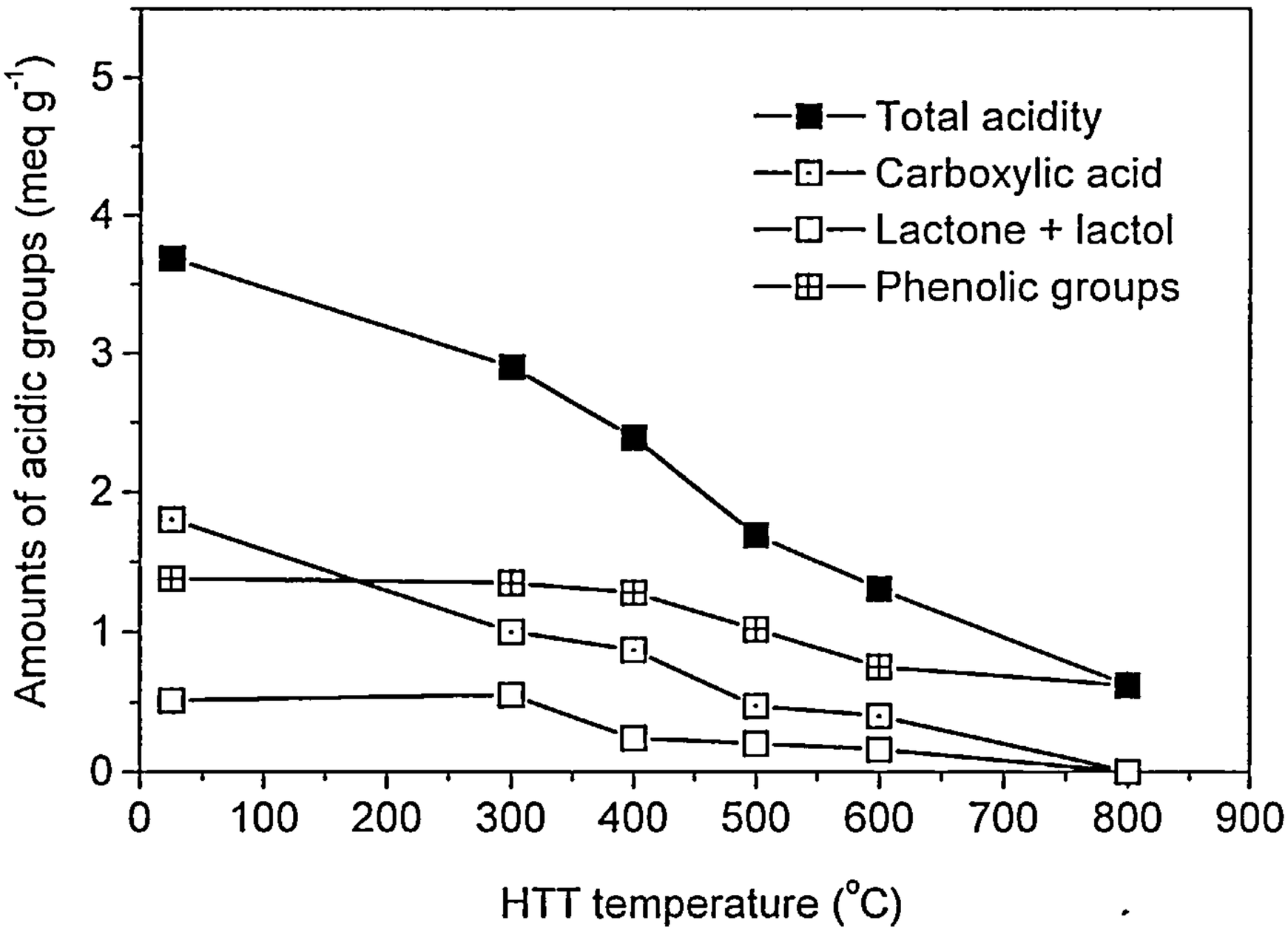

Figure 6.1 The variation of surface acidic groups with heat treatment for CN1

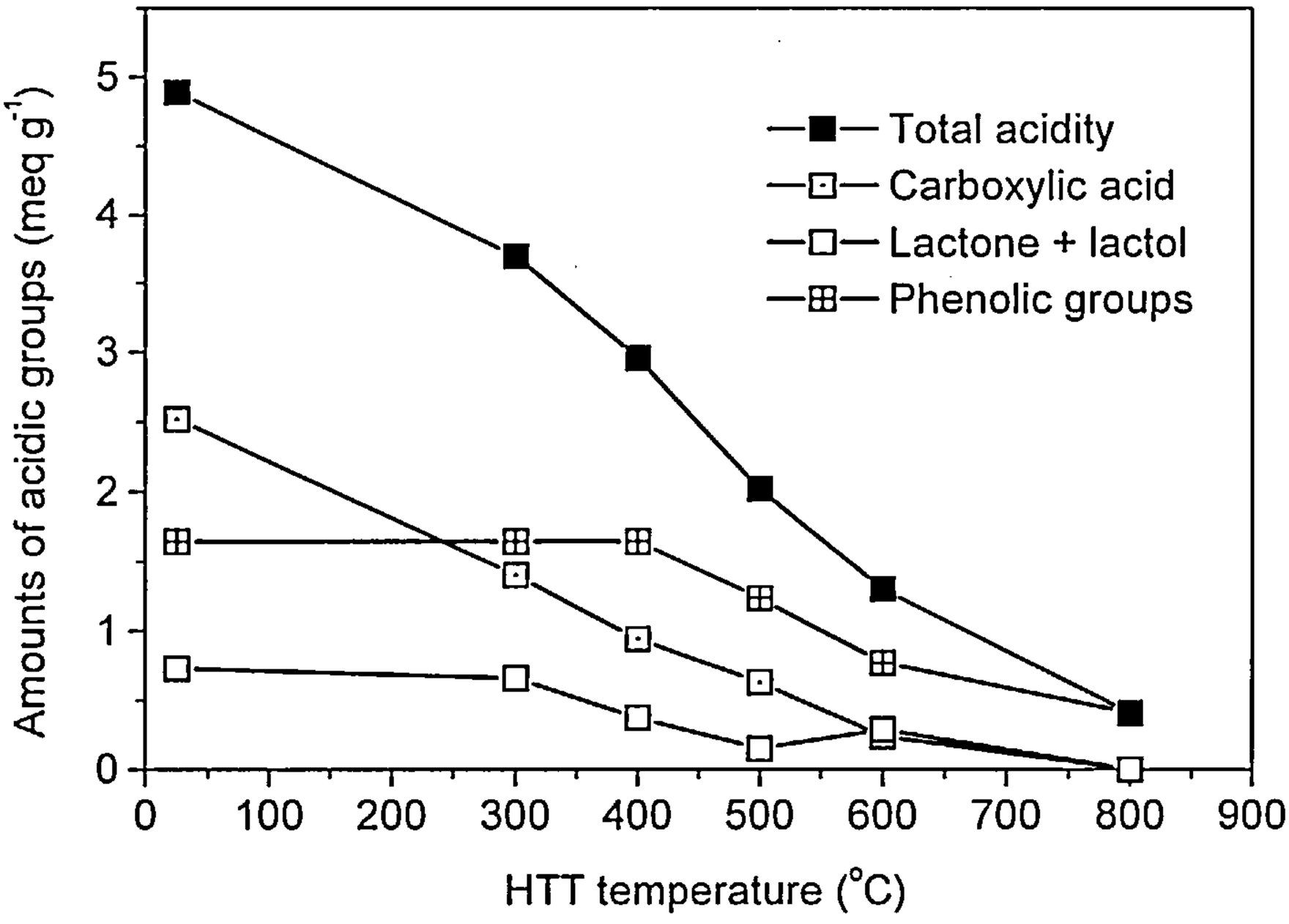

Figure 6.2 The variation of surface acidic groups with heat treatment for CN2

Temperature Programmed Desorption

Temperature programmed desorption (TPD) experiments were carried out to characterise surface oxygen and nitrogen functionality from their thermal stability by monitoring evolved CO, CO_2, H_2O and NO. The interpretation of TPD is complex especially at high temperature where surface mobility is significant [*4*]. However, it is generally accepted that at low temperatures CO_2 is mainly due to the decomposition of carboxylic acid groups and its derivatives, anhydride, lactone and lactol groups, whereas CO is derived from the decomposition of phenolic hydroxyl, carbonyl, quinone, ether, pyrone, carboxylic acid and anhydride groups [*5,6*]. **Figures 6.3**, **6.4**, **6.5** and **6.6** show the CO and CO_2 TPD profiles of the oxidised carbon CN1, CN2 and their heat treatment derivatives. The CO_2 TPD evolution profile of carbon C1 is not illustrated in the figures due to the negligible amount of CO_2 evolved during TPD, which is consistent with the above titration results which show that neither Na_2CO_3 nor $NaHCO_3$ react with carbon C1 indicating that carboxylic groups and their derivatives were not present.

Two well resolved peaks were observed in the carbon dioxide TPD for both oxidised carbons, CN1 and CN2, at about 270 °C and 700 °C respectively, while the profiles were complex consisting of a number of unresolved additional peaks. Heat treatment results in decomposition of the surface oxygen functional groups and this results in significant changes in the TPD profiles. The starting points of CO_2 evolution increased gradually with increasing heat treatment temperature, but in general CO_2 evolution starts below the HTT of the sample. The initial CO release occurred at higher temperatures than the corresponding CO_2 and the CO evolution reached a maximum at 600 °C.

The temperature programmed CO_2 desorption profiles of the nitrogen-rich carbons are shown in **Figure 6.7**. It apparent that these carbons do not contain any strongly acidic oxygen functional groups which decompose to give CO_2 below ~600 °C. This reflects the heat treatment temperature of the carbons during preparation process. The release of NO is due to the decomposition of nitrogen functional groups in carbon. Detectable level of NO were only found in the TPD products of the nitrogen rich-carbon *i.e.* CA, CNA and PAN1 carbons. **Figure 6.8** shows that the NO TPD profiles are different for the three nitrogen-rich carbons, indicating that the composition of the nitrogen functional groups on the carbon surface are different. However it is difficult to assign the original nitrogen functional groups present on carbon surface based on the NO TPD profiles.

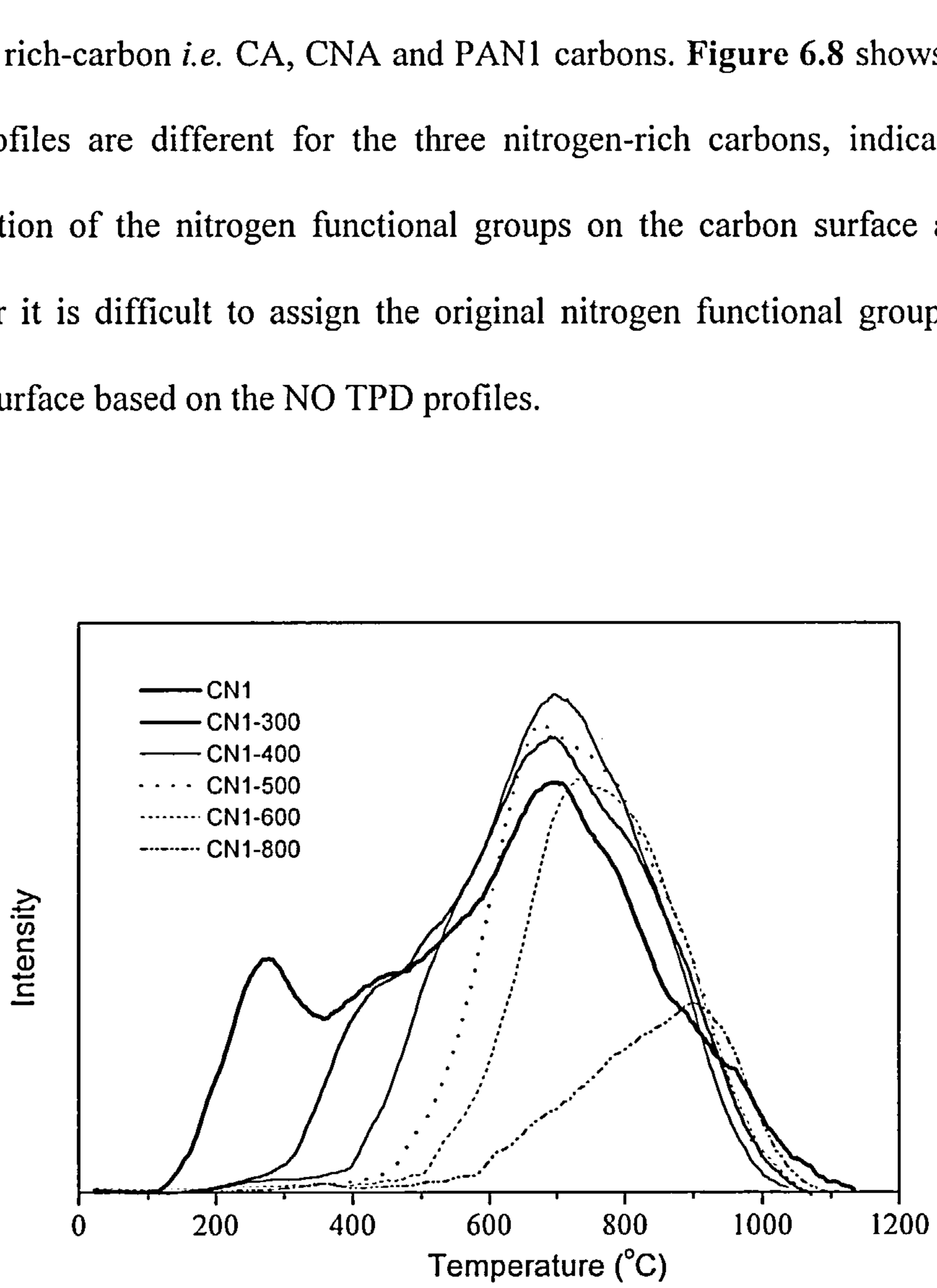

Figure 6.3 Temperature programmed CO_2 desorption profiles for CN1 and its heat treated derivatives

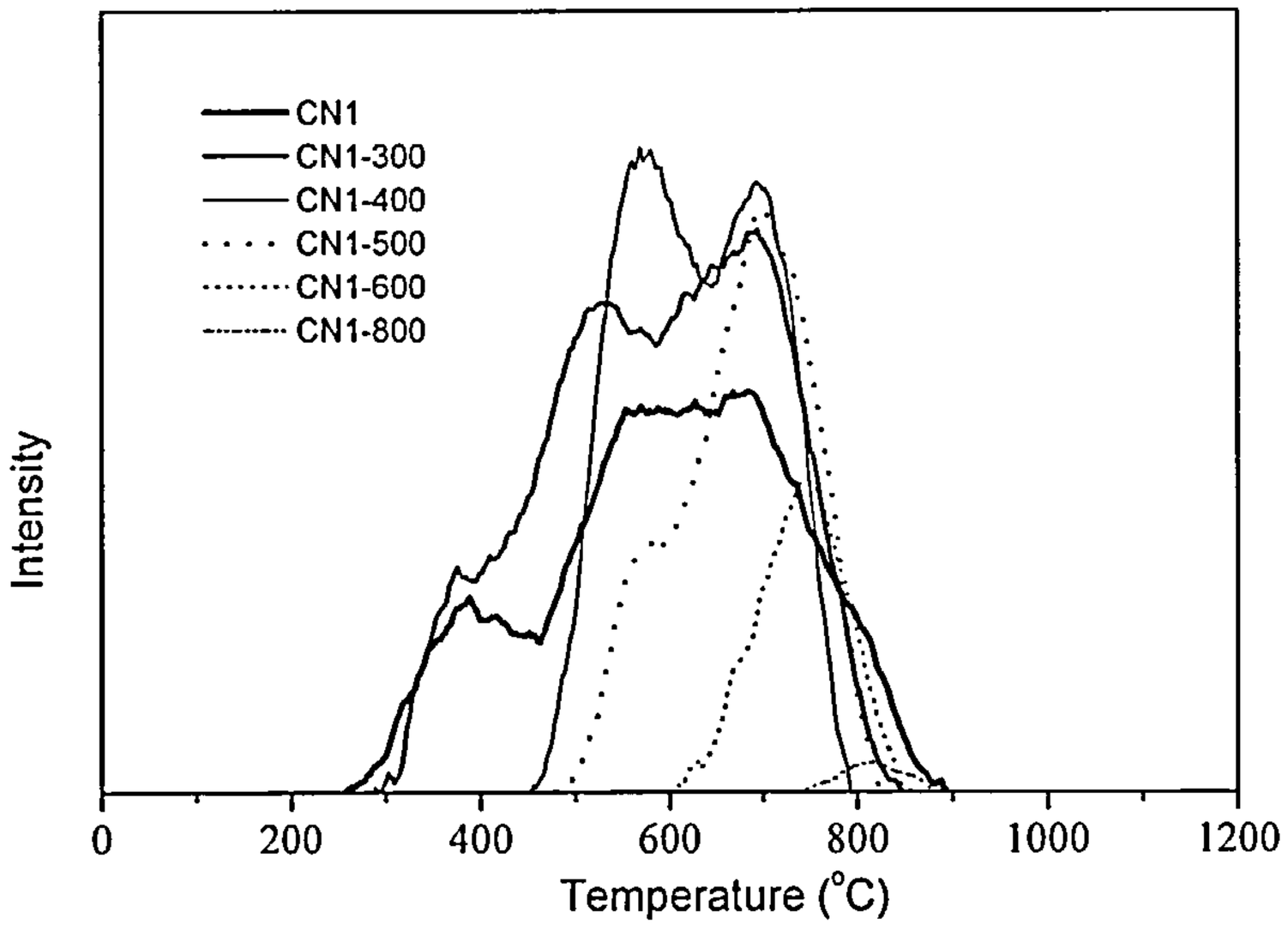

Figure 6.4 Temperature programmed CO desorption profiles for CN1 and its heat treated derivatives

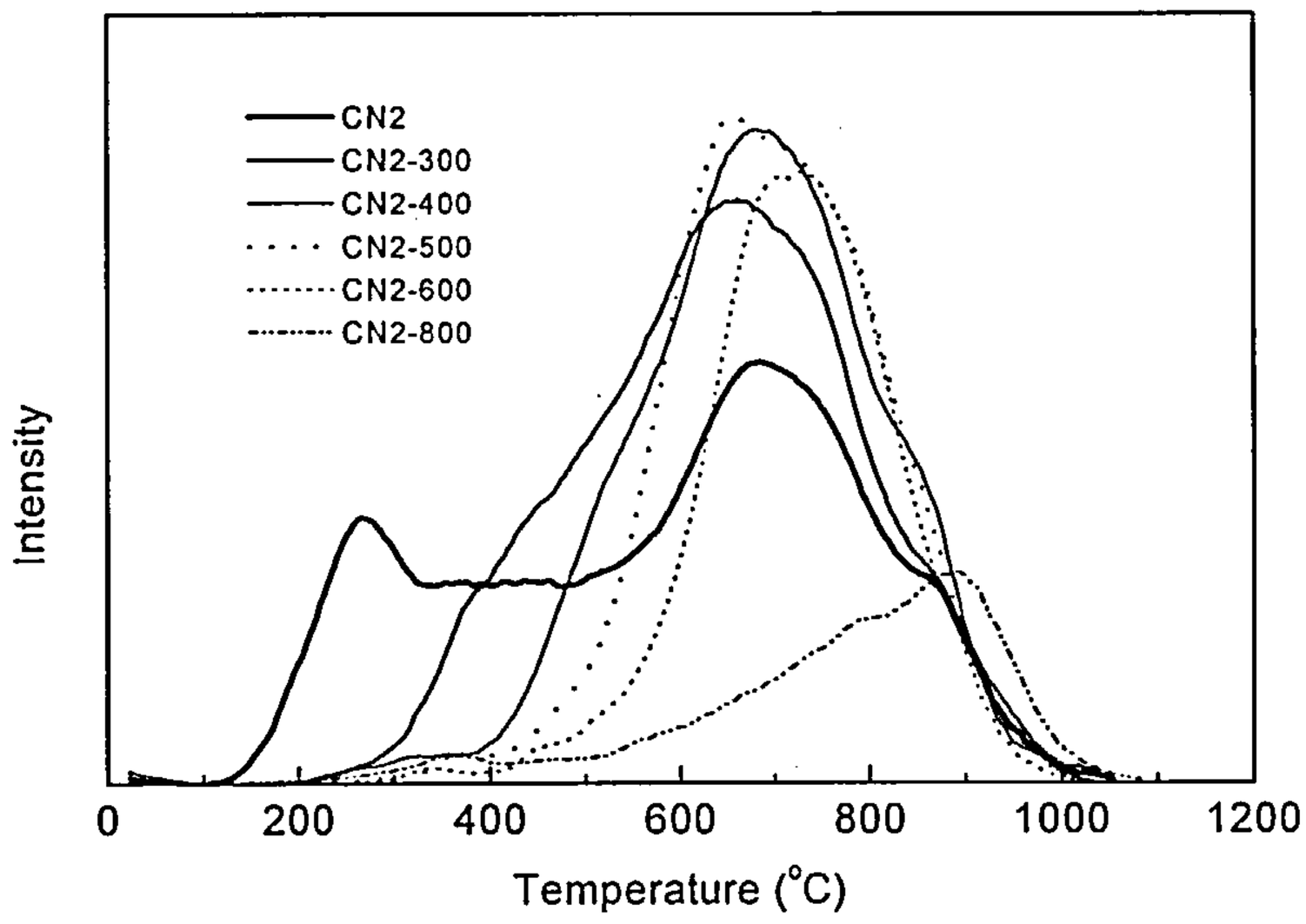

Figure 6.5 Temperature programmed CO_2 desorption profiles for CN2 and its heat treated derivatives

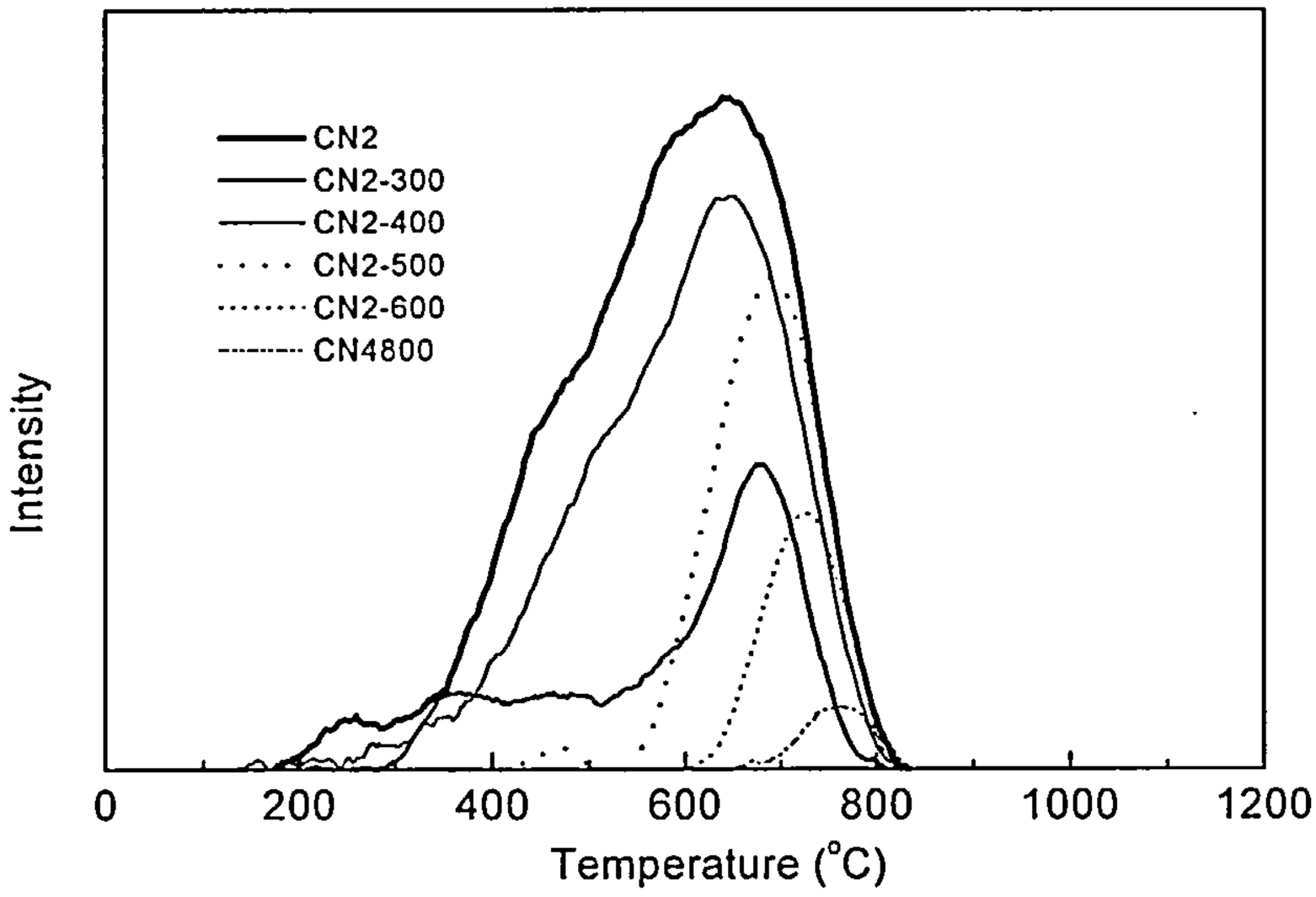

Figure 6.6 Temperature programmed CO desorption profiles for CN2 and its heat treated derivatives

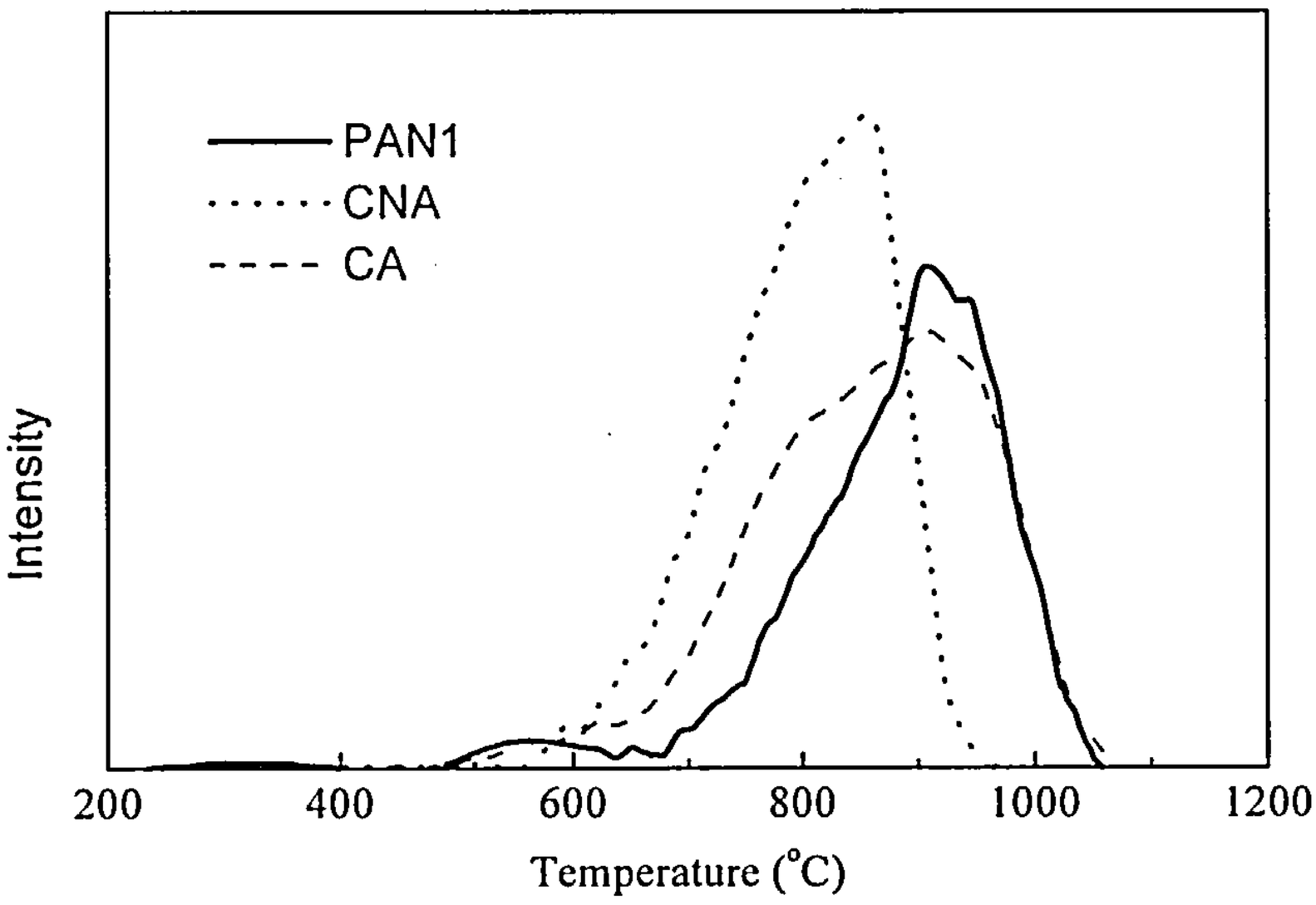

Figure 6.7 Temperature programmed CO_2 desorption profiles for the nitrogen rich- carbons

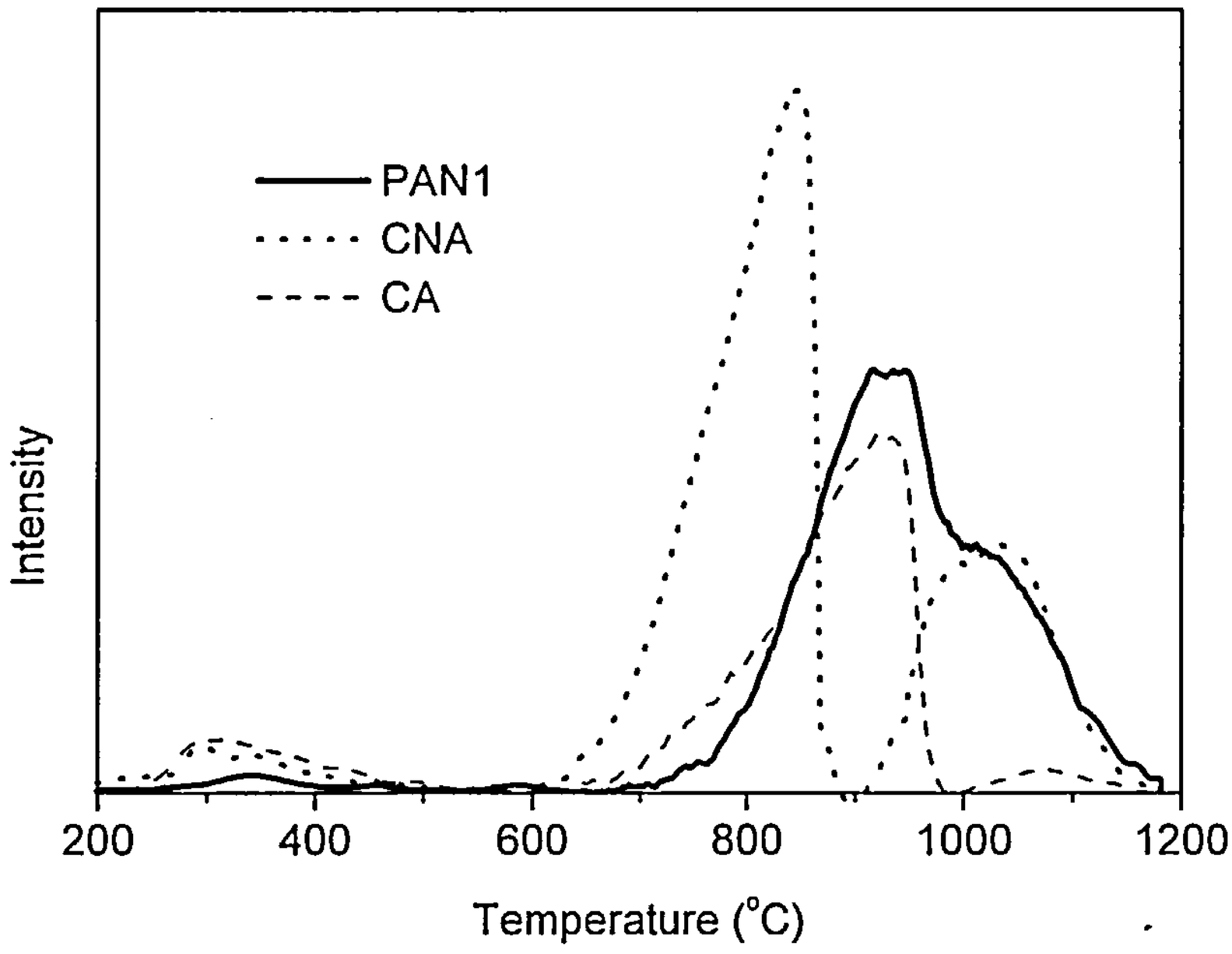

Figure 6.8 Temperature programmed NO desorption profiles for the nitrogen rich- carbons

Nitrogen X-ray Absorption Near Edge Structure Spectroscopy (XANES)

The nitrogen X-ray absorption near edge structure (XANES) spectroscopy results are illustrated in **Figure 6.9**. It is apparent that the nitrogen XANES spectrum of PAN1 shows three well resolved peaks at 399.8, 401.1 and 402.6 eV. Comparison with the spectra of standard compounds in previous work [*7*] allows the assignment of the three well resolved peaks to pyridinic, pyridone and pyrrolic functionality respectively. This is in good agreement with the nature of nitrogen functionality present in partially gasified PAN chars [*7*]. The nitrogen XANES spectrum of the nitrogen rich carbon CNA obtained by the combination of HNO_3 oxidation and NH_3

treatment shows a strong well resolved peak at 399.7 eV and two weak peaks at 401.8 and 404.4 eV. The peak at 399.7 eV is due to pyridinic nitrogen functionality whereas the 401.8 eV peak is assigned as pyridone functional groups. The XPS studies [*8*] of nitrogen functionality in the active carbon obtained by HNO_3 oxidation followed by ammonia treatment also suggested the presence of pyridinic and pyridone nitrogen functional groups. Although the assignment of 404.4 eV peak to aromatic amine is not unequivocal in this study, amine groups have been suggested to be present in the ammonia treated carbon by XPS studies [*9,10*]. The nitrogen XANES spectrum of oxidised carbon CN2 shows three peaks with the peak at 401.1 eV assigned to pyridone groups whereas the two strong well resolved peaks at 403.5 and 405 eV being assigned to pyrrolic and possibly pyridine N-oxide groups respectively.

Fourier Transform Infrared (FTIR) Spectroscopy

The FTIR spectra of original carbon C1, oxidised carbon CN2, heat treated CN2 and CN2 reacted with bases of different strength are presented in **Figures 6.10** and **6.11**. For carbon C1, the bands observed at 2852 and 2921 cm^{-1} were assigned to symmetric and asymmetric C-H stretching vibrations in aliphatic CH, CH_2 and CH_3 groups. The band at 1635 cm^{-1} is a characteristic peak for carbon materials [*11*] and is probably ascribable to carbonyl groups which are highly conjugated in the graphene layer such as quinone and/or ionoradical structure C=O [*12*]. This is consistent with the basic nature of the carbon. The broad weak peak at 1182 cm^{-1} is assigned to C-O stretching vibrations in phenolic groups.

Two additional bands were observed at 1576 and 1717 cm^{-1} in the IR spectrum of CN2 while the relative intensity of the broad band at 1182 cm^{-1} increased

considerably and the peak at 1635 cm^{-1} was obscured by the new bands at 1576 cm^{-1} and 1717 cm^{-1}. The 1717 cm^{-1} band is characteristic of stretching vibrations of carbonyl groups C=O in carboxylic acid groups. The carboxylic acid groups should also have an absorption band at ~3400 cm^{-1}. However, the intense broad peak at 3400 cm^{-1} region in the spectrum of CN2 is not an unequivocal identification of O-H stretching vibrations in carboxylic acid groups because of the possibility of adsorbed water being present in the sample. The broad band at 1182 cm^{-1} has contributions from both C-O stretching and O-H bending modes in phenolic, carboxylic acid groups [*12,13*]. The 1576 cm^{-1} band has contributions from the aromatic ring stretching mode and conjugated carbonyl groups, such as quinone type C=O and/or C⁻=O ionoradical structures. Secondly, the reaction between COOH groups in the carbon and KBr during the preparation of the sample disc cannot be ruled out completely. The resultant carboxylate groups COO^- should display a strong asymmetric COO^- vibrations band in the range 1550 ~ 1610 cm^{-1} and a weak symmetric COO^- stretching band in the range 1360 ~ 1450 cm^{-1} [*14,15*]. The absence of bands at 1830 and 1760 cm^{-1} confirm the absence of carboxylic anhydride in carbon CN2.

The FTIR spectra of CN2 treated with $NaHCO_3$, Na_2CO_3 and NaOH to selectively neutralise different acidic groups are shown in **Figure 6.10**. It is evident that there are changes in the IR spectra of CN2 after reaction with bases of different strength. The relative intensity of 1717 cm^{-1} band assigned to carboxylic acid decreased significantly, accompanied by an increase in the intensity of the 1576 cm^{-1} band assigned to carboxylate groups. The reactions also brought about a decrease in the 1182 cm^{-1} band intensity which was assigned as C-O stretching and O-H bending mode in carboxylic acid and phenolic groups [*12,13*]. Although the band at 1717 cm^{-1} decreased in relative intensity, it did not shift to higher wave number after CN2 was

reacted with $NaHCO_3$. Therefore, it can be inferred that lactone groups were probably absent in oxidised carbon CN2.

The changes in FTIR spectra of CN2 after heat treatment are shown in **Figure 6.11**. It is apparent that the bands at 1182, 1576 and 1717 cm^{-1} decrease with increasing HTT. Heat treatment to 400 °C results in the band at 1717 cm^{-1} shifting to 1734 cm^{-1} which is assigned as lactone groups. Since the absorption bands due to anhydride were not observed, it is proposed that carboxylic acid groups decompose with partial intermolecular rearrangements to form lactone groups. The concentration of lactone groups were decreased gradually at heat treatment temperatures > 400 °C as inferred from the changes in 1734 cm^{-1} band intensity and the titration studies above. The reduction of the band intensities at 1182 and 1576 cm^{-1} region for heat treatment at 600 °C suggests that considerable decomposition of phenolic and quinone groups had occurred. The band at 1635 cm^{-1} split into two bands at 1585 and 1623 cm^{-1}. The 1623 cm^{-1} band was assigned to the quinone type carbonyl oxygen double bond conjugated with the carbon basal plane. The band at 1585 cm^{-1} in CN2-800 was assigned to ionoradical structure C⁼⁼O caused by heat treatment or further chemisorption of oxygen at room temperature [*12,16*].

The surface nitrogen functional groups of the activated carbons were also studied using FTIR and the resultant spectra are shown in **Figure 6.12**. The 1635 cm^{-1} band in the IR spectrum of carbon C1 is probably ascribable to carbonyl groups which are highly conjugated as quinone in the graphene layer as suggested above. After treatment of carbon C1 with ammonia three additional bands were observed at 1512, 1541 and 1570 cm^{-1} in the IR spectrum of CA. They are possibly assigned to pyridinic, pyridonic and indolic (or pyrrolic) structures [*14,17*] while the band at 1635

cm^{-1} is probably due to carbonyl groups (C=O) in quinone and pyridone structures. The 1717 cm^{-1} band in the IR spectrum of CN2 is characteristic of stretching vibrations of carbonyl groups C=O in carboxylic acid groups whereas the 1576 cm^{-1} band is probably a composite band which has contributions from the aromatic ring mode, conjugated carbonyl groups and carboxylate COO^- groups. The reaction of CN2 with ammonia completely eliminated the carboxylic acid groups on the carbon surface. The bands at 1512, 1541 and 1570 cm^{-1} are possibly due to pyridinic, pyridonic and indolic(or pyrrolic) structures. This assignment can be supported by the suggestion [*18*] that the reaction of carboxylic acid groups on carbon surfaces with ammonia at elevated temperature brought about the formation of pyridinic and pyrrolic structures on the carbon surface. The C=O band of pyridonic structure might be obscured by the new bands. The IR spectrum of PAN1 shows similar bands to that of CA suggesting the presence of pyridinic, pyridonic, indolic (or pyrrolic) structures on the carbon surface. The absence of 2000 - 2200 cm^{-1} bands suggested that the cyano-nitrogen functional groups are absent on the carbon surface.

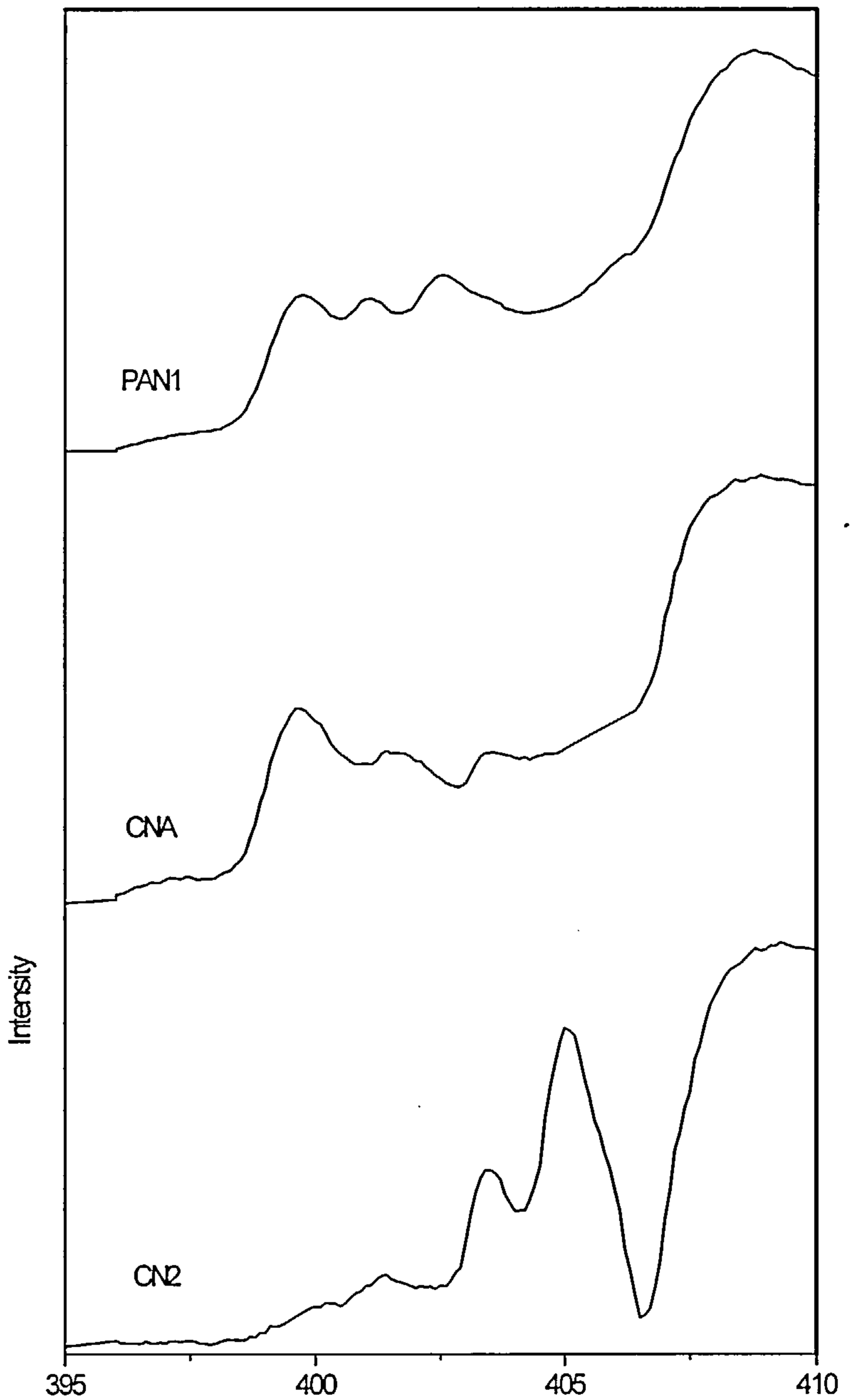

Figure 6.9 Nitrogen XANES spectra of the nitrogen rich carbons

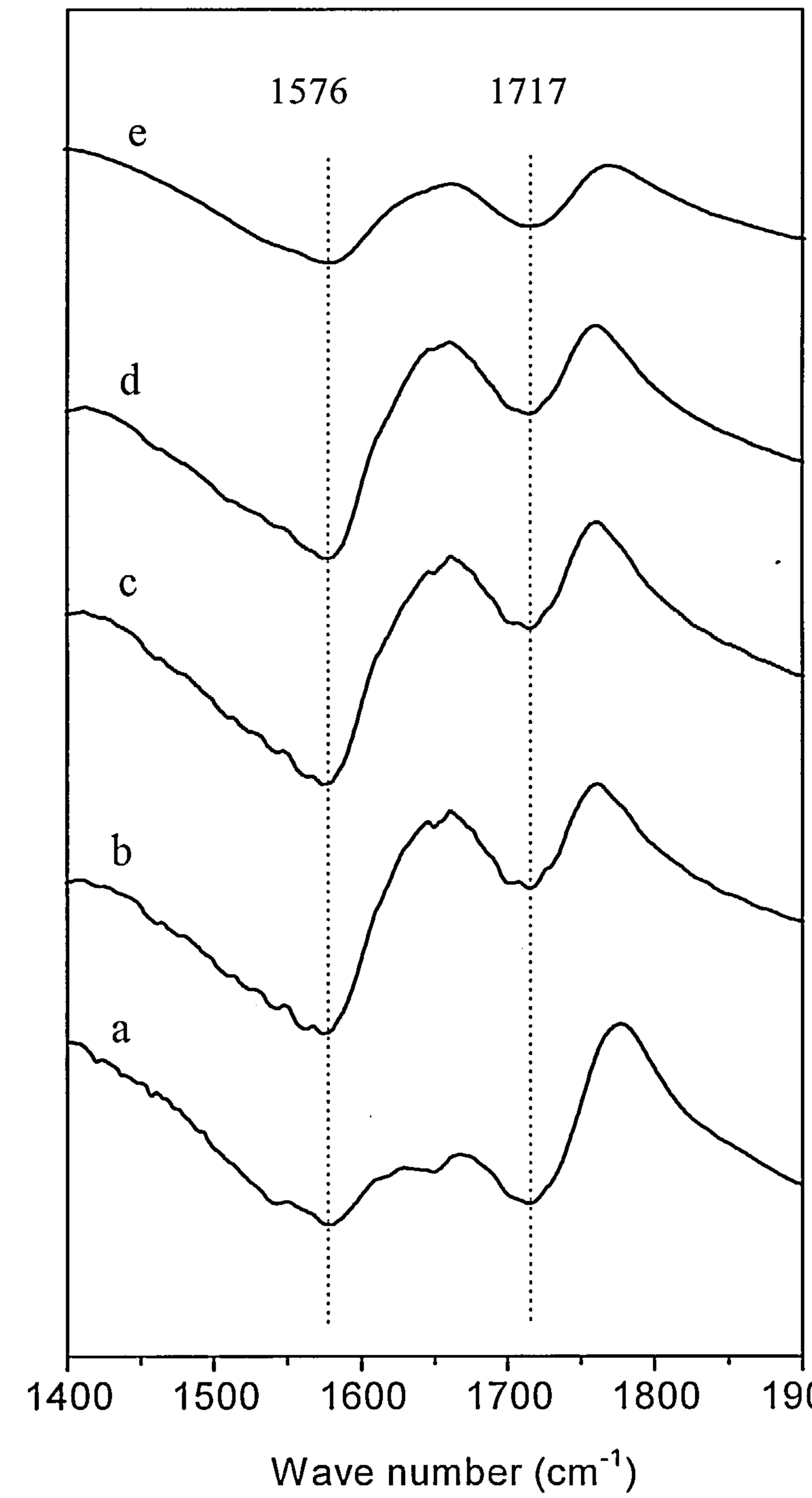

Figure 6.10 FTIR spectra of a) CN2, b) CN2-$NaHCO_3$, c) CN2-Na_2CO_3, d) CN2-NaOH and e) CN2 after adsorption of cadmium

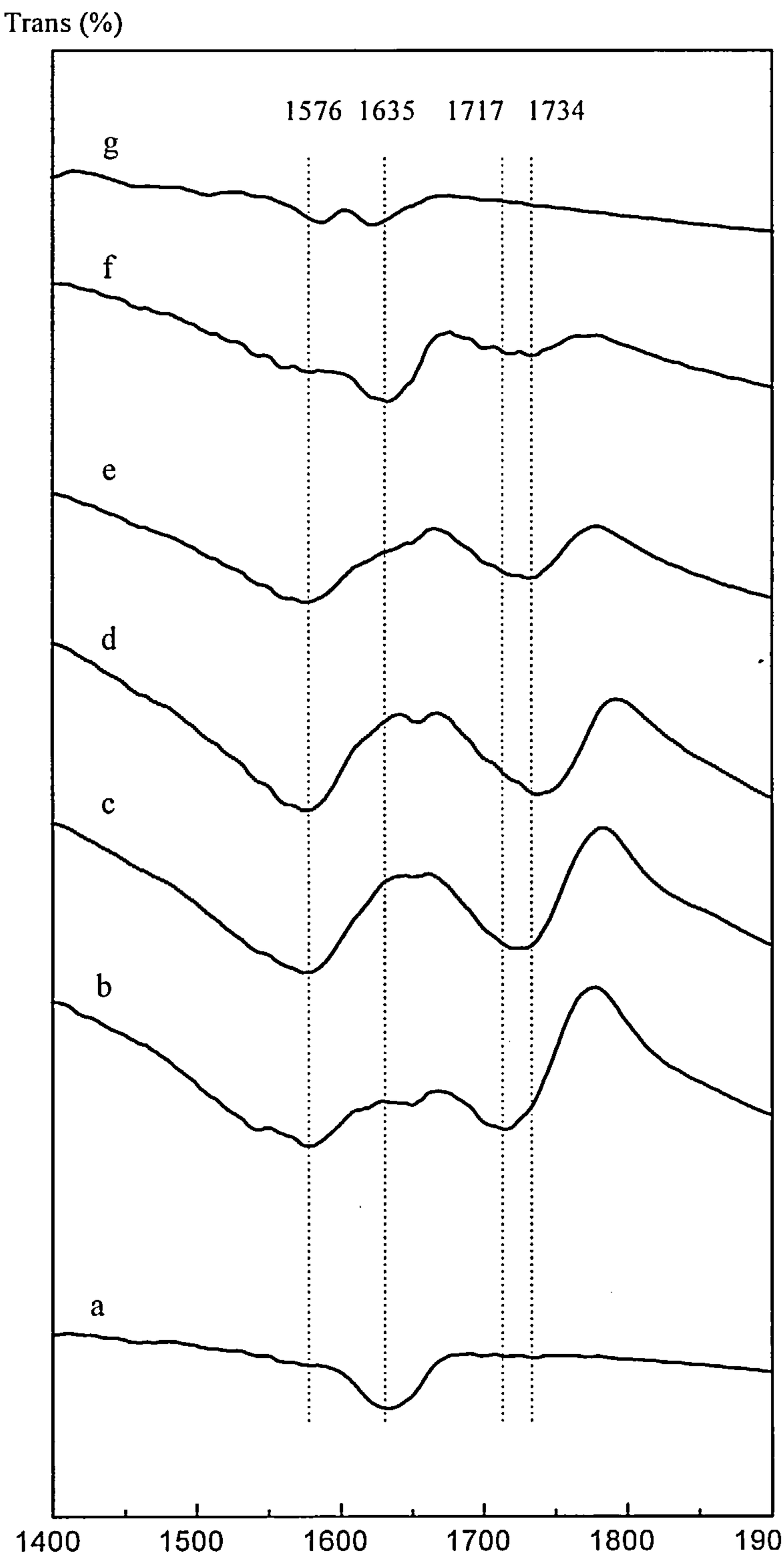

Figure 6.11 FTIR spectra of a) original carbon C1, b) CN2, c) CN2-300, d) CN2-400, e) CN2-500, f) CN2-600, g) CN2-800

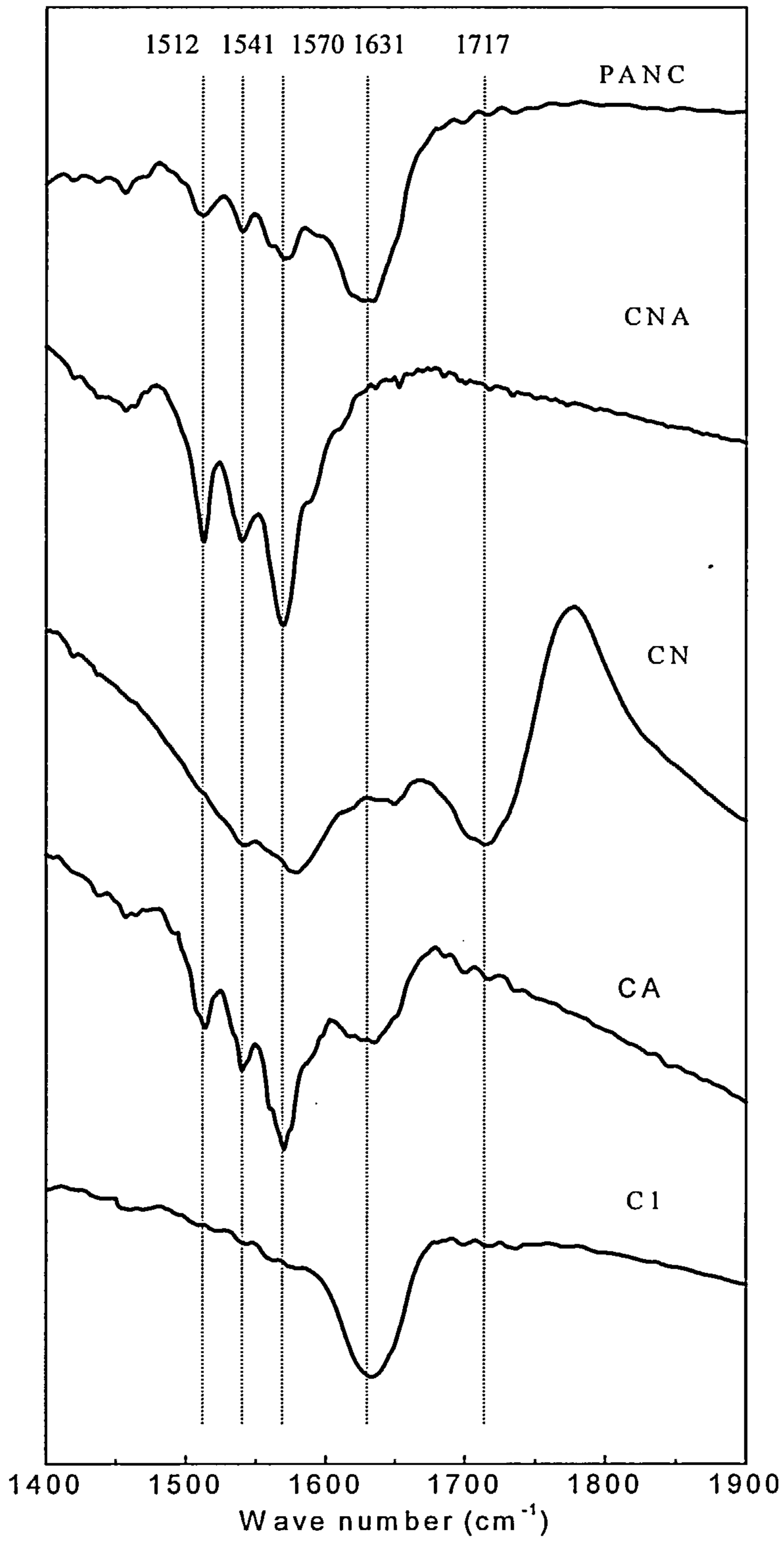

Figure 6.12 FTIR spectra of carbon C1, CA, CN, CNA and PAN1

6.2 Adsorption of Gold and Silver Cyanide Species From Aqueous Solution

6.2.1 Gold and Silver Cyanide Species Present in Solution

Figure 6.13 shows the Raman spectra of $KAu(CN)_2$, $KAu(CN)_2/KCN$, $KAg(CN)_2$, $KAg(CN)_2/KCN$ and KCN aqueous solutions. It is apparent that there are three Raman peaks for $KAg(CN)_2/KCN$ solution with CN^-/Ag^+ mole ratio of 4.5 whereas only two peaks are observed for the corresponding $KAu(CN)_2/KCN$ aqueous solution. In $KAu(CN)_2/KCN$ aqueous solution, the two Raman peaks at 2079 cm^{-1} and 2165 cm^{-1} are assigned as free cyanide ion CN^- and $Au(CN)_2^-$ respectively in agreement with the Raman spectra of solutions of pure KCN and $KAu(CN)_2$. In $KAg(CN)_2/KCN$ aqueous solution, comparison with the Raman spectra of KCN and $KAg(CN)_2$ solutions leads to the assignment of the bands at 2079 cm^{-1} and 2141 cm^{-1} to CN^- and $Ag(CN)_2^-$ respectively. The Raman peak at 2109 cm^{-1} obtained for higher CN^-/Ag^+ mole ratio (4.5) is attributed to $Ag(CN)_3^{2-}$, based on the assignment of Chantry *et al* [***19***]. $Ag(CN)_3^{2-}$ is the dominant silver species in the solution of CN^-/Ag^+ ratio of 4.5 whereas only a small amount of $AgCN)_2^-$ exists. The geometry of silver (I) tricyano complex is thought to be tetrahedral by the formation of complex $Ag(CN)_3(H_2O)^{2-}$ [***20***]. This indicates that $Ag(CN)_2^-$ concentration is comparatively low in the presence of excess free cyanide ions in solution. Jones *et al* [***20***] also observed additional peaks in the infrared spectra at high CN^-/Ag^+ mole ratios which were assigned to the presence of $Ag(CN)_4^{3-}$ ion in solution.

The infrared spectra of solid $KAu(CN)_2$, $KAg(CN)_2$ and the aqueous solutions of $KAu(CN)_2$, $KAu(CN)_2/KCN$, $KAg(CN)_2$ and $KAg(CN)_2/KCN$ are shown in **Figure**

6.14. One peak is observed for $KAu(CN)_2$ and $KAg(CN)_2$ solutions at 2147 cm^{-1} and 2135 cm^{-1} respectively whereas $KAg(CN)_2$ / KCN solution shows three peaks at 2135 cm^{-1}, 2104 cm^{-1} and 2080 cm^{-1} and $KAu(CN)_2$ / KCN solution shows two peaks at 2147 cm^{-1} and 2080 cm^{-1}. The IR peaks at 2147 cm^{-1} for $KAu(CN)_2$ solution and 2135 cm^{-1} for $KAg(CN)_2$ solution are assigned as $Au(CN)_2^-$ and $Ag(CN)_2^-$ respectively. These data are in good agreement with above Raman spectroscopy results and with the work of Jones et al [*20*]. This indicates that there is no detectable dissociation for $Au(CN)_2^-$ and $Ag(CN)_2^-$ in aqueous system. The two peaks at 2147 cm^{-1} and 2080 cm^{-1} for $KAu(CN)_2$ / KCN solution are assigned as $Au(CN)_2^-$ and free cyanide ion CN^-. A new species is derived in $KAg(CN)_2$ / KCN aqueous solution with CN / Ag mole ratio of 6 which gave a IR peak at 2104 cm^{-1}. This dominant species in solution is attributed to $Ag(CN)_3^{2-}$ based on previous assignment [*19-21*].

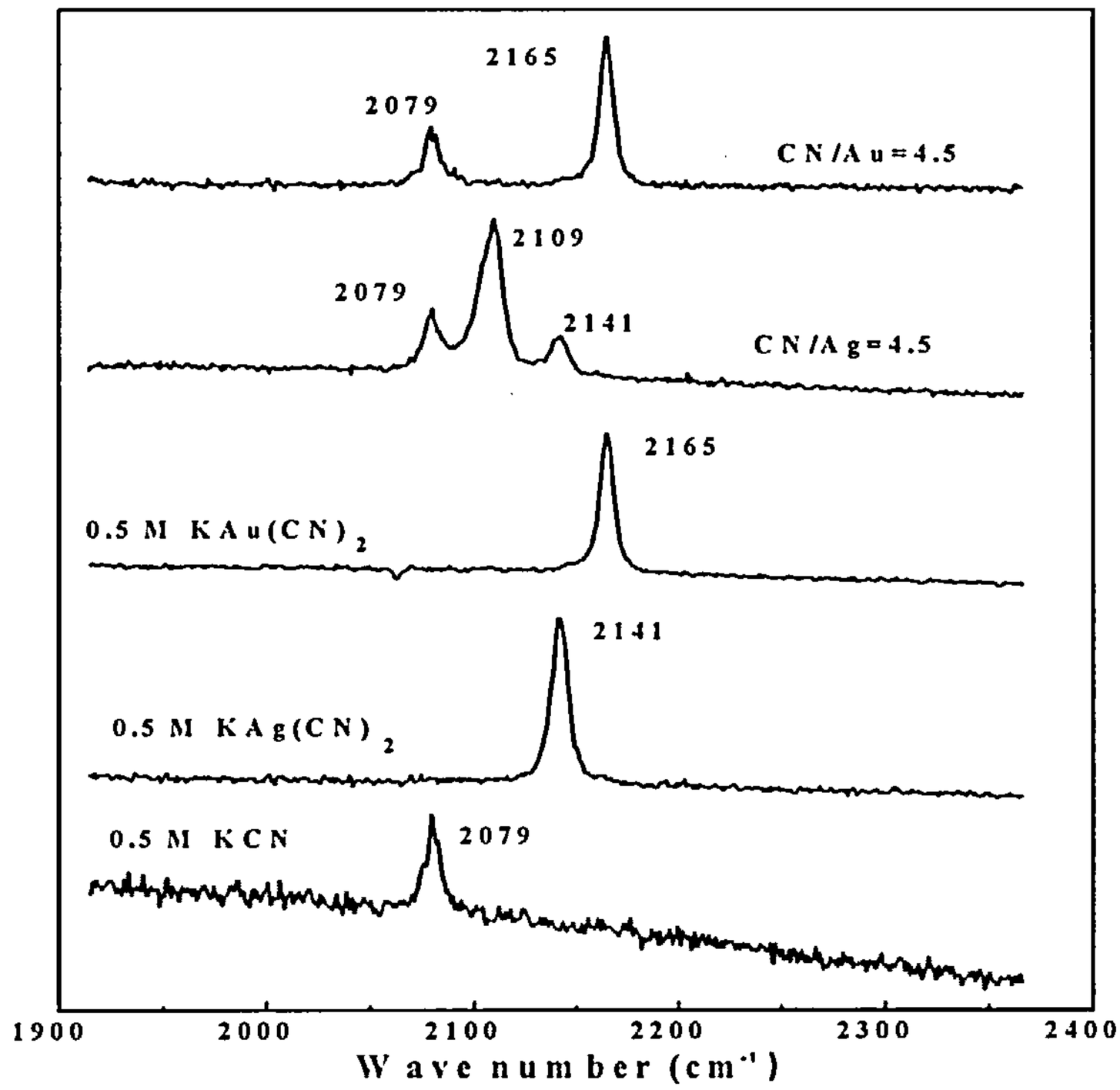

Figure 6.13 Raman spectra of aqueous KCN, $KAu(CN)_2$ and $KAg(CN)_2$ solutions

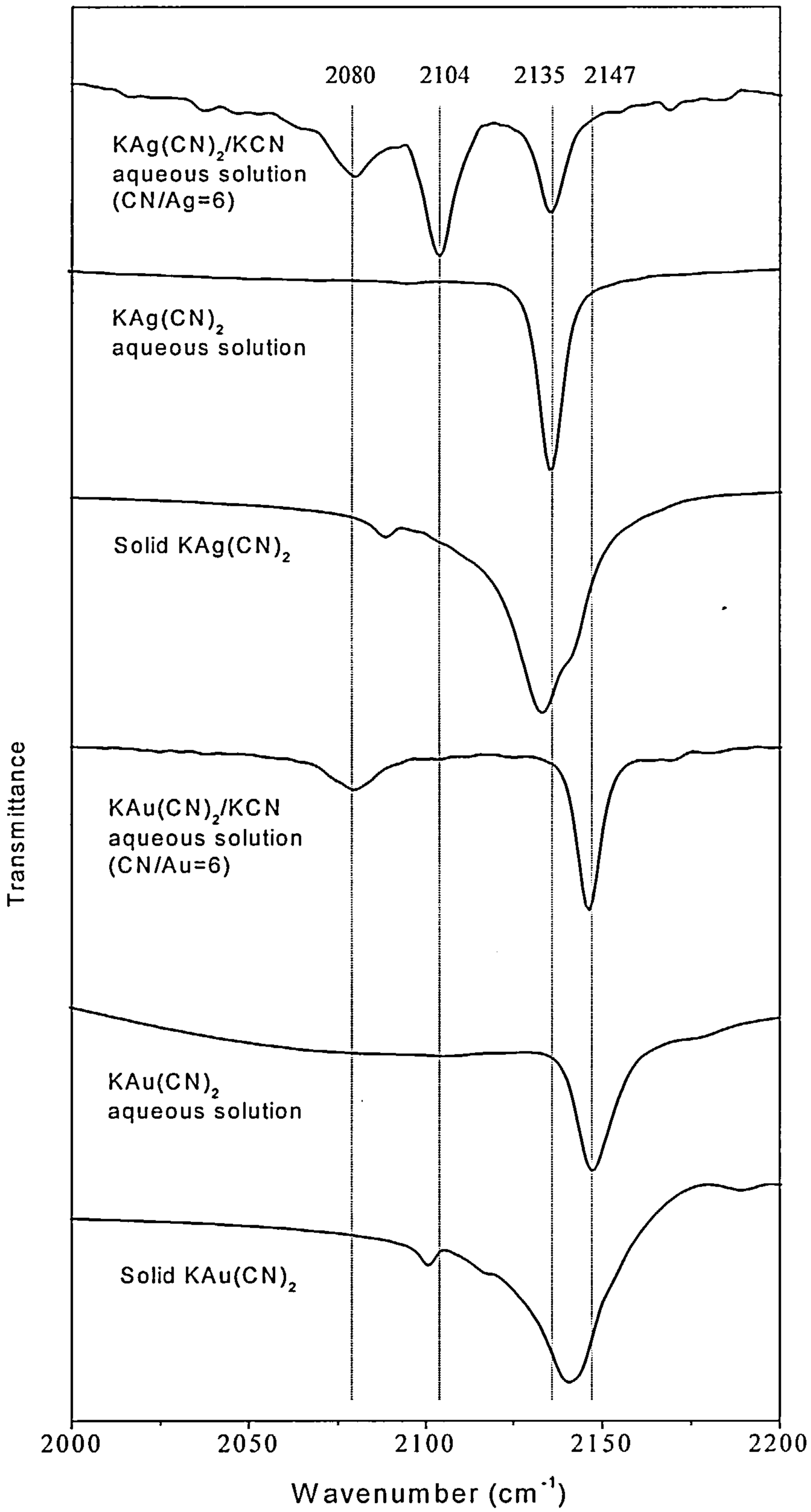

Figure 6.14 Infrared spectra of $KAu(CN)_2$, $KAg(CN)_2$ and their aqueous solutions

6.2.2 Effect of Burn-off of Active Carbons on Gold and Silver Adsorption Capacities

Figure 6.15 shows gold cyanide ionic species adsorption isotherms in the presence of buffer solution at pH 10 for the set of carbon derived from coconut shell. The relations between carbon burn-off and gold and silver adsorption capacities are evident. The gold adsorption capacities increase appreciably with increasing extent of activation of the active carbons.

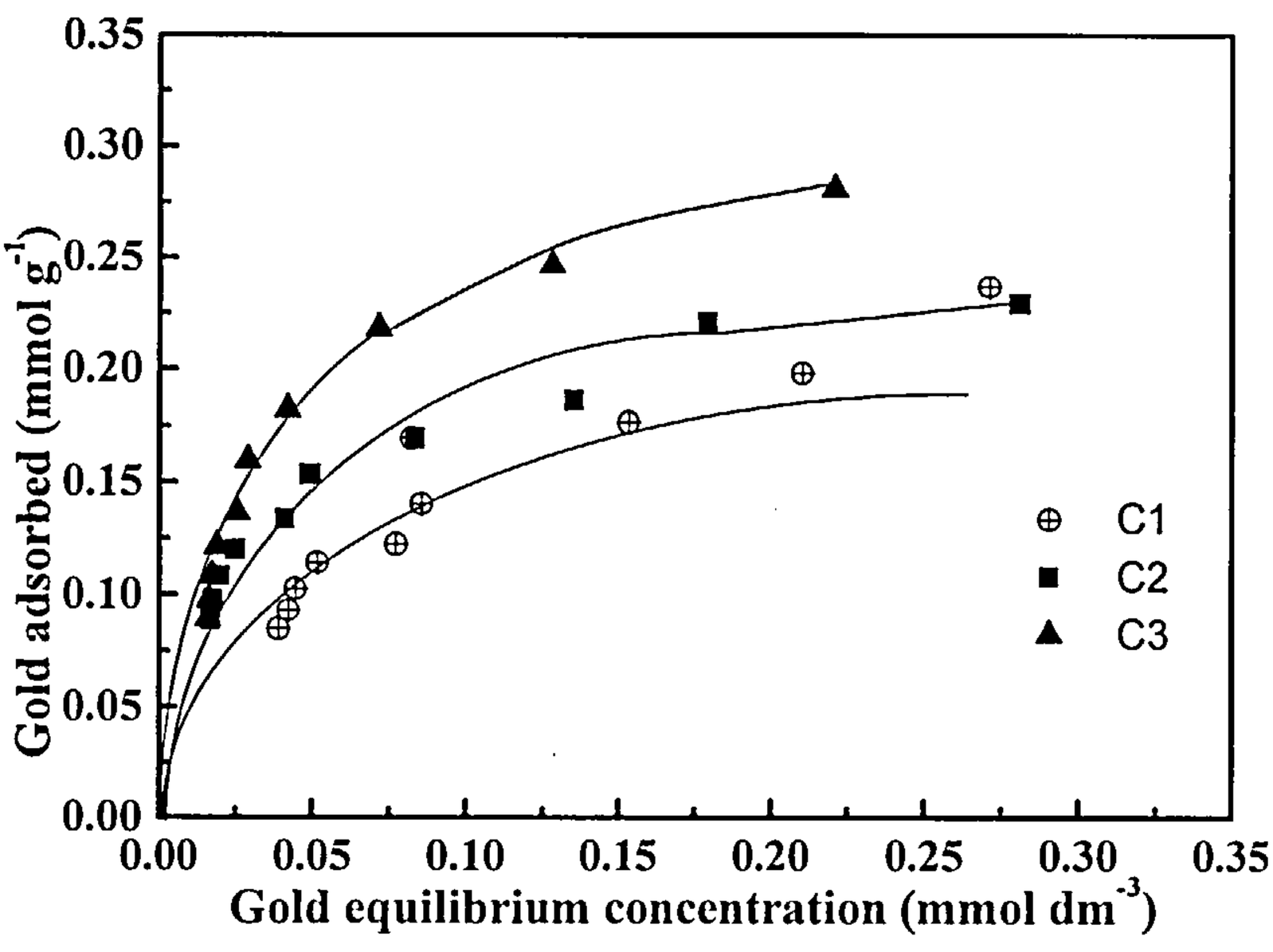

Figure 6.15 A comparison of $Au(CN)_2^-$ adsorption isotherms in the presence of CN^- (4 mmol dm^{-3}) at pH 10 for coconut shell derived active carbons

6.2.3 Effect of Nitric Acid and Ammonia Treatment on Gold and Silver Adsorption

Figure 6.16 shows a comparison of $KAu(CN)_2$ adsorption isotherms in borate buffer solution (pH 10) for C1, CN2 and CNA. It is apparent that nitric acid oxidation treatment significantly decreased gold adsorption capacity. Gasification of CN2 in ammonia to form CNA dramatically increased the total pore volume, nitrogen content and gold adsorption capacity. However the gold capacity was still lower than original untreated C1 carbon. The decrease in the adsorption capacity of gold on oxidised carbon is probably due to the blockage of the micropores by functional groups, the destruction of graphene layers and the more negative acidic surface formed after oxidation which is detrimental to the adsorption of aurocyanide anions.

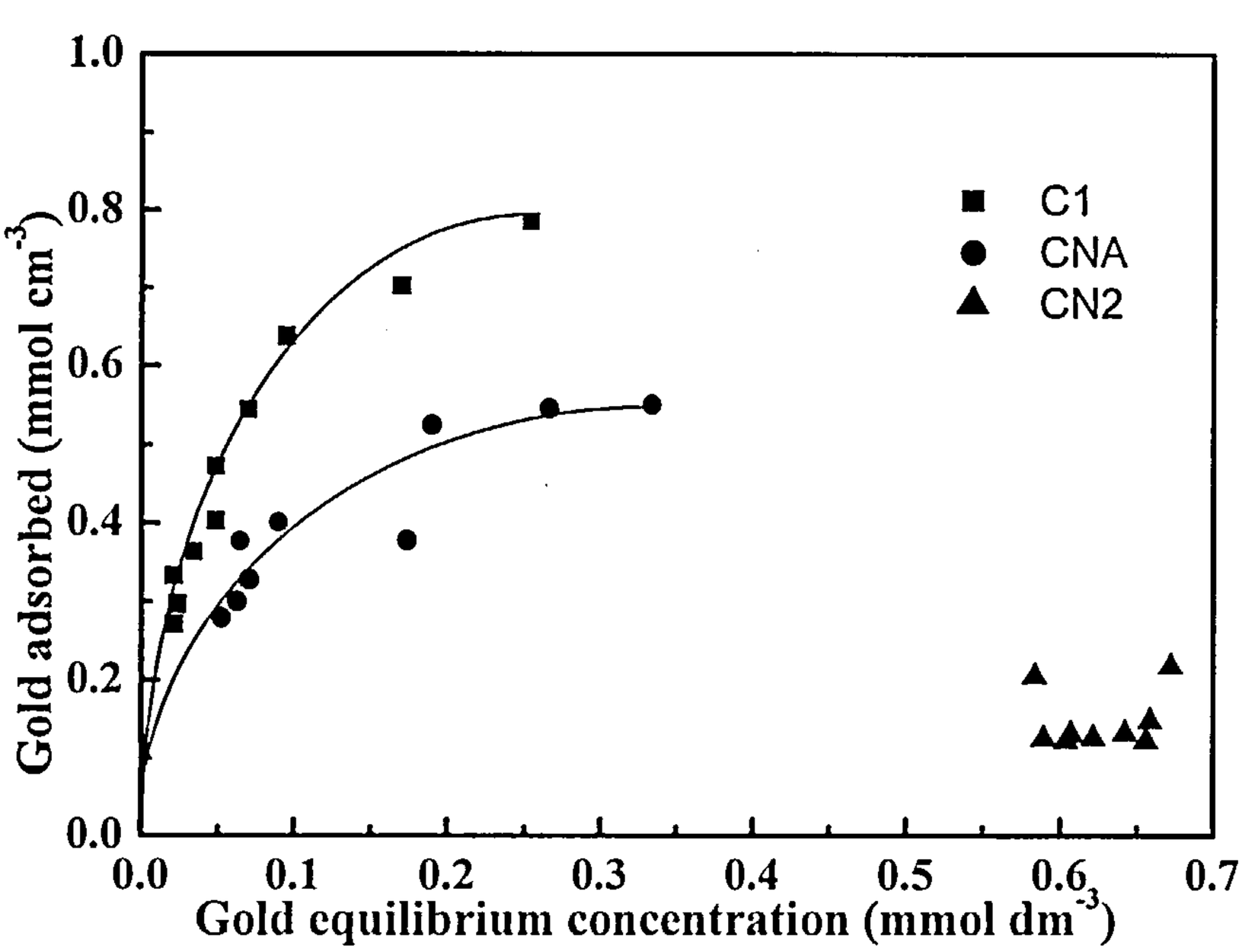

Figure 6.16 A comparison of $Au(CN)_2^-$ adsorption isotherms normalised to total pore volume in the presence of CN^- (4 mmol dm^{-3}) at pH 10 for C1, CN2 and CNA

6.2.4 Effect of Alcohols on Gold Adsorption Capacity of Carbons

The influence of primary alcohols on gold adsorption capacity of active carbon C1 is shown in **Figure 6.17**. The concentration of butan-1-ol in $KAu(CN)_2$ solution was 0.67 mol dm^{-3}, which was lower than that of ethanol (1.19 mol dm^{-3}). Both alcohols have adverse effects on gold cyanide adsorption on carbon C1. There is very strong competitive adsorption of alcohols and gold cyanide species on the carbon. Butan-1-ol has a larger effect on gold cyanide species adsorption on the carbon than ethanol in spite of the lower concentration in solution and this is probably related to the more hydrophobic nature of butanol compared with ethanol.

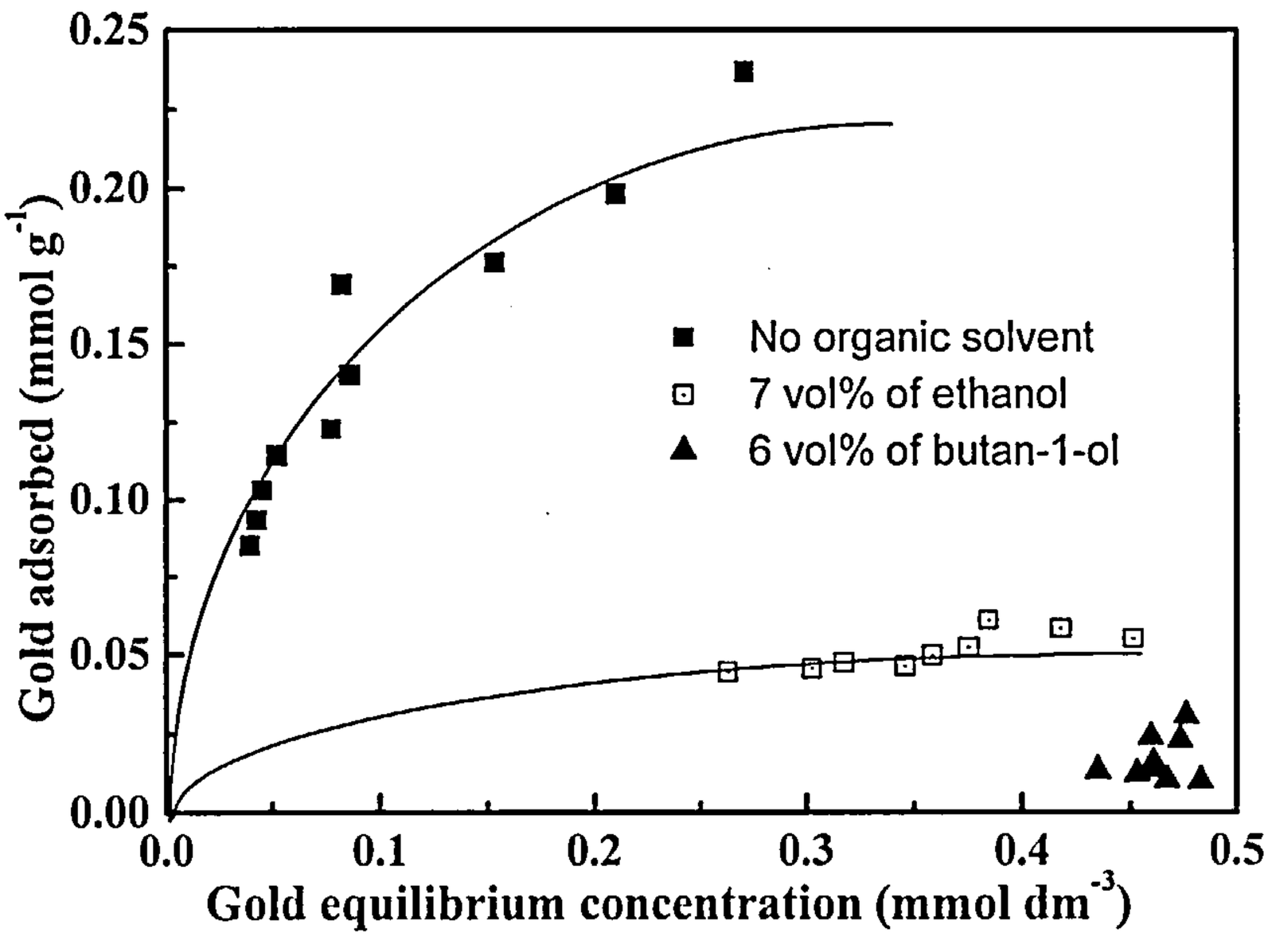

Figure 6.17 Effect of alcohols on $Au(CN)_2^-$ adsorption isotherms in the presence of CN^- (4 mmol dm^{-3}) at pH 10 (borate buffer) on C1

6.2.5 Effect of Free Cyanide Ions on Gold and Silver Adsorption

Figure 6.18 shows the adsorption isotherms of $KAu(CN)_2$ and $KAu(CN)_2$/KCN aqueous solutions at 25 °C, while **Figure 6.19** compares the adsorption capacities of $KAu(CN)_2$ on C1 with and without the presence of free cyanide at 70 °C. The results show that similar amounts of aurocyanide species are adsorbed on carbon C1 at 25 °C with different CN^-/Au^+ ratios. This indicates that excess free cyanide ion has little effect on the adsorption capacity of gold cyanide at 25 °C. In contrast, when the temperature was increased to 70 °C, excess free cyanide ions in solution markedly decreased the adsorption of gold cyanide on carbon C1. This provides sound evidence and basis for the elution of gold from activated carbon which is carried out at higher temperature and in the presence of excess free cyanide ions. In order to confirm the reaction between free cyanide and surface functional groups of carbon, the carbon was treated with aqueous solution of potassium cyanide by refluxing for 4 hours followed by Soxhlet extraction with water to remove residual cyanide in carbon. The treated carbon was then subjected to the adsorption of $KAu(CN)_2$ in the absence of free cyanide at 25 °C and the result is shown in **Figure 6.20**. It is apparent that after the carbon was treated with KCN at 70 °C, the adsorption capacity of was decreased significantly. This indicates that there was a reaction between CN^- and the oxygen functionality on the carbon surface with the products having an adverse effect on the adsorption of gold cyanide species. But this was not as large as the decrease in adsorption capacity in the presence of free CN^- ions.

Figure 6.21 shows the silver adsorption isotherms at different CN^-/Ag^+ ratios at 25 °C. It is evident that excess free cyanide ion in solution significantly decreased the

adsorption of silver cyanide species on carbon C1 with higher CN^-/Ag^+ ratio causing larger decreases in the silver adsorption capacity. The formation of $Ag(CN)_3^{2-}$ etc is one of the reasons why gold is adsorbed to a greater extent than silver on activated carbon. **Figure 6.22** shows the effect of excess free CN^- on the adsorption of silver cyanide on peat derived active carbon P1. The adsorption capacity of silver cyanide was reduced by free CN^- ions, however the extent of the decrease in silver adsorption on P1 is smaller in comparison with coconut shell carbon C1.

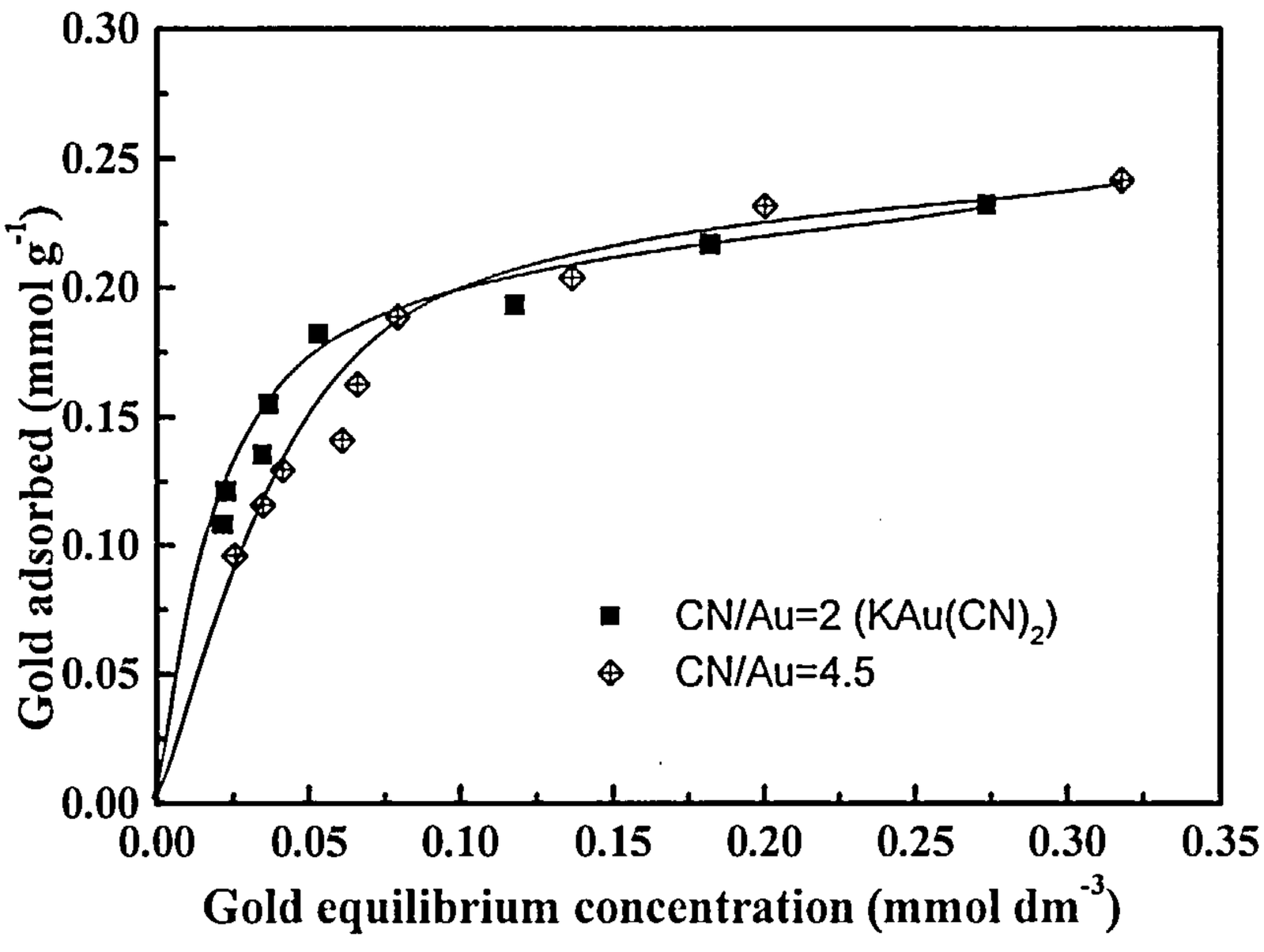

Figure 6.18 The effect of excess free CN^- on the adsorption of gold cyanide species on C1 active carbon at 298 K

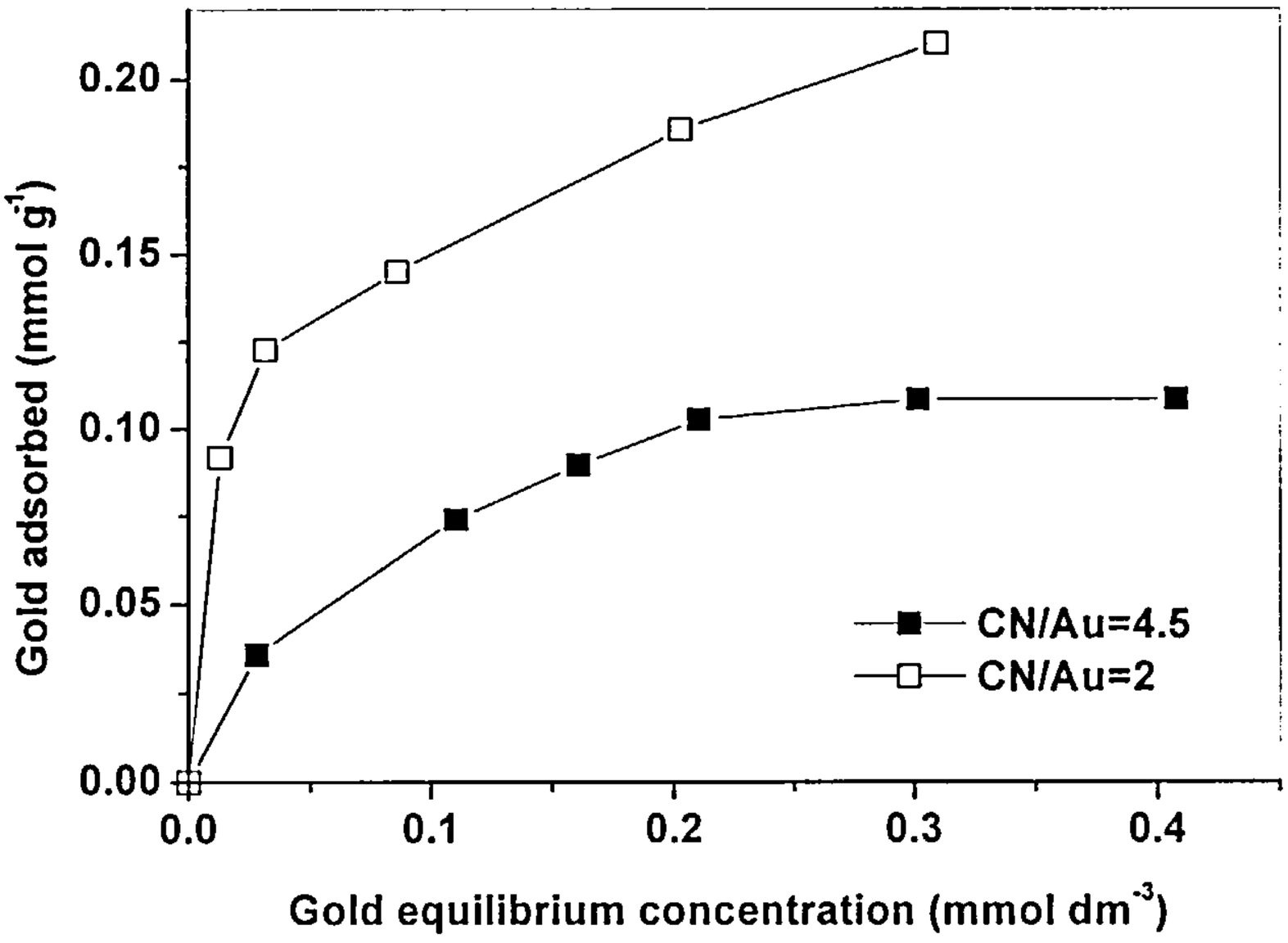

Figure 6.19 The effect of excess free CN^- on the adsorption of gold cyanide species on C1 active carbon at 343 K

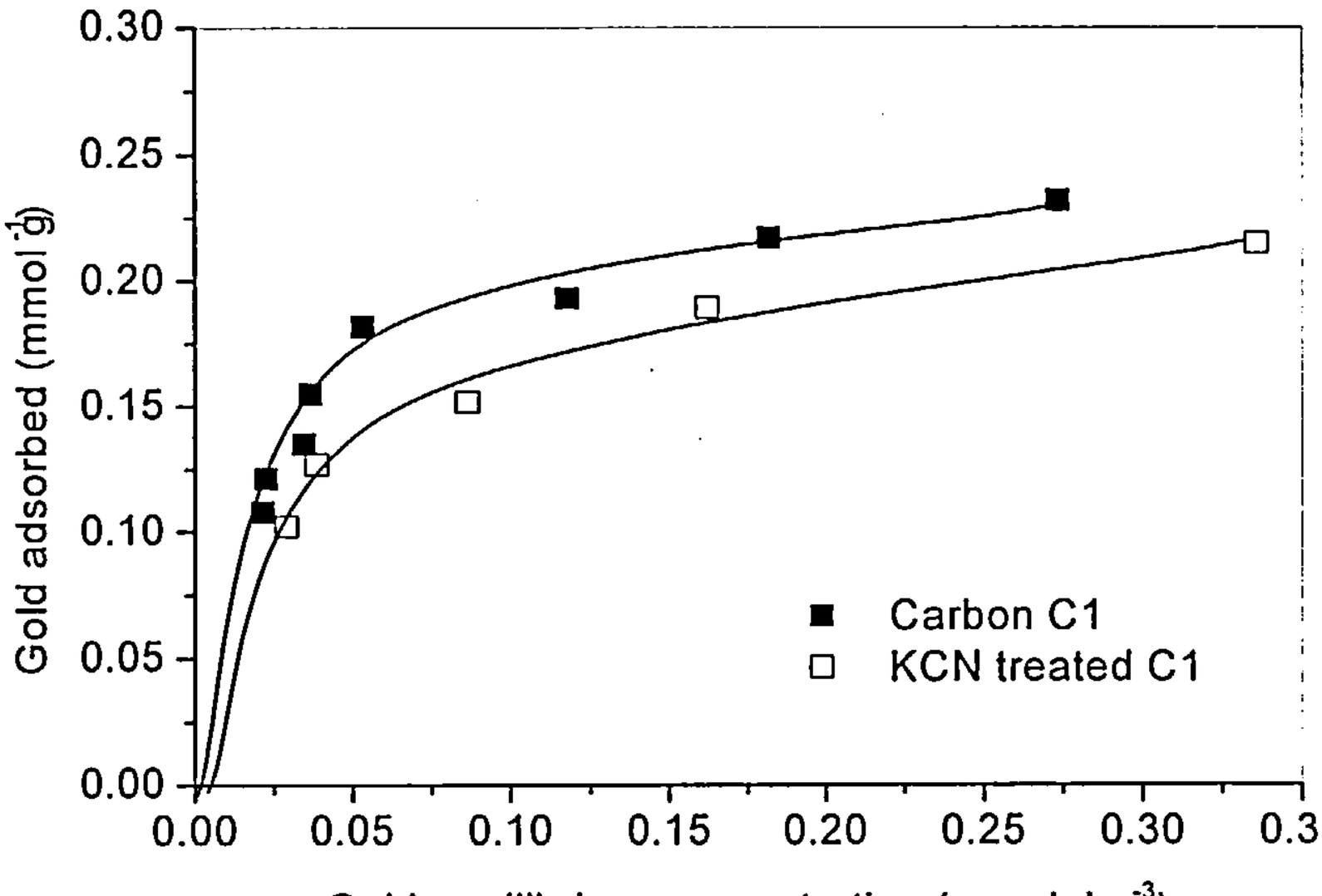

Figure 6.20 Effect of KCN treatment of C1 active carbon on the adsorption of $KAu(CN)_2$ at 298 K

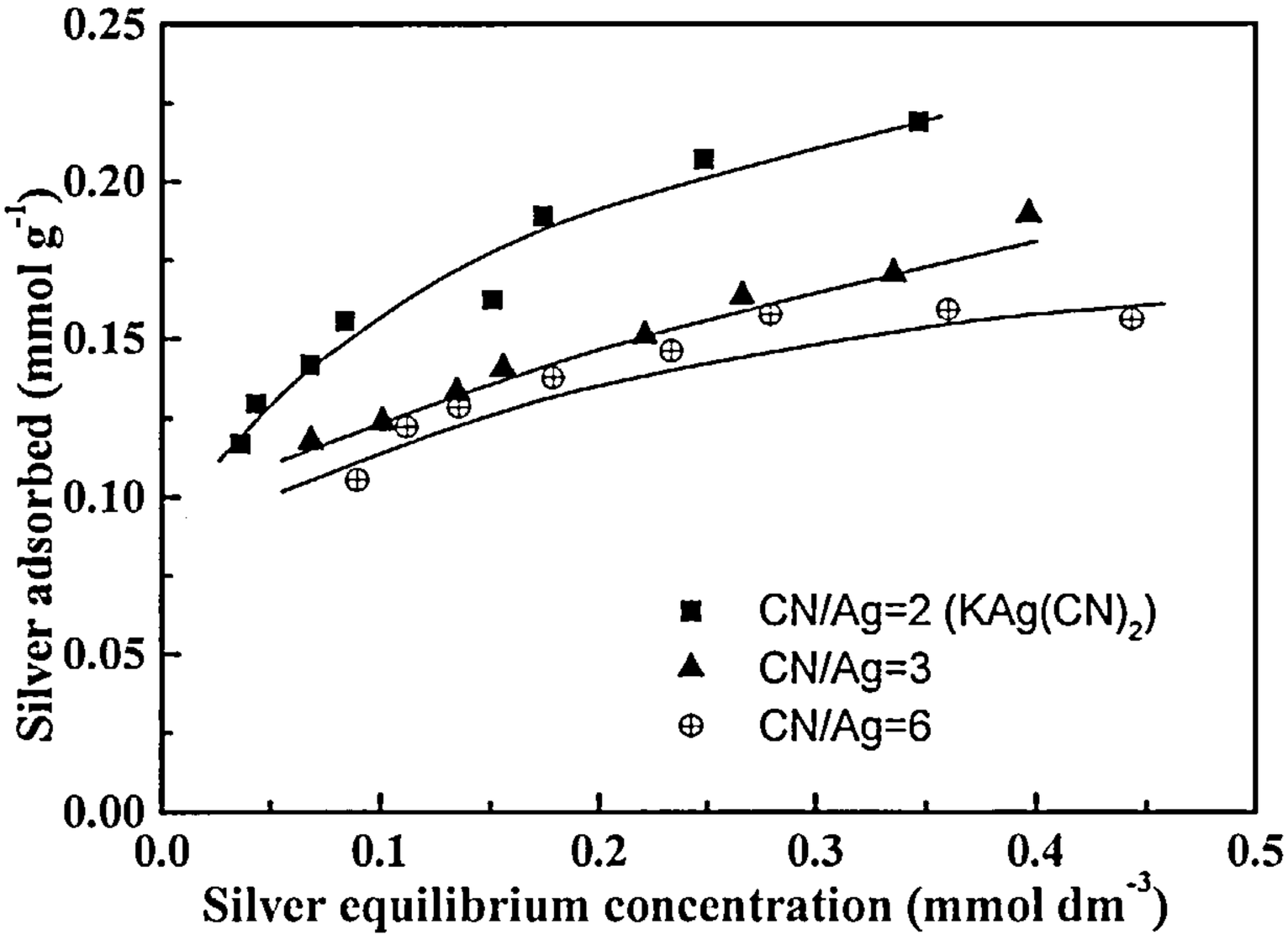

Figure 6.21 The effect of excess free CN^- on the adsorption of silver cyanide species on C1 active carbon at 298 K

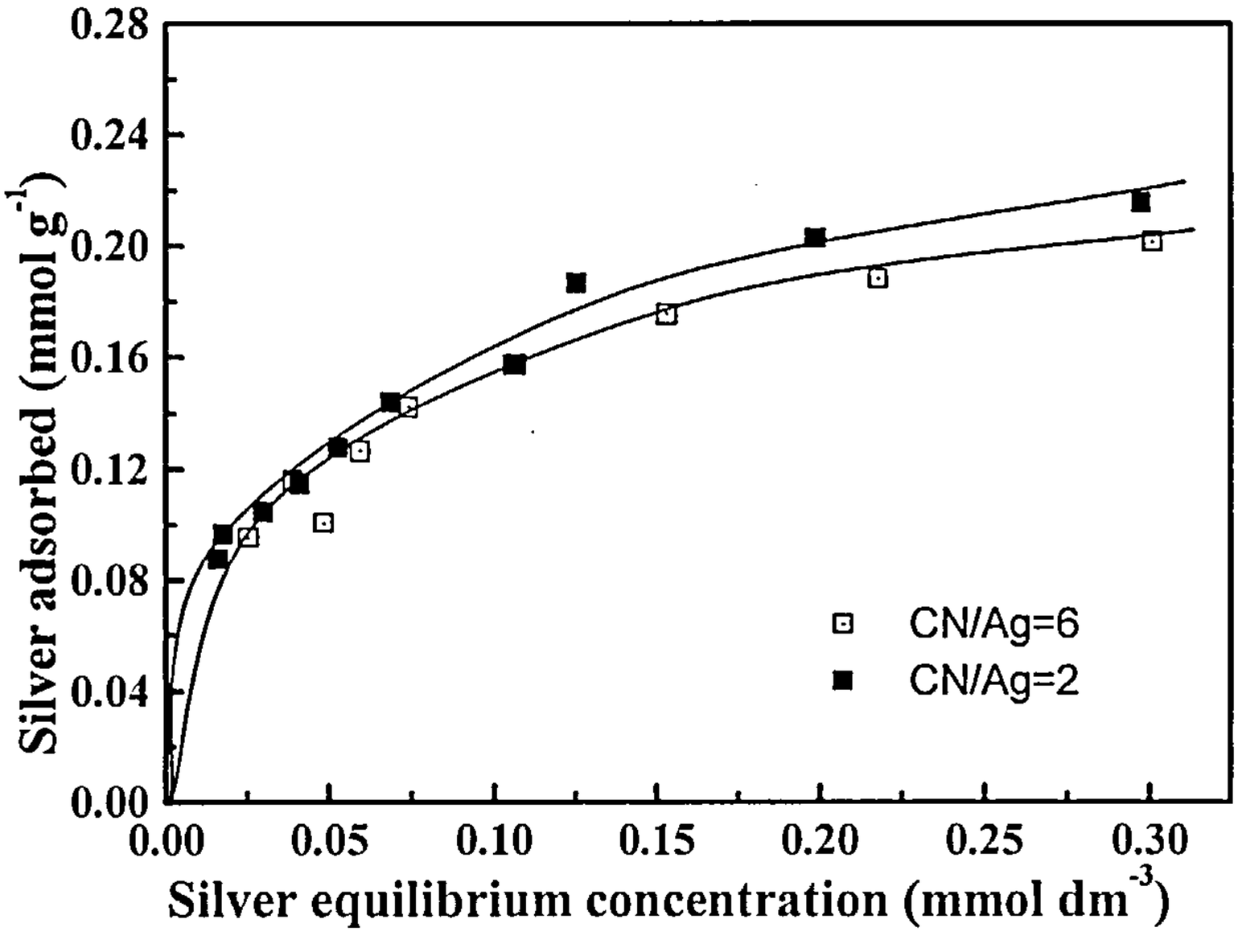

Figure 6.22 The effect of excess free CN^- on the adsorption of silver cyanide species on peat based carbon P1 at 298 K

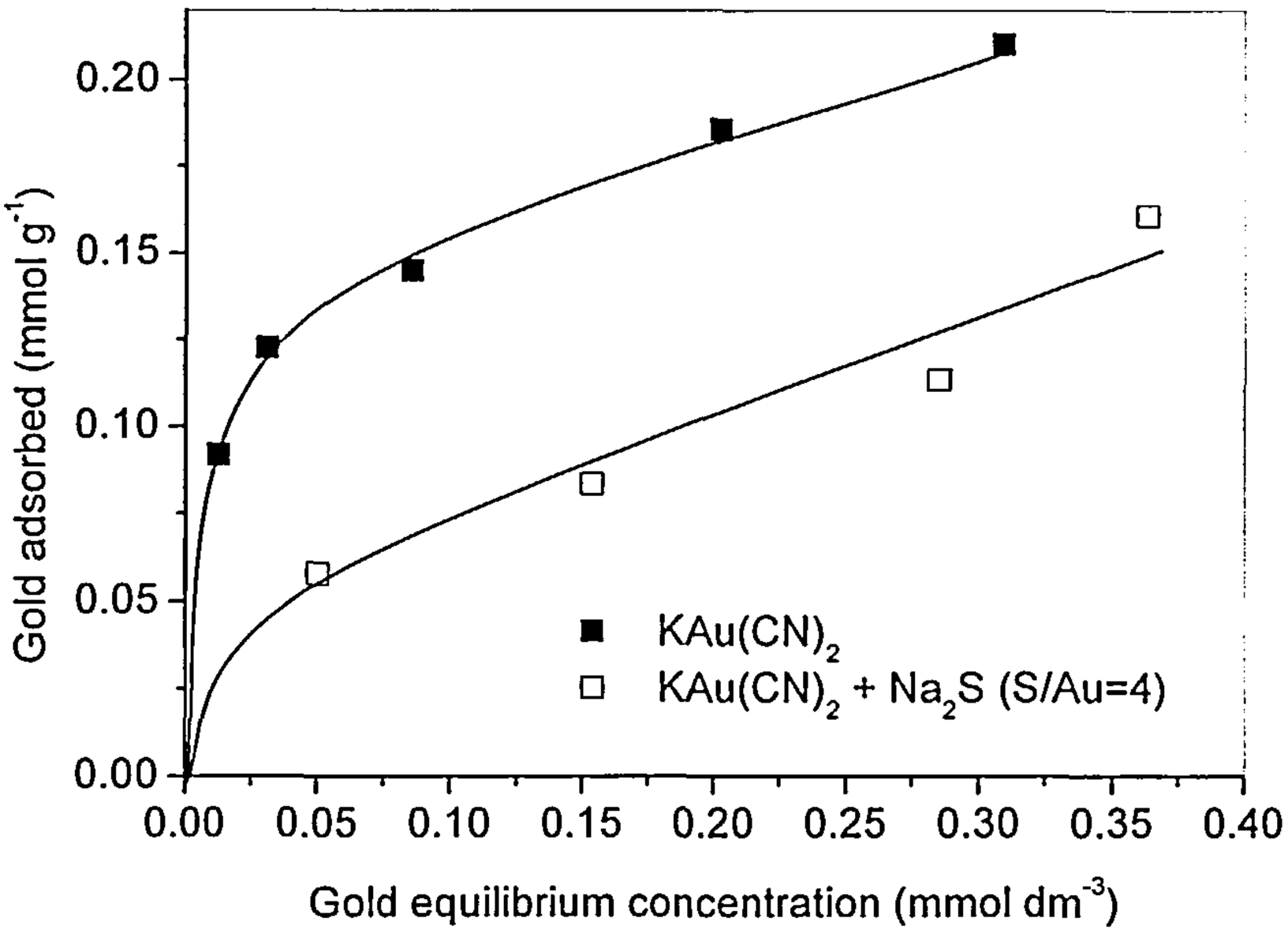

Figure 6.23 Effect of sodium sulphide present in solution on the adsorption of gold cyanide species on carbon C1 at 343 K

6.2.6 Effect of Sodium Sulphide on the Adsorption of Gold

The effect of sodium sulphide on the adsorption of gold cyanide on active carbon C1 at 70 °C is shown in **Figure 6.23**. It is apparent that the sodium sulphide present in solution is detrimental to the adsorption of gold cyanide species on carbon. The extent of decrease in gold adsorption capacity in the presence of sodium sulphide is similar to the effect of excess free cyanide ions present in solution. Therefore sodium sulphide can also be used to enhance the elution of gold from activated carbon after loading. However, due to the environmental concern and the problem in recycling process the sulphide has no significant advantages over sodium cyanide in the elution process.

6.2.7 Effect of Nitrogen Functionality on the Adsorption of Gold and Silver

The gold and silver cyanide adsorption capacities of PAN derived carbons are compared with peat derived carbon P1 and coconut shell derived carbon C2 in **Figures 6.24** and **6.25** respectively. The aurocyanide anion adsorption capacities on both P1 and C2 are appreciably higher than on the PAN derived carbons, PAN1 and PAN2. The silver cyanide adsorption on P1 was higher than PAN1 which has similar silver cyanide adsorption capacity to C2. The nitrogen contents of PAN1 (9.3 wt%) and PAN2 (9.5 wt%) were much higher than that of P1 (0.3 wt %), C2 (< 0.1%). The results indicate that the role of nitrogen functional groups present in the active carbon on gold and silver adsorption is negligible whereas the pore structure is important.

6.2.8 Effect of Degassing Treatment Prior to Adsorption

Basically the surface of active carbon is comprised of hydrophobic graphene layers and small amount of hydrophilic functional groups. Due to the hydrophobic nature of carbon surface, the contact with aqueous solution may not be complete, which could impact the accessibility of gold cyanide complex to the porous structure and restrict the surface available. This is true especially for micropores where there might be gas trapped in the porous structure which might restrict access to the pores. Therefore the carbon was degassed at room temperature prior to adsorption of gold. **Figure 6.26** shows the effect of degassing treatment on the adsorption of gold cyanide species on carbon P1. It is evident that there is little difference in gold adsorption capacity on P1 before and after degassing treatment. This indicates that air trapped in micro pores does not play an important role in the gold adsorption.

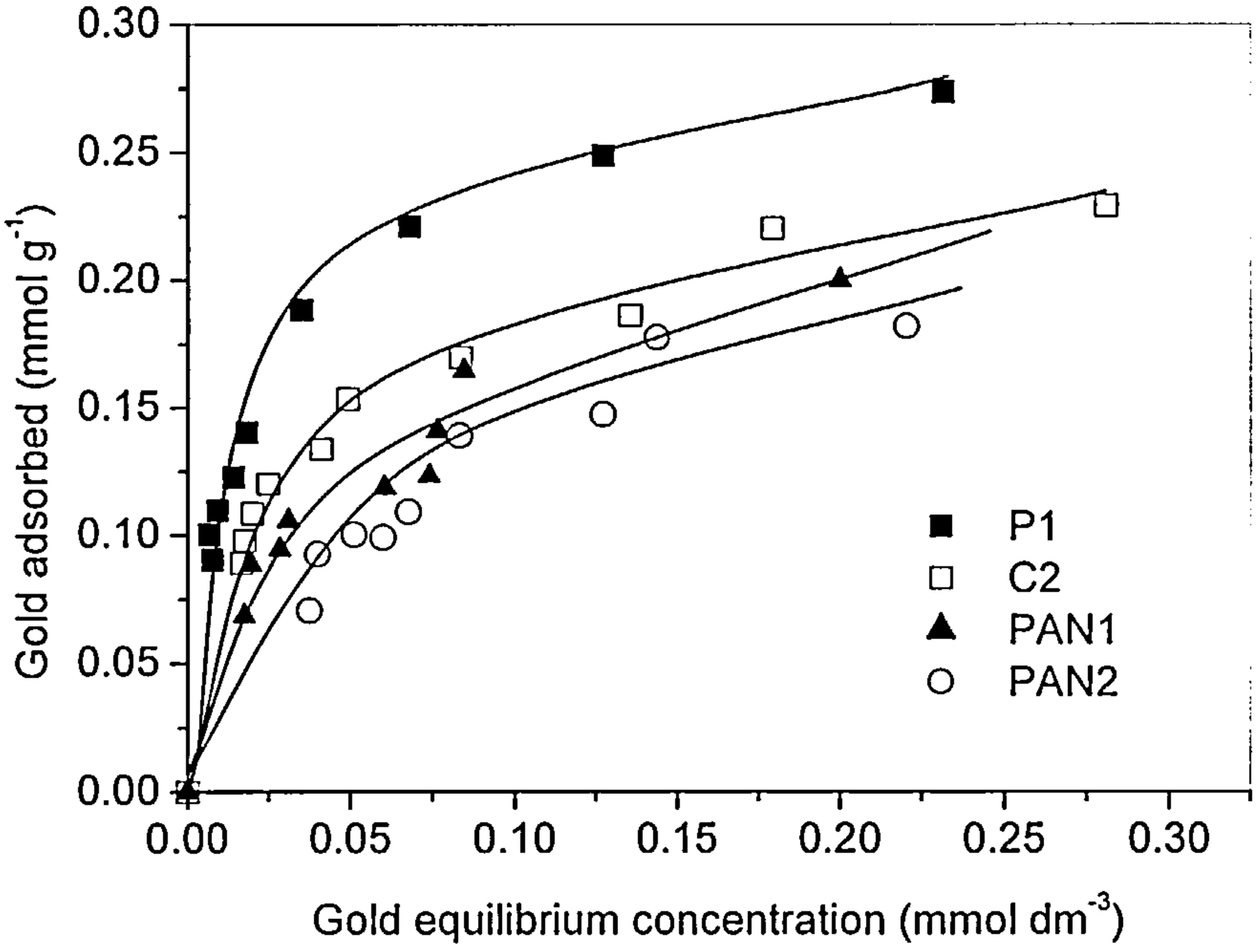

Figure 6.24 A comparison of gold adsorption isotherms in the presence of CN^- (4 mmol dm^{-3}) at pH 10 for P1, C2, PAN1 and PAN2

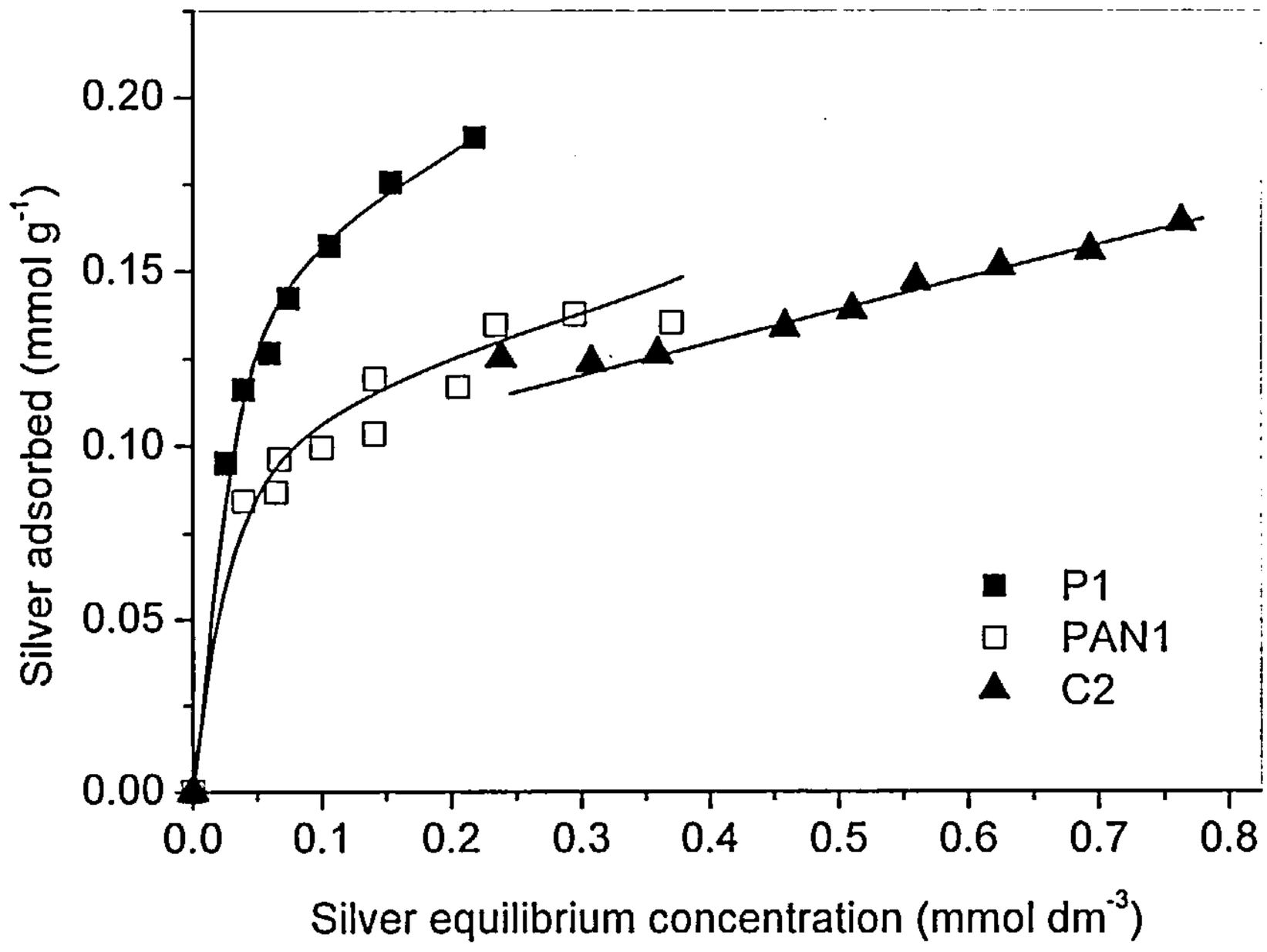

Figure 6.25 A comparison of silver adsorption isotherms in the presence of CN^- (2 mmol dm^{-3}) at pH 10 for P1, C2 and PAN1

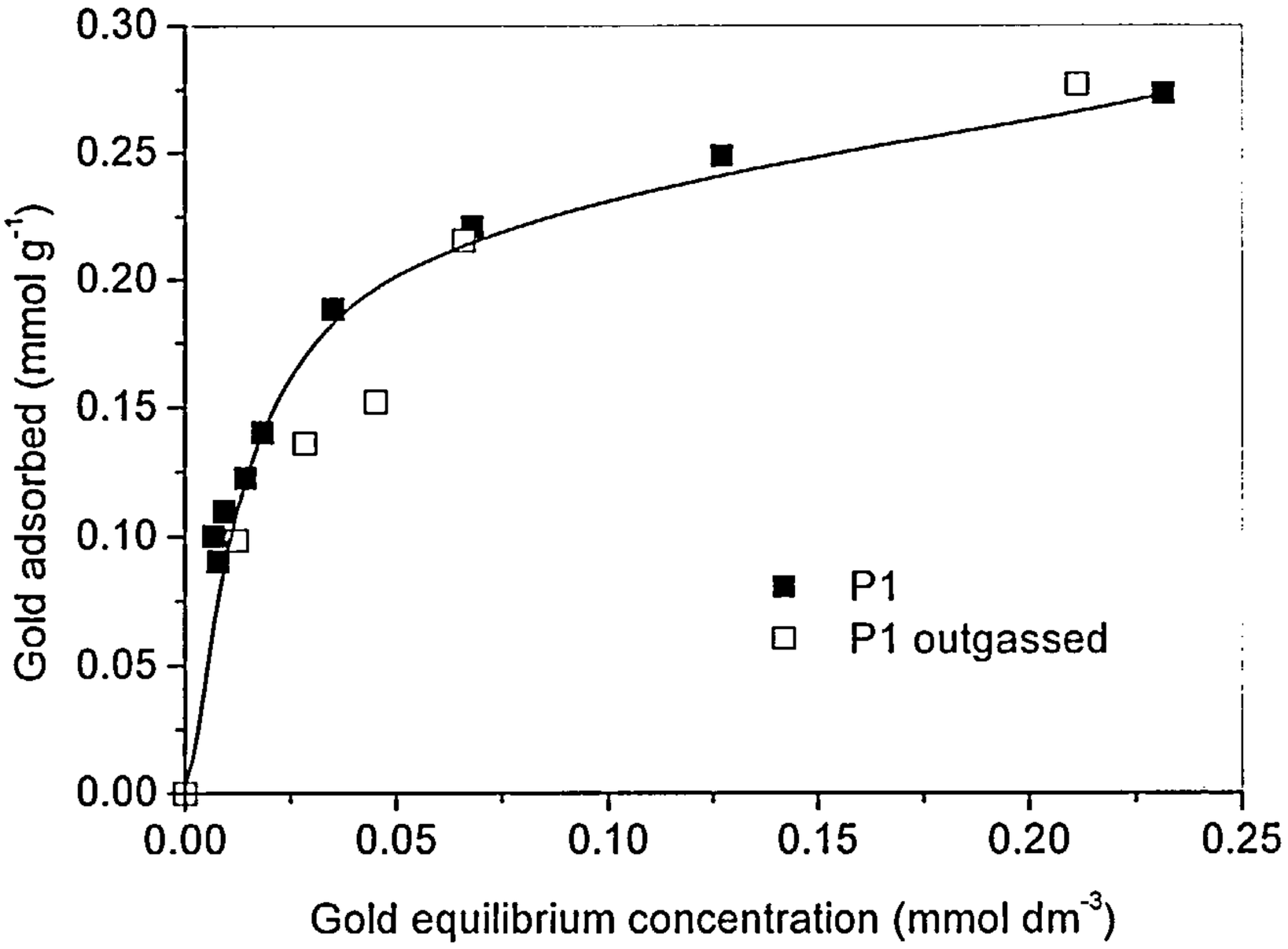

Figure 6.26 Effect of degassing treatment prior to adsorption on the adsorption of gold on carbon P1

6.3 Adsorption of Heavy Metal Cations on Oxygen Sites in Carbon

6.3.1 Adsorption of Cadmium

The adsorption kinetics of cadmium on HNO_3 oxidised carbon CN2 were studied in order to assess the time required for equilibrium to be achieved. The results showed that equilibrium was achieved within ~ 3 hours (see **Figure 6.27**). However the solutions were left for 48 hours to ensure complete equilibration.

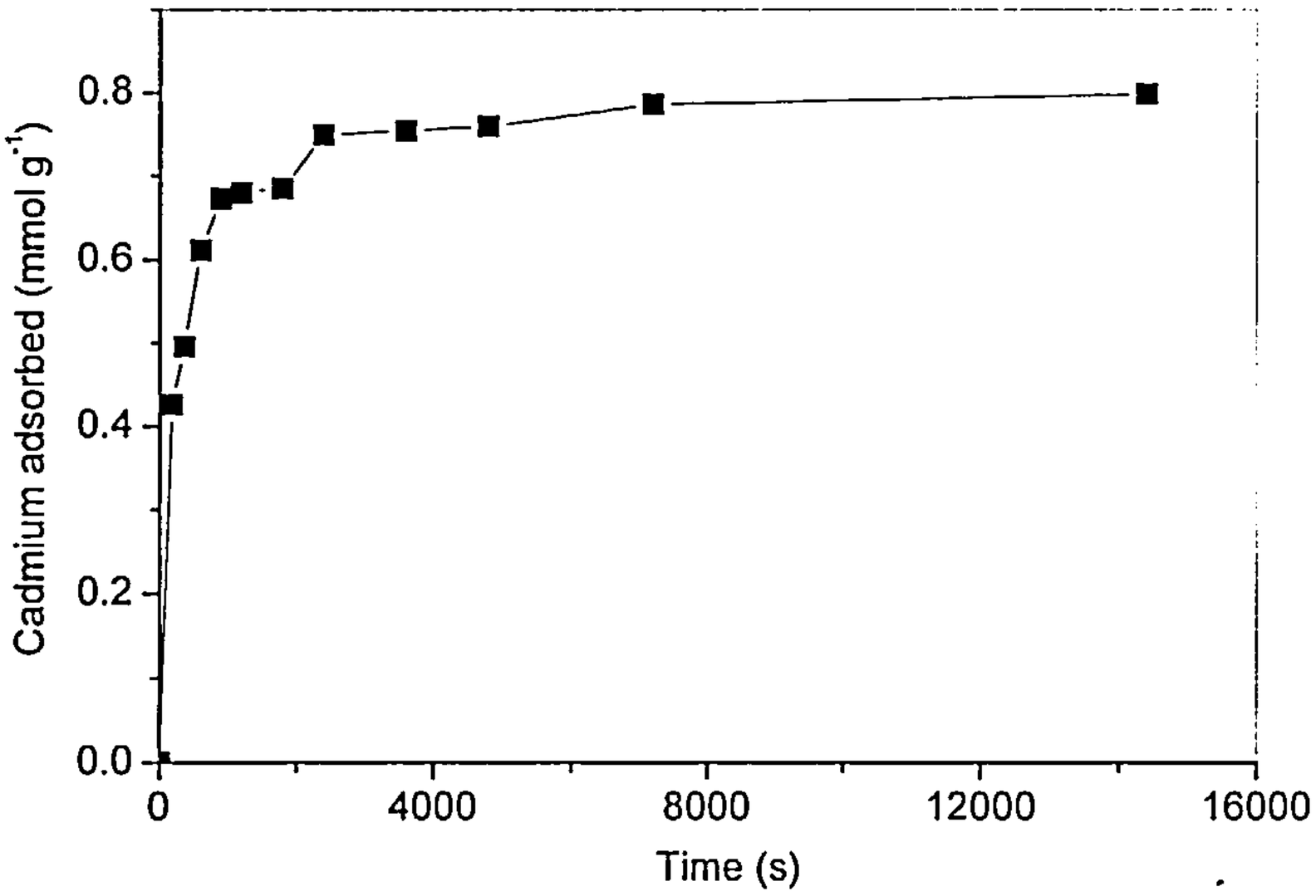

Figure 6.27 A plot of adsorbed amount *vs* time for cadmium on oxidised carbon CN2

The adsorption isotherms of cadmium on various carbons are shown in **Figures 6.28** and **6.29**. It is apparent that the adsorption capacities of cadmium were dramatically enhanced after the carbon C1 was oxidised with HNO_3. After CN1 and CN2 were subjected to progressive decomposition of surface oxygen functional groups by heat treatment at elevated temperatures, the adsorption capacities of Cd^{2+} on the carbons were reduced significantly. Comparison of the adsorption isotherms of cadmium on CN1 and CN2 shows that CN2 has higher capacity for cadmium. This indicates that higher extent of oxidation treatment by HNO_3 incorporated more oxygen functionality responsible for cadmium adsorption. The greatest reduction of the adsorption capacities of cadmium is observed for the carbons heated treated to 300

°C for 1 hour. This indicates that the acidic oxygen functional groups eliminated at ~ 300 °C which were assigned as mainly carboxylic acid groups play a very important role in the adsorption of cadmium cation.

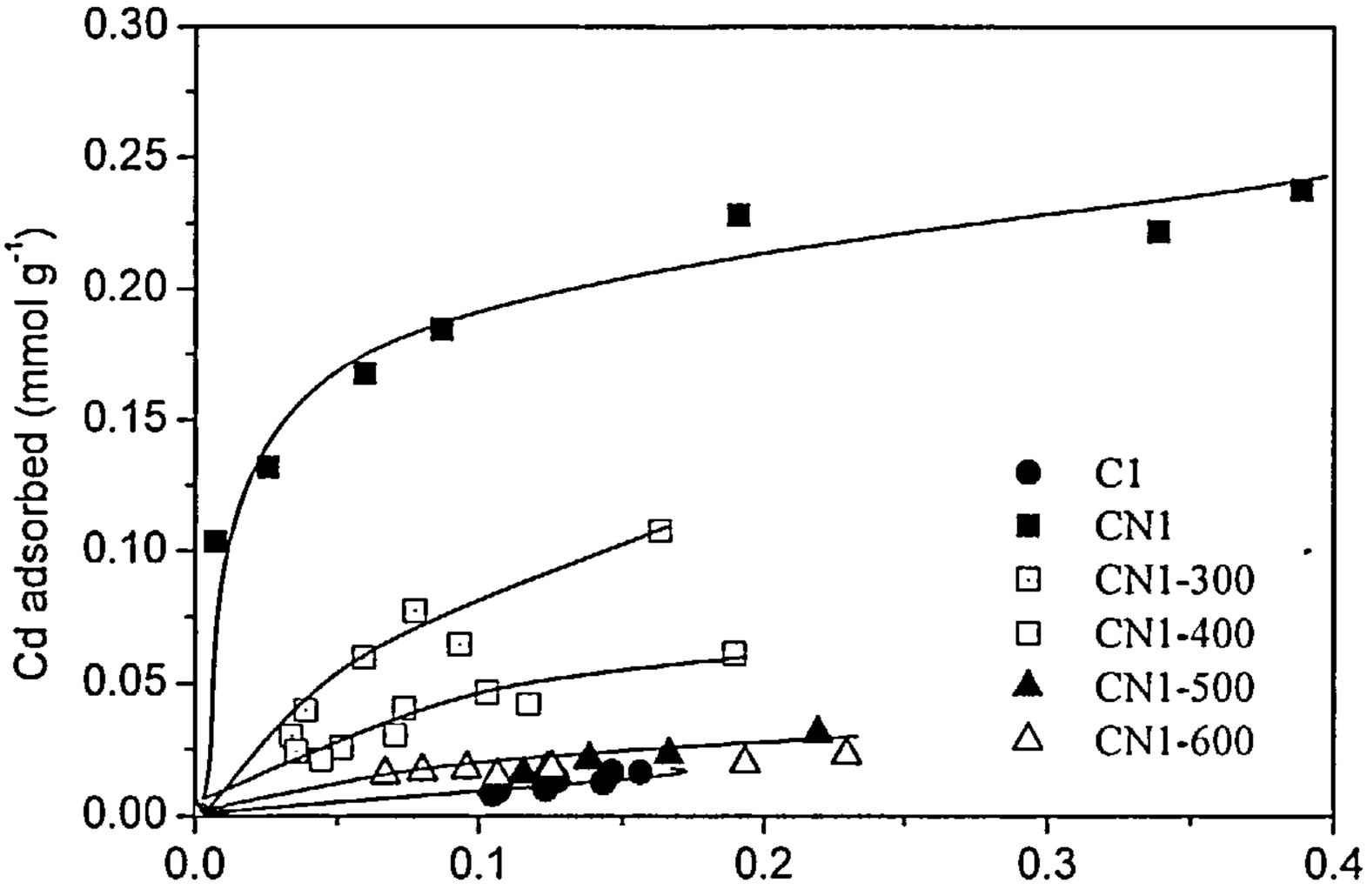

Figure 6.28 A comparison of adsorption isotherms of cadmium on oxidised carbon CN1 and heat treated derivatives

The changes in pH of residual solution after cadmium adsorption on various carbons were also monitored in this study. It was found that the pH decreased after adsorption of cadmium on HNO_3 treated carbons and their heat treated derivatives below 600 °C. Comparison of the cadmium adsorption studies with the corresponding blank reference studies showed that the release of protons from carbon when contacting with cadmium solution was entirely ascribed to the adsorption of cadmium which displaced the protons from the carbon surface. The relation between the amounts of adsorbed cadmium and that of released protons after adsorption on

oxidised carbon CN2 is shown in **Figure 6.30**. It is evident that the ratio of released H^+ to adsorbed Cd^{2+} is approximately 2 in the lower concentration range used in this study. The ratio decreased slightly at higher concentrations. The amounts of corresponding desorbed cadmium from carbon CN2 are also shown in **Figure 6.30**. It is apparent that little cadmium was desorbed from carbon CN2 by Soxhlet extraction using water. This was confirmed by EDA studies of the surface of CN2 after adsorption of cadmium followed by Soxhlet extraction with water. **Figure 6.31** shows the micrograph and cadmium distribution for a typical particle. It is apparent that the cadmium distribution is relatively uniform across the surface of the particle and that the cadmium was adsorbed irreversibly on the oxygen surface sites in the carbon. Therefore the carboxylic acid groups on the surface of carbon CN2 are probably the main sites for the adsorption of cadmium cations with the ion exchange of cadmium cations with the protons of carboxylic acid groups.

The relations between adsorbed cadmium and released H^+ for CN2-300 and CN2-400 are shown in **Figure 6.32**. It is apparent that after heat treatment of CN2 to eliminate some surface oxygen functional groups, the ratio of H^+/Cd^{2+} decreased in addition to the reduction of cadmium capacity. The H^+/Cd^{2+} ratio for adsorption on CN2-300 is slightly greater than 1 at lower concentration and less than 1 at higher concentration. The H^+/Cd^{2+} for adsorption on CN2-400 is much lower than that of CN2-300 and CN2 and this ratio also decreases with increasing equilibrium concentration.

In order to further investigate the adsorption mechanism of cadmium, the oxidised carbon CN2 was treated with NaOH to neutralise the acidity on the carbon surface and displace H^+ with Na^+. Adsorption of cadmium on Na^+ ion exchanged carbon was studied and the amounts of released Na^+ and adsorbed Cd^{2+} were

monitored (see **Figure 6.33**). At lower concentration the amount of desorbed Na^+ during cadmium adsorption is approximately twice that of adsorbed Cd^{2+}, indicating that cation exchange mechanism may be involved in the cadmium adsorption. At higher concentrations the Na^+/Cd^{2+} ratio is less than 2 and decreases gradually with increasing equilibrium Cd^{2+} concentration.

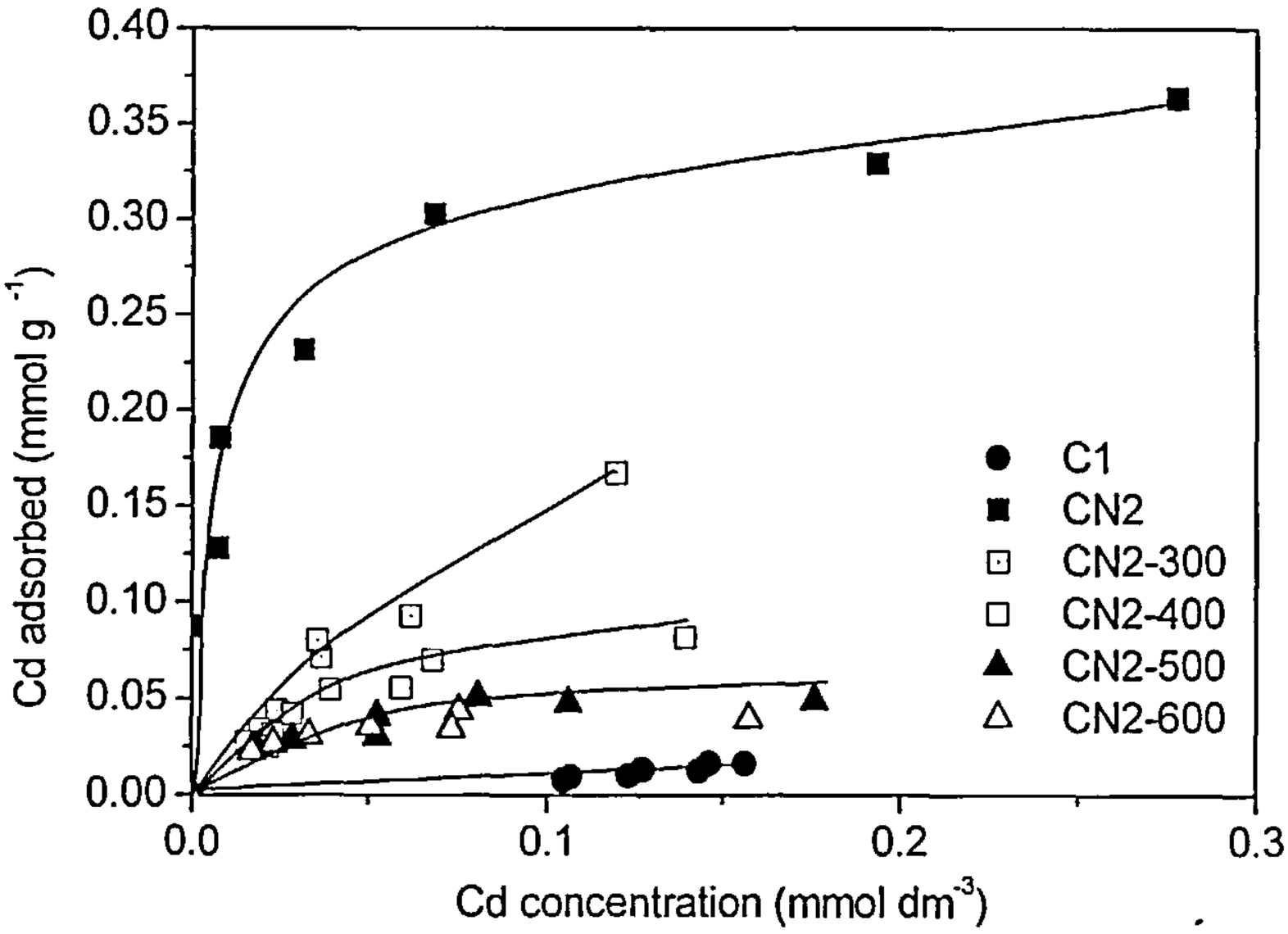

Figure 6.29 A comparison of adsorption isotherms of cadmium on oxidised carbon CN2 and heat treated derivatives

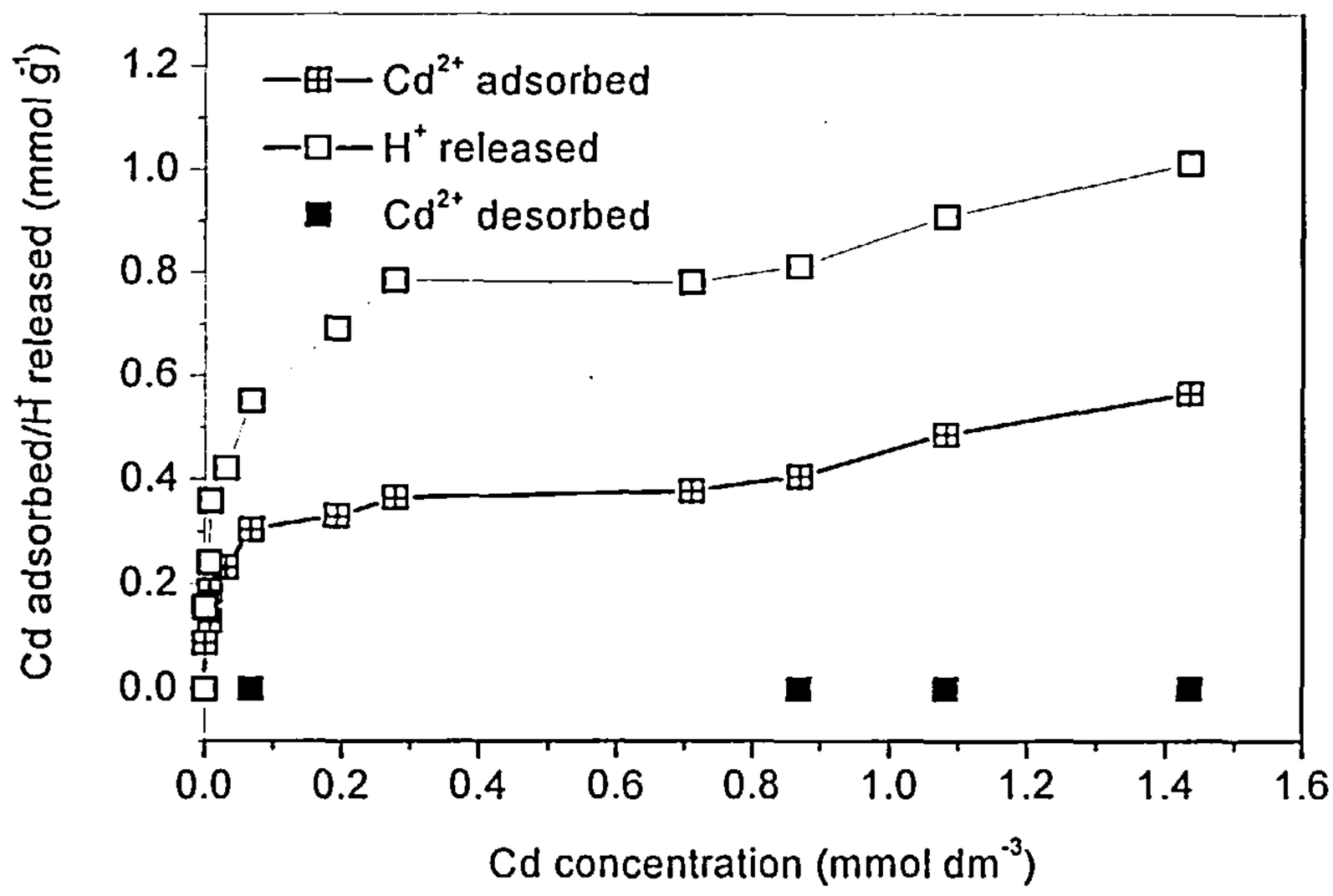

Figure 6.30 A comparison of the amounts of adsorbed cadmium ions on oxidised carbon CN2 with that of released H^+ from the carbon after adsorption and desorbed cadmium ions by Soxhlet extraction

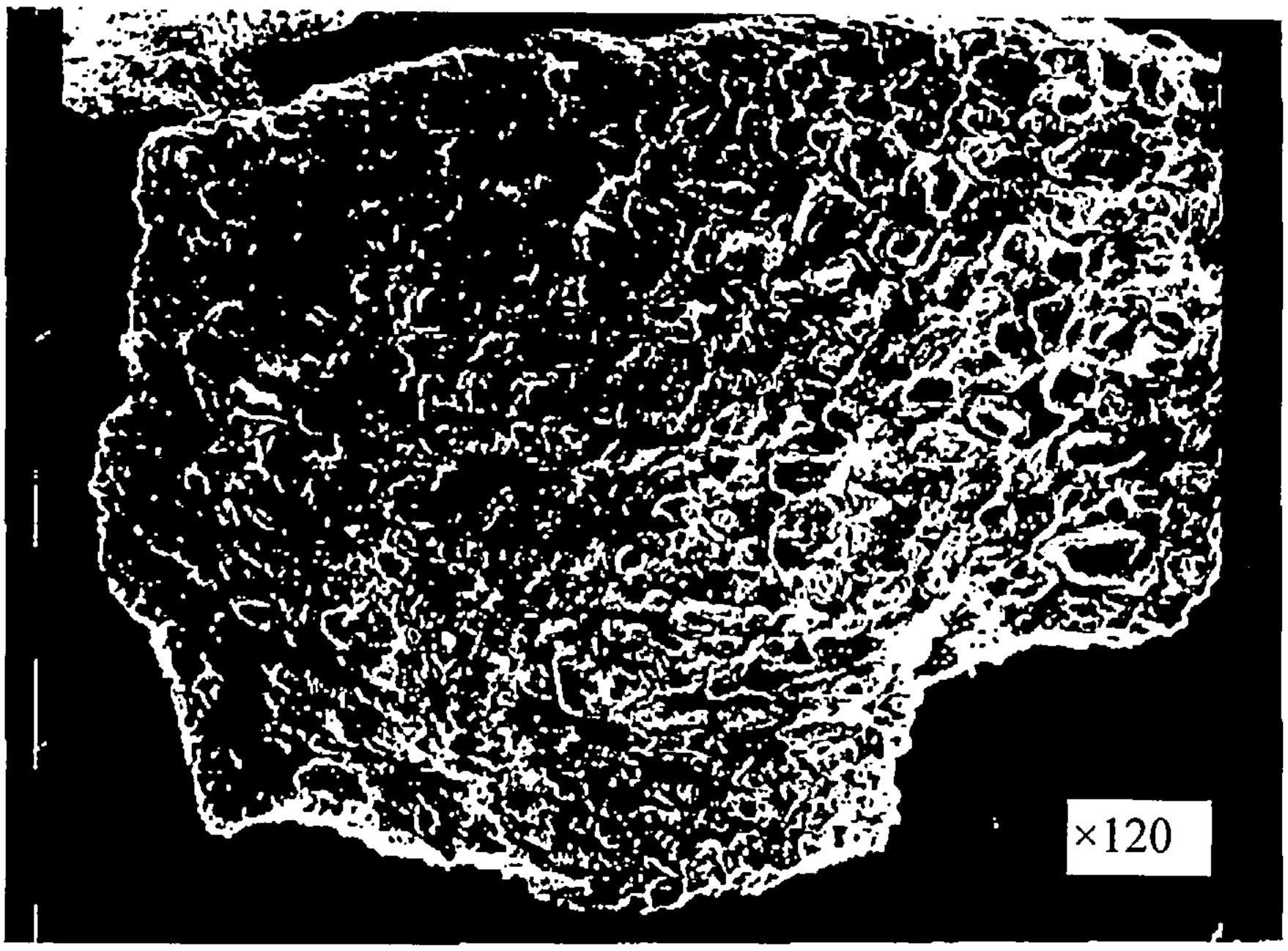

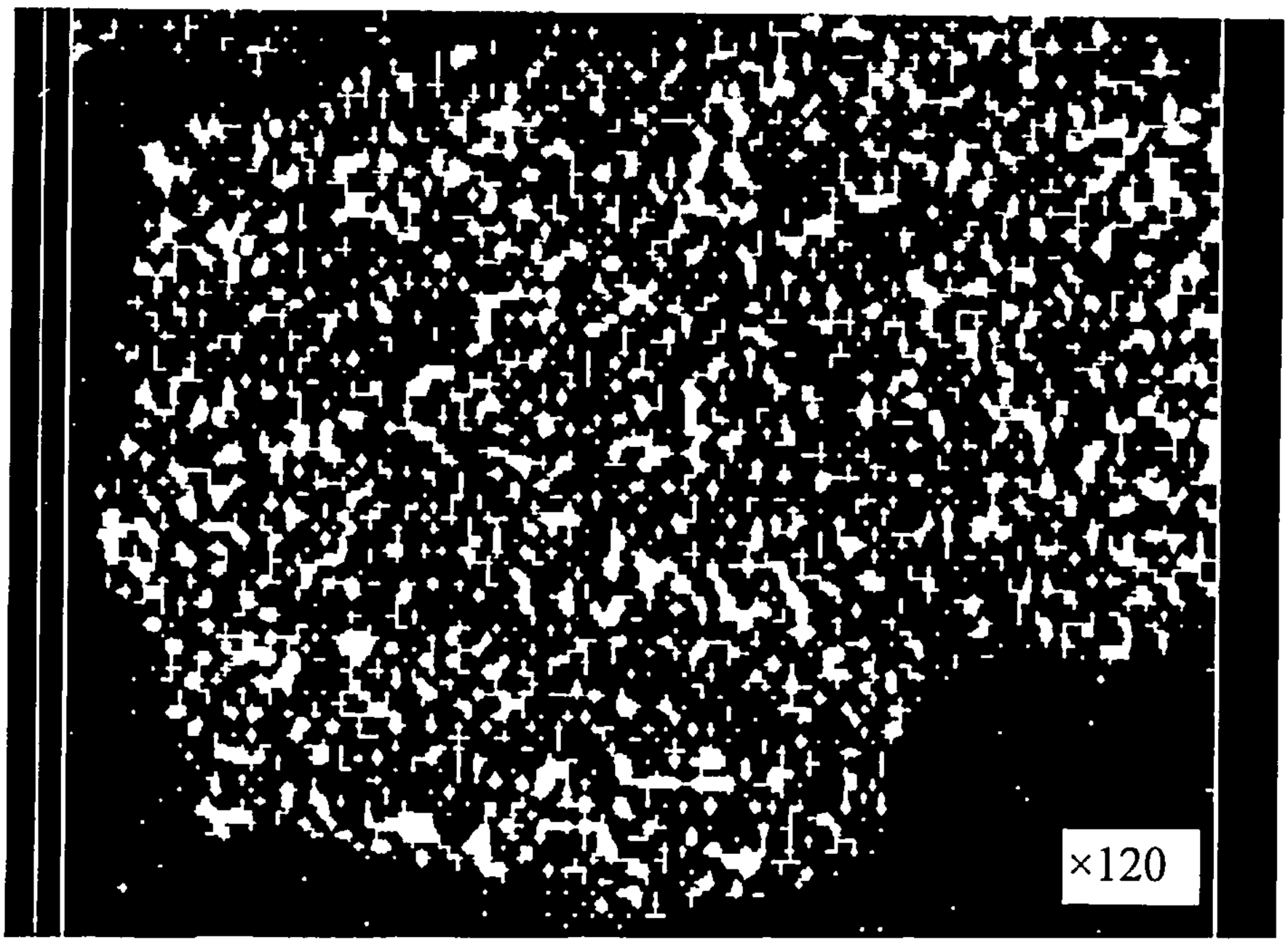

Figure 6.31 EDA micrograph and cadmium distribution of a typical particle of CN2 after adsorption of cadmium followed by 48 hours Soxhlet extraction with water

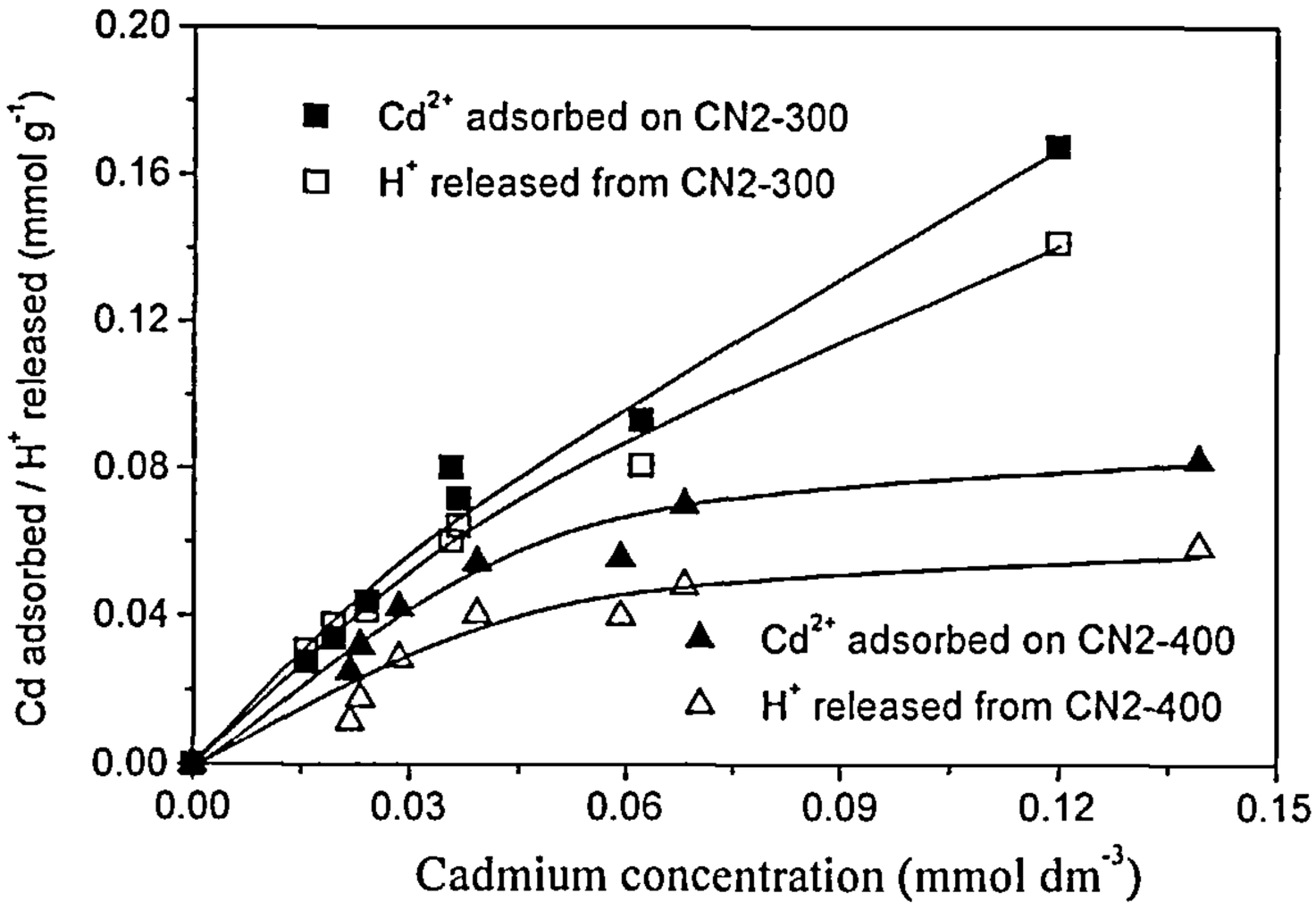

Figure 6.32 A comparison of the amounts of adsorbed cadmium ions with that of released H^+ for the carbons CN2-300 and CN2-400

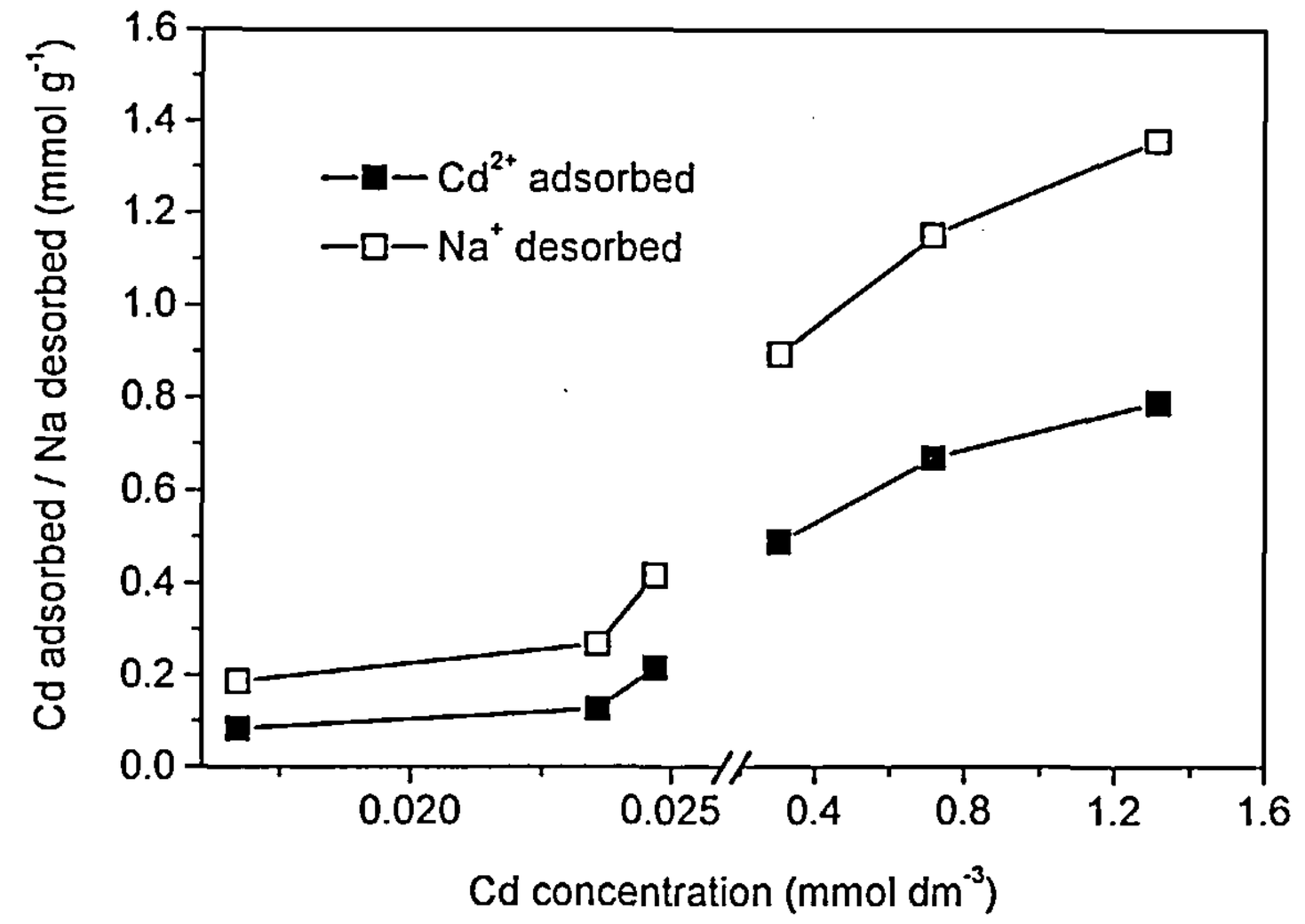

Figure 6.33 A comparison of the amounts of adsorbed cadmium ions with that of released Na^+ for carbon CN2 after reaction with NaOH

6.3.2 Heats of Adsorption and Desorption of Cadmium on Carbon

The heats of adsorption and desorption of cadmium ions on carbon were measured by the following procedure (see **Figure 6.34**). 1) The carbon was equilibrated by passing water until a steady baseline was achieved. 2) Cadmium nitrate solution was passed over the sample and the heat of adsorption (***Adsorption 1***) was measured by calibration of the thermal profile against a known current/voltage/time calibration peak. After the adsorption and calibration were finished, the water was passed over the sample to obtain the heat of desorption (***Desorption 1***). 3) When a steady baseline was achieved after desorption 1, the cadmium nitrate was passed over the sample bed again to obtain the heat of adsorption for the second adsorption (***Adsorption 2***). 4) Finally, the heat of desorption for the second cycle was obtained by passing water over the sample (***Desorption 2***).

The enthalpies of adsorption and desorption of cadmium on oxidised carbon CN2 are shown in **Figure 6.35**. There is a large difference between adsorption 1 and other isotherms, while little difference is observed among the desorption 1, adsorption 2 and desorption 2. This difference remains relatively constant in the concentration range used in this study. It is apparent that both of reversible and irreversible adsorption are involved in the adsorption of cadmium on oxidised carbon CN2. The irreversible adsorption is shown from the difference between the heat of adsorption 1 and desorption 1, adsorption 2 and desorption 2. The reversible adsorption is reflected by the similar isotherms of the heat of desorption 1, adsorption 2 and desorption 2.

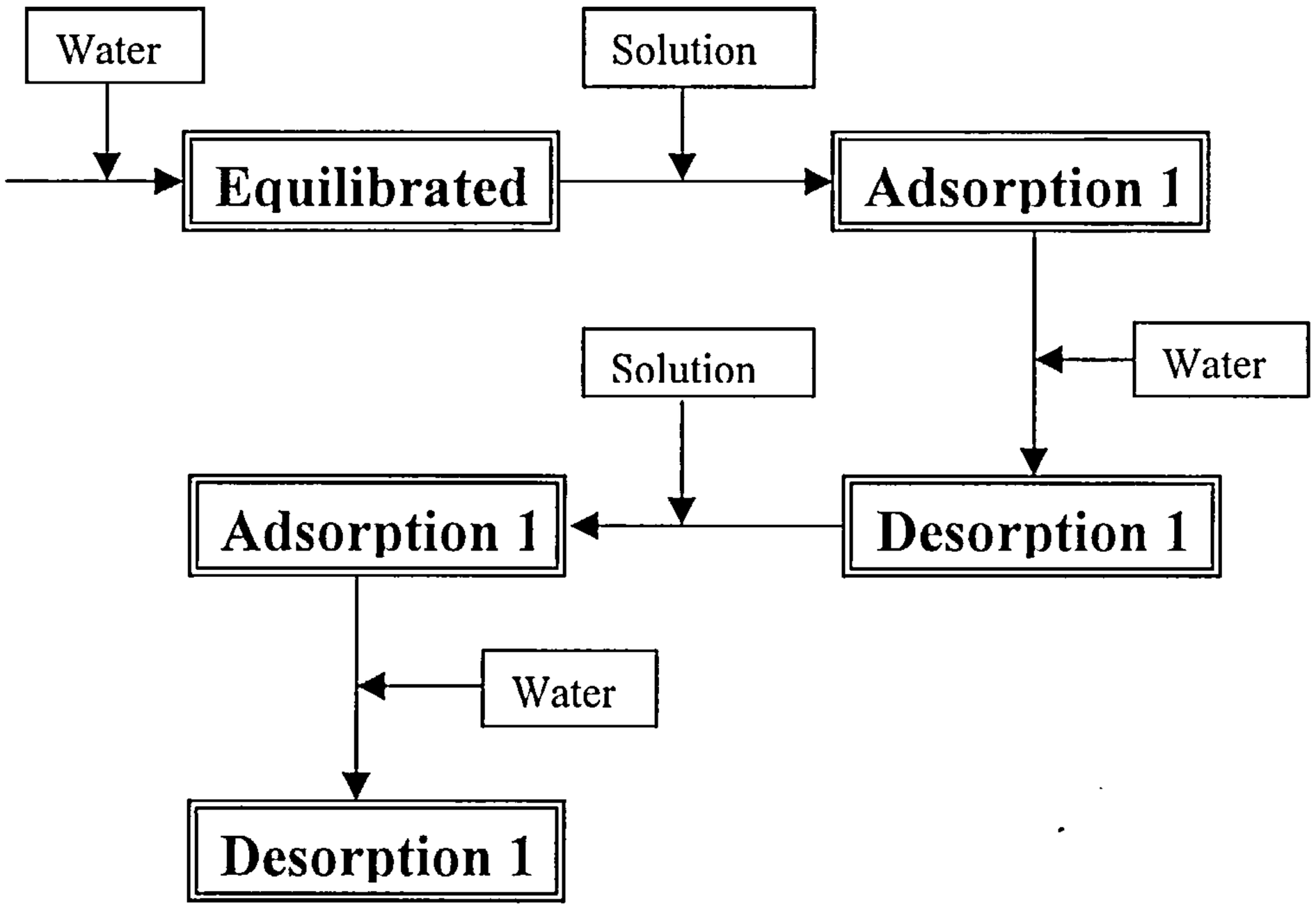

Figure 6.34 A flowchart of the measurement of heats of cadmium adsorption and desorption on activated carbon

The heats of adsorption and desorption of cadmium on carbon CN2-300 are shown in **Figure 6.36**. It is evident that there is little difference between the graphs, indicating reversible process for CN2-300.

Comparison of **Figures 6.35** and **6.36** shows that the heat of adsorption on CN2-300 is higher than that on CN2, though the adsorption capacity of cadmium on CN2-300 is much less than that of CN2. The enthalpy of adsorption increases further after the oxidised carbon was heat treated at 500 °C, as shown in **Figure 6.37**.

The molar heats of adsorption of cadmium ions on CN2, CN2-300 and CN2-500 are shown in **Figure 6.38**. It is evident that the molar heats of adsorption increase with increasing concentration for all three carbons indicating differences in the adsorption

sites and mechanism. The enthalpy of adsorption for cadmium on CN2 is very low and similar to that observed for ion exchange reactions in resins (0.0-0.5 $kJmol^{-1}$) [*22*]. The enthalpy of adsorption of cadmium ions on carbon C 1 (untreated) at a concentration of 1 $mmoldm^{-3}$ was 70 $kJmol^{-1}$. Previous studies of Groszek [*23*] of the adsorption of cadmium ions on Chemviron BPL carbon reported a value of 89 $kJmol^{-1}$ at the same concentration. It is apparent that oxidation treatment reduced the molar enthalpy of adsorption dramatically to ~ 0.2 $kJmol^{-1}$. The enthalpy of adsorption for cadmium ions on CN2 is relatively uniform compared with its heat treated derivatives. The enthalpy of adsorption increases after the oxidised carbon was heat treated, as shown in **Figure 6.38**. This indicates that the changes in adsorption mechanism resulting from the changes in surface functional groups during heat treatment.

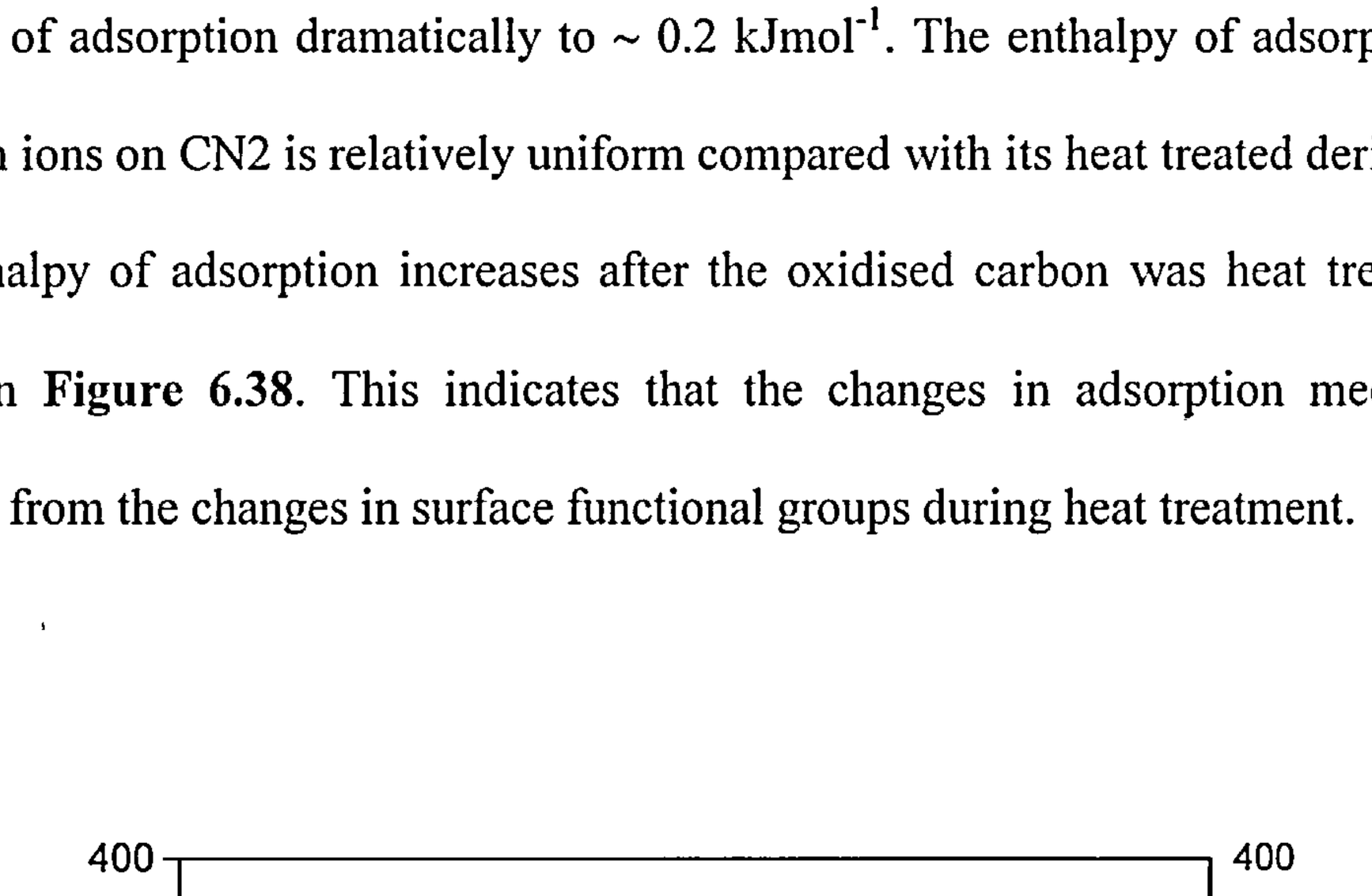

Figure 6.35 Enthalpies of adsorption and desorption of cadmium on carbon CN2

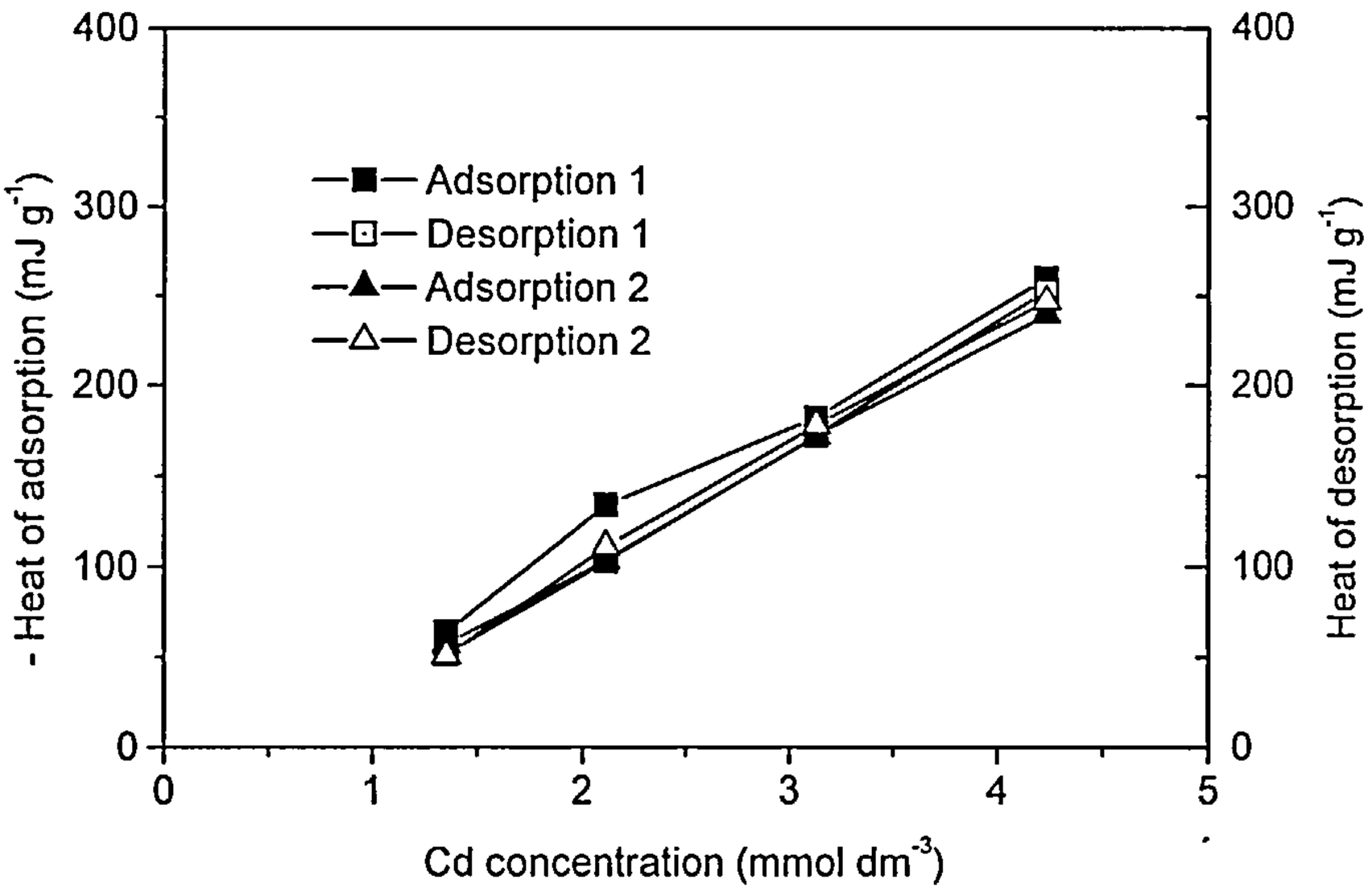

Figure 6.36 Enthalpies of adsorption and desorption of cadmium on carbon CN2-300

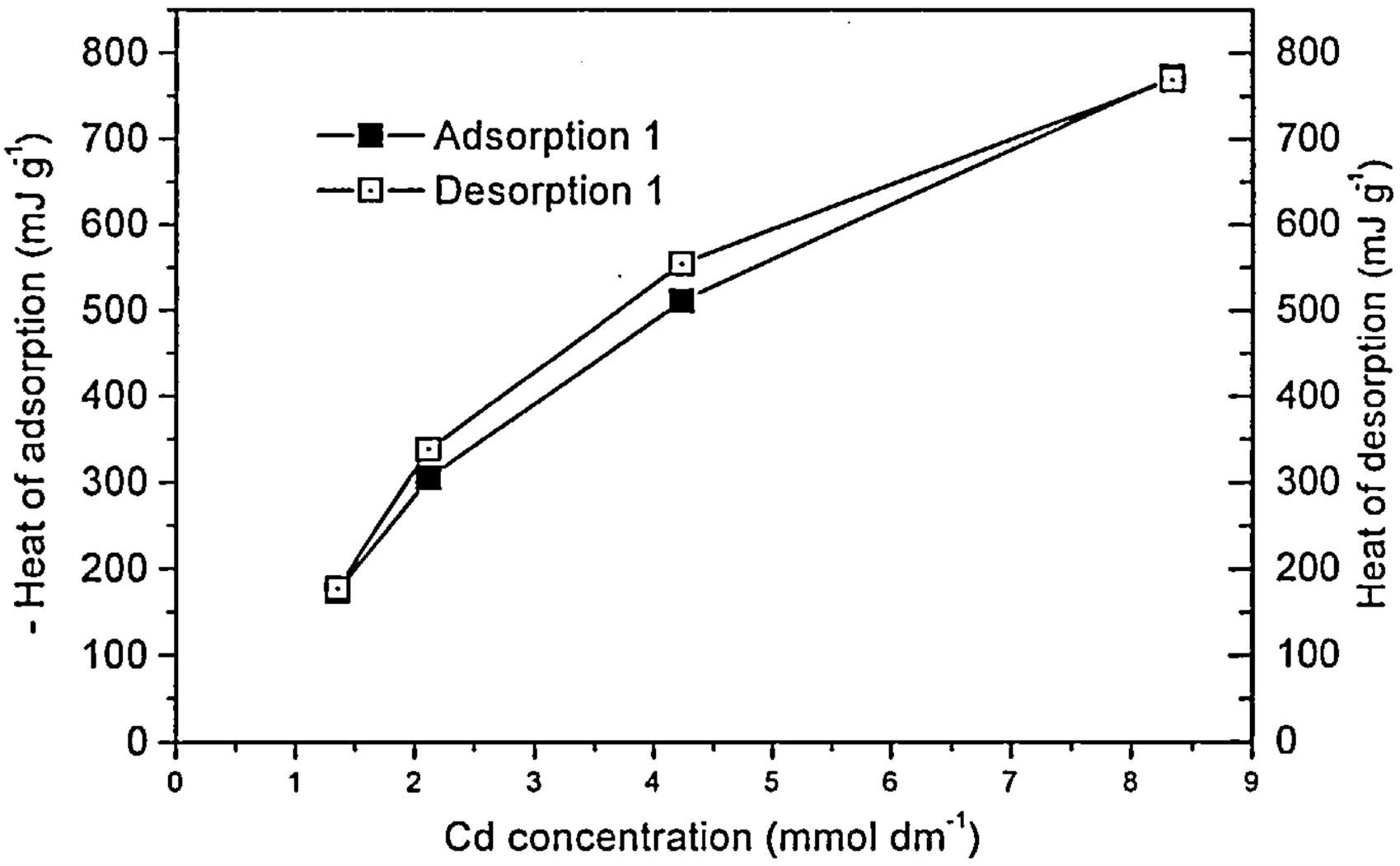

Figure 6.37 Enthalpies of adsorption and desorption of cadmium on carbon CN2-500

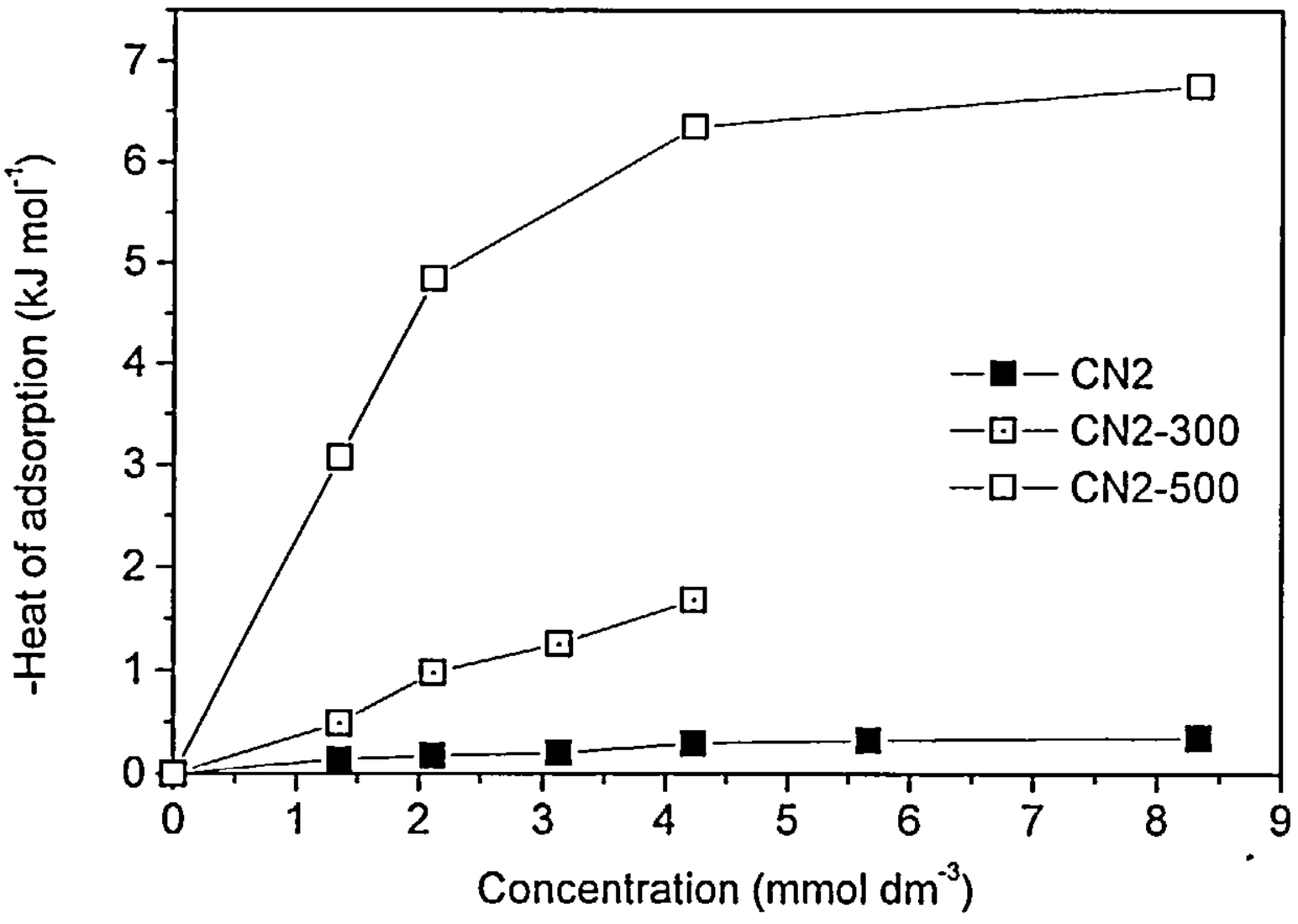

Figure 6.38 The molar heat of adsorption of cadmium on various carbons

6.3.3 Comparison of the Adsorption of Various Metal Cations on Oxidised Carbon

Figure 6.39 shows the adsorption isotherms of various metal cations on oxidised carbon CN2. It is apparent that copper cation has the highest adsorption capacity on CN2. Both cadmium and copper are adsorbed to a greater extent than nickel and calcium cations whereas the latter two species show similar adsorption capacities on CN2. It is of importance to investigate the selectivity of the oxidised carbon towards different metal cations since the real waste water is not comprised of single metal species.

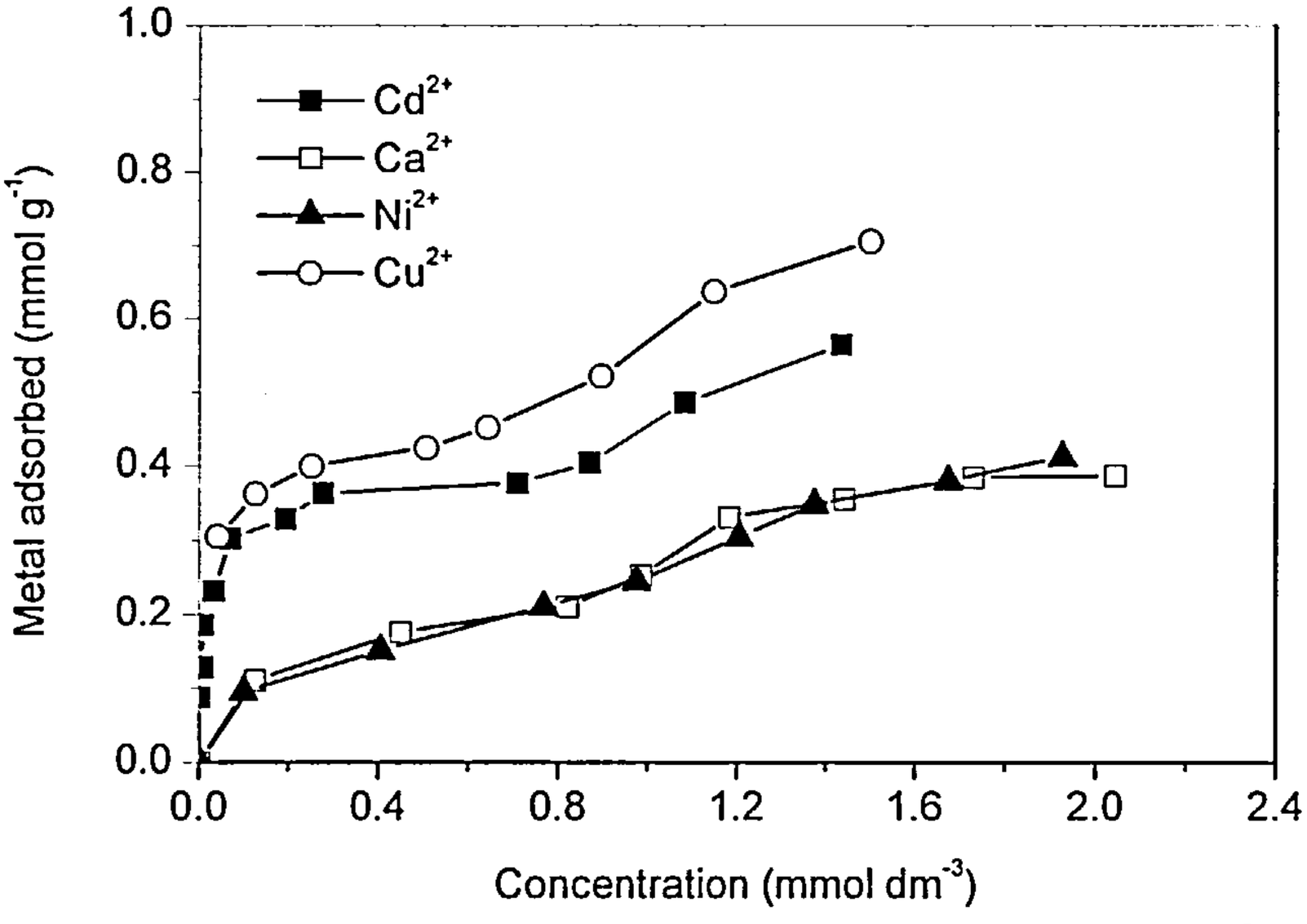

Figure 6.39 A comparison of adsorption of various metal cations on oxidised carbon CN2

6.4 Adsorption of Transition Metal Cations on Nitrogen Sites in Carbon

A comparison of isotherms of adsorption of cadmium cations on carbon C1, CA, CNA and PAN1 at pH 4.1 is shown in **Figure 6.40**. It is apparent that at low concentration all four carbon have similar adsorption capacity for cadmium ions. With increasing concentration, the nitrogen-rich carbons CA, CNA and PAN1 adsorbed more cadmium than carbon C1. This indicates that nitrogen functionality on carbon surface enhanced cadmium adsorption.

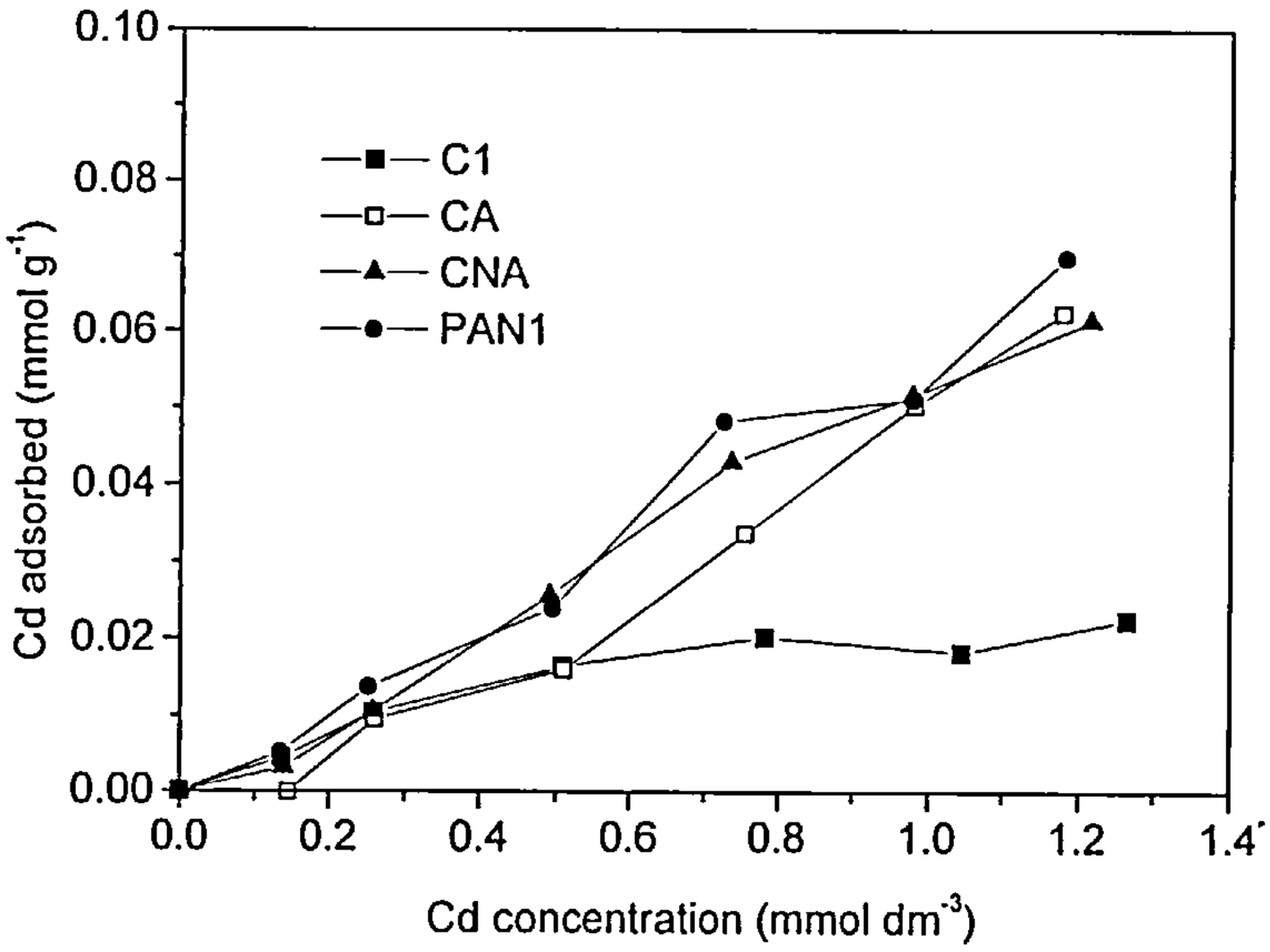

Figure 6.40 A comparison of adsorption isotherms of Cd^{2+} on carbon C1, CA, CNA and PAN1 at pH 4.1 (adjusted using acetate buffer)

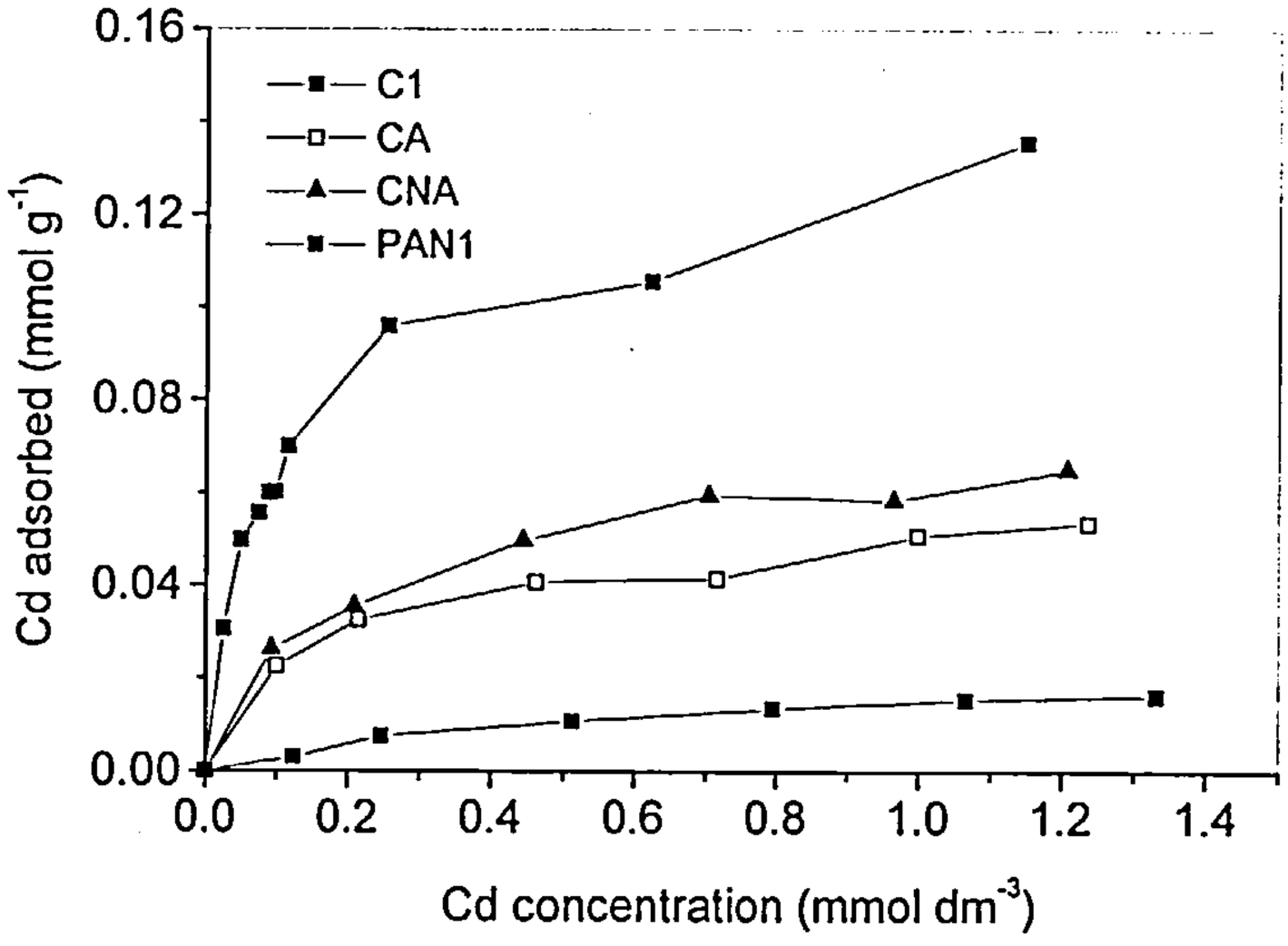

Figure 6.41 A comparison of adsorption isotherms of Cd^{2+} on carbon C1, CA, CNA and PAN1 at pH 7

Figure 6.41 shows the adsorption isotherms of cadmium ions on above four carbons at pH 7. It is apparent from **Figs 6.40** and **6.41** that cadmium ions were adsorbed to a greater extent on the nitrogen carbons CA, CNA and PAN1 than on C1. Comparison of **Figure 6.40** and **6.41** shows that the adsorption capacities of cadmium ions on C1 are similar at pH 4.1 and pH 7 indicating that pH does not greatly affect the cadmium ion adsorption on carbon C1. On the contrary, the adsorption capacities of cadmium ions on nitrogen-rich carbons were greatly influenced by pH with higher pH enhancing the adsorption significantly. There is no correlation between the adsorption of cadmium ions with the surface areas and pore volumes of CA, CNA and PAN1.

The adsorption isotherms of nickel and copper cations on carbon C1, CA, CNA and PAN1 are shown in **Figures 6.42** and **6.43** respectively. It is evident that the adsorption of Ni^{2+} and Cu^{2+} were enhanced by the surface nitrogen functionality incorporated through ammonia treatment (CA and CNA) or inherited from the precursor (PAN1). The capacities of the adsorption Ni^{2+} and Cu^{2+} are in the following order: PANC > CNA, CA > C, consistent with the order of nitrogen contents of the carbons.

The effect of incorporated nitrogen functionality in the active carbon on the adsorption calcium cation was also investigated (see **Figure 6.44**). In contrast to the adsorption of transition metal cations, the ammonia treatment of carbon C1 to give carbon CA and CNA with much higher nitrogen content did not improve the adsorption of alkali earth metal cation Ca^{2+}.

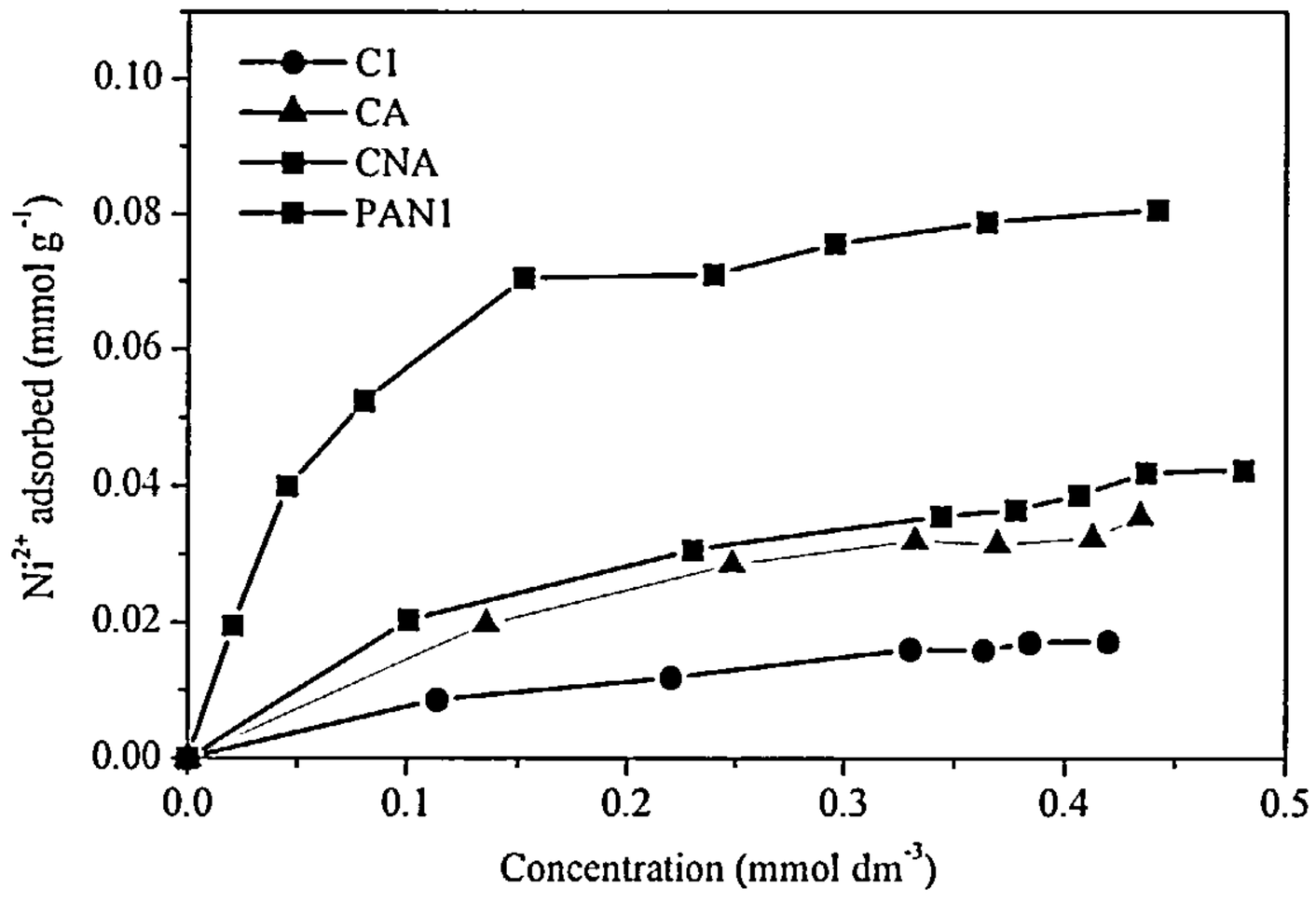

Figure 6.42 A comparison of adsorption isotherms of Ni^{2+} on carbon C1, CA, CNA and PAN1

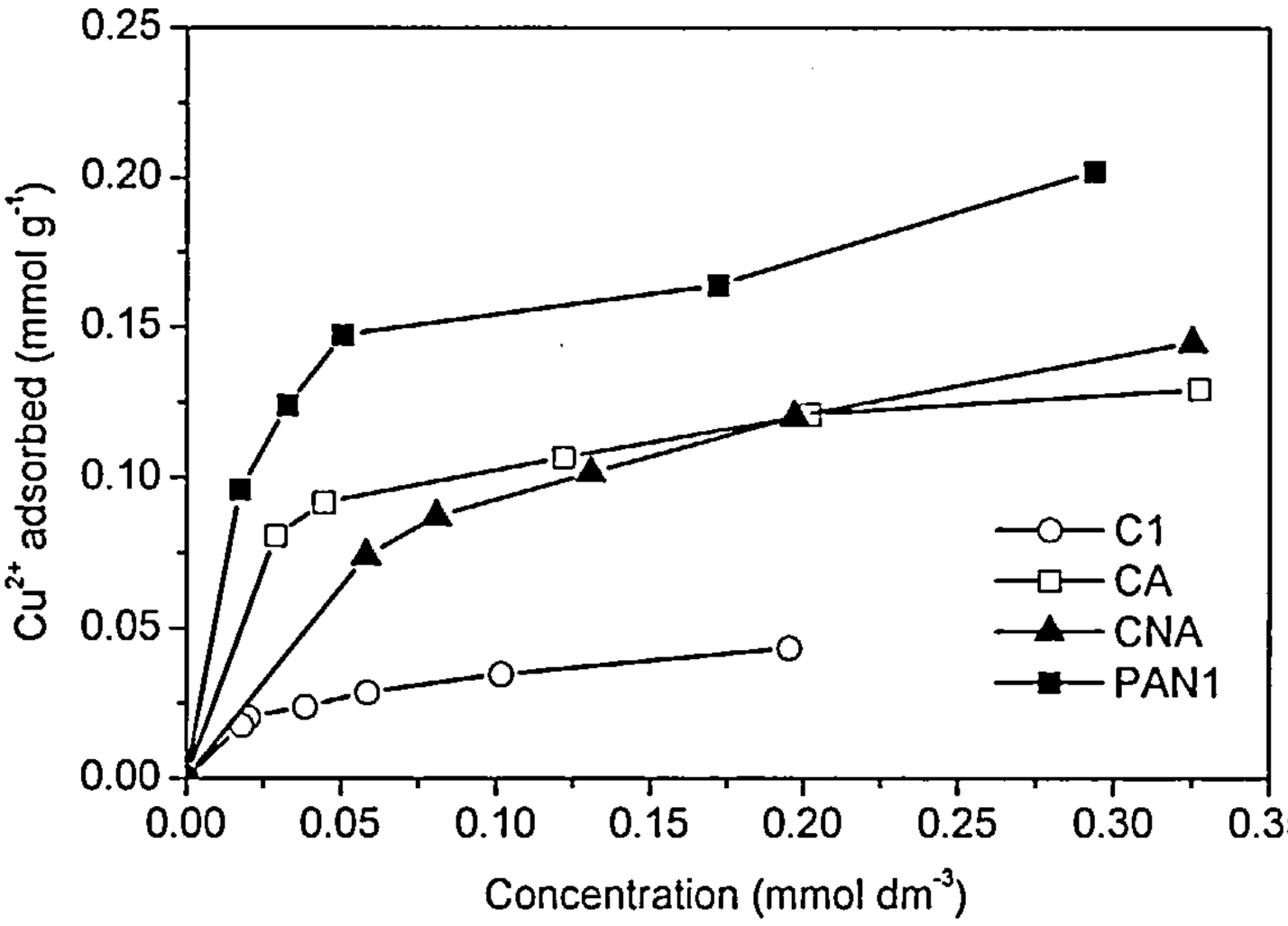

Figure 6.43 A comparison of adsorption isotherms of Cu^{2+} on carbon C1, CA, CNA and PAN1

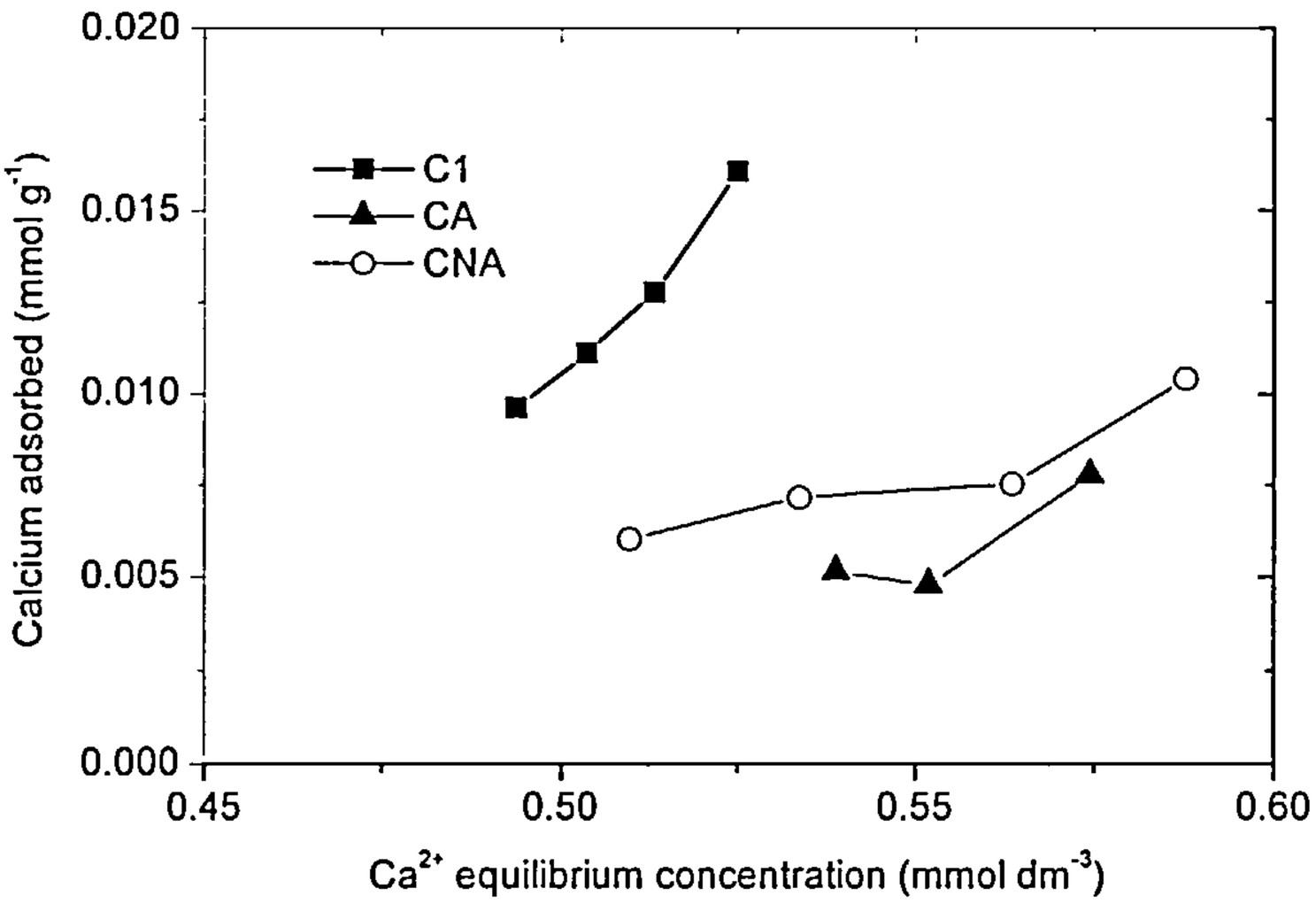

Figure 6.44 Effect of nitrogen functionality on the adsorption of alkali earth metal cation Ca^{2+}

References

1. Leon y Leon, C.A. and Radovic, L.R. In *Chemistry and Physics of Carbon* 1992, Vol.24, 213.
2. Boehm, H.P. *Advan. Catal.* **1966**, *16*, 179.
3. Boehm, H.P. and Bewer, G. In *Proc. 4th Inter London Carbon and Graphite Conf.* 1974, p344.
4. Turner, J.A. and Thomas, K.M. *Langmuir*, in press.
5. Moreno-Castilla, C.; Ferro-Garcia, M.A.; Joly, J.P.; Bautista-Toledo, I.; Carrasco-Marin, F. and Rivera-Utrilla, J. *Langmuir* **1995**, *11*, 4386.
6. de la Puente, G.; Pis, J.J.; Menendez, J.A. and Grange, P. *J. Ana. Pyro.* **1997**, *43*, 125.
7. Zhu, Q; Money, S.L; Russell, A. E and Thomas, K.M. *Langmuir* **1997**, *13*, 2149.
8. Jansen, R. J. J. and van Bekkum, H. *carbon,* 1995, **33**, 1021.
9. Kurth, R.; Tereczki, B. and Boehm, H. P. *Ext. Abstr. 15th Bienn. Conf. On Carbon*, Philadelphia, PA, 1981, p244.
10. Stöhr, B.; Boehm, H. P. and Schlögl, R. *Carbon*, 1991, **29**, 707.
11. Akhter, M.S.; keifer, J.R.; Chughtai, A.R. and Smith, D.M. *Carbon* **1985**, *23*, 589.
12. Zawadzki, J. In *Chemistry and Physics of Carbon* 1989, Vol.21, p147.
13. Biniak, S.; Szymanski, G.; Siedlewski, J. and Swaiatkowski, A. *Carbon* **1997**, *35*, 1799.
14. Nakanishi, K. *Infrared Absorption Spectroscopy-Practical*, Hoden-Day, Inc., San Francisco and Nankodo Company Limited, Tokyo, 1962.
15. Lin-Vien, D.; Colthup, N.B.; Fateley, W.G. and Grasselli, J.G. *The Handbook of Infrared and Raman characteristic Frequencies of Organic Molecules*, Academic Press, Inc., London, 1991.
16. Puri, B.R. In *Chemistry and Physics of Carbon*, Edited by Walker (Jr.), P.L. 1970, Vol.6, p191.
17. Lambert, J. B.; Shurvell, H. F.; Lightner, D. A. and Cooks, R. G. *Introduction to Organic Spectroscopy*, Macmillan Publishing Company, New York & Collier Macmillan Publishers, London.
18. Jansen, R. J. J. and van Bekkum, H. *Carbon*, 1994, **32**, 1507.

19.Chantry, G.W. and Plane, R.A., *J. Chem. Phys.*, 1960, **33**(3), 736.

20.Jones, L. H. and Penneman, R. A., *J. Chem. Phys.*, 1954, **22**(6), 965.

21.Chantry, G.W. and Plane, R.A., *J. Chem. Phys.*, 1961, **35**(3), 1027.

22.Harland, C.E. *Ion Exchange: Theory and Practice*, 2nd Edition, Royal Society of Chemistry, Cambridge, **1994**.

23.Groszek. A.J., In *Proceedings of Carbon 92*, Essen, Germany, Deutsche Keramische Geselleschaft, 1992, p278.

Chapter 7

DISCUSSION

7.1 Adsorption Sites in Active Carbons and Interaction Between Gold or Silver Cyanide Complexes and the Carbon Surface

The adsorption sites in active carbons can be divided into two major types: a) hydrophobic surfaces comprising of the graphene layers; and b) oxygen and nitrogen functional groups which are primarily hydrophilic. This provides two main possibilities for the adsorption of gold and silver cyanide adsorption species: 1) adsorption by interaction between the π orbitals of the graphene layers and $Au(CN)_2^-$ species; or 2) an ion exchange mechanism involving the functional groups. Despite the extensive industrial application of this technology, the mechanism of the adsorption of metal cyano complexes, including gold, silver etc., on carbon is not fully understood. Extensive research has been carried out in the past decades on the adsorption of aurocyanide species on active carbons. The mechanism involving the adsorption of gold as an ion pair $M^{n+}[Au(CN)_2]_n$ was proposed [*1*] after the observation that the 'spectator cations', *e.g.* Ca^{2+}, Mg^{2+}, K^+, Na^+ etc., in the adsorption medium increased the gold adsorption on carbon. This proposed mechanism was widely accepted in gold adsorption studies [*2-6*]. X-ray photoelectron spectroscopy (XPS) [*2,7-11*], Fourier transform infrared spectroscopy (FTIR) [*11,12*] and Mössbauer Spectroscopy [*13-15*] were employed in investigations of the adsorption of

aurocyanide species on carbon. It was suggested [*2*] that the adsorption of the ion pair $M^{n+}[Au(CN)_2]_n$ was followed by the subsequent partial reduction of $Au(CN)_2^-$ to $Au(CN)_x$. However, while it was proposed that AuCN formed during $Au(CN)_2^-$ adsorption [*8,16,17*], other studies clearly showed that $Au(CN)_2^-$ adsorbs intact without any chemical change [*7,9-11*]. The adsorbed $Au(CN)_2^-$ ions were transformed to tetramer $Au_4(CN)_5^-$ after treated by acid [*2,4*]. The pH in the range 1 - 10 had no effect on adsorbed gold cyanide species whereas the oligomers $Au_x(CN)_{x+1}^-$ were formed during drying on the carbon surface after adsorption from acidic solution [*9*]. Surface oxygen functionality was assumed to play an important role in gold adsorption [*16,18-20*]. However, the concentration of oxygen groups on the carbon surface was not found to correlate with gold adsorption characteristics [*21-23*]. According to some studies [*9,10,21-23*], the graphene layers are the dominant sites for gold cyanide adsorption.

The presence of ethanol and butan-1-ol in $KAu(CN)_2$ aqueous solution reduces $Au(CN)_2^-$ adsorption on activated carbon with butan-1-ol having the more adverse effect. This implies that the adsorbed $Au(CN)_2^-$ species occupies similar surface sites on the activated carbon to the organic species in aqueous solution and that there is competitive adsorption between $KAu(CN)_2$ and organic solvents for the hydrophobic graphene layer surface. Alcohols display the ability of displacing aurocyanide species from carbon surfaces. Fleming *et al* [*24*] attributed the adverse effects of organic solvents on gold adsorption on carbon to the mass transfer barrier which resulted from the adsorption of organic solvent on the surface of carbon. However this mechanism cannot satisfy the markedly improved elution of gold from active carbon by organic solvents such as ethanol and acetone *etc* [*25*]. The highly hydrophobic graphene layers show preferential adsorption for organic materials from water. In a homologous series

of organic solvents, the adsorption on carbon is higher for butan-1-ol compared with ethanol due to the larger hydrophobic part of the molecule. The adverse effects of organic solvents on the adsorption of $Au(CN)_2^-$ on activated carbon are indicative of the basal planes of activated carbon being the main sites for the adsorption of gold cyanide ions. This provides the reasonable explanation for detrimental effects of benzene and heptane on gold adsorption on carbon [*24*] and for the observation that polar organic solvents such as ethanol, acetone and acetonitrile markedly improve the elution of gold from activated carbon [*25*]. An interesting phenomenum was noted [*5,26*] that chemically activated carbons have a poor affinity for gold cyanide species. This also suggests the key role played by the graphene layers in carbon on gold adsorption since chemically activated carbons are more disordered than active carbons prepared by gasification [*27*].

Cho and Pitt [*28*] found that $Au(CN)_2^-$ ion was preferentially adsorbed on carbon compared to the $Ag(CN)_2^-$ ion. They explained this observation using solvation energy theory which predicts that ions with high ratio of radius to charges are specifically adsorbed due to the larger ionic radius of gold (137 pm) compared to silver (126 pm). However the structures of the $Au(CN)_2^-$ and $Ag(CN)_2^-$ determined by X-ray crystallography [*29,30*] indicate that the sizes of the molecules are very similar.

The following resonance structures exist [*31*] for metal dicyano species.

$$N\equiv C\text{-}M\text{-}C\equiv N \leftrightarrow N^-=C=M^+=C=N^- \qquad (7.1)$$

I II

The resonance is determined by the electronegativity and oxidation state of the central metal. Since higher electronegativity favours higher contribution from I,

$Au(CN)_2^-$ has a greater contribution of form I than $Ag(CN)_2^-$. According to the mechanism postulated by Klauber [*7*], $Au(CN)_2^-$ is adsorbed on the graphene layers via weak π donation from the carbon surface to the central metal atom, with the estimated charge transfer 0.3-0.5 of an electronic charge [*10*].

X-ray photoelectron spectroscopy (XPS) and infrared spectroscopy have been used study the adsorption of $Au(CN)_2^-$ on carbons. The results are consistent with the adsorbed species being $Au(CN)_2^-$ with weak donation of π electrons from the active carbon to the gold. No evidence was found to support the ion-pair adsorption model. The bonding in $M(CN)_2^-$ ions involves strong σ donor and weak π back bonding to the CN^- and this will influence the interaction between $Au(CN)_2^-$ and.$Ag(CN)_2^-$ anions and graphene layers of active carbon. Jones [*31*] showed that the carbon-nitrogen force constant increases with increase in metal-cyanide σ-bonding and decrease in metal-cyanide π bonding in metal cyanide complexes. The metal-carbon π bonding in $M(CN)_2^-$ species was in the order $Au(CN)_2^- > Ag(CN)_2^-$. Electronegativity and oxidation state considerations indicate that, the extent of π back bonding is in the following order for some dicyano complexes, $Hg(CN)_2 > Au(CN)_2^- > Ag(CN)_2^- > Cu(CN)_2^-$, and this order is coincident with the decreasing order of the adsorption capacity [*2*,*32*] and $\nu(C{\equiv}N)$.

Davidson [*1*] established that the addition of 'spectator cations' could appreciably enhance the gold adsorption following the sequence, $Ca^{2+} > Mg^{2+} > H^+ > Li^+ > Na^+ > K^+$. He proposed a mechanism involving the adsorption of gold as ion pair $M^{n+}[Au(CN)_2]_n$, where the ion pair is adsorbed on the carbon surface more firmly for alkaline earth metal compared with alkali metal cation. This model appears reasonable since carbon shows greater affinity for neutral molecules. Ibrado *et al* [*11*] questioned

the ion pair theory and suggested that the adsorbed gold species on active carbon surfaces is most likely the unpaired $Au(CN)_2^-$ rather than $M^{n+}[Au(CN)_2]_n$ ion pairs, and that the cations are employed to preserve the electroneutrality as counter ions in the electrical double layer. However they did not explain why gold adsorption can be increased by the 'spectator cations'.

7.2 Possible Bonding Formed During Adsorption of $Au(CN)_2^-$ and $Ag(CN)_2^-$

The adsorption of gold and silver on carbon is related to the electronic structure of their cyano complexes. $Au(CN)_2^-$ is a linear structure with the cyanide groups acting as σ electron donor to gold and as π acceptor for d electrons from gold. In terms of Molecular Orbital Theory, molecular orbital formula for cyanide ion should be expressed as $(\sigma 2s)^2 (\sigma^* 2s)^2 (\pi 2p_y)^2 (\pi 2p_z)^2 (\sigma 2p)^2$. The outermost configuration of Au^+ is typically represented by empty 6s and 6p orbitals and fully filled 5d orbital with regard to coordination with ligands due to their approximately similar energy levels. Two $6s6p_x$ hybrid orbitals are formed in Au^+ for gold dicyano complex to accept the σ donation from the CN^- whereas the π backbonding involves the back donation of electrons from d orbitals of gold to π^*2p empty orbitals. The interaction between $Au(CN)_2^-$ and basal plane can be described in **Figure 7.1**.

7.3 Relation of Adsorption Capacities with Gold and Silver Species in Solutions

It has been found [*27*] that free cyanide ions caused a decrease in the adsorption of silver cyanide species on charcoal. Similar results have been observed in this study.

However the extent of the effect appears to be different for coconut and coal derived active carbons. Cho *et al* inferred that there is competitive adsorption between the cyanide ions and the silver cyanide ions for the active sites. If the concentration of CN^- increased, the CN^- ions may be adsorbed on the active sites on the carbon surface, resulting in a decrease in the adsorption of silver cyanide species. However, the existence of various silver cyanide species in $KAg(CN)_2$/KCN aqueous solution was not discussed.

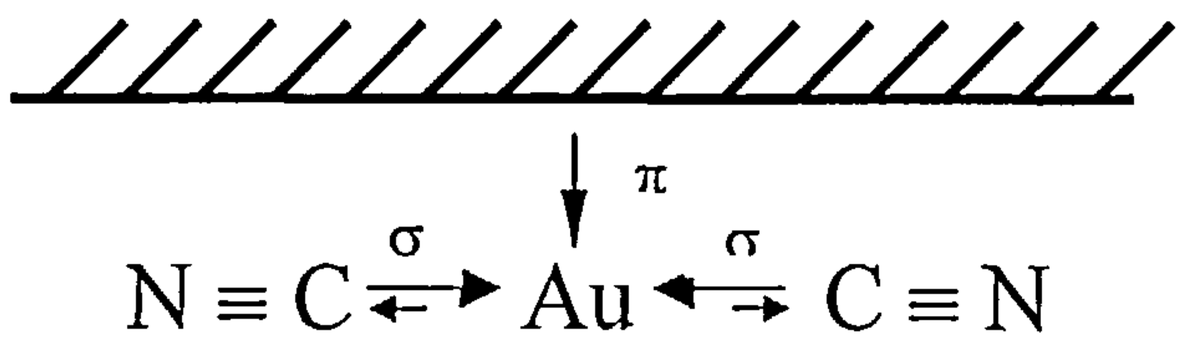

Figure 7.1 A schematic diagram of possible bonding between $Au(CN)^{2-}$ and graphene layers during adsorption

The excess free cyanide ions in $KAu(CN)_2$/KCN and $KAg(CN)_2$/KCN aqueous solutions resulted in significant differences in the species present in the two solutions. There is only one gold species present in $KAu(CN)_2$/KCN solution, $Au(CN)_2^-$, whereas higher coordination number silver species, $Ag(CN)_3^{2-}$ ions were present in $KAg(CN)_2$/KCN aqueous solution. It is well known that the following equilibria exist in $Ag(CN)_2^-/CN^-$ aqueous solution which are determined by the extent of excess CN^- [*31*,*33*].

$$Ag(CN)_2^- + CN^- \rightleftharpoons Ag(CN)_3^{2-} \qquad (7.2)$$

$$Ag(CN)_3^{2-} + CN^- \rightleftharpoons Ag(CN)_4^{3-} \qquad (7.3)$$

$Ag(CN)_2^-$ is linear in structure [*30*] while the geometry of $Ag(CN)_4^{3-}$ ion is tetrahedral. The structure of $Ag(CN)_3^{2-}$ is thought to be present as the tetrahedral $Ag(CN)_3(H_2O)^{2-}$ complex in solution[*33*].

The amount of silver adsorbed on carbon decreases noticeably with increasing CN^-/Ag^+ ratio whereas gold adsorption capacities are similar for different CN^-/Au^+ ratios at 25 °C. Taking the above mentioned equation (1) and (2) into consideration, with increasing concentration of free cyanide ions, the amount of $Ag(CN)_2^-$ decreases while $Ag(CN)_3(H_2O)^{2-}$ or $Ag(CN)_4^{3-}$ increases. According to the mechanism postulated by Klauber [*7*], $Au(CN)_2^-$ is adsorbed via π electron donation from the graphene layers of active carbon to the central gold atom. It is proposed that $Ag(CN)_2^-$ is adsorbed while $Ag(CN)_3(H_2O)^{2-}$ and $Ag(CN)_4^{3-}$ anions are not adsorbed on the carbon via π donor mechanism because of their tetrahedral structure. The amount of silver adsorbed on carbon in the presence of excess CN^- is lower as a result of equilibria involving $Ag(CN)_2^-$, $Ag(CN)_3(H_2O)^{2-}$ and $Ag(CN)_4^{3-}$ in solution and the equilibria will change as the $Ag(CN)_2^-$ species is adsorbed on the active carbon. The carbon porous structure will be a factor since the accessibility of the available surface to the various silver cyanide species will vary for different carbons and this will influence the equilibria. In contrast, excess cyanide ions show little effect at 25 °C on the adsorption of $Au(CN)_2^-$ which is the only gold cyanide species present in solution. It is apparent that competitive adsorption between CN^- and $Au(CN)_2^-$ is comparatively small. However excess free cyanide ions present in $KAu(CN)_2$ solution at 70 °C decreased the adsorption of $Au(CN)_2^-$. It is proposed that [*34*] the cyanide that is decomposed on the surface of the carbon changes the functional groups on the surface in such a way that the surface becomes less receptive for adsorption. The following

possible reactions between cyanide and the functional groups on the carbon surface were proposed [*6*]:

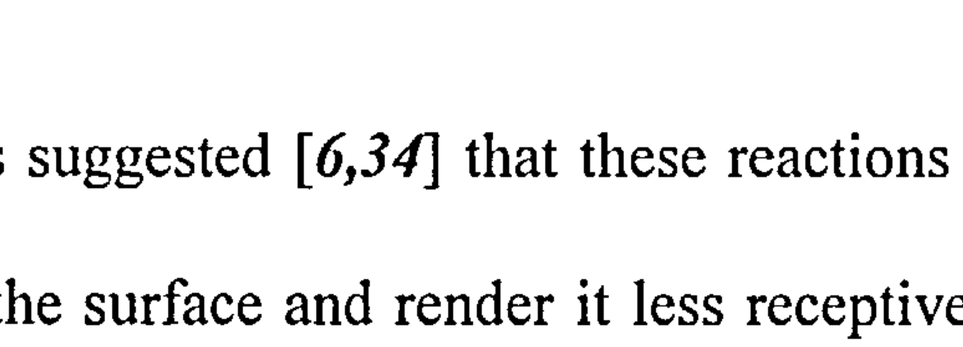

$$R-\overset{\overset{O}{\|}}{C}-R + CN^- \rightleftharpoons R-\overset{\overset{O^-}{\|}}{\underset{\underset{CN}{|}}{C}}-R \qquad (7.4)$$

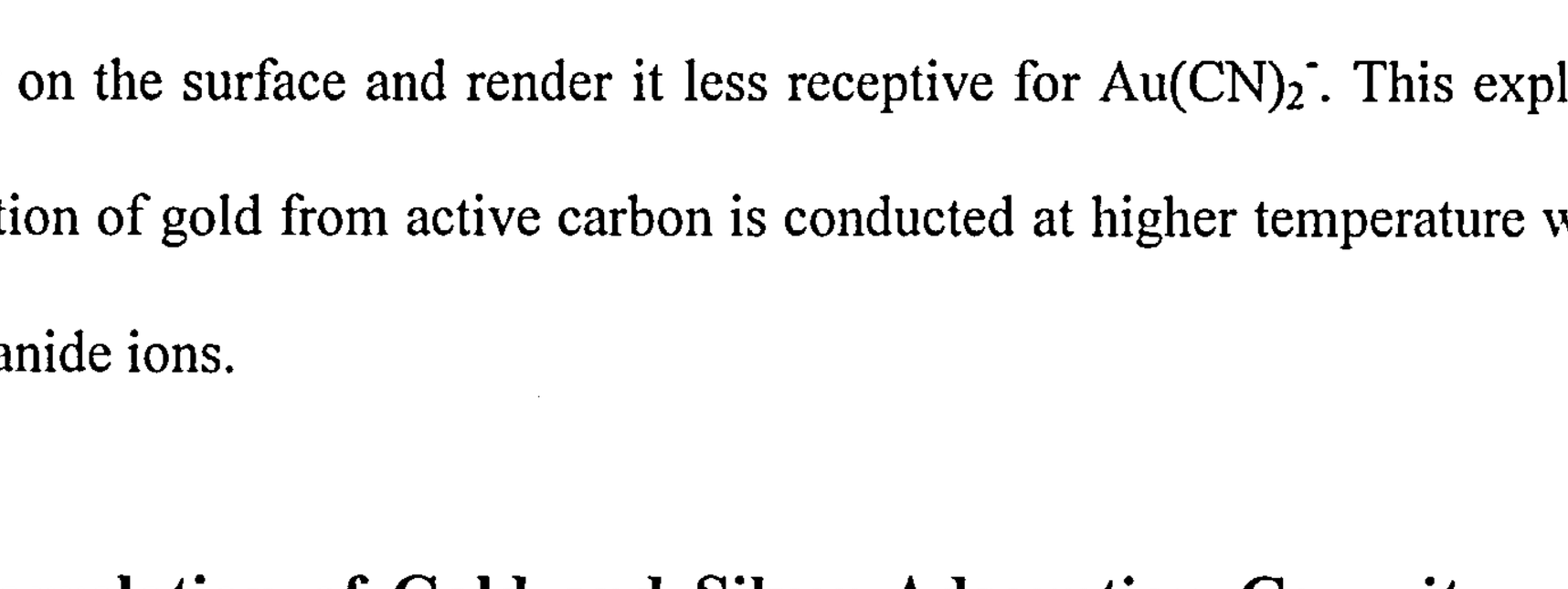

$$-\underset{|}{\overset{|}{C}}-\underset{\|}{C}- + CN^- \rightleftharpoons -C=\underset{\underset{O^-}{|}}{C}- + HCN \qquad (7.5)$$

It was suggested [*6,34*] that these reactions would increase the negative charge density on the surface and render it less receptive for $Au(CN)_2^-$. This explained why the elution of gold from active carbon is conducted at higher temperature with excess free cyanide ions.

7.4 Correlation of Gold and Silver Adsorption Capacity with Pore Structure

The results show that $KAu(CN)_2$ and $KAg(CN)_2$ adsorption capacities of carbon in buffer solution at pH 10 have a good correlation with total pore volume determined from nitrogen adsorption. The gold and silver adsorption capacities increase with increasing total pore volume for both the coal [*35*] and coconut shell derived carbons. The micropore volume does not change greatly during activation for the coconut derived carbons whereas the change for the coal based carbons is greater [*35*].

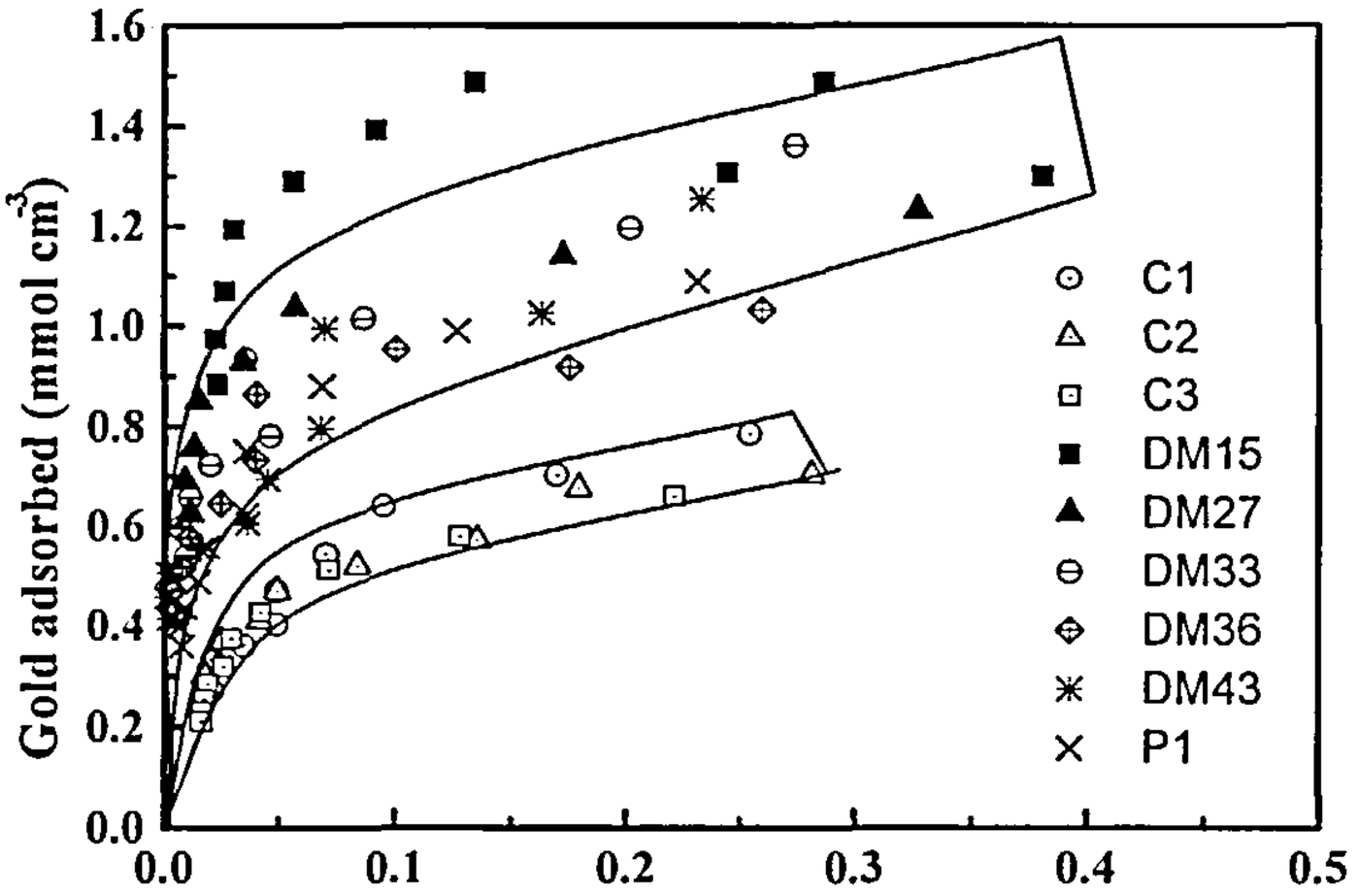

Figure 7.2 The gold adsorption normalised to pore volume as a function of gold equilibrium concentration of solution (the amounts of gold adsorbed on carbons are normalised on a basis of total pore volume from N_2 adsorption at 77 K)

Figures 7.2 and **7.3** show the gold and silver cyanide adsorption isotherms normalised to total pore volume respectively for coal and coconut shell based carbons with varying extents of activation. The DM series carbons were derived from coal and the adsorption of gold and silver were carried out by Steele [*35*]. It is apparent from these results that though gold and silver adsorption isotherms vary widely on a weight basis, the amounts of adsorbed gold and silver normalised to total pore volume are similar for the carbons derived from the same precursor. Coal based carbons have higher gold and silver adsorption normalised to total pore volume than coconut shell based carbons. It appears that the carbon precursor structure influences the gold and silver cyanide normalised adsorption capacity. The most reasonable explanation involves the pore size distribution. Although the activation procedure and after-treatment employed mainly determine the chemical nature of the surface oxides, the

porous structure and pore size distributions are to a certain extent pre-determined by the nature of precursor materials.

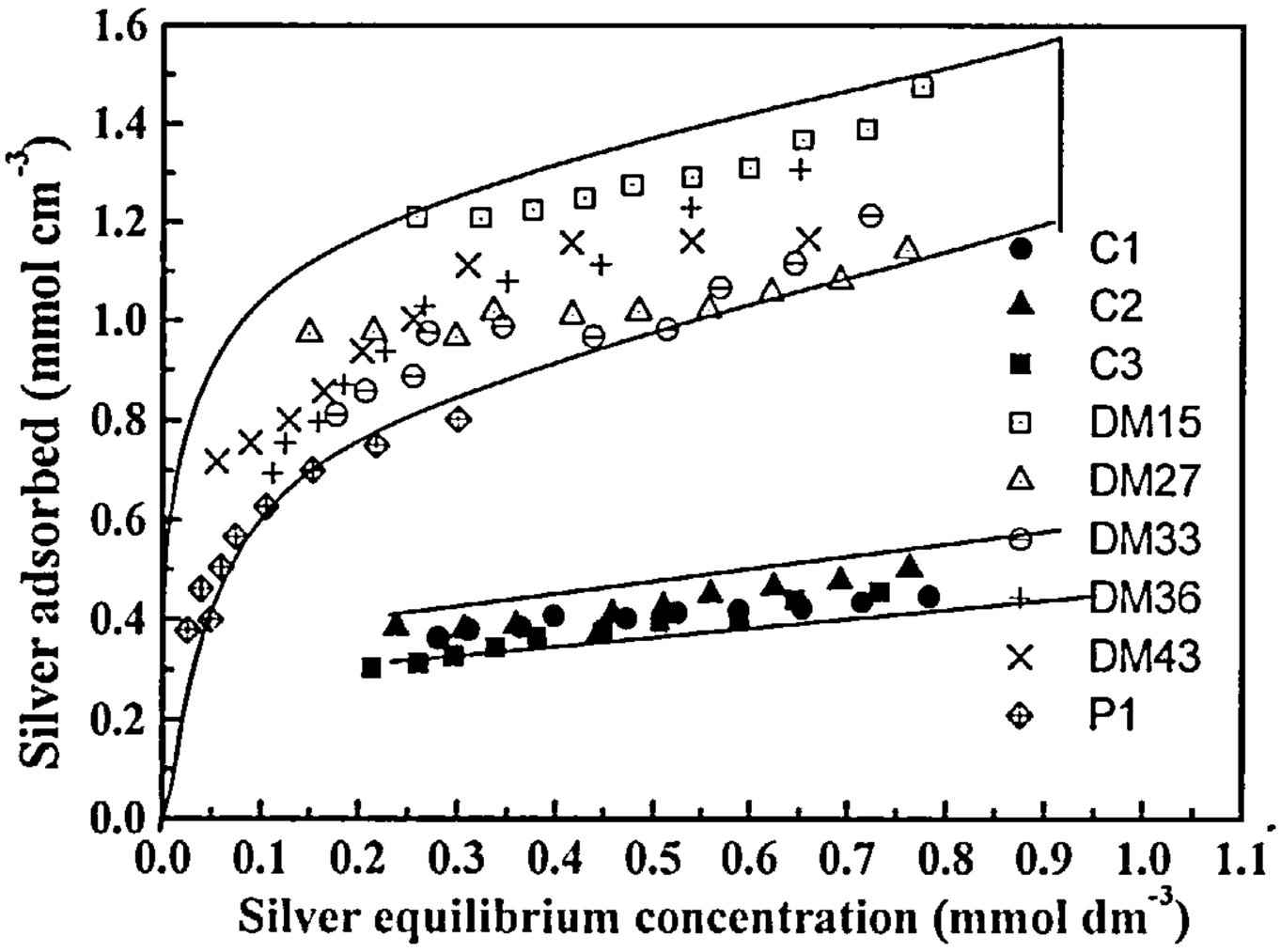

Figure 7.3 The silver adsorption normalised to pore volume as a function of silver equilibrium concentration of solution (the amounts of silver adsorbed on carbons are normalised on a basis of total pore volume from N_2 adsorption at 77 K)

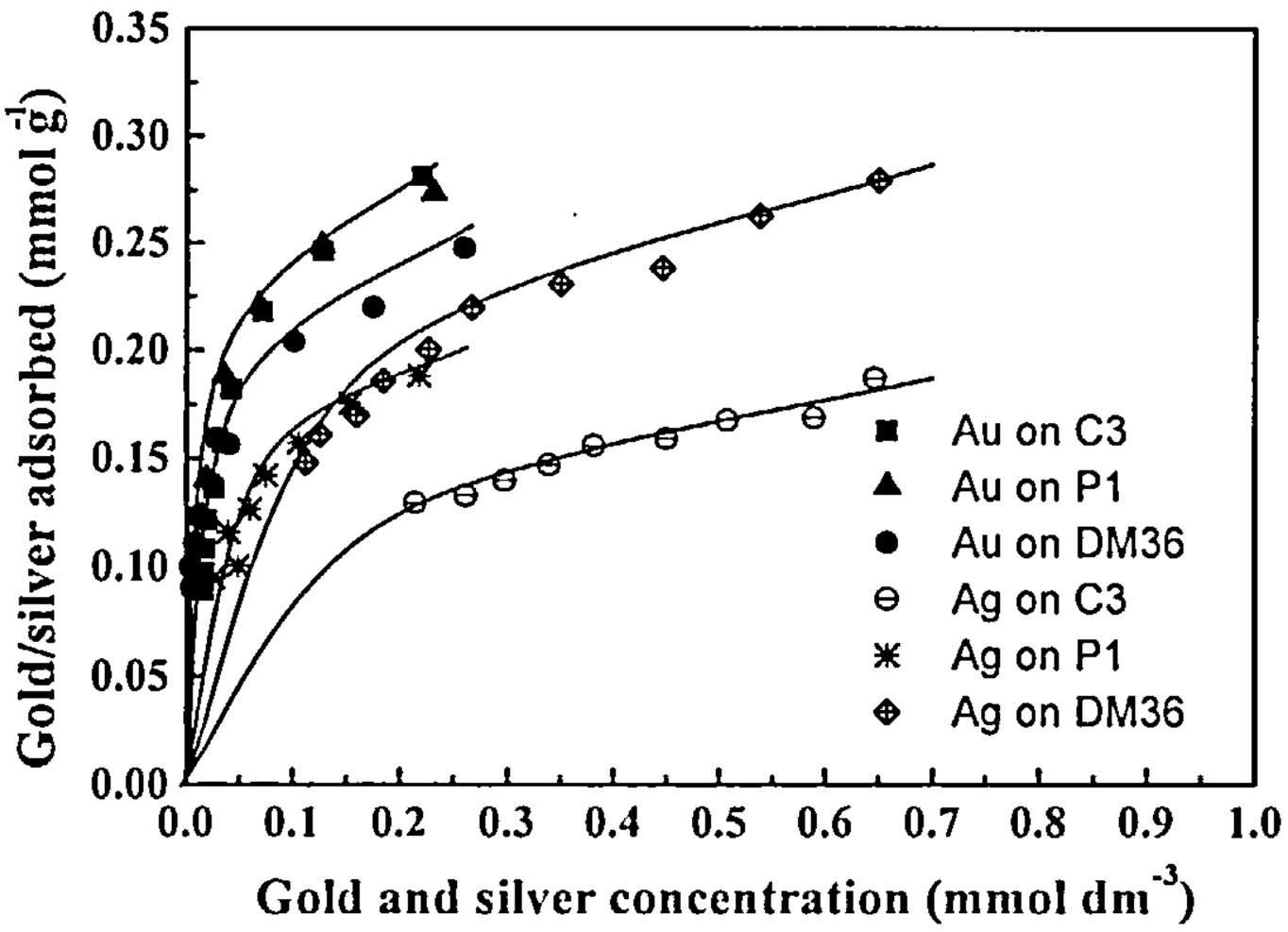

Figure 7.4 A comparison of gold and silver adsorption isotherms in the presence of CN^- at pH 10 on carbons from different precursors

Figure 7.4 shows the gold and silver cyanide adsorption isotherms on C3, P1, and DM36 and these isotherms are similar for gold adsorption. However, P1 and DM36 have higher silver cyanide adsorption capacities than C3, despite C3 having much higher surface area and pore volume. This suggests that a greater proportion of the porous structure in carbon C3 is not accessible to $Ag(CN)_2^-$, $Ag(CN)_3H_2O^{2-}$ and $Ag(CN)_4^{3-}$ ions than in carbons P1 and DM36. There are equilibria involving $Ag(CN)_2^-$ (ads), $Ag(CN)_2^-$ (aq), $Ag(CN)_3H_2O^{2-}$ (aq) and $Ag(CN)_4^{3-}$ (aq) in silver cyanide solution due to the presence of free CN^- which influence the adsorption of $Ag(CN)_2^-$ whereas there is only one gold species $Au(CN)_2^-$ (aq) in $KAu(CN)_2/CN^-$ aqueous. The ions $Ag(CN)_3H_2O^{2-}$ and $Ag(CN)_4^{3-}$ which are not adsorbed to significant extents on the carbon have a much larger size than $Ag(CN)_2^-$ and the equilibria in the porous structure will vary accordingly. Thus in the presence of free CN^-, coconut shell carbons have a higher selectivity for the adsorption of $Au(CN)_2^-$ compared with coal and peat derived carbons due to differences in the porous structure. Therefore the specific surface areas, micropore and total pore volumes cannot act as reasonable evaluation parameters of gold and silver adsorption capacities for the carbons from different precursors. Pore structure and pore size distributions are more important factors in controlling gold adsorption capacity.

A comparison of the pore size distributions between coal (DM36), peat (P1) and coconut shell (C1) based carbons, is shown in **Figure 7.5**. The amounts of porosity above ~ 2 nm are fairly similar and the main difference appears to be the much higher pore volume for porosity < 2 nm. The dimension of $Au(CN)_2^-$ ion is ~ 500 pm in spherical cross-section by ~1 nm long [*13*], and hence adsorption in the microporous structure should be possible. However the results indicate that the porosity > 2 nm is

probably responsible for adsorption of gold and silver cyanide species since similar gold adsorption isotherms are observed for the three carbons.

Nitric acid oxidation treatment of C1 carbon to form CN2 carbon resulted in significant decrease in total pore volume and micropore volume. The gold and silver adsorption capacity of CN2 was drastically reduced compared to C1. This is probably due to the decrease in total pore volume and the formation of more hydrophilic surface due to incorporation of oxygen functional groups which are not involved in and may be detrimental to the adsorption of $Au(CN)_2^-$ anion.

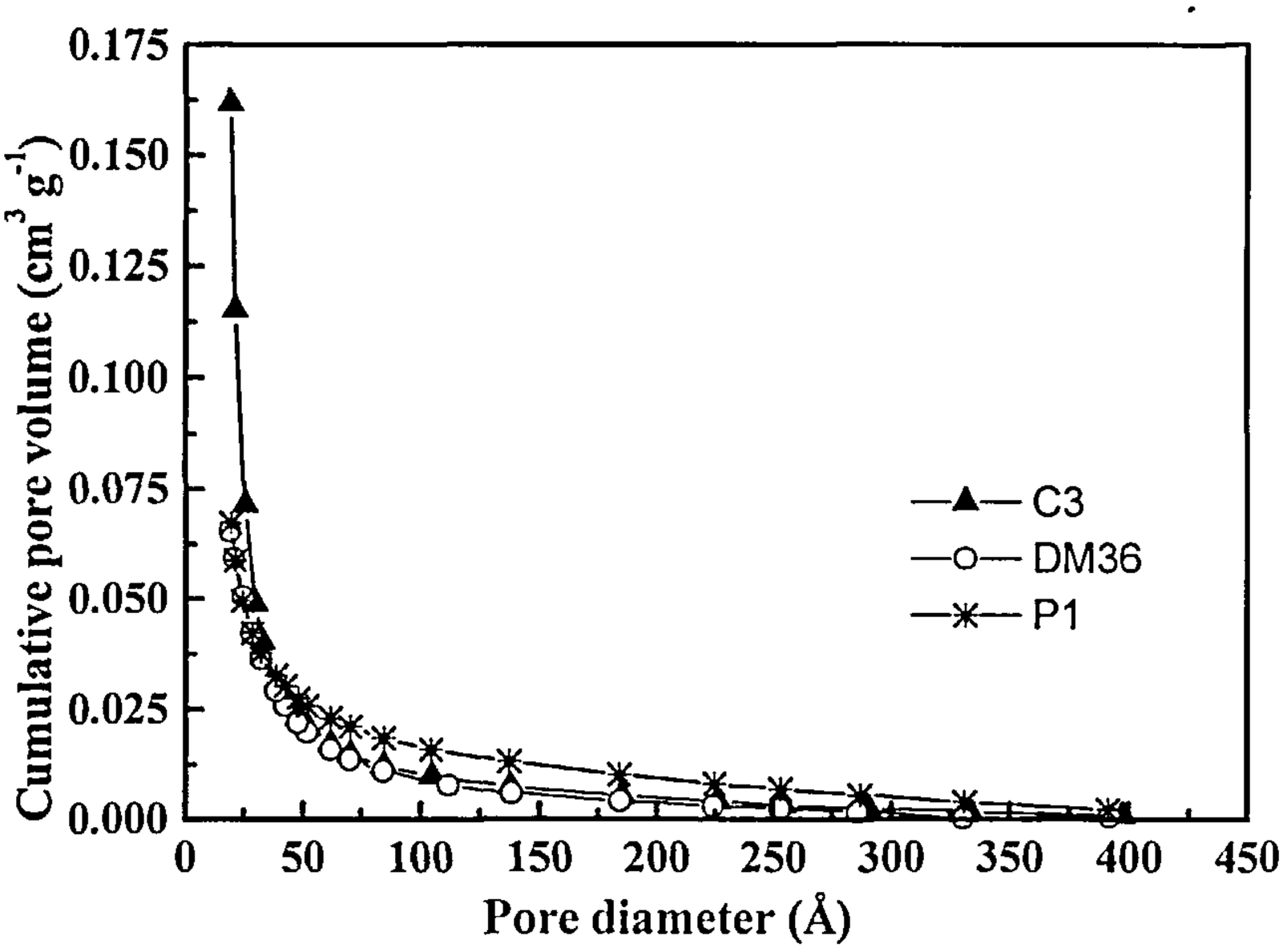

Figure 7.5 Pore size distribution of carbons from different precursors

Although oxygen and nitrogen were introduced into the carbon by nitric acid oxidation and ammonia activation treatment, no evidence of improvement of gold adsorption from incorporated oxygen and nitrogen functionality was observed. On the contrary, CN2 and CNA with higher nitrogen contents adsorbed less gold per unit

total pore volume compared with C1. The difference of gold adsorption density probably is a result of the variation of pore size distribution for these carbons. Similarly the total pore and micropore volumes of carbons PAN1 and PAN2 are quite similar to those of DM33 and DM36 but the nitrogen contents are much higher. However the adsorption characteristics of gold and silver cyanide species are quite similar suggesting that nitrogen functional groups do not have a significant effect. The results by Ibrado *et al* [*21*] also showed that the adsorption of gold cyanide was not related to the amount of oxygen groups on carbon surface. A good correlation between gold adsorption and basic surface groups was made in a recent study [*20*]. However the differences in the porous structures were not taken into consideration. The increase in gold adsorption capacity results from the development of the pore structure leading to increased accessibility to the graphene layer. The major role played by surface functionalities probably is to improve the wetting of the surface.

7.5 Effect of Oxygen Functionality on the Adsorption of Cadmium

The oxidation of active carbons by nitric acid involves the incorporation of surface functional groups which result in significant modification on the surface chemistry of the activated carbon. Heat treatment eliminates oxygen functional groups progressively. The nature of oxygen groups present in carbon were determined by a combination of FTIR, TPC and selective neutralisation studies. The oxygen functional groups present in HNO_3 oxidised carbon can be divided into carboxylic acid, phenolic and quinone groups. No strong evidence was observed to support the existence of lactone groups. The titration studies show that heat treatment at 300 °C eliminated more than half of the carboxylic acid groups, whereas other oxygen functional groups

were removed to a much smaller extent. The lactone groups were possibly formed during heat treatment at lower than 400 °C and began to decompose at higher than 400 °C. Small amounts of nitrogen functional groups were also incorporated by the oxidation procedure.

The oxidation with nitric acid brought about the reduction of surface areas, micropore and total pore volumes of the oxidised carbons. However, the adsorption capacities of active carbon for cadmium ions were enhanced dramatically by the nitric acid treatment of the active carbon. Heat treatment of the oxidised carbons increased the surface area and pore volumes while the adsorption capacities for cadmium were decreased dramatically. Carbon CN2 had lower total and micropore volumes than CN1 and C1 but adsorbed greater quantities of Cd^{2+} than CN1 and C1. These observations indicate that the cadmium adsorption capacities of the carbons are not influenced significantly by the changes in the porous structure of the activated carbons during nitric acid oxidation. The amounts of nitrogen incorporated into the carbon structure did not change significantly with heat treatment and therefore this is not a factor. The adsorption of cadmium correlated with surface acidic oxygen functional groups present in carbon. The cadmium adsorption capacity was increased dramatically after significant amounts of acidic oxygen groups were introduced by HNO_3 oxidation. However various types of oxygen surface groups do not make the same contribution to the adsorption cadmium. Carboxylic acid surface groups are the least thermally stable. Although heat treatment at 300 °C only decreased the oxygen contents of CN1 and CN2 slightly, it produced the greatest reduction of cadmium adsorption capacities. This is indicative of the oxygen present as carboxylic acid groups contributing most to the adsorption of cadmium. However, the role of other oxygen functional groups in cadmium adsorption cannot be excluded completely.

The FTIR spectra strongly suggest the formation of carboxylate after the adsorption of cadmium ions on HNO_3 oxidised carbon. The FTIR spectrum of oxidised carbon CN2 after adsorption of cadmium (see **Figure 6.10**) shows that relative intensity of carboxylic acid band at 1717 cm^{-1} decreased relative to the carboxylate 1576 cm^{-1} band intensity increased correspondingly. This provides direct evidence that cation exchange with carboxylic acid groups is involved in cadmium adsorption on activated carbon. Attempts to detect CdO stretching vibration for CN2 after adsorption of cadmium using both infrared and Raman spectroscopy were unsuccessful.

The adsorption capacity of cadmium was decreased correspondingly with the elimination of carboxylic acid groups by heat treatment. The ratio of H^+/Cd^{2+} is approximately 2 for oxidised carbon CN2 in the concentration range used in this study and decreases slightly at higher concentration. It is apparent that surface carboxylates compounds $(RCOO)_2Cd$ were formed during adsorption of Cd^{2+} with 2 protons being displaced by one cadmium cation. This was confirmed by the ratio of Na^+/Cd^{2+} during cadmium adsorption on the NaOH-neutralised CN2. At higher concentration, the ratio of Na^+/Cd^{2+} decreases slightly, indicating other mechanisms may be involved in the adsorption in addition to the cation exchange mechanism.

The possible modes of coordination of the carboxylate to the cadmium cation are illustrated in **Figure 7.6**. The coordination modes I and II represent the cation exchange reaction with one cadmium cation displacing two protons or sodium cations [*3-39*]. Studies of the crystal structures of metal carboxylate complexes shows that the carboxylate can form a monodendate ligand, a bidendate chelate or a bridging bidendate structures . In the case of H^+/Cd^{2+} or Na^+/Cd^{2+} ratios < 2 the nitrate anion must also be involved in order to balance the charge. It is also possible for the less

acidic phenolic groups to co-ordinate to the cadmium ions. However the major changes in the adsorption capacity are associated with functional groups which decompose on heat treatment to give mainly carbon dioxide. It is possible that phenolic groups are involved for adsorption on carbons heat treated to higher temperatures.

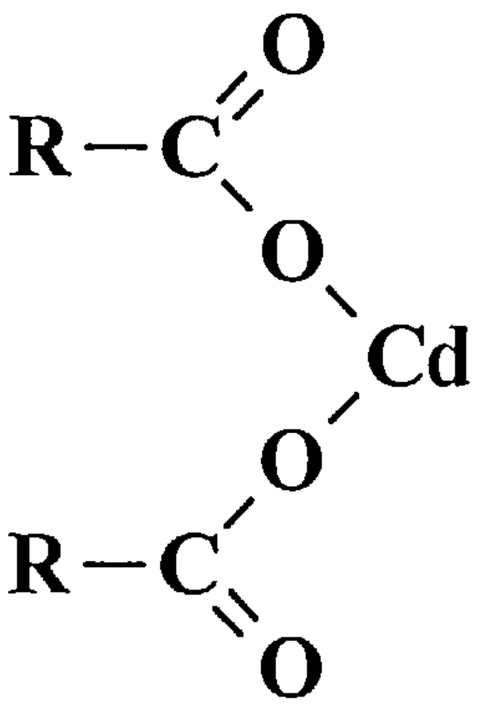

(I)

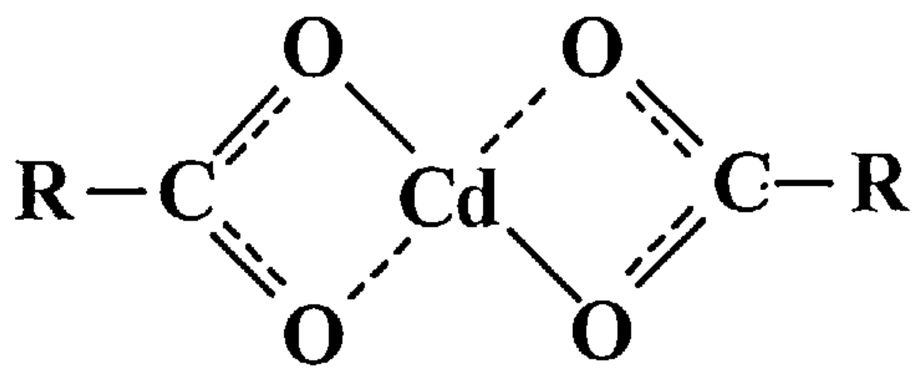

(II)

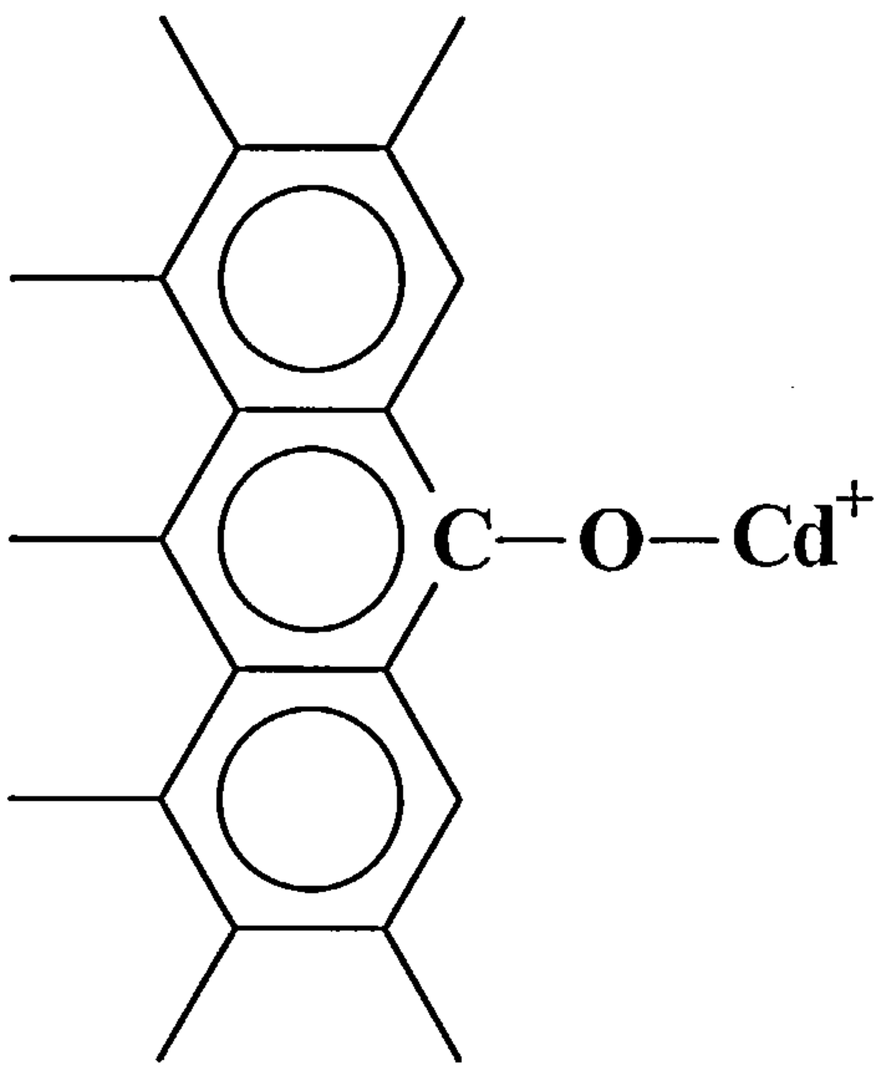

(III)

Figure 7.6 Possible modes of carboxylate coordination with cadmium cation

Comparison of **Figure 6.31** and **Figure 6.34** shows that after CN2 was treated with NaOH solution, the adsorption capacity for cadmium was enhanced appreciably. This is because neutralisation of weekly acidic surface functional groups with strong alkali solution gives a salt of the weak acid-strong base which is more dissociated than weak acid and in this form could be termed as a strong exchanger [***40***]. The following equations illustrate the ion exchange behaviour of the weakly acid and neutralised version where a short equilibrium arrow denotes an unfavourable direction of exchange:

$$\overline{RCOOH} + H_2O \leftrightharpoons \overline{RCOO^-} + H^+ \qquad (1)$$

$$\overline{RCOO^-} + H^+ + A^+_{aq} \leftrightharpoons \overline{RCOO^-} + \overline{A^+} + H^+_{aq} \qquad (2)$$

$$\overline{RCOOH} + NaOH \longrightarrow \overline{RCOO^-} + Na^+ + H_2O \qquad (3)$$

$$RCOO^- + Na^+ + A^+_{aq} \rightleftharpoons \overline{RCOO^-} + \overline{A^+} + Na^+_{aq} \qquad (4)$$

For the adsorption of cadmium on CN2-300, the ratio of H^+/Cd^{2+} is approximately 1:1. The contribution from cation exchange to the adsorption of cadmium decreases with increasing heat treatment temperatures of the carbon and with the reduction of the amounts of carboxylic acid groups. In addition to the ion exchange, another mechanism of adsorption of cadmium on carbon may involve the interaction between other oxygen surface groups and cadmium cations by the formation of hydrogen bonding. The hydrogen bonding is formed by the interaction of oxygen surface groups and hydrated cadmium cations [***41***] with charge balance involving nitrate ions.

Both reversible and irreversible adsorption of cadmium on oxidised carbon CN2 and heat treatment derivatives are involved. In the lower concentration range, the

adsorption is dominated by the ion exchange between surface carboxylic acid groups and cadmium cations which results in irreversible adsorption. When the carboxylic acid groups were removed by heat treatment or reacted with the Cd^{2+} ions, the reversible physisorption takes place. This possibly involves hydrogen bonding between other surface oxygen groups and hydrated cadmium ions [*41*], which may result in the reversible adsorption of cadmium. There is also the possibility of the Cd^{2+} ion interacting with the phenolic groups in the carbon.

7.6 Effect of Nitrogen Functionality on the Adsorption of Transition Metal Cations

There have been numerous studies of surface oxygen functional groups [*35,42-45*], nitrogen functional groups on active carbon surface have not been studied extensively [*46-48*] and the reports on the effects of nitrogen functional groups present in active carbon on the adsorption of metal species are rather limited [*49*]. X-ray photoelectron spectroscopy (XPS) was used to identify the nitrogen functional groups present on carbon surface [*46-51*]. However, XPS studies of carbon suffer from the lack of spectral resolution. The spectra usually had broad overlapping bands which were difficult to differentiate various forms of nitrogen. The newly developed technique X-ray absorption near-edge structure (XANES) spectroscopy has shown advantages over XPS in determining nitrogen functionality present in coals [*52, 53*] and in chars [*54*] in terms of better resolution.

The characterisation of the of nitrogen functional groups on the carbon surface is crucial to the understanding of the adsorption mechanism of metal cations on the active carbon. XANES has the advantages over XPS in determining the nature of

nitrogen in carbon of better resolution which allow more precise interpretation. The interpretation of IR spectra is more difficult than that of XANES due to the overlap with other bands. The forms of nitrogen present on the carbon surface either incorporated by ammonia treatment or inherited from precursor are determined to be pyridinic, pyridonic, pyrrolic (or indolic) and possibly amine-like structures. These nitrogen functional groups are usually located at the edges of the graphene layers. It is plausible that quaternary nitrogen structure was incorporated into the graphene layers, however no strong evidence was observed to support its presence on carbon surface due to lake of appropriate references compounds. The pyridinic, pyrrolic (or indolic), pyridonic structures should give C=C, C=N and C=O absorption bands in the IR region near 1500 - 1600 cm^{-1}. The graphene layer sites and quinone C=O also show bands in the similar region. Therefore it is of much difficulty to differentiate those functional groups on IR bands. The absence of the bands in 2200 cm^{-1} region indicated that the nitrile groups C≡N were absent in all the carbons used in this study.

The adsorption capacities of transition metal cation species did not correlate with surface area and pore volumes. Nitrogen functional groups present on the carbon surface substantially enhanced the adsorption of transition metal cations Cd^{2+}, Ni^{2+} and Cu^{2+} with the carbon of higher nitrogen content having greater adsorption capacity. The influence of oxygen functional groups was minimal since the stronger acidic oxygen functional groups were absent which can increase the metal adsorption through cation exchange reaction. Therefore the enhancement of the adsorption of transition metal cations was undoubtedly ascribed to the nitrogen functional groups present on carbon surface. The nitrogen functional groups may act as ligands which can coordinate with transition metal cations. The transition metal cations were probably bound to the nitrogen sites through the formation of coordination compounds

which is illustrated in **Figure 7.7**. It is apparent that all the nitrogen functional groups present on the surface of carbon can coordinate with transition metal cations [*55*] thereby increasing the adsorption of transition metal cation species. Alkali earth metal cation can only form complex with chelate agents. They can not coordinate with most nitrogen containing ligands such as pyridinic, pyrrolic, pyridonic and amine-like structures [*56*]. Thus ammonia treatment of the carbon did not increase the adsorption of calcium cation Ca^{2+} as observed above.

The pH of the solution does not greatly affect the adsorption of cadmium on carbon C1 indicating that the hydrolysis of cadmium ions to form $Cd(OH)^{+}$ or $Cd(OH)_2$ contributes little to the adsorption on the carbon surface. The increased adsorption capacities of cadmium ions with increasing pH on nitrogen rich carbons are mainly due the effect of pH on the behaviour of the nitrogen functional groups. The nitrogen functional groups are basic which would be protonated at low pH forming the pyridinium ions therefore decreasing the availability of these sites for the adsorption of cadmium. Cu^{2+} was adsorbed to a great extent than Cd^{2+} and Ni^{2+} on nitrogen rich carbons. The selectivity was due to the difference in the stability constant of the coordination compounds of the transition metal cations and the nitrogen functional groups. The coordination compounds with higher stability constant would be adsorbed to a greater extent.

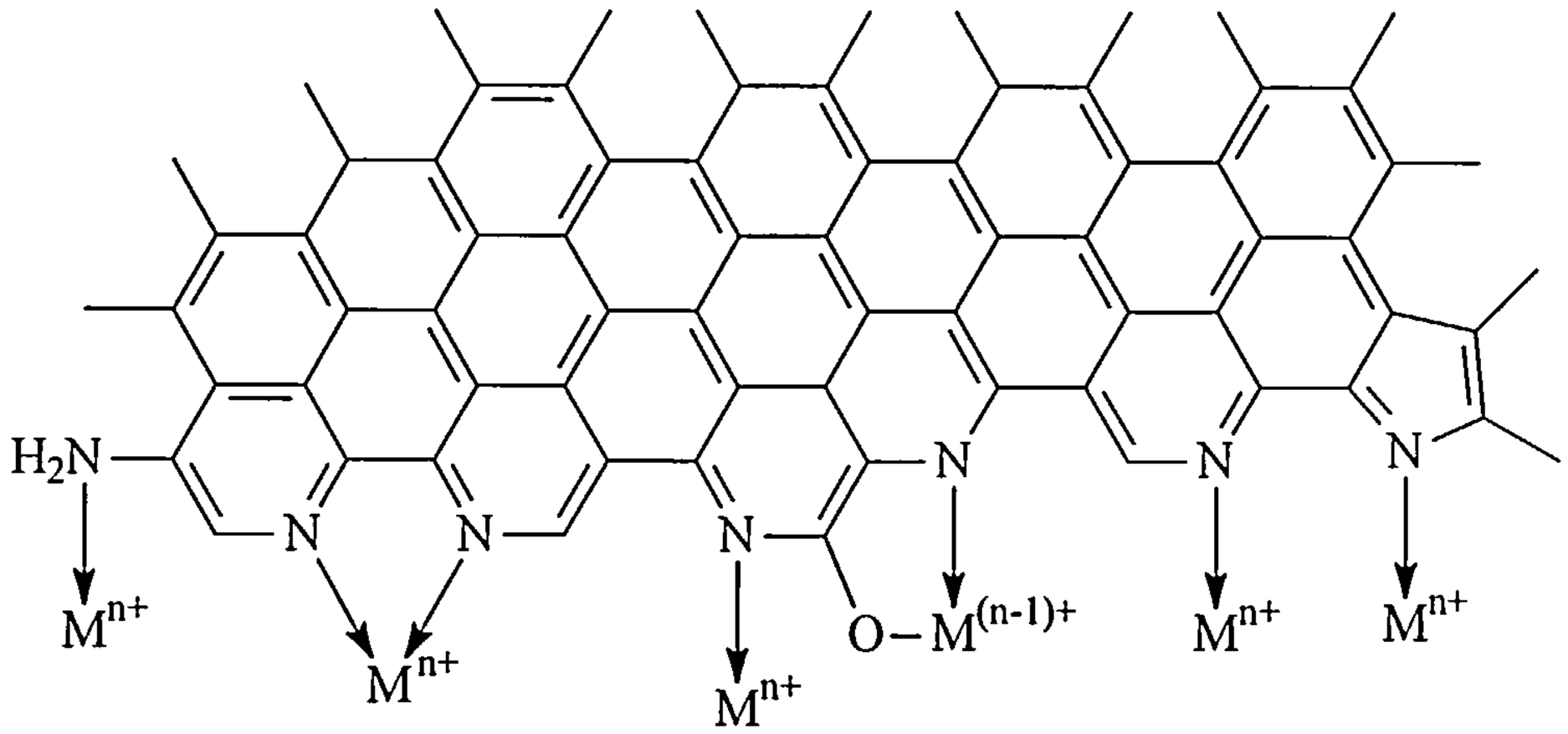

Figure 7.7 A schematic diagram of possible bonding of transition metal cations with surface nitrogen functional groups in activated carbon during adsorption

References

1. Davidson, R.J., *J. S. Afr. Inst. Min. Metall.*, 1974, **75**, 67.
2. McDougall, G.J., Hancock, R.D., Nicol, M.J., Wellington, O.L. and Copperthwaite, R.G., *J. S. Afr. Inst. Min. Metall.,* 1980, **80,** 344.
3. McDougall, G.J., Adams, M.D. and Hancock, R.D., *Hydrometallurgy*, 1987, **18**, 125.
4. Adams, M.D., McDougall, G.J. and Hancock, R.D., *Hydrometallurgy*, 1987, **18,** 139.
5. Adams, M.D., McDougall, G.J. and Hancock, R.D., *Hydrometallurgy*, 1987, **19,** 95.
6. Adams, M.D. and Fleming, C.A., *Metall Trans.*, 1989, **20B**, 315.
7. Klauber, C., *Surface Science*, 1988, **203**, 118.
8. Cook, R., Crathorne, E.A., Monhemius, A.J. and Perry, D.L., *Hydrometallurgy*, 1989, **22**, 171.
9. Jones, W.G., Klauber, C. and Linge, G., in *Proceedings of 19th Biennial Carbon Conference*, American Carbon Society, Pennsylvania State University, 1989, p. 38.
10. Klauber, C., *Langmuir*, 1991, **7**, 2153.
11. Ibrado, A.S. and Fuerstenau, D.W., *Minerals Engineering,* 1995, **8**(4/5), 441.
12. Van der Merwe, P.F. and Van Derventer, J.S.J., *Chem. Eng. Cmmun.*, 1988, **65**, 121.
13. Cashion, J.D., Cookson, D.J., Brown, L.J. and Howard, D.G., *Industrial Application of the Mössbauer Effect,* New York, 1987.
14. Cashion, J.D., McGrath, A.C., Volz, P. and Hall, J.S., *Trans. Inst. Min. Metall.*, 1988, **97**, 129.
15. Kongolo, K., Bahr, A., Friedl, J. and Wagner, F.E., *Metall. Trans.*, 1990, **21B**, 239.
16. Tsuchida, N. and Muir, D.M., *Metall. Trans.*, 1986, **17B**, 529.
17. VanDeventer, J.S.J. and Van Der Merwe, P.F., *Metall. Trans. B*, 1993, **24B**, 433.
18. Dixon, S.N., Cho, E.H. and Pitt, C.H., *AME. Inst. Chem. Eng. Symposium Series*, 1978, **147**, Part 173, 75.
19. Tsuchida, N. and Muir, D.M., *Metall. Trans.*, 1986, **17B**, 523.

20. Papirer, E., Polania-Leon, A., Donnet, J.B. and Montagnon, P., *Carbon*, 1995, **33**, 1131.

21. Ibrado, A.S., Fuerstenau, D.W., Kongolo, K., Bahr, A., Friedl, J. and Wagner, F.E., *Metall. Trans.*, 1990, **21B**, 239.

22. Ibrado, A.S. and Fuerstenau, D.W., *Hydrometallurgy*, 1992, **30**, 243.

23. Miller, J.D. and Sibrell, P.L., in *EPD Congress' 91, Min. Metas and Mat. Soc. AIME,* University of Utah, 1991, p. 647.

24. Fleming, C.A. and Nicol, M.J., *J. S. Afr. Inst. Min. Metall.*, 1984, **84**(4), 85.

25. Heinen, H. J., Peterson, D. G. and Lindstrom, R. E., *U.S. Patent*, 4, 208, 378, 17th Jun, 1980.

26. McDougall, G.J., in *Proceedings of The International Gold and Silver Conference*, Perth, Australia, 1988 p59.

27. McDougall, G.J., *J. S. Afr. Inst. Min. Metall.*, 1991, **91**, 109.

28. Cho, E.H. and Pitt, C.H., *Metall. Trans.*, 1979, **10B**, 159.

29. Rosenzweig, A. and Cromer, D.T., *Acta Cryst.*, 1959, **12**, 709.

30. Hoard, J.L., *Z. Kristallogr.*, 1933, **84**, 231.

31. Jones, L.H., *Inorganic Chemistry*, 1962, **2**, 77.

32. McDougall, G.J. and Hancock, R.D., *Gold Bulletin*, 1981, **14**(4), 138.

33. Jones, L. H. and Penneman, R. A., *J. Chem. Phys.*, 1954, **22**(6), 965.

34. Van Deventer, J.S.J and van der Merwe, P.F., *Metallurgical and Materials Transaction B*, 1994, **25B**, 829.

35. Steele, C.J., *Gold Adsorption on Activated Carbon*, PhD Thesis, University of Newcastle upon Tyne, 1997.

36. Nakamoto, K. *Infrared and Raman Spectra of Inorganic and Coordination Compounds*, 5th Edition, John Wiley & Sons, New York, 1986.

37. Simon-Kutscher, J.; Gericke, A. and Hühnerfuss, H. *Langmuir* **1996**, *12*, 1027.

38. Finnie, K. S.; Bartlett, J. R. and Woolfrey, J. L. *Langmuir* **1998**, *14*, 2744.

39. Clegg, W.; Little, I. R. and Straughan, B. P. *Inorg. Chem.*. **1988**, *27*, 1916.

40. Harland, C.E. *Ion Exchange: Theory and Practice*, 2nd Edition, Royal Society of Chemistry, Cambridge, **1994**.

41. Corapcioglu, M.O. and Huang, C.P. *Water Research* **1987**, *21*, 1031.

42. Mattson, J. S. Mark, Jr. H. B. *Activated Carbon: Surface Chemistry and adsorption from Solution*, Marcel Dekker, New York, 1971.

43. Moreno-Castilla, C.; Ferro-Garcia, M.A.; Joly, J.P.; Bautista-Toledo, I.; Carrasco-Marin, F. and Rivera-Utrilla, J. *Langmuir* **1995**, *11*, 4386.

44. de la Puente, G.; Pis, J.J.; Menendez, J.A. and Grange, P. *J. Ana. Pyro.* **1997**, *43*, 125.

45. Zawadzki, J. In *Chemistry and Physics of Carbon* 1989, Vol.21, p147.

46. Jansen, R. J. J. and van Bekkum, H. *carbon,* 1995, **33**, 1021.

47. Jansen, R. J. J. and van Bekkum, H. *Carbon*, 1994, **32**, 1507.

48. Vinke, P.; van der Eijk, M.; Verbree, M.; Voskamp, A. F. and van Bekkum, H. *Carbon*, 1994, **32**, 675.

49. Abotsi, G.M.K. and Scaroni, A.W. *Carbon* **1990**, *28*, 79.

50. Pels, J.R., Kapteijn, F., Moulijn, J.A., Zhu, Q. and Thomas, K.M., *Carbon*, 1995, **33**, 1641.

51. Stanczyk, K., Dziembaj, R., Piwowarska, Z. and Witkowski, S. *Carbon*, 1995, **33**, 1383.

52. Mitra-Kirtley, S.; Mullin, O. C.; Branthaver, J. F.; Gramer, S. P. *Energy and Fuel*, 1993, 7, 1128.

53. Mullin, O. C.; Mitra-Kirtley, S.; Elp, J. V. and Gramer, S. P. *Appl. Spectrosc.* 1993, **47**, 1268.

54. Zhu, Q.; Money, S. L.; Russell, A. E. and Thomas, K. M. *Langmiur*, 1997, **13**, 2149.

55. Constable, E. C. *Metals and Ligand Reactivity*, VCH Verlagsgesellschaft, Weinheim (Germany) & VCH Publisher, New York (USA), 1996.Ferro-Garcia, M. A.; Rivera-Utrilla, J.; Rodriguez-Gordillo, J. and Bautista-Toledo, I. *Carbon*, 1988, **26**, 363.

56. Kettle, S.F.A, *Physical Inorganic Chemistry – A Coordination Chemistry Approach*, Oxford University Press, Oxford, 1996.

Chapter 8

CONCLUSIONS

8.1 Overall Conclusions

The mechanisms of adsorption of gold cyanide anionic species and heavy metal cationic species on active carbon are different. The main sites for the adsorption of gold and silver cyanide species are the graphene layers in active carbon and the adsorption capacity is related to the porous structure, *i.e.* total pore volume and pore size distribution. The heavy metal cationic species are adsorbed on oxygen functional groups via ion exchange mechanism while the cationic species are adsorbed on nitrogen surface groups via a coordination mechanism similar to ligands in inorganic chemistry. There is no relationship established between the adsorption of heavy metal cations and the porous structure.

8.2 Specific Conclusions

Incorporation of Oxygen Functionality into Active Carbon

Acidic oxygen functional groups were incorporated into activated carbon by HNO_3 oxidation. Carboxylic acid groups together with some phenol and quinone groups were introduced by the oxidation process. No strong evidence was observed to support the existence of lactone groups in the oxidised carbon. The functional groups had a range of thermal stabilities with carboxylic acid groups being the least stable.

The titration studies show that heat treatment at 300 °C eliminated more than half of the carboxylic acid groups, whereas other oxygen functional groups were removed to a much less extent. The lactone groups were possibly formed during heat treatment at lower than 400 °C and began to decompose at higher than 400 °C. Small amounts of nitrogen functional groups were also incorporated by the oxidation procedure. The oxidation with nitric acid brought about the reduction of surface areas, micropore and total pore volumes of the oxidised carbons.

Incorporation of Nitrogen Functionality into Active carbon

Various nitrogen functional groups were incorporated into the coconut shell derived active carbon by treatment with ammonia and nitric acid oxidation followed by ammonia at elevated temperature. Active carbons with high nitrogen content were also produced from the carbonisation of polyacrylonitrile (PAN). The possible nitrogen functional groups present in the active carbons are pyridinic, pyrrolic (or indolic), pyridonic, ammonia amine-like structures and probably quaternary nitrogen. Pyrrolic nitrogen can be converted to pyridinic nitrogen with increasing heat treatment temperature (HTT). Quaternary nitrogen is probably formed from the conversion of pyridinic nitrogen during the condensation process when the nitrogen atoms are incorporated in the graphene layers replacing carbon atoms. Pyridonic groups are probably formed on carbon oxidation during activation process.

Adsorption of Gold and Silver Cyanide Anionic Species on Graphene Layers

Adsorption of gold and silver cyanide ionic species on active carbon correlates with total pore volume of a given type of carbon precursor. Coal based carbons have

higher gold and silver adsorption capacities normalised to the total pore volume than coconut shell based carbons due to their differences in pore size distribution. A fraction of micropores are not accessible for gold and silver cyanide species whereas mesopores play an important role in the adsorption. There is little evidence for carbon surface oxygen and nitrogen functional groups playing an important role in gold adsorption under the conditions used in this study. The adsorption characteristics of silver cyanide ionic species are influenced by solution equilibria. Raman spectroscopy study has shown that $Ag(CN)_3H_2O^{2-}$ is the dominant species in silver solution containing excess free cyanide with CN/Ag ratio of 4.5, while only $Au(CN)_2^-$ exists with excess free cyanide ions. Silver cyanide species adsorption is reduced significantly by excess free cyanide ions in solution by the formation of tetrahedral $Ag(CN)_3(H_2O)^{2-}$ and $Ag(CN)_4^{3-}$ thereby reducing the concentration of $Ag(CN)_2^-$ which is preferentially adsorbed on carbon. This is an explanation of why silver adsorption capacity is lower than gold with the excess free cyanide ions in solutions. Coconut shell derived carbons have higher selectivity for gold than silver in the presence of free CN^- compared with coal and peat derived carbons and this is related to the porous structure of the active carbons. The concentration of cyanide ions can be used to control the selectivity for gold adsorption compared with silver adsorption. Alcohols in solution are detrimental to gold adsorption on carbon by competitive adsorption on the hydrophobic graphene layer surface. This is indicative of the graphene layers in active carbon being the main sites for gold adsorption. The adsorption of $Au(CN)_2^-$ and $Ag(CN)_2^-$ ions on carbon is related to the electronic structure of the ions with the adsorption interaction related to the electron donation via π orbitals from the graphene layers to the metal atom. Hence the adsorption of gold and silver cyanide species on

active carbons is a function of solution equilibria, carbon porous structure and the bonding in the metal cyanide species.

Adsorption of Heavy Metal Cationic Species on Acidic Oxygen Sites in Carbon

Cadmium adsorption did not correlate with the porous structures of the activated carbons. Cadmium adsorption was dramatically enhanced after the carbon was oxidised and decreased significantly after heat treatment to progressively eliminate the oxygen functional groups of various thermal stability, thereby establishing a link between acidic oxygen functional groups and cadmium adsorption with the carboxylic acid groups contributing most to the cadmium adsorption. However, different types of oxygen surface groups do not make the same contribution to the adsorption cadmium. The oxygen present as carboxylic acid groups contributing most to the adsorption of cadmium. The ratio of H^+/Cd^{2+} for oxidised carbon and Na^+/Cd^{2+} for Na^+ ion exchange form of the carbon after adsorption were approximately 2 coinciding with the stoichiometry of cation exchange. Both reversible and irreversible adsorption were observed in cadmium adsorption on oxidised carbon. The adsorption is dominated by irreversible process at relatively low equilibrium adsorbate concentration whereas reversible adsorption occurs at higher concentration when the cadmium concentration is in excess of the amounts of acidic groups. The irreversible adsorption is ascribed to cation exchange with carboxylic acid groups while reversible adsorption probably resulting from the hydrogen bonding between surface functional groups and hydrated cadmium cations also occurs. After heat treatment to eliminate surface acidic oxygen functional groups, the irreversible adsorption is decreased markedly.

Adsorption of Heavy Metal Cationic Species on Basic Nitrogen Sites in Carbon

Surface nitrogen functional groups in active carbons markedly increased the adsorption capacities of the transition metal cationic species Cd^{2+}, Ni^{2+} and Cu^{2+}. In contrast, the ammonia treatment of the carbon did not enhance the adsorption of alkali earth metal cation Ca^{2+} on the carbon. The nitrogen functional groups can act as ligands which coordinate with transition metal cations. Therefore it can be inferred that the adsorption of transition metal cations on nitrogen containing surface may involve the interaction of nitrogen functional groups with transition metal cations by the formation of coordination bond to the carbon surface. The adsorption of cadmium ions on coconut shell derived carbon was not greatly affect by the variation of pH at the range of 4-7 whereas cadmium was adsorbed to a much greater extent at pH 7 than at pH 4.1 for the nitrogen-rich carbon. The results indicate that pH in above range does not greatly affect the hydrolysis of Cd^{2+} to form $Cd(OH)^{+}$ and $Cd(OH)_2$ which contribute to the adsorption of Cd^{2+} on the carbon surface. The nitrogen functional groups are basic which would be protonated at low pH forming the pyridinium ions therefore decreasing the availability of the adsorption sites for the adsorption of Cd^{2+} on the carbon. Copper cations were adsorbed to a great extent than cadmium and nickel on nitrogen rich carbons. The selectivity was due to the difference in the stability constant of the coordination compounds of the transition metal cations and the nitrogen functional groups in the carbon. The coordination compounds of with higher stability constant would be adsorbed to a greater extent.

Publications Related to the Work

(1) JIA, Y.F. and THOMAS, K.M., Adsorption of Cadmium Ions on Oxygen Surface Sites in Activated Carbon, *Langmuir*, 2000, **16**, pp1114-22.

(2) JIA, Y.F., STEELE, C.J., HAYWARD, I.P. and THOMAS, K.M., Mechanism of Adsorption of Gold and Silver Species on Activated Carbons, *Carbon*, 1998, **36**, pp1299-1308.

(3) JIA, Y.F. and THOMAS, K.M., Adsorption of Transition Metals on Surface Nitrogen Sites in Activated carbon, In *Proceedings of Annual ASICS Conference*, Brighton, UK, September 1999, p32.

(4) JIA, Y.F. and THOMAS, K.M., Adsorption of Cadmium Cations on Surface Oxygen Sites of Oxidised Carbon, In *Proceedings of 24th Biennial Conference on Carbon*, Charleston, South Carolina, USA, July 1999, p472.

(5) JIA, Y.F. and THOMAS, K.M., Effects of Nitrogen Functionality in Activated Carbon on the Adsorption of Transition Metal Cations, In *Proceedings of 24th Biennial Conference on Carbon*, Charleston, South Carolina, USA, July 1999, p476.

(6) JIA, Y.F. and THOMAS, K.M., Adsorption of heavy metal cation species on activated carbon, *Environmental Application of Carbon*, oral presentation on British Carbon Conference (SCI), Loughborough, April, 1999.

(7) JIA, Y.F., ZHU, Q. and THOMAS, K.M., The Influence of Carbon Surface Functionality on the Adsorption of Metals from Solution, in the *proceedings of International Conference on Carbon*, Strasbourg, France, 1998, p347.

(8) GROSZEK, A.J., STEELE, C.J., JIA, Y.F., THOMAS, K.M., New Flow Method For The Determination of Gold Adsorption Capacity and Kinetics on Carbons, in the *Proceedings of Biennial Conference on Carbon,* Pennsylvania, USA, 1997, Vol. I, p24.

(9) ELLYATT, W., HARDING, A.W., JIA, Y.F., ROY, S.C., THOMAS, K.M., TURNER, J., ZHU, Q., The Effect of Carbon Functionality on Electrocatalysis, *Scientific Report*, Vol. 2 p913, Synchrotron Radiation Department, Daresbury Laboratory, 1995-1996